



**UNIVERSITY OF
CYPRUS**

DEPARTMENT OF CHEMISTRY

**MATERIALS BASED ON
FUNCTIONAL STAR
POLYMERS: NETWORKS,
CELL TRANSFECTANTS, AND
HYBRID METAL-ORGANIC
NANOPARTICLES**

DOCTOR OF PHILOSOPHY DISSERTATION

ELENI J. KEPOLA

April 2020



**UNIVERSITY OF
CYPRUS**

DEPARTMENT OF CHEMISTRY

**MATERIALS BASED ON
FUNCTIONAL STAR
POLYMERS: NETWORKS,
CELL TRANSFECTANTS, AND
HYBRID METAL-ORGANIC
NANOPARTICLES**

Dissertation Submitted to the University of Cyprus in Partial
Fulfillment of the Requirements for the Degree of Doctor of
Philosophy

ELENI J. KEPOLA

April 2020

ELENI J. KEPOLA

Eleni J. Kepola, 2020

Validation Page

Doctoral Candidate: Eleni J. Kepola

Doctoral Thesis Title: MATERIALS BASED ON FUNCTIONAL STAR POLYMERS: NETWORKS, CELL TRANSFECTANTS, AND HYBRID METAL-ORGANIC NANOPARTICLES

*The present doctoral dissertation was submitted in partial fulfillment of the requirements for the Degree of Doctor of Philosophy at the Department of Chemistry and was approved on the 30th April 2020 by the members of the **Examination Committee***

Examination Committee:

Research Supervisor:

Costas S. Patrickios, Professor

Department of Chemistry, University of Cyprus

Committee Coordinator:

Savvas N. Georgiades, Assistant Professor

Department of Chemistry, University of Cyprus

Committee Member (Internal):

Anastasios J. Tasiopoulos, Professor

Department of Chemistry, University of Cyprus

Committee Member (External):

Triantafyllos Stylianopoulos, Assistant Professor.....

Department of Mechanical and Manufacturing Engineering, University of Cyprus

Committee Member (External):

John C. Plakatouras, Professor

Department of Chemistry, University of Ioannina, Greece

Declaration of Doctoral Candidate

The present doctoral dissertation was submitted in partial fulfillment of the requirements for the degree of Doctor of Philosophy of the University of Cyprus. It is a product of original work of my own, unless otherwise mentioned through references, notes, or any other statements.

Eleni J. Kepola

.....[Signature]

ELENI J. KEPOLA

Περίληψη

Αυτή η Διδακτορική Διατριβή πραγματεύεται με τη σύνθεση και τη μελέτη νέων υλικών βασισμένων σε λειτουργικά αστεροειδή πολυμερή: (α) αυτοσυναρμολογούμενα, αμφιφιλικά πολυμερικά συμπλέγματα (amphiphilic polymer conetworks, APCNs) που περιλαμβάνουν διασυνδεδεμένα αστεροειδή πολυμερή, (β) αποικοδομήσιμα πολυμερικά πλέγματα που περιλαμβάνουν αστεροειδή πολυμερή που φέρουν διασπώμενες διασταυρώσεις, γ) κατιονικά αστεροειδή πολυμερή ικανά να σχηματίζουν σύμπλοκα με γενετικό υλικό και να το μεταφέρουν σε (βιολογικά) κύτταρα (επιμόλυνση), δ) υβριδικά πολυμερικά νανοσωματίδια με μεταλλικούς πυρήνες και ε) πολυμερικά πλέγματα διασυνδεδεμένα στα άκρα με μέταλλα. Όλες οι παραπάνω πολυμερικές συνθέσεις έγιναν με «ζωντανές» μεθόδους πολυμερισμού / ελεγχόμενες, κυρίως, όπου χρησιμοποιήθηκε ο πολυμερισμός μεταφοράς ομάδας (group transfer polymerization, GTP), αλλά επίσης και ο πολυμερισμός μεταφοράς αλυσίδας αντιστρεπτής προσθήκης-απόσπασης (reversible addition-fragmentation chain transfer, RAFT), για την εξασφάλιση καλά καθορισμένων δομών πολυμερών και επιβεβαιώθηκαν με τη χρήση κατάλληλων μεθόδων χαρακτηρισμού μεγέθους και σύστασης, π.χ. χρωματογραφία αποκλεισμού μεγέθους (gel permeation chromatography, GPC) και φασματοσκοπία πυρηνικού μαγνητικού συντονισμού πρωτονίων (^1H nuclear magnetic resonance, NMR), αντίστοιχα.

Τα σημαντικότερα αποτελέσματα της εργασίας αυτής είναι ίσως εκείνα από το κομμάτι των APCNs, που συντέθηκαν με GTP και βασίζονται σε διάφορα συνδεδεμένα στο τέλος, «με έναρξη από τον πυρήνα» αμφιφιλικά αστεροειδή συμπολυμερή μεθακρυλικού μεθυλεστέρα (methyl methacrylate, MMA, υδρόφοβο συστατικό) και μεθακρυλικού 2-(διμεθυλαμινο)αιθυλεστέρα (2-(dimethylamino)ethyl methacrylate, DMAEMA, υδρόφιλο συστατικό), που καλύπτει πολλά μήκη βραχιόνων, συνθέσεις και αλληλουχίες. Ενώ τα περισσότερα δείγματα επέδειξαν μικροφασικό διαχωρισμό με διάταξη μικρής εμβέλειας, όπως συνήθως συμβαίνει με τα APCNs στη βιβλιογραφία, το πιο υδρόφοβο δείγμα, με μία συγκεκριμένη αλληλουχία, παρουσίασε μια φυλλώδη μορφολογία με διάταξη μεγάλης εμβέλειας τόσο σε νερό όσο και σε ξηρή μορφή, όπως αποδείχτηκε από μετρήσεις χρησιμοποιώντας σκέδαση νετρονίων υπό μικρές γωνίες (small-angle neutron scattering, SANS) σε D_2O , μικροσκοπία ατομικής δύναμης (atomic force microscopy,

AFM) μετά από θερμική ανόπτηση σε ξηρό δείγμα και στο νερό και μικροσκοπία πολωμένου φωτός στο νερό. Η παρατηρούμενη δομή με διάταξη μεγάλης εμβέλειας επιβεβαιώθηκε με επανάληψη των πειραμάτων χαρακτηρισμού και επανάληψη της συγκεκριμένης σύνθεσης τουλάχιστον δύο φορές και στη συνέχεια εκ νέου πραγματοποίηση του δομικού χαρακτηρισμού που παρήγαγε τα αποτελέσματα. Η αντοχή σε θλίψη του εξαιρετικά διατεταγμένου δείγματος ήταν επίσης ανώτερη από εκείνη των ομολόγων του, δείχνοντας ότι η καλή δομή συνοδεύεται από βελτίωση αυτής της ιδιότητας.

Ενώ ο αριθμός των βραχιόνων στους πρωτεύοντες πυρήνες των προαναφερθέντων "έναρξης από τον πυρήνα" αστεροειδών πολυμερών θα μπορούσε να προσδιοριστεί με χρήση στατικής σκέδασης φωτός, ο αριθμός των βραχιόνων στους δευτερεύοντες πυρήνες δεν μπορούσε να προσδιοριστεί εντός του διασταυρωτή, πράγμα που ώθησε την σύνθεση, μέσω GTP, παρόμοιων πλεγμάτων βασισμένων σε διασυνδεδεμένα αστεροειδή ομοπολυμερή "έναρξης από τον πυρήνα" του MMA (απλούστερο σύστημα μοντέλου) που περιλαμβάνει αποικοδομήσιμους πυρήνες που προκύπτουν από τη χρήση ενός διασπώμενου διασταυρωτή του οποίου η αποικοδόμηση μέσα στους πρωτεύοντες πυρήνες θα επέτρεπε τον επιθυμητό προσδιορισμό του αριθμού βραχιόνων στους δευτερεύοντες πυρήνες. Αν και η σύνθεση των πολυμερικών πλεγμάτων και η υδρολυτική αποικοδόμηση τους επιτεύχθηκαν αμφότερα, τα αποτελέσματα δεν ήταν καθοριστικά καθώς η αποικοδόμηση συνοδεύτηκε από ανασυνδυασμό των τμημάτων των υδρολυμένων πρωτευόντων πυρήνων.

Η επόμενη μελέτη αφορά τη σύνθεση αστεροειδών ομοπολυμερών «έναρξης από το βραχίονα» του μεθακρυλικού γλυκιδυλεστέρα (glycidyl methacrylate, GMA) χρησιμοποιώντας πολυμερισμούς GTP και RAFT και με την προσκόλληση αμινών μέσω των εποξειδικών δακτυλίων, όπου προέκυψαν πέντε αστεροειδή πολυμερή με ολιγοαμίνες, που φέρουν από 2 έως 6 άτομα αζώτου, ακολουθούμενη από τη χρήση κάθε δείγματος για την επιμόλυνση κυττάρων μυοβλαστών ποντικού C2C12, με ένα πλασμίδιο που κωδικοποιεί μια φθορίζουσα πρωτεΐνη, τη λουσιφεράση πυγολαμπίδας. Από τα αποτελέσματα ανιχνεύθηκε ένα φαινόμενο περιττού - ζυγού, σε σχέση με τον αριθμό των ατόμων αζώτου που προσδέθηκαν στις ολιγοαμίνες, τόσο ως προς την αποτελεσματικότητα στην επιμόλυνση όσο και ως προς την κυτταροτοξικότητα, επιβεβαιώνοντας τα αποτελέσματα της βιβλιογραφίας σε επιμόλυνση με πολυπεπίδια διασυνδεδεμένα με τις ίδιες ολιγοαμίνες, έτσι με τη δική

μας εργασία παρουσιάστηκε για πρώτη φορά ένα τέτοιο φαινόμενο περιττού – ζυγού σε απολύτως αβιοτικούς επιμολυντές.

Για το επόμενο μέρος της παρούσας Διδακτορικής Διατριβής συντέθηκαν υβριδικά πολυμερικά νανοσωματίδια με μεταλλικούς πυρήνες. Για το σκοπό αυτό χρησιμοποιήθηκε για πρώτη φορά ο πολυμερισμός RAFT για τη σύνθεση διαφόρων διαδρομερών συν- και τρι-πολυμερών που περιλαμβάνουν ένα μικρό μέρος από μεθακρυλικό 2- (ακετοακετοξύ) αιθυλεστέρα (2-(acetoacetoxy)ethyl methacrylate, AcEMA) όπου συμπλοκοποιείται με μέταλλα και ένα μεγαλύτερο μέρος, από μη πολικό μεθακρυλικό λαυρυλεστέρα (lauryl methacrylate, LauMA) και χρησιμοποιήθηκε ως φθορίζον μονομερές ο μεθακρυλικός 9-ανθρυλομεθυλεστέρας (9-anthrylmethyl methacrylate, AnMMA) τυχαία ενσωματωμένο στα τριπολυμερή εντός του τμήματος του polyLauMA. Τέσσερα διαφορετικά μέταλλα συμπλοκοποιήθηκαν με τα διαδρομερή σε διάφορους διαλύτες, και συντέθηκαν υβριδικά μεταλλικά-οργανικά νανοσωματίδια όπου χαρακτηρίστηκαν σε σχέση με το μέγεθος και το σχήμα τους με χρήση σκέδασης φωτός και AFM.

Τέλος, επεκτείνοντας τη στρατηγική μεταλλικών νανοσωματιδίων στην προηγούμενη ενότητα, στο τελευταίο τμήμα αυτού του PhD, ετοιμάσαμε υδρόφοβα πλέγματα συνδεδεμένα στα άκρα με μέταλλα. Ο πολυμερισμός RAFT χρησιμοποιήθηκε και πάλι για τη σύνθεση, αυτή τη φορά, των τριαδρομερών συμπολυμερών ABA των AcEMA-LauMA-AcEMA. Τα τερματικά μέρη, polyAcEMA αυτών των τριαδρομερών στη συνέχεια συμπλοκοποιήθηκαν με παλλάδιο και χρυσό, τα οποία οδήγησαν στο σχηματισμό πλεγμάτων. Οι διάμετροι των μεταλλικών πυρήνων διασταύρωσης προσδιορίστηκαν χρησιμοποιώντας μικροσκοπία μετάδοσης ηλεκτρονίων υψηλής ανάλυσης και βρέθηκαν να είναι περίπου 5 - 65 nm, ενώ τα μεγέθη των κρυσταλλιτών των μετάλλων μέσα σε αυτούς τους πυρήνες προσδιορίστηκαν χρησιμοποιώντας περίθλαση ακτίνων-X σε σκόνη και εκτιμήθηκαν να είναι γύρω στο 4.5 - 5.5 nm.

Abstract

This PhD Thesis deals with the synthesis and study of novel materials based on functional star polymers: (a) self-assembling, amphiphilic polymer conetworks (APCN) comprising interconnected star polymers, (b) degradable polymer networks comprising star polymers bearing cleavable crosslinks, (c) cationic star polymers capable of forming complexes with genetic material and transferring it to (biological) cells (transfection), (d) hybrid polymer nanoparticles with metal cores, and (e) metal-end-linked polymer conetworks. All of the above polymer syntheses involved living / controlled polymerization methods, mostly group transfer polymerization (GTP), but also reversible addition-fragmentation chain transfer (RAFT) polymerization, to secure well-defined polymer structures, as subsequently confirmed using appropriate size and composition characterization methods, *i.e.*, gel permeation chromatography (GPC) and ^1H nuclear magnetic resonance (NMR) spectroscopy, respectively.

The most important results from the Thesis are perhaps the ones from the part on APCNs, synthesized by GTP, and based on various end-linked “core-first” amphiphilic star block copolymers of methyl methacrylate (MMA, hydrophobic component) and 2-(dimethylamino)ethyl methacrylate (DMAEMA, hydrophilic component), covering several arm lengths, compositions and block sequences. While most samples exhibited microphase separation with short-range order, as is usually the case with APCNs in the literature, the most hydrophobic sample, with a particular block sequence, exhibited a lamellar morphology with long-range order both in water and in the bulk, as evidenced by measurements using small-angle neutron scattering (SANS) in D_2O , atomic force microscopy (AFM) after thermal annealing in the bulk and water, and polarized light microscopy in water. The observed structure with long-range order was confirmed by repeating the characterization experiments several times, and also repeating the particular synthesis at least twice and then again performing the structural characterization which reproduced the results. The compressive strength of the highly-ordered sample was also superior to that of its homologues, manifesting that good structure is accompanied with property improvement.

While the number of arms in the primary cores of the above-mentioned “core-first” star polymers could be determined using static light scattering, the number of arms in

the secondary cores could not be determined within the crosslinked material, which motivated the synthesis, via GTP, of similar networks based on interconnected “core-first” star homopolymers of MMA (simpler model system) comprising degradable cores arising from the use of a cleavable crosslinker whose disassembly in the primary cores would enable the desired determination of the number of arms in the secondary cores. Although the synthesis of the designed polymer networks and their hydrolytic disassembly were both achieved, the results were not conclusive as the disassembly was accompanied by recombination of the moieties of the hydrolyzed primary cores.

The next project involved synthesis of “arm-first” star homopolymers of glycidyl methacrylate (GMA) using both GTP and RAFT polymerization, and the attachment, through the epoxide rings, onto the resulting stars of five oligoamines, bearing from 2 to 6 nitrogen atoms, followed by the use of each sample for transfecting C2C12 mouse myoblast cells with a plasmid encoding for a fluorescent protein, firefly luciferase. The results detected an odd-even motif, with respect to the number of nitrogen atoms in the oligoamine grafts, both regarding transfection efficiency and cytotoxicity, corroborating literature results on polypeptide-based transfectants grafted with the same oligoamines, and with our present work constituting the first demonstration of such an odd-even effect with totally abiotic transfectants.

For the following part of this Doctoral Thesis, hybrid polymer nanoparticles with metal cores were fabricated. To this end, RAFT polymerization was first utilized to synthesize several diblock co- and ter-polymers comprising a metal-chelating short block of 2-(acetoacetoxy)ethyl methacrylate (AcEMA) and a longer, relatively non-polar, block of lauryl methacrylate (LauMA), with the 9-anthrylmethyl methacrylate (AnMMA) fluorescent monomer randomly incorporated in the terpolymers within the LauMA block. Four different metals were complexed with the diblocks in various solvents, and the formed hybrid metal-organic nanoparticles were characterized in terms of their size and shape using light scattering and AFM.

Finally, extending the metal nanoparticle strategy in the previous section, in the last part of this PhD, we prepared metal-end-linked hydrophobic conetworks. RAFT polymerization was again employed to synthesize, this time, ABA triblock copolymers of AcEMA-LauMA-AcEMA. The polyAcEMA end-blocks of these triblocks were subsequently complexed with palladium and gold, which led to

network formation. The diameters of the metal crosslinking cores were determined using high-resolution transmission electron microscopy and found to be around 5 – 65 nm, whereas the sizes of the metal crystallites within these cores were determined using powder X-ray diffraction and estimated to be around 4.5 – 5.5 nm.

ELENI J. KEPOLA

Acknowledgement

Coming to the end of my Doctoral Thesis I would like to extend my warmest thanks to various individuals who contributed all these years to the success of my work.

First, I would like to extend my thanks to my Research Advisor Professor Costas S. Patrickios for his help, support, and continuous guidance that he provided to me throughout this research work.

Next, I would like to thank Professor Epameinondas Leontides from our Department, for making available to us his polarized light microscope, and his valuable help in conducting the polarized light microscopy experiments. Many thanks also go to Associate Professor Theodora Krasia-Christoforou from the Department of Mechanical and Manufacturing Engineering of the University of Cyprus, for her valuable advice in all metal experiments (solutions and networks). Also, I would like to thank Dr. Charalambos Papatryphonos and Professor Charis Theocharis from our Department, for making available to us the powder X-ray Diffractometer, and their help in conducting the experiments.

I would like also to thank the European Regional Development Fund and the Republic of Cyprus through Cyprus Research Promotion Foundation (infrastructure projects IPE/ NEKYP/0311/27) which funded; through the Cyprus Research Promotion Foundation (infrastructure project IPE/ NEKYP/0311/27) the current research work enabled the purchase of the AFM and DLS/SLS instruments. We are also grateful to the A. G. Leventis Foundation, and the Cyprus Research Promotion Foundation and the Regional Development Fund (project NEKYP/0308/02) for the establishment of the NMR infrastructure at the University of Cyprus.

For the SANS experiments and measurements, I would like to thank Dr. Ralf Schweins and Dr. Ingo Hoffmann from the Institut Laue-Langevin (ILL) Grenoble, France, Dr. Marie-Sousai Appavou from the Jülich Center for Neutron Science (JCNS), Garching in Germany, Dr. Paul D. Butler from the National Institute of Standards and Technology (NIST), Gaithersburg, Maryland, and Dr. Michael Gradzielski and Dr. Miriam Simon from the Stranski Laboratorium für Physikalische und Theoretische Chemie, at the Institut für Chemie, of the Technische Universität Berlin in Germany.

I would like to thank Dr. Florian Johann (Asylum) for his help with the AFM measurements in water and Dr. Christian Krumm and Professor Joerg C. Tiller from Department of Biochemical and Chemical Engineering, of the Technische Universität Dortmund in Germany, for the analysis of the AFM images.

I would like to thank Professor Chrys Wesdemiotis and Dr. Michelle Kushnir, from the Department of Chemistry and the Integrated Biosciences Program, of the University of Akron, in the United States for conducting mass spectroscopy measurements for some of my polymer (the cores of the star polymers).

Furthermore, many thanks go to Assistant Professor Triantafyllos Stylianopoulos and Dr. Chrysovalantis Voutouri from Department of Mechanical and Manufacturing Engineering, of the University of Cyprus for the measurements mechanical properties.

I also thank Dr. Nikolaos P. Mastrogiannopoulos and Professor Leonidas A. Phylactou from the Department of Molecular Genetics, Function & Therapy, at the Cyprus Institute of Neurology and Genetics for their help with the gene delivery experiments.

I would also like to express my gratitude to Professor Yoshihito Osada of RIKEN, Wako, Saitama, Japan, for his valuable comments and suggestions on the part of my work on amphiphilic polymer conetworks.

Many thanks to Professor Patrick Théato from Karlsruhe Institute of Technology (KIT), Institute for Chemical Technology and Polymer Chemistry for his valuable help in the experiments of oligoamine-grafted polymers.

I would also like to thank Dr. Kyriaki Paphiti for her help with the synthesis of the oligoamine-grafted polymers and the experiments on gene delivery, and also for her valuable help and advice all these years.

I would also like to thank the members of my Doctoral Examination Committee: Assistant Professor Savvas N. Georgiades, Professor Anastasios J. Tasiopoulos, Assistant Professor Triantafyllos Stylianopoulos and Professor John C. Plakatouras.

In the end, I would like to express my sincere thanks to my family and my husband Mr. Floros Zorpas for the help and support they were offered to me throughout the years of my Doctoral studies.

Experiments carried out by Collaborators

In this PhD thesis some scientific measurements were performed by external partners. The name of these external partners together with the measurements they made for us are summarized below:

1. SANS experiments and measurements for the amphiphilic polymer conetworks in D₂O: Dr. Ralf Schweins, Dr. Ingo Hoffmann, Dr. Marie-Sousai Appavou, Dr. Paul D. Butler, Professor Michael Gradzielski and Dr. Miriam Simon.
2. AFM images in the 3.1 & 3.2 Sections: Dr. Christian Krumm and Professor Joerg C. Tiller.
3. Mass Spectrometry experiments for the cores of the amphiphilic polymer conetworks: Professor Chrys Wesdemiotis and Dr. Michelle Kushnir.
4. Determination of the mechanical properties of the amphiphilic polymer conetworks: Assistant Professor Triantafyllos Stylianopoulos and Dr. Chrysovalantis Voutouris.
5. Powder-XRD experiments: Dr. Charalambos Papatryphonos and Professor Charis Theocharis.

To my father, who left too early from my life but he was close to me all the time.

Publications

1. E. J. Kepola, E. Loizou, C. S. Patrickios, E. Leontidis, C. Voutouri, T. Stylianopoulos, R. Schweins, M. Gradzielski, C. Krumm, J. C. Tiller, M. Kushnir, C. Wesdemiotis,, ‘Amphiphilic End-linked Conetworks Based on “Core-first” Star Copolymers: Structure Formation with Long-range Order,’ *ACS Macro Letters* **2015**, *4*, 1163-1168.
Number of Citation: 35
2. E. J. Kepola, K. Kyriacou, C. S. Patrickios, M. Simon, M. Gradzielski, M. Kushnir and C. Wesdemiotis, “Amphiphilic Polymer Conetworks Based on Interconnected Hydrophobic Star Block Copolymers: Synthesis and Characterization”, *Macromolecular Symposia* **2017**, *372*, 69 – 86.
Number of Citation: 2
3. E.J. Kepola and C. S. Patrickios, “Networks Based on “Core-First” Star Polymers End-Linked Using a Degradable Ketal Cross-Linker: Synthesis, Characterization, and Cleavage”, *Macromolecular Chemistry and Physics* **2018**, *219*, 1700404.
Number of Citation: 2
4. K. S. Pafiti, E. J. Kepola, M. C. Vlasίου, C. S. Patrickios, , E. Yamaaki, N. P. Mastrogiannopoulos, L. A. Phylactou and P. Théato, ‘Oligoamino-grafted-Poly(Glycidyl Methacrylate) Star and Linear Homopolymers: Odd-Even Correlated Transfection Efficiency,’ **in preparation for submission in ACS Biomaterials Science and Engineering**
5. E. J. Kepola, T. Krasia-Christoforou, C. S. Patrickios, ‘Metal-bearing Nanoparticles From the Chelation-driven Self-assembly of Diblock Co- and Ter- polymers: Preparation and Characterization with Atomic Force Microscopy and Dynamic Light Scattering,’ **in preparation for submission in European Polymer Journal**.
6. E. J. Kepola, T. Krasia-Christoforou, C. Papatryfonos, C. Theocharis, C. S. Patrickios, E. Vasile, ‘Metal-end-linked Polymer Conetworks from the Chelation-driven Self-assembly of ABA Triblock Copolymers: Preparation and Characterization,’ **in preparation for submission in European Polymer Journal**

7. E. J. Kepola, C. S. Patrickios, N. P. Mastroiannopoulos, L. A. Phylactou ‘Polymeric Micelles from Poly[(2-acetoacetoxy)ethyl methacrylate]-Poly[(2-dimethylamino)ethyl methacrylate] Block Copolymer and Au, for Gene Delivery,’ **in preparation for submission in Biomacromolecules.**

ELENI J. KEPOLA

Table of Contents

	Pages
CHAPTER 1: INTRODUCTION	1-20
1.1 Objective and Innovation.	1
1.2. Literature review.	3
<i>1.2.1. Polymer Networks.</i>	3
1.2.1.1. Amphiphilic Polymer Conetworks (APCNs).	3
1.2.1.2. Degradable Quasi-model Polymer Networks.	4
<i>1.2.2. Oligoamine-grafted Glycidyl Methacrylate Polymers.</i>	4
<i>1.2.3. Metal-organic Coordination Polymers and Networks.</i>	6
1.3. Theoretical Background.	6
<i>1.3.1. Degradable Ketal Crosslinker and Hydrolysis.</i>	6
<i>1.3.2. Odd-even Effect.</i>	7
<i>1.3.3. Discovery and General Characteristics of plasmid-DNA.</i>	7
1.3.3.1. Plasmid-DNA.	7
1.3.3.2. Application of plasmid-DNA.	8
1.3.3.3. Transfection of DNA (plasmid-DNA).	9
<i>1.3.4. Metal Nanoparticles(MNPs).</i>	9
<i>1.3.5. Polymerization Methods.</i>	10
1.3.5.1. Group Transfer Polymerization (GTP).	10
1.3.5.2. Reversible Addition–fragmentation Chain-transfer Polymerization (RAFT).	11
<i>1.3.6. Methods for Polymer and Networks Characterization.</i>	14
1.3.6.1. Gel Permeation Chromatography (GPC-HPLC).	14
1.3.6.2. Nuclear Magnetic Resonance Spectroscopy (¹ H, ¹³ C-NMR).	14
1.3.6.3. Static Light Scattering (SLS).	15
1.3.6.4. Dynamic / Static Light Scattering (DLS/SLS).	16
1.3.6.5. Atomic Force Microscopy (AFM).	16
1.3.6.6. Small-angle Neutron Scattering (SANS).	17
1.3.6.7. High-resolution Transmission Electron Microscopy (HR-TEM).	18
1.3.6.8. Polarized Light Microscopy.	19
1.3.6.9. Powder X-Ray Diffraction (<i>p</i> -XRD).	19

1.3.6.10. Mass Spectrometry (MS).	20
1.3.6.11. Compression Test.	20
CHAPTER 2: EXPERIMENTAL PART	22-41
2.1. Chemical Reagents and Solvents.	22
2.2. Purification of Monomers and Solvents for the Polymerizations.	23
2.3. Synthesis of the AnMMA Monomer, the Chain Transfer Agent and the Degradable Cross-linker.	24
2.3.1. <i>Synthesis of the AnMMA Monomer.</i>	24
2.3.2. <i>Synthesis of the 1,4-BTBTPB Chain Transfer Agent .</i>	24
2.3.3. <i>Synthesis of the DMOEP Hydrolyzable Cross-linker.</i>	25
2.4. Synthesis of Polymers and Polymer Networks.	26
2.4.1. <i>GTP Synthesis of EGDMA-MMA-DMAEMA-EGDMA Amphiphilic Polymer Conetworks Based on End-linked Core-first Star Block Copolymers.</i>	26
2.4.2. <i>GTP Synthesis of Hydrolyzable MMA Networks Cross-linked with DMOEP and EGDMA.</i>	27
2.4.3. <i>RAFT and GTP Synthesis of Linear and Star "Arm-first" GMA Homopolymers.</i>	28
2.4.3.1. <i>GMA "Arm-first" Star Homopolymer by GTP.</i>	29
2.4.3.2. <i>Linear and "Arm-first" Star Homopolymes of GMA by RAFT Polymerization.</i>	29
2.4.4. <i>RAFT Synthesis of the AcEMA-LauMA Diblock Copolymers and the Linear AcEMA-LauMA-AnMMA Diblock Terpolymers.</i>	30
2.4.4.1. <i>Synthesis of the Diblock Copolymers.</i>	30
2.4.4.2. <i>Synthesis of Diblock Terpolymers.</i>	31
2.4.5. <i>RAFT Synthesis of AcEMA-LauMA-AcEMA Triblock Copolymers.</i>	31
2.4.6. <i>RAFT Synthesis of Linear AcEMA₅₀-b-DMAEMA₂₀₀ Copolymer.</i>	32
2.5. Characterization Methods for all the Polymers and Polymer Networks.	32
2.5.1. <i>Gel Permeation Chromatography (GPC-HPLC.)</i>	32
2.5.2. <i>Nuclear Magnetic Resonance Spectroscopy (¹H and ¹³C NMR).</i>	33
2.5.3. <i>Extractables of Amphiphilic Polymer Conetworks and Degradable Polymer Networks.</i>	33
2.5.4. <i>Static Light Scattering (SLS).</i>	33
2.5.5. <i>Dynamic / Static Light Scattering (DLS/SLS).</i>	35
2.5.6. <i>Mass Spectroscopy (MS) in the Core of the Star Polymer in Amphiphilic Polymer Conetwork.</i>	35

2.5.7. <i>Degrees of Swelling (DS).</i>	35
2.5.7.1. <i>Degrees of Swelling in Organic Solvent.</i>	36
2.5.7.2. <i>Degrees of Swelling in Water at Different pHs.</i>	36
2.5.8. <i>Polarized Light Microscopy.</i>	36
2.5.9. <i>Small-angle Neutron Scattering (SANS).</i>	37
2.5.10. <i>High-resolution Transmission Electron Microscopy (HR-TEM).</i>	37
2.5.11. <i>Atomic Force Microscopy (AFM).</i>	38
2.5.11.1. <i>AFM for Amphiphilic Polymer Conetwork.</i>	38
2.5.11.2. <i>AFM for Metal-bearing Nanoparticles.</i>	38
2.5.11.3. <i>AFM for Au-end-linked Polymer Conetworks.</i>	38
2.5.12. <i>Powder X-ray Diffraction (p-XRD).</i>	39
2.5.13. <i>Compression Tests of Amphiphilic Polymer Conetworks.</i>	39
2.6. Hydrolysis of the Degradable Conetworks.	39
2.7. Derivatization of Linear and Star GMA Homopolymers with Several Amines.	40
2.8. DNA Transfer Using Oligoamine-grafted-GMA Polymers and AcEMA₅₀-LauMA₂₀₀-linear/Au.	41
2.8.1. <i>Plasmid DNA / Polymer Transient Transfections.</i>	41
2.8.2. <i>Firefly Luciferase Assay.</i>	42
2.8.3. <i>Determination of Cell Viability.</i>	42
2.9. Complexation of all the diblock and triblock copolymers (AcEMA-LauMA-AnMMA) with Metal Ions and Reduction in Nanoparticles.	42
2.9.1. <i>Complexes with Au Metal Ions.</i>	42
2.9.2. <i>Complexes with Pd or Ni Metal Ions.</i>	43
2.10. Preparation of the metal-end-linked polymer conetworks with Pd(CH₃COO)₂ or HAuCl₄·3H₂O.	43
CHAPTER 3: RESULTS AND DISCUSSION	44-140
3.1. Amphiphilic Polymer Conetworks Based on End-Linked “Core-First” Star Block Copolymers: Structure Formation with Long-Range Order.	47
3.1.1. <i>GPC Traces of the Star (Co)polymers.</i>	48
3.1.2. <i>Molecular Weights and Compositions of the Star (Co)polymers.</i>	51
3.1.3. <i>Average Number of Arms in Star Polymers.</i>	53
3.1.4. <i>Extractables from the (Co)networks.</i>	54
3.1.5. <i>Species Identification in the EGDMA Core.</i>	55
3.1.6. <i>Effect of pH on the Aqueous Degrees of Swelling.</i>	56

3.1.7. <i>Effect of (Co)polymer Composition and Architecture on the Degrees of Swelling.</i>	58
3.1.8. <i>Structure of the Conetworks in the Bulk and in Water.</i>	59
3.1.8.1. <i>Structure in the Bulk.</i>	59
3.1.8.2. <i>Structure in Solution.</i>	64
3.1.9. <i>Anisotropic Nanophases.</i>	67
3.1.10. <i>Mechanical Properties.</i>	69
3.1.11. <i>Confirmation of the APCN Long-range Structure.</i>	70
3.1.12. <i>Conclusions.</i>	70
3.2. Amphiphilic Polymer Conetworks Based on End-Linked “Core-First” Hydrophobic Star Block Copolymers: Synthesis and Characterization.	72
3.2.1. <i>Species Identification in the EGDMA Core.</i>	74
3.2.2. <i>GPC Traces of Star (Co)polymers.</i>	76
3.2.3. <i>Molecular Weights and Compositions</i>	78
3.2.4. <i>Extractables.</i>	80
3.2.5. <i>Effect of pH on the Aqueous Degrees of Swelling.</i>	81
3.2.6. <i>Structure of the Conetworks in Water.</i>	84
3.2.7. <i>Anisotropic Nanophases.</i>	91
3.2.8. <i>Conclusions.</i>	92
3.3. Networks Based on “Core-first” Star Hydrophobic Homopolymers End-linked Using a Degradable Ketal Cross-Linker: Synthesis, Characterization and Cleavage.	93
3.3.1. <i>Synthesis and Characterization of the DMOEP Crosslinker.</i>	94
3.3.2. <i>Synthesis of Hydrolyzable End-Linked Networks of MMA Based on EGDMA and DMOEP Crosslinkers.</i>	95
3.3.3. <i>GPC Traces of the Star Homopolymers.</i>	96
3.3.4. <i>Molecular Weights, Absolute Molecular Weights and Composition.</i>	100
3.3.5. <i>Extractables.</i>	102
3.3.6. <i>Degrees of Swelling in THF.</i>	103
3.3.7. <i>Size and Composition of the Polymer Network Hydrolysis Products.</i>	104
3.3.8. <i>Conclusions.</i>	105
3.4. Oligoamine-grafted Glycidyl Methacrylate Linear and Star Homopolymers: Odd-Even Correlated Transfection Efficiency	106
3.4.1. <i>Synthesis Oligoamine-grafted Glycidyl Methacrylate Linear and Star Homopolymers.</i>	107

3.4.2. <i>Molecular Weights and Compositions.</i>	107
3.4.3. <i>Derivatization of GMA the Linear and Star Homopolymers with the Oligoamines.</i>	108
3.4.4. <i>Evaluation of the Oligoamine-grafted PolyGMAs as Plasmid DNA Transfectants.</i>	110
3.4.5. <i>Conclusions.</i>	114
3.5. Metal-bearing Nanoparticles From the Chelation-driven Self-assembly of Diblock Co- and Ter-polymers: Preparation and Characterization with Atomic Force Microscopy and Dynamic Light Scattering.	115
3.5.1. <i>Synthesis and Characterization of the AnMMA Monomer.</i>	115
3.5.2. <i>Synthesis of Linear Diblock AcEMA-b-LauMA Copolymers AcEMA-b-(LauMA-co-AnMMA) Terpolymers.</i>	116
3.5.3. <i>Molecular Weights and Compositions.</i>	117
3.5.4. <i>Polymer Complexation with Three Different Metals (Au, Pd, Ni) in Selective and Non-selective Organic Solvents.</i>	118
3.5.5. <i>Characterization of Nanoparticles Stability in Organic Solvents.</i>	119
3.5.6. <i>Surface Morphology.</i>	121
3.5.7. <i>Absolute Molecular Weights and Radii of the Nanoparticles.</i>	126
3.5.8. <i>Conclusions.</i>	127
3.6. Metal-end-linked Polymer Conetworks from the Chelation-driven Self-assembly of ABA Triblock Copolymers: Preparation and Characterization.	129
3.6.1. <i>RAFT Synthesis of AcEMA-LauMA-AcEMA Triblock Copolymers.</i>	129
3.6.2. <i>Molecular Weights and Compositions.</i>	129
3.6.3. <i>Complexation with Metals Leading to the Formation of Hybrid Networks</i>	130
3.6.4. <i>Degrees of Swelling in n-Hexane.</i>	131
3.6.5. <i>Size of the Au and Pd crystallites in the Au- and Pd-end-linked polymer conetworks.</i>	133
3.6.6. <i>Diameters of the nanoparticles within the Au- and Pd-end-linked polymer conetworks.</i>	134
3.6.7. <i>Surface Morphology of the Au-end-linked Conetworks.</i>	135
3.6.8. <i>Conclusions.</i>	138
3.7. Synthesis of a linear AcEMA₅₀-b-DMAEMA₂₀₀ Copolymer Complexed with Au for use in Gene Delivery.	139
3.7.1. <i>Molecular Weights and Compositions.</i>	139

3.7.2. <i>Luciferase Expression and Cytotoxicity.</i>	140
3.7.3. <i>Conclusions.</i>	141
CHAPTER 4: CONCLUSIONS AND FUTURE WORK	142-145
4.1. Conclusions.	142
4.2. Future Work.	145
CHAPTER 5: BIBLIOGRAPHY	146-160
ANNEX I	161

ELENI J. KEPOLA

List of Figures

Figure 1.1. Illustration of a bacterium containing both chromosomal DNA and plasmids.

Figure 1.2. Group transfer polymerization (GTP) mechanism.

Figure 1.3. Chemical structure of a dithioester chain transfer agent for RAFT polymerization.

Figure 1.4. RAFT polymerization steps.

Figure 2.1. Synthetic sequences followed for the preparation of the end-linked MMA homopolymer networks based on interconnected “core-first” star polymers.

Figure 3.1. Graphical representation of the various projects under taken in this PhD Thesis.

Figure 3.2. Schematic representation of the procedure followed for APCN preparation via sequential GTP.

Figure 3.3. Schematic representations of the “core-first” star (co)polymer building blocks, precursors to the eight (co)networks. E, M and D are further abbreviations for EGDMA, MMA and DMAEMA, respectively. The hydrophobic MMA units are shown in red, the hydrophilic DMAEMA units are presented in light blue, the first EGDMA cores are displayed in grey, and the second EGDMA cores are painted black.

Figure 3.4. GPC traces of all the soluble precursors to the (co)networks based on the end-linked “core-first” star (co)polymers. The traces for the EGDMA core oligomers, the “core-first” star homopolymers, and the “core-first” star block copolymers are shown in grey dotted lines, in light green dashed lines, and in blue continuous lines, respectively.

Figure 3.5. MALDI-TOF spectrum of the EGDMA oligomeric core of a star polymer, involving various conjugates of EGDMA with the MTS initiator (I).

Figure 3.6. pH-Dependence of the swelling and ionization degrees of all the (co)polymer (co)networks.

Figure 3.7. Degrees of swelling of all the (co)polymer (co)networks in pure (blue) and in acidic (red) water, and in THF (green), plotted against (co)network

composition for the two (co)network architectures: MMA-*b*-DMAEMA (open symbols) and DMAEMA-*b*-MMA (closed symbols). M is MMA and D is DMAEMA.

Figure 3.8. Atomic force microscopy phase images of all the (co)networks of this study in the bulk before thermal annealing. Image dimensions are 1000 nm × 1000 nm. E is EGDMA, D is DMAEMA and M is MMA.

Figure 3.9. Atomic force microscopy phase images of all the (co)networks of this study in the bulk, after thermal annealing at 105 °C. Image dimensions are 500 nm × 500 nm. E is EGDMA, D is DMAEMA and M is MMA.

Figure 3.10. Structure formation with long-range order exhibited by Sample EGDMA₁-*b*-MMA₃₀-*b*-DMAEMA₁₀-*b*-EGDMA₁ in water, as observed using AFM (phase mode). Secondary assembly in water: hydrophilic cores organized in 2D to give lamellae.

Figure 3.11. Small-angle neutron scattering profiles of the unprocessed (not thermally-annealed) (co)networks in D₂O. These data were collected at the National Institute of Standards and Technology (NIST), in Gaithersburg, Maryland in the USA. E is EGDMA, D is DMAEMA and M is MMA.

Figure 3.12. Small-angle neutron scattering profiles of the thermally-annealed (at 105 °C) (co)networks in D₂O. These data were collected at the Jülich Center for Neutron Scattering (JCNS) in Garching, Germany. E is EGDMA, D is DMAEMA and M is MMA.

Figure 3.13. Polarized light microscopy images of all the (co)networks swollen in water. E is EGDMA, D is DMAEMA and M is MMA.

Figure 3.14. Compressive (a) stress and (b) strain at break, and (c) Young's modulus of all (co)networks equilibrium-swollen in water.

Figure 3.15. Small-angle neutron scattering profiles of EGDMA₁-*b*-MMA₃₀-*b*-DMAEMA₁₀-*b*-EGDMA₁ in D₂O. (a) Originally-synthesized sample, and, (b) repeated synthesis. These SANS data were collected at the Institut Laue-Langevin (ILL) in Grenoble, France.

Figure 3.16. Structure formation with long-range order exhibited by sample EGDMA₁-*b*-MMA₃₀-*b*-DMAEMA₁₀-*b*-EGDMA₁ in water, as observed using (a)

AFM (phase mode), (b) SANS, and (c) polarized light microscopy, with image dimensions $625 \mu\text{m} \times 625 \mu\text{m}$.

Figure 3.17. Schematic representations of the “core-first” star block copolymer building blocks, precursors to the six conetworks. E, M and D are further abbreviations for EGDMA, MMA and DMAEMA, respectively. The hydrophobic MMA units are shown in red, the hydrophilic DMAEMA units are presented in light blue, the first EGDMA cores are displayed in grey, and the second EGDMA cores are painted black.

Figure 3.18. MALDI-TOF spectra of the EGDMA oligomeric cores of the star block copolymer precursors to the six amphiphilic polymer conetworks, each exhibiting various peaks corresponding to conjugates between the EGDMA crosslinker and the MTS initiator.

Figure 3.19 GPC traces for all soluble precursors to the six amphiphilic polymer conetworks, and the extractables from the conetworks. The traces of the EGDMA core oligomers are shown in black dashed lines, those of the MMA star homopolymers are presented in red dashed-dotted lines, those of the MMA-DMAEMA star block copolymers are displayed in blue dashed-double dotted lines, and those of the extractables are exhibited in green dotted lines.

Figure 3.20. pH-Dependence of the swelling and ionization degrees for all amphiphilic polymer conetworks equilibrated in aqueous media. In the figure labels, E, M and D are further abbreviations for EGDMA, MMA and DMAEMA, respectively.

Figure 3.21. Degrees of swelling of all the amphiphilic polymer conetworks in pure water, in acidic water, and in tetrahydrofuran (THF). (a) Effect of the composition of the arm of the star block copolymer. (b) Effect of the degree of polymerization of the arm of the star block copolymer. In the x -axis labels, M and D represent further abbreviations for MMA and DMAEMA, respectively.

Figure 3.22. Small-angle neutron scattering (SANS) profiles for all the amphiphilic polymer conetworks in D_2O in the pure state (obtained by dividing by the factor A that takes into account incomplete filling of the cells). The curves fitted with eqs. 1 and 2 are given as solid lines. (a) Effect of the composition of the arm of the star

block copolymer. (b) Effect of the degree of polymerization of the arm of the star block copolymer.

Figure 3.23. Small-angle neutron scattering (SANS) profile for sample #1 (EGDMA₁-*b*-MMA₅-*b*-DMAEMA₁₅-*b*-EGDMA₁ in D₂O) showing the scattering of subdomains with a size of ~ 0.8 nm at high q and a schematic representation of the corresponding structures (right).

Figure 3.24. Polarized light microscopy images for all the amphiphilic polymer conetworks, in the dried state and in water-swollen states.

Figure 3.25. Chemical reaction leading to the formation of the 2,2-di(methacryloyloxy-1-ethoxy)propane (DMOEP) crosslinker accompanied by the formation of the mono-substituted side-product 2-[(2-methoxypropan-2-yl)oxy]ethyl methacrylate (m-HEMA).

Figure 3.26. (a) ¹H and (b) ¹³C NMR spectra of the 2,2-di(methacryloyloxy-1-ethoxy)propane (DMOEP) crosslinker in *d*₆-DMSO.

Figure 3.27. (a) ¹H and (b) ¹³C NMR spectra of 2-[(2-methoxypropan-2-yl)oxy]ethyl methacrylate (m-HEMA) in *d*₆-DMSO.

Figure 3.28 Synthesis and hydrolysis of networks based on end-linked “core-first” star MMA homopolymers using the four possible combinations of degradable and non-degradable crosslinkers.

Figure 3.29. GPC traces of all the precursors to all MMA homopolymer networks synthesized, the extractables from the networks, and the hydrolysis products of the networks. The traces of the cores appear in red dotted curves, those of the star homopolymers in blue dashed lines, those of the hydrolysis products in green dashed-dotted lines, and those of the extractables in black continuous lines.

Figure 3.30. GPC traces of the GMA₂₀-*star* and GMA₁₀₀-*star* homopolymers together with those of their linear precursors.

Figure 3.31. Synthetic routes followed for the preparation of the oligoamine-grafted GMA₁₀₀-*star* and GMA₁₀₀-*linear* homopolymers through RAFT polymerization and subsequent oligoamine grafting onto the ethylene oxide ring.

Figure 3.32. ¹H NMR spectrum of the GMA₁₀₀-*star* homopolymer in CDCl₃, overlaid with those of the oligoamine-grafted GMAs: (GMA₁₀₀-EDA)-*star*, (GMA₁₀₀-

DETrA)-*star*, (GMA₁₀₀-TrETA)-*star*, (GMA₁₀₀-TEPA)-*star* and (GMA₁₀₀-PEHA)-*star* in D₂O.

Figure 3.33. Dependence of Luc expression and cell viability on the amount of polymer at a constant amount of plasmid DNA for the (GMA₂₀-amine)-*star* homopolymers.

Figure 3.34. Dependence of Luc expression and cell viability on the amount of polymer at a constant amount of plasmid DNA for the (GMA₁₀₀-amine)-*star* homopolymers.

Figure 3.35. Dependence of Luc expression and cell viability on the amount of polymer at a constant amount of plasmid DNA for the (GMA₁₀₀-amine)-*linear* homopolymers.

Figure 3.36. Chemical reaction leading to the formation of the monomer 9-anthrylmethyl methacrylate (AnMMA) via the esterification of 9-anthracenemethanol with methacryloyl chloride.

Figure 3.37. (a) ¹H and (b) ¹³C NMR spectra of the purified AnMMA monomer in CDCl₃.

Figure 3.38. Synthesis of the diblock copolymers and terpolymers by RAFT polymerization.

Figure 3.39. Fabrication of metal-bearing nanoparticles in selective and non-selective organic solvents.

Figure 3.40. Photographs of one linear diblock copolymer and one linear diblock terpolymer complexed with three different metals (Au, Ni, Pd) in four different solvents. The photographs were taken after 24 h and 72 h from the complexations. A: Benzene, B: CHCl₃, C: Cyclohexane, D: n-Hexane.

Figure 3.41. AFM images (4 μm x 4 μm) of the hybrid metal-organic nanoparticles cast from solutions in four different organic solvents.

Figure 3.42. Synthetic route followed for the preparation of the AcEMA-LauMA-AcEMA triblock copolymers by the two-step sequential RAFT polymerization using a bifunctional CTA in 1,4-dioxane at 65 °C.

Figure 3.43. Schematic representation of the procedure followed for the formation of the metal-end-linked ABA triblock copolymer conetworks, and photographs of the final products.

Figure 3.44. Dependence of the degrees of swelling in *n*-hexane on the degree of polymerization of the LauMA mid-block of the Au- and Pd-end-linked-conetworks.

Figure 3.45. *p*-XRD profiles of the (a) Pd- and (b) Au-end-linked AcEMA-LauMA-AcEMA copolymer conetworks.

Figure 3.46. TEM images of four polymer conetworks, two based on Au- and two based Pd- end-linked ABA triblock copolymers.

Figure 3.47. Atomic force microscopy phase images of the four conetworks with Au in benzene with the theoretical size of their nanoparticles and the average sized calculated from the AFM images.

Figure 3.48. Comparison of the results of Luc expression (left) for the two transfections (red results after Au complexation and blue before complexation) and cytotoxicity (right).

List of Tables

Table 2.1. Indicative values of dn/dC for each polymerization step used in SLS.

Table 3.1. Molecular weight (relative) and composition characteristics of the soluble precursors to the (co)networks based on end-linked “core-first” star (co)polymers.

Table 3.2. Characteristics of the extractables from the amphiphilic polymer conetworks of this study, including their sol fraction, composition and molecular weight.

Table 3.3. Locations of peak maxima in the SANS profiles of all the (co)networks in D_2O , both before and after thermal annealing, and corresponding correlation distances.

Table 3.4. Molecular weights and identification of the species with general formula $MTS_x\text{-EGDMA}_y$, present in the MALDI-TOF mass spectrum of core 2 (Figure 3.18), corresponding to the star block copolymer precursor to the amphiphilic polymer conetwork with chemical structure $EGDMA_1\text{-}b\text{-}MMA_{22.5}\text{-}b\text{-}DMAEMA_{7.5}\text{-}b\text{-}EGDMA_1$.

Table 3.5. Compositions, molecular weights, and molecular weight dispersities of the soluble precursors to the amphiphilic polymer conetworks. The calculated number of arms of the star polymers is also listed.

Table 3.6. Characteristics of the extractables from the amphiphilic polymer conetworks of this study, including their sol fraction, composition and molecular weights.

Table 3.7. Position of the intensity maximum, q_{max} , distance between the scattering centers, d , hydrophobic volume fraction, Φ , radius of hydrophobic core, R , and star aggregation number (both obtained from the peak position q_{max}) within the unit cell for the amphiphilic polymer conetworks of this study in D_2O , as obtained using small-angle neutron scattering.

Table 3.8. Parameters obtained from fitting the SANS data with eqs. 1-2: hard sphere volume fraction Φ_{HS} , radius R_{sph} , hard sphere radius R_{HS} , fraction of the MMA contained in the hydrophobic domains, B , and fractal exponent n .

Table 3.9. Relative number-average molecular weights, M_n , and absolute weight-average molecular weights, M_w , and DMOEP content in the precursors to the polymer networks. The calculated numbers of arms of the star polymers are also listed.

Table 3.10. Percentage, and molecular weight and composition characteristics of the extractables from the networks.

Table 3.11. Degrees of swelling of the networks in THF.

Table 3.12. Size and composition characteristics of the polymer network hydrolysis products.

Table 3.13 Theoretical structures, monomer and crosslinker conversions, molecular weights, molecular weight dispersities, arm DPs and number of arms of the GMA star homopolymers.

Table 3.14. Molecular weights and compositions of the linear diblock copolymers and terpolymers determined using GPC and ^1H NMR, respectively.

Table 3.15. Radii of the major micelle populations and their mean values obtained from the AFM images in Figure 3.41.

Table 3.16. Absolute molecular weights and size characteristics of the nanoparticles formed by the AcEMA₂₀-*b*-(LauMA₇₂-*co*-AnMMA₈) terpolymer and its complexes with three metals in four solvents.

Table 3.17. Chemical structures, molecular weights and compositions of the prepared metal-chelating AcEMA-LauMA-AcEMA triblock copolymers.

Table 3.18. Degrees of swelling in *n*-hexane of the gold- and palladium-end-linked AcEMA-LauMA-AcEMA triblock copolymer conetworks.

Table 3.19. Sizes of the Au and Pd metal crystallites in the dried Au- and Pd-end-linked AcEMA-LauMA-AcEMA triblock copolymer conetworks.

Table 3.20. Chemical structures, molecular weights, monomer conversion and compositions of the prepared AcEMA₅₀-*b*-DMAEMA₂₀₀-linear copolymer.

Abbreviations

AcEMA	2-Acetoacetoxy Ethyl Methacrylate
AFM	Atomic Force Microscopy
AIBN	2,2'-Azobis(isobutylnitrile)
AnMMA	9-Anthrylmethyl Methacrylate
APCN	Amphiphilic Polymer Conetwork
APN	Amphiphilic Polymer Network
ATRP	Atom Transfer Radical Polymerization
<i>B</i>	Mass fraction
1,4-BTBTBPB	1,4-Bis[2-(thiobenzoylthiol)prop-2-yl]benzene
CDCl ₃	Deuterated Chloroform
CHCl ₃	Chloroform
¹³ C NMR	Carbon Nuclear Magnetic Resonance
2-CPDB	2-Cyanoprop-2-yl dithiobenzoate
CTA	Group Transfer Agent
<i>d</i>	Distance between the scattering centers
DCM	Dichloromethane
DETrA	Diethylene Triamine
DLS	Dynamic Light Scattering
DMAc	Dimethyl Acetamide
DMAEMA	2-(Dimethylamino)ethyl Methacrylate
DMOEP	2,2-Dimethacryloyloxy-1-ethoxy Propene
DNA	Deoxyribonucleic acid
DP	Degree of Polymerization
DPPH	2,2-Diphenyl-1-picrylhydrazyl hydrate
DS	Degree of Swelling
EDA	Ethylene Diamine
EGDMA	Ethylene Glycol Dimethacrylate

Et ₃ N	Triethylamine
Gly	Glycidyl Methacrylate
GMA	Glycidyl Methacrylate
GPC	Gel Permeation Chromatography
GTP	Group Transfer Polymerization
HEMA	2-Hydroxyethyl Methacrylate
¹ H NMR	Proton Nuclear Magnetic Resonance
HR-TEM	High-resolution Transmission Electron Microscopy
LauMMA	Lauryl Methacrylate
MaCl	Methacryloyl chloride
MMA	Methyl Methacrylate
M _n	Number-average molecular weight
MNP	Metal Nanoparticle
MOP	2-Methoxypropene
M _p	Peak molecular weight
MS	Mass Spectrometry
MTS	1-Methoxy-1-Trimethylsiloxy-2-Methyl Propene
M _w	Weight-average molecular weight
MW	Molecular weight
<i>n</i>	Fractal exponent
N _{agg}	Aggregation number
PAsp	Poly(Aspartic acid)
PBLA	Poly(β-Benzyl-L-Aspartate)
PEHA	Pentaethylene Hexamine
PGlu	Poly(Glutamic acid)
PMMA	Poly(Methyl Methacrylate)
pTSA	<i>p</i> -Toluenesulfonic Acid
<i>p</i> -XRD	Powder X-Ray Diffraction
q _{max}	Valume of q at intensity maximum

R	Radius of hydrophobic core
RAFT	Reversible Addition-Fragmentation chain Transfer polymerization
R_{HS}	Hard sphere radius
RNA	Ribonucleic acid
R_{sph}	Radius
SANS	Small-Angle Neutron Scattering
SLS	Static Light Scattering
TBABB	Tetrabutylammonium Bibenzoate
TEPA	Tetraethylene Pentamine
THF	Tetrahydrofuran
TrETA	Triethylene Tetramine
Φ	Hydrophobic volume fraction
Φ_{HS}	Hard sphere volume

CHAPTER 1: INTRODUCTION

1.1. Objective and Innovation.

Synthetic polymers can form complexes with a plethora of compounds of various sizes. These complexes attract the interest of the science and technology communities.¹ This complexation proceeds via different mechanisms, from non-selective adsorption (dispersion forces, 2– 4 kJ mol⁻¹),² up to electrostatic complexation (ionic bonds, 250 kJ mol⁻¹),² and coordination bonds (~100 kJ mol⁻¹).² The present work deals with three complex systems of synthetic polymers: one with metals³ through coordination bonds, the second with genetic material⁴ through ionic interactions and also polymer networks consisting of covalently interconnected monomers crosslinked with covalent bonds either degradable or non-degradable. At the end, a complex copolymer system was developed contacting both metal and genetic material.

Regarding the first system, metals have important electrical, magnetic, optical and catalytic properties,^{5,6} leading to their use in variety of applications.⁷ Here, metals are initially introduced as cations which are subsequently reduced to the metallic form possessing the above properties. Because complexation with the cation (metal ion) usually results in the formation of an insoluble compound, the presence of a soluble fragment in the polymer is required to stabilize the complex. This is achieved by using block copolymers bearing one segment for complexation and one for stabilization.⁸⁻¹⁰

Concerning the second system, electrostatic complexation of positively charged polymers with negatively charged genetic material, DNA or RNA, is of great importance in genetic therapy as well as a diagnostic tool.¹¹⁻¹² Due to the low concentrations herein, the complexes remain soluble in water, and, usually, no stabilizing portion of the polymer is required. In this embodiment, the positively charged polymer enters in excess, so that the complex has an overall positive charge, which will help its entry into the cell through the negatively charged cell membrane. In addition, in the case of DNA, electrostatic complexation also results in the necessary shrinkage of this huge biomolecule to facilitate its endocytosis.

Amphiphilic polymer conetworks (APCN) self-assemble in water, phase separating at the nanoscale, and yielding hydrophilic and hydrophobic domains of nanoscopic

dimensions, as well as a huge interfacial area between the nanophases. These attributes endow APCNs with a great utility in a variety of applications, including uses as the material for soft extended-wear contact lenses,¹³ matrices for drug delivery¹⁴ and tissue engineering,¹⁵ and porous scaffolds for phase transfer (bio-)catalysis.¹⁶ In the past 20 years, we developed many quasi-model (“almost ideal”) polymer network families, based on end-linked linear chains or star copolymers with important development as the introduction of degradability, either through a degradable crosslinker¹⁷⁻²⁴ or through a degradable bifunctional initiator,²⁵⁻³⁰ with the latter being more demanding than the former, arising from the difficulties associated with the synthesis, purification and the stability of degradable bifunctional initiators.

In this work, the following research objectives were set, all of which include the synthesis of well-defined polymers of different architectures using controlled polymerizations:

- a) Synthesis of two different families of APCNs based on end-linked “core-first” star block copolymers aiming at structure formation with long-range order.³¹⁻³²
- b) Synthesis of networks based on “core-first” star polymers end-linked using a degradable ketal crosslinker.³³
- c) Synthesis of oligoamine-grafted glycidyl methacrylate linear and star homopolymers, to check for any odd-even correlated transfection efficiency on gene delivery.
- d) Synthesis of metal-bearing nanoparticles from the chelation-driven self-assembly of diblock co- and ter-polymers.
- e) Synthesis of metal-end-linked polymer conetworks from the chelation-driven self-assembly of ABA triblock copolymers.
- f) Synthesis with a combination of the two complexing motifs, with the preparation of crosslinked copolymers with one segment complexing with genetic material and the other with metal, with the ultimate aim of transferring genetic material.

1.2. Literature review.

1.2.1. Polymer Networks.³⁴⁻³⁶

Polymer networks are polymeric systems, in which the polymer chains are interconnected with crosslinkers. These materials have the property of being insoluble in every solvent, but they have the ability to absorb a quantity of solvent resulting in swelling. Polymer networks may consist of a single kind of monomer and are called homopolymer networks or two or more kinds of monomers and are called copolymer networks. These networks can be further classified into hydrophilic, hydrophobic and amphiphilic, depending on the nature of the monomer repeating. Hydrophilic networks contain at least one type of hydrophilic monomer and are compatible with polar solvents, while the hydrophobic networks contain at least one type of hydrophobic monomer and are compatible with non-polar solvents. Amphiphilic (co)networks contain both, hydrophilic and hydrophobic monomer units, sometimes each type located in separate blocks, and they therefore, can absorb both polar and non-polar solvents. An interesting property of polymer networks is volume phase transition,³⁷ *i.e.* the ability to change their volume in response to external stimuli in their environment, such as temperature,³⁸ pH,³⁹ electric field,⁴⁰ and irradiation.⁴¹ Depending on the type of crosslinking between the polymer chains, the networks can be classified into irreversibly crosslinked polymer networks and into reversibly crosslinked polymer networks. The irreversibly crosslinked networks are inters with permanent irreversible bonds, whereas, the reversibly crosslinked networks are interconnected with physical non-covalent bond or inconnected dynamic covalent bonds.

1.2.1.1. Amphiphilic Polymer Conetworks (APCNs).

Amphiphilic polymer conetworks are those networks that are composed of both hydrophobic and hydrophilic monomer repeating units.⁴² When the hydrophobic monomer repeating units are located in hydrophobic segments (blocks) consisting of three or more units, this gives sufficient driving force for self-organization to occur in the presence of water (selective solvent for the hydrophilic phase) and the formation of different morphologies.⁴³ In these morphologies, there are two microphases, the hydrophilic and the hydrophobic. The hydrophilic phase is swollen

with water, while the hydrophobic one is shrunk and without solvent (water) and consists only of aggregated hydrophobic segments. Thus, the degree of swelling in water of APCNs is lower than that of a pure hydrophilic network. The reduced swelling degree and the formation of hydrophobic aggregates increase the mechanical strength of the APCNs. Regarding the latter, the hydrophobic aggregates function as energy dissipation centers during deformation.⁴⁴ The presence of crosslinker in the APCNs reduces the flexibility and mobility of polymer chains, thereby impeding, to some extent, their facile self-organization in a selective solvent and yielding morphologies less perfect than in the absence of crosslinks.

1.2.1.2. Degradable Quasi-model Polymer Networks.

Patrickios and coworkers⁴⁵⁻⁵⁰ studied, for many years, quasi-model polymer network systems, including polyampholytic ones,⁴⁵⁻⁴⁶ comprising positively and negatively ionizable polymer segments,⁴⁷⁻⁴⁸ and double-hydrophilic ones, comprising both hydrophilic polymer segments, of which one was ionizable and the other nonionic.⁴⁹⁻⁵⁰ Another important development within quasi-model polymer networks was the introduction of degradability, either through a degradable crosslinker¹⁷⁻²⁴ or through a degradable bifunctional initiator,²⁵⁻³⁰ with the latter being more demanding than the former, arising from the difficulties associated with the synthesis, purification and the stability of degradable bifunctional initiators.

1.2.2. *Oligoamine-grafted Glycidyl Methacrylate Polymers.*

Studies in past decades indicated that a combination of a high transfection efficiency with a low cytotoxicity can be achieved if a high MW uncharged polymer, grafted with a low MW ionizable poly(ethylene imines) is employed. Studies on such polymers showed that transfection efficiency and cytotoxicity, in most cases, were connected with the type and number of amine-repeating units in each graft, and, the presence of other functional groups in these grafts.⁵¹⁻⁵⁷ To this end, Dou et al.⁵¹ synthesized a series of linear and star shaped poly(β -benzyl-*L*-aspartate)s (PBLA) *via* ring opening polymerization initiated by ethylene diamine an (EDA) or EDA-functionalized cyclodextrin core followed by aminolysis with cationic poly[(2-dimethylamino)ethyl methacrylate) with one terminal primary amino group

(PDMAEMA-NH₂). Evaluation of these systems for DNA delivery indicated that star-shaped polymers exhibited better transfection efficiency. Itaka et al.⁵²⁻⁵⁴ carried out a comparative study of poly(aspartic acid) (PAsp) and poly(glutamic acid) (PGlu) grafted with diethylene triamine, P[Asp(DET)] and P[Glu(DET)], respectively. In contrast to P[Glu(DET)], P[Asp(DET)] was shown to possess self-degrading ability. The latter led the lack of both cytotoxicity *in vitro* and pro-inflammatory action *in vivo* together with high transfection efficiency. Chen and coworkers⁵⁵ presented the synthesis of multi-armed polyaspartate-*graft*-OEI (PA-*g*-OEI) copolymers by grafting OEI with MW of 423, 600 and 1800 g mol⁻¹. All polymers were found to exhibit good capacity in condensing nucleic acids (pDNA or siRNA) into nanosized particles, while PA-*g*-OEI with OEI of MW of 1800 g mol⁻¹ was also found to have improved transfection efficiency and lower cytotoxicity compared to PEI25k. Moreover, Wagner and coworkers⁵⁶ studied the synthesis of comb-like structures consisting of an oligolysine peptide backbone modified at the ϵ -amino groups with four different artificial oligo(amino acid)s, succinyl-diethylene triamine (Sdt), succinyl-triethylene tetramine (Stt), succinyl-tetraethylene pentamine (Stp) and succinyl-pentaethylene hexamine (Sph) and showed that the best performing oligomers were those containing the Stp or Sph building blocks. More recently, Salakhieva et al.⁵⁷ studied a series of cationic polyaspartamides with different (dialkylamino)alkyl and alkyl or hydroxyalkyl groups. Polyaspartamides bearing both cationic (dialkylamino)propyl and additional alkyl or hydroxyalkyl side groups were found to present enhanced DNA-condensing and transfection properties.

In the spirit of the above studies, Kataoka and coworkers⁵²⁻⁵⁴ performed a systematic investigation on the effect of the number of aminoethylene repeating units in the side chains of PBLA-derived *N*-substituted polyaspartamides on DNA and mRNA transfection efficiency. These researchers observed that polyaspartamides grafted with oligomers bearing an even number of ethylene imine units displayed a higher DNA transfection efficiency, without marked cytotoxicity, compared with those grafted with oligomers bearing an odd number of ethylene imine units.

1.2.3. Metal-organic Coordination Polymers and Networks.

Metal-organic coordination polymers⁵⁸⁻⁶¹ are nanoporous crystalline materials constructed by metal ions and rigid organic linkers equipped with two or more ligation sites to form supramolecular polymer networks in the crystalline state. Recent extensive studies have been focused on new molecular designs of the supramolecular polymer networks and their applications such as catalysis, energy storage, separation, and nanomaterials.⁶²⁻⁶⁵

There are several studies on well-defined supramolecular polymer networks⁶⁶ *via* metal–ligand coordination. Rowan et al.⁶⁷⁻⁶⁹ demonstrated the preparation of supramolecular polymer networks *via* metal–ligand coordination, where mechano-, chemo-, and thermo-responsivenesses were investigated. Krasia et el.⁷⁰⁻⁷² presented similar materials and the study of their mechanical and magnetic properties.

Although metal–ligand coordination has a high potential for applications of supramolecular polymer networks,⁷³⁻⁷⁶ because of the number of the reports on physical properties of supramolecular materials *via* metal–ligand coordination. This was initially hampered by the difficulty in preparing such materials with sufficient homogeneity, a problem that has relatively recently been solved.⁷⁷⁻⁷⁹

1.3. Theoretical Background.

1.3.1. Degradable Ketal Crosslinker and Hydrolysis.

Degradable crosslinkers are crosslinkers which they have at least one covalent bond that can be broken, due to the application of heating,⁸⁰⁻⁸² chemicals⁸³⁻⁸⁶ or enzymes,⁸⁷⁻⁸⁹ resulting in the cleavage of the branching points due to the crosslinker. The irreversible cleavage of the covalent bond of the crosslinker is expected to form fragments which cannot recombine or react with another part of the polymer, and form another covalent crosslink. After the breaking of crosslinker, at least two of the pieces which were produced, remain embedded in the polymer to which they belong. The crosslinkers are typically polymerized by free radical polymerization. Recently, however, such crosslinkers were polymerized *via* controlled polymerization, such as group transfer polymerization (GTP), reversible addition-fragmentation chain transfer (RAFT) polymerization and atom transfer radical polymerization (ATRP). The main applications of polymers containing degradable crosslinkers is the delivery of drugs⁹⁰⁻

⁹¹ and the manufacture of electronic boards through positive lithography.⁹² There are degradable crosslinkers with ketal, acetal, ester *etc.* in their structures. In this work, a degradable crosslinker with a ketal unit in its structure was used, because ketals degrade very easily.

A ketal⁹³⁻⁹⁶ has two alkyl groups as substituents which are cleaved quite easily in slightly acidic conditions but they are stable under basic and neutral conditions. The rate of hydrolysis of such groups depends on the type of alkyl groups bound to the carbon. The effect of substituents on the rate of hydrolysis increases as the capacity of electron increases. Specifically, the more powerful electron donors speed up the hydrolysis, because of the stabilization of carbocation obtained after cleavage of the leaving group. Then, water is introduced, which is the nucleophile, which leads to degradation and formation of alcohol and a ketone. These materials can be used, as biodegradable orthopaedic implants,⁹³ in imprint lithography,⁹⁴ in drug delivery⁹⁵ and as matrices for protein delivery.⁹⁶

1.3.2. *Odd-even Effect.*

The effect of the number⁵³⁻⁵⁴ of aminoethylene repeating units in the side chains of polymer on DNA and mRNA transfection efficiency is important. Polymer grafted with oligomers bearing an even number of nitrogen units were shown to attain a higher DNA transfection efficiency, without marked cytotoxicity, compared with those grafted with oligomers bearing an odd number of nitrogen units.

1.3.3. *Discovery and General Characteristics of plasmid-DNA.*

1.3.3.1. *Plasmid-DNA.*

Joshua Lederberg introduced the term *plasmid*, in 1952, to refer to “any extrachromosomal hereditary determinant.”⁹⁷ The term's early usage included any bacterial genetic material that exists extrachromosomally for at least part of its replication cycle, but because that description includes bacterial viruses, the notion of *plasmid* was refined over time to comprise genetic elements that reproduce autonomously, Figure 1.1⁹⁸ In 1968, it was decided that the term *plasmid* should be adopted as the term for extrachromosomal genetic element.⁹⁹

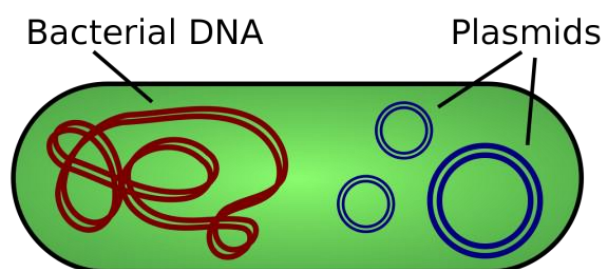


Figure 1.1. Illustration of a bacterium containing both chromosomal DNA and plasmids.

Thus, a *plasmid* is a small, extrachromosomal DNA molecule within a cell that is physically separated from chromosomal DNA and can replicate independently. While chromosomes are large and contain all the essential genetic information for living under normal conditions, plasmids are usually very small and contain only additional genes that may be useful in certain situations or conditions. Artificial *plasmids* are widely used as vectors in molecular cloning, serving to drive the replication of recombinant DNA sequences within host organisms. In the laboratory, *plasmids* may be introduced into a cell *via* transformation.

1.3.3.2. Application of *plasmid*-DNA.

Plasmids are considered replicons, units of DNA capable of replicating autonomously within a suitable host. However, plasmids, like viruses, are not generally classified as life.¹⁰⁰ Plasmids are transmitted from one bacterium to another, even of different species, mostly through conjugation.¹⁰¹ This host-to-host transfer of genetic material is one mechanism of horizontal gene transfer, and *plasmids* are considered part of the mobilome. Unlike viruses, which encase their genetic material in a protective protein coat called a capsid, *plasmids* are "naked" DNA and do not encode genes necessary to encase the genetic material for transfer to a new host. However, some classes of *plasmids* encode the conjugative "sex" pilus necessary for their own transfer. The size of the *plasmid* varies from 1 to over 200 kbp,¹⁰² and the number of identical *plasmids* in a single cell can range anywhere from one to thousands under some circumstances.

1.3.3.3. Transfection of DNA (*plasmid*-DNA).

Transfection is the process of transferring foreign molecules to cells either for study purposes (gene function and protein expression) or for therapeutic purposes (gene therapy) or diagnostics. Such molecules can be genetic material (such as DNA, RNA, plasmid DNA, and siRNA) but also proteins (such as antibodies).

Transfection of *plasmid*-DNA¹⁰³ (and generally with genetic material) in cells can be accomplished by direct transfer of "naked" *plasmid*-DNA, by complexation *via* electrostatic interactions but also by chemical binding of *plasmid*-DNA to various systems such as cationic polymers, lipids, liposomes, cations proteins and aptamers. Also, *plasmid*-DNA transfection can be performed using viruses such as retroviruses, adenoviruses, and adenovirus-associated viruses.

The "gene gun" method (mainly for DNA) may also be applied in which gold nanoparticles (Au) are used for the transfer of genetic material. At the same time, the transfection can be carried out hydrodynamically and by electroporation. During electroporation in the cells, an electric field is applied, thus creating holes in the cell membranes from which the genetic material enters.

1.3.4. Metal Nanoparticles (MNPs).

The unique size dependent properties and the high surface to volume ratios of metal nanoparticles (MNPs) are some of the reasons which have led to an increased interest in these materials for general scientific fields. Consequently, MNPs are among the most promising candidates for several applications in photonics, optoelectronics, catalysis etc.¹⁰⁴ The ability of amphiphilic block copolymers to create various organized nanomorphologies in solution due to microphase separation, makes them ideal templates for the localization of metals on the nanoscale.¹⁰⁵⁻¹⁰⁶

β -Ketoester moieties in polymers can act as strong bi-dentate ligands for different metal ions such as Co(II), Fe(II) and Cu(II), yielding sterically stabilized colloidal hybrid nanomaterials.¹⁰⁷

1.3.5. Polymerization Methods.

1.3.5.1. Group Transfer Polymerization (GTP).¹⁰⁸⁻¹¹²

Group transfer polymerization (GTP) was developed by Owen W. Webster and coworkers in Dupont laboratories in the USA in the early 1980s. The development of GTP constituted a crucial step for the progress of anionic polymerizations.

GTP, in principle, retains the important advantage of anionic polymerization in that the polymer ends remain active even after full monomer consumption, thereby enabling further polymerization. It is a basic method of controlled polymerization of methacrylic monomers which is carried out even at room temperature and requires silicone ketene acetals or other silicon compounds as initiators and nucleophilic reagents as catalysts (such as fluoride, difluoride, cyanide, azide, Lewis acids). It gives "living" polymers with a narrow MW distribution, where the degree of polymerization is controlled by the molar ratio of monomer to initiator.

GTP has the following important advantages:

1. Quantitative yield of polymerization,
2. Narrow molecular weight distribution,
3. Ability to prepare polymers with various architectures, such as block copolymers, star polymers, branched polymers and polymer networks.
4. Relatively high polymerization reaction rate and
5. Conduction of polymerization at room temperature.

Disadvantages of GTP are:

1. The relatively small size of polymers that can be prepared, with an upper limit of MW for linear polymers of about 50000 g mol^{-1} corresponding to $DP \leq 500$;
2. Application only to specific types of monomers: methacrylates and acrylates,
3. Its high sensitivity to moisture and acidic impurities (which deactivate its active centers).

For many years, the mechanism of GTP was a subject of controversy among scientists until the dissociative mechanism, shown in Figure 1.2, was adopted. Initially, the

nucleophilic catalyst is complexed with the silicone ketene acetal and, through a cleavage step, the active enol anion is formed which is subsequently added to the monomers. The enol anion is then joined to the Me_3SiNu group and thus the terminal silicate ketene acetal is reformed.

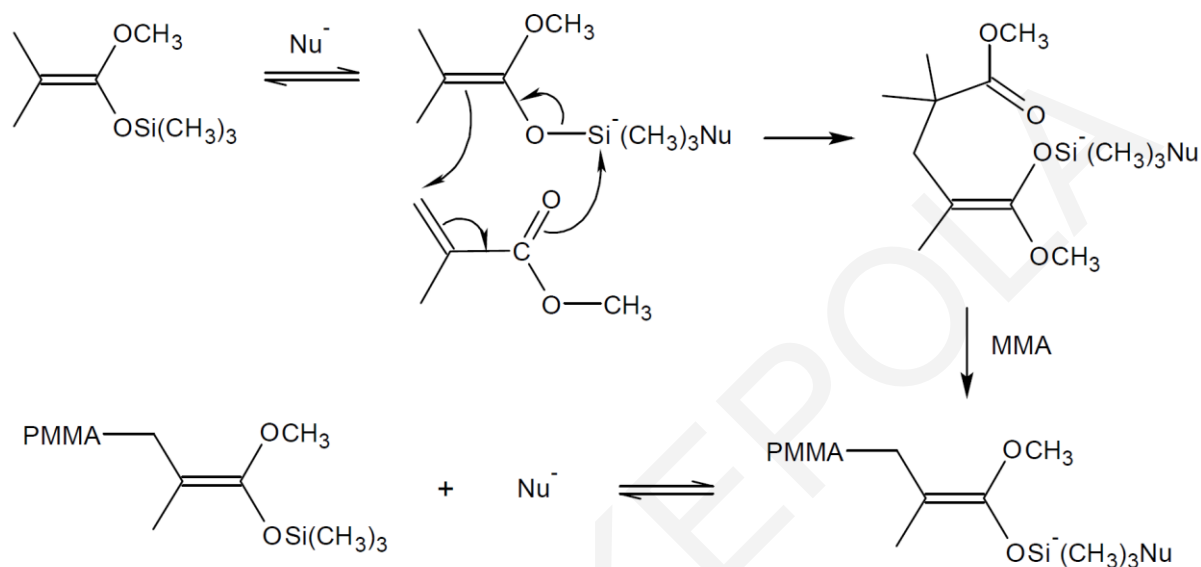


Figure 1.2. Group transfer polymerization (GTP) mechanism.

1.3.5.2. Reversible Addition-fragmentation Chain-transfer Polymerization (RAFT).¹¹³

RAFT polymerization was developed by Moad and colleagues in Australia in 1998 and belongs to controlled radical polymerizations. It is a polymerization method which can polymerize a wide range of monomers, including monomers with functional groups such as $-\text{OH}$, $-\text{COOH}$, $-\text{CONR}_2$, $-\text{NR}_2$ and $-\text{SO}_3\text{Na}$ without the need for the protection and deprotection of these groups, while a wide variety of architectures including block copolymers, star polymers, and other complex architectures can be obtained.

RAFT polymerization requires the presence of dithioester or trithiocarbonate compounds which act very effectively as group transfer agents (CTAs) with reversible addition-detachment. The best known CTAs are thiocarbonylthio compounds of the

form Z-C(=S)-S-R (Figure 1.3) in which the group Z determines the rates of addition and removal.

In order for CTAs to be effective, the following conditions must be met:

1. The rates of addition and fragmentation (removal) should be similar to the rate of polymerization propagation, in order to ensure the fast consumption of the original CTA and the rapid equilibrium between active and inactive compounds. To favor radical addition, the Z group must activate the C = S bond.
2. In order to ensure the progress of polymerization to the desired extent, the leaving group R must be a good leaving group as a radical and be capable of reactivating polymerization ($R = \text{CH}_2\text{Ph}$, $\text{C}(\text{CH}_3)_2\text{Ph}$, $\text{C}(\text{CH}_3)_2\text{CN}$). If this is not the case, there is an increased risk of delaying the mechanism and the occurrence of adverse reactions *via* radicals, such as, for example, premature termination.

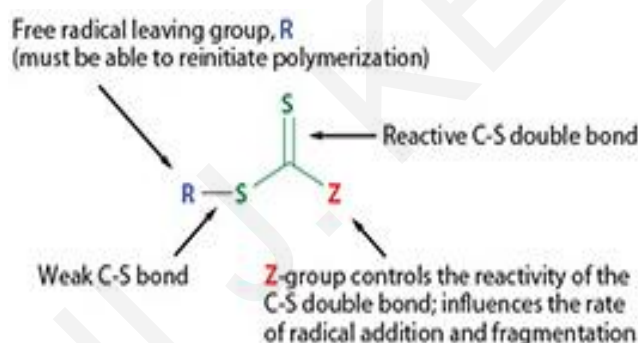


Figure 1.3. Chemical structure of a dithioester chain transfer agent for RAFT polymerization.

The mechanism of RAFT polymerization is illustrated in Figure 1.4. The figure shows that the polymerization initiation and termination occur as in conventional free radical polymerization. The first stage of polymerization involves the cleavage of the primer to radicals. These radicals (P_n^\bullet) initiate polymerization by reacting with the monomer. In the second step, the dissociation radical (P_n^\bullet) is added to the thiocarbonyl this (1), followed by cleavage of the intermediate radical which results in the formation of a polymeric-dithioester (3) and a new radical (R^\bullet). The reaction of the new radical (R^\bullet) with a monomer molecule creates a new propagation radical (P_m^\bullet). The rapid

equilibrium between the active propagation radicals (P_n^\bullet and P_m^\bullet) and the inert thiocarbonylthio polymer (3) results in an equal chance for all chains to grow and produce low polydispersity polymers. The core of the RAFT path is the principal equilibrium that occurs in the chain equilibrium / propagation reaction with the k_{addP} and $k_{-\text{addP}}$ kinetic constants controlling the equilibrium position. In the addition step, the k_{addP} kinetic constant controls the intermolecular reaction between the free polymeric radicals and the RAFT polymeric reagent which leads to the formation of macro-RAFT radical (4), while the $k_{-\text{addP}}$ kinetic constant can be interpreted as the inverse of the lifetime of the intermediate macro-RAFT radical (4). In the last step, intermolecular termination of the free radical polymerization results in the formation of inactive polymers. When polymerization is complete, most chains retain the thiocarbonylthio terminal group and can be isolated as stable materials.

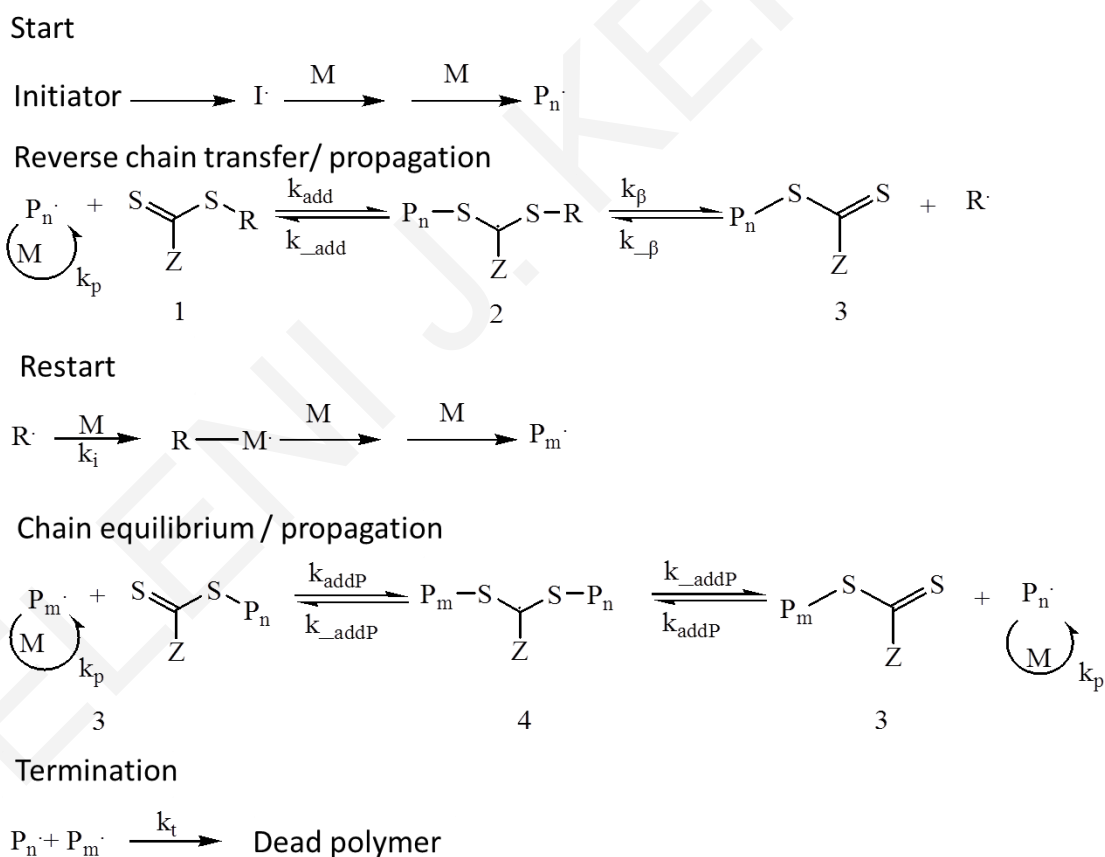


Figure 1.4. RAFT polymerization steps

1.3.6. Methods for Polymer and Networks Characterization.

1.3.6.1. Gel Permeation Chromatography (GPC-HPLC).¹¹⁴

Gel permeation chromatography was first developed in 1955 by Lathe and Ruthven.¹⁵⁵ The term gel permeation chromatography can be traced back to J.C. Moore in 1964.¹⁵⁶ Gel permeation chromatography is a type of size exclusion chromatography (SEC) that separates analyses on the basis of size, typically in organic solvents. The technique is often used for the analysis of polymers. GPC system is necessary to separate polymers, both to analyze them as well as to purify the desired product. When characterizing polymers, it is important to consider the dispersity (D) as well the molecular weight. Polymers can be characterized by a variety of definitions for molecular weight including the number average molecular weight (M_n), the weight average molecular weight (M_w) and the size average molecular weight (M_p).

1.3.6.2. Nuclear Magnetic Resonance Spectroscopy (^1H , ^{13}C -NMR).¹¹⁵

Nuclear magnetic resonance spectroscopy was discovered by Isidor Isaac Rabi, who received the Nobel Prize in Physic in 1944. NMR is a spectroscopic technique to observe local magnetic fields around atomic nuclei. As the fields are unique or highly characteristic to individual compounds, in modern organic chemistry practice, NMR spectroscopy is the definitive method to identify monomolecular organic compounds. Similarly, chemists use NMR to identify polymers and other complex molecules. Besides identification, NMR spectroscopy provides detailed information about the structure, dynamics, reaction state, and chemical environment of molecules. The most common types of NMR are ^1H - (proton) and ^{13}C - (carbon) NMR spectroscopy, but it is applicable to any kind of sample that contains nuclei possessing spin.

The nuclei that can be studied by NMR are the nuclei that exhibit non-zero spin, that is, all nuclei with an excessive number of protons or an unnecessary number of neutrons. The exact frequency required for tuning depends on the strength of the external magnetic field and the type of core. Basically, the transition frequency is proportional to the intensity of the magnetic field, as shown by the equation $\omega_o = \gamma \cdot B_o$. The frequency ω_o is called the Larmor frequency, while the γ constant is called gyromagnetic.

The resonance position of a nucleus is expressed relative to a standard substance added to the sample. Tetramethylsilane (TMS) is usually taken as a standard substance. The chemical shift expresses the difference in the resonance frequency between the protons of the sample and the protons of the TMS. The chemical shift is usually expressed on the δ -scale based on the ratio: $\delta = (\nu_\delta - \nu_\alpha) / \nu_o$ where ν_δ is the resonance frequency of the proton in question (in Hz), ν_α the resonance frequency of the protons of the reference substance, *i.e.*, TMS, and is the operating frequency of the spectrometer. The parameter δ , the chemical shift, is a dimensionless number and is expressed in ppm. The chemical shift depends on the electron environment of the nucleus. Most shielded nuclei appear in a high magnetic field (right), while less shielded nuclei appear in a low field (left).

NMR spectra can be obtained in solutions with solvents containing no protons (e.g. CCl₄) or secondary solvents (e.g. CDCl₃) where a small amount of TMS has been added. Protons having the same environment, *i.e.* having the same degree of shielding, are usually magnetically equidistant presenting the same value δ .

1.3.6.3. Static Light Scattering (SLS).¹¹⁶

Static light scattering is a technique in physical chemistry that measures the intensity of the scattered light to obtain the average molecular weight M_w of a macromolecule like polymers. Measurement of the scattering intensity at many angles allows calculation of the root mean square radius, also called the radius of gyration R_g . By measuring the scattering intensity for many samples of various concentrations, the second virial coefficient A_2 , can be calculated.

For static light scattering experiments, a high-intensity monochromatic light, usually a laser, is launched in a solution containing the macromolecules. One or many detectors are used to measure the scattering intensity at one or many angles. To measure the average molecular weight directly without calibration from the light scattering intensity, the laser intensity, the quantum efficiency of the detector, and the full scattering volume and solid angle of the detector needs to be known.

For polymers and polymer complexes which are of a monodisperse nature as determined by static light scattering, a Zimm plot¹⁵⁷⁻¹⁵⁸ is a conventional means of deriving the parameters such as R_g , molecular mass M_w and the second virial

coefficient A_2 . Experiments are performed at several angles and at least 4 concentrations. The basis for the Zimm diagram is equation 1.1:

$$\text{Equation 1.1: } \frac{Hc}{\Delta R(\theta, c)} = \left(\frac{1}{M_w} + 2A_2c \right) \left(1 + \frac{1}{3} q^2 R_g^2 \right)$$

where θ is the scattering angle, ΔR the Rayleigh factor, M_w the mean weight MW, the polymer concentration, $q = (4n/v) \sin(\theta/2)$ and R_g the gyrosopic radius. The optical constant H given by equation 1.2:

$$\text{Equation 1.2: } H = 4\pi^2 n_o^2 (dn/dc)^2 / (N_{AV} \lambda_o^4)$$

where n_o the solvent refractive index number, dn/dc the solvent specification index, N_{AV} the Avogadro number, and λ_o the wavelength of the optical radiation (laser) used in the air.

1.3.6.4. Dynamic / Static Light Scattering (DLS/SLS).¹¹⁶

Dynamic light scattering (DLS) and SLS can be complimentary and can sometimes be done within a single commercial instrument. As we describe the SLS theory above, we can see the DLS which is a technique in physics that can be used to determine the size distribution profile of small particles in suspension or polymers in solution. In the scope of DLS, temporal fluctuations are usually analyzed by means of the intensity or photon auto-correlation function. DLS can also be used to probe the behavior of complex fluids such as concentrated polymer solutions.

1.3.6.5. Atomic Force Microscopy (AFM).¹¹⁷

Atomic force microscopy is a type of scanning probe microscopy, with demonstrated resolution on the order of fractions of a nanometer, more than 1000 times better than the optical diffraction limit. The information is gathered by "feeling" or "touching" the surface with a mechanical probe. Piezoelectric elements that facilitate tiny but accurate and precise movements on command enable precise scanning. AFM can be used to measure the forces between the probe and the sample as a function of their mutual separation. This can be applied to perform force spectroscopy, to measure the

mechanical properties of the sample, such as the sample's Young's modulus. Also, for imaging, the reaction of the probe to the forces that the sample imposes on it can be used to form an image of the three-dimensional shape (topography) of a sample surface at a high resolution. The surface topography is commonly displayed as a pseudo color plot.

1.3.6.6. Small-angle Neutron Scattering (SANS).¹¹⁸

SANS was applied to polymer science in the early 1970s¹⁵⁹⁻¹⁶⁰ The SANS technique is a powerful technique for determining the shape and size of particles between 1 and 300 nm. This technique requires the presence of a source of neutrons which may come from nuclear reactors or accelerators from nuclear reactions. In their production, neutrons have a very high energy to be used in scattering experiments and must therefore be slowed down (with neutron retarders) until their kinetic energy corresponds to room temperature (hot neutrons) or lower (cold neutrons). Neutrons are characterized by a de Broglie wavelength of $\lambda = \frac{h}{(m_n v)} \approx 1 - 10 \text{ \AA}$, where m_n is

the mass of the neutron and v its velocity. The de Broglie length is comparable to typical atomic dimensions, so neutron scattering is analyzed by the Debye-Gans scattering theory of large particles. Neutrons are quite heavy particles and, unlike X-rays, are not scattered by electrons. Neutrons have magnetic moment but have zero electric dipole moment and zero electric charge, so they have negligible interaction with electrons. Neutrons are scattered only by the nuclei of atoms with which the interaction is very strong but also extremely short-range (10^{-15} m).

Studies of the structure of polymer networks using scattering techniques require the use of suitable structural models. Starting from a polymer solution, we can say that the radiation is scattered by the spontaneous thermodynamic concentration fluctuations around the equilibrium state described by the average volume fraction of the polymer, ϕ , and the corresponding osmotic compressibility factor. In the neutron scattering of polymeric grids, the modulus of elasticity (G) played by the fact that the polymeric grid chains are interconnected plays an important role. The presence of this modulus modifies the system's response. Thus, the dynamic concentration fluctuations that scatter radiation from the expanded grids are no longer controlled only by the osmotic compressibility coefficient of a polymer solution, but also by a longitudinal osmosis factor (M_{os}) derived from molecular motions. Concentration fluctuations are

also caused by the elastic forces in the networks. Such static concentration fluctuations, which are also caused by the elastic barriers on the network due to chemical crossings, are more distant than the osmotic fluctuations and thus cause strong scattering in the low q range of the spectrum.

Therefore, for networks consisting of elastic polymer chains, the scattered intensity can be described by the sum of the dynamic and static components. Based on the above, the resulting relationship for the intensity of scattered radiation is:

$$\text{Equation 1.1: } I(q) = I_{dyn}(q) + I_{stat}(q) = \Delta\rho^2 \left[\frac{kT\phi^2}{M_{os}} \frac{1}{1+q^2\xi^2} + f(s) \exp(-q\Xi)^s \right]$$

Where $f(s)$ is the normalizing agent and takes the form of:

$$\text{Equation 1.2: } f(s) = \frac{2\pi^2 s \langle \delta\phi^2 \rangle \Xi^3}{\Gamma\left(\frac{3}{s}\right)}$$

where s a constant that depends on the structure of the network and gets such a value as to best fit Equation 1.1 to the network neutron scattering data, Ξ the statistical correlation length (magnitude of the static concentration fluctuations) and ξ the correlation length for polymer-polymer interactions.

Among the various applications of SANS to polymer characterization-namely, polymer solutions, the structure of crystalline morphology, polymer blends and block copolymers and polymer networks are very suitable to being investigated by SANS because of the following reasons: (1) Scattering contrast can be easily bestowed on the sample simply by producing a gel in a deuterated solvent or by immersing in a deuterated solvent. This also significantly lowers the incoherent scattering arising from H-containing materials. (2) Special sample measurements, such as high-pressure measurements, shear deformation measurements and stretching measurements under temperature and humidity control, can be easily realized with quartz, sapphire and/or metal windows because of the strong penetration power of a neutron beam.

1.3.6.7. High-resolution Transmission Electron Microscopy (HR-TEM).

High-resolution transmission electron microscopy is an imaging mode of specialized transmission electron microscopes (TEMs) that allows for direct imaging of the atomic structure of the sample. HR-TEM is a powerful tool to study properties of materials on the atomic scale, such as metals and nanoparticles. At present, the highest point resolution realized in phase contrast TEM is around 0.5 \AA (0.050 nm).¹⁶² At these small scales, individual atoms of a crystal and its defects can be resolved. One of the difficulties with HR-TEM is that image formation relies on phase contrast. In phase-contrast imaging, contrast is not necessarily intuitively interpretable, as the image is influenced by aberrations of the imaging lenses in the microscope. The latter can be estimated from the so-called Thon ring pattern appearing in the Fourier transform modulus of an image of a thin amorphous film.

1.3.6.8. Polarized Light Microscopy.¹⁶³

Polarized light microscopy can mean any of a number of optical microscopy techniques involving polarized light, include illumination of the sample with it. Directly transmitted light can, optionally, be blocked with a polariser orientated at 90 degrees to the illumination. These illumination techniques are most commonly used on birefringent samples where the polarized light interacts strongly with the sample and so generating contrast with the background. Polarized light microscopy was used for the study of the anisotropic phases in the water-swollen conetworks.

1.3.6.9. Powder X-Ray Diffraction (*p*-XRD).¹⁶⁴

Powder diffraction is a scientific technique using X-ray, neutron, or electron diffraction on powder or microcrystalline samples for structural characterization of materials. An instrument dedicated to performing such powder measurements is called a powder diffractometer. Powder diffraction stands in contrast to single crystal diffraction techniques, which work best with a single, well-ordered crystal. The source is often x-rays, because they are the only kind of energy with the correct frequency for inter-atomic-scale diffraction.

Relative to other methods of analysis, powder diffraction allows for rapid, non-destructive analysis of multi-component mixtures without the need for extensive sample preparation. This gives laboratories, the ability to quickly analyze unknown

materials and perform materials characterization in such fields as metallurgy, mineralogy, forensic science, archeology, condensed matter physics, and the biological and pharmaceutical sciences.

1.3.6.10. Mass Spectrometry (MS).¹²⁰

Mass spectrometry is an analytical technique that measures the mass-to-charge ratio of ions. The results are typically presented as a mass spectrum, a plot of intensity as a function of the mass-to-charge ratio. Mass spectrometry is used in many different fields and is applied to pure samples as well as complex mixtures. These spectra are used to determine the elemental or isotopic signature of a sample, the masses of particles and of molecules, and to elucidate the chemical identity or structure of molecules and other chemical compounds. In a typical MS procedure, a sample, which may be solid, liquid, or gaseous, is ionized, for example by bombarding it with electrons. This may cause some of the sample's molecules to break into charged fragments or simply become charged without fragmenting. These ions are then separated according to their mass-to-charge ratio, for example by accelerating them and subjecting them to an electric or magnetic field: ions of the same mass-to-charge ratio will undergo the same amount of deflection.¹⁶⁵ The ions are detected by a mechanism capable of detecting charged particles, such as an electron multiplier. Results are displayed as spectra of the signal intensity of detected ions as a function of the mass-to-charge ratio. The atoms or molecules in the sample can be identified by correlating known masses to the identified masses or through a characteristic fragmentation pattern.

1.3.6.11. Compression Test.

The mechanical properties of the water-swollen APCNs were characterized in confined compression using an Instron 5944 mechanical testing system (Instron, Norwood, MA). According to the confined compression protocol, specimens with a size of 6 mm were confined within a metallic chamber. The bottom side of the chamber was in contact with a filter paper to allow fluid but not the solid material of the specimen to pass through the pores of the filter. At the top side of the chamber, a piston compressed the specimens to a specified strain (90%) with a strain rate of 0.05 mm s^{-1} . This was the slowest strain rate the used mechanical testing system could apply in order to diminish any viscoelastic effects. The specimens were compressed

up to 90% strain and the developed force was recorded. From the measured force and the initial cross-sectional area of the specimen, the first Piola-Kirchhoff stress was calculated. The Young's modulus was measured from the slope of the linear part of the stress strain curve of the specimens. The stress and strain at break were taken at the point of failure of the specimen.

ELENI J. KEPOLA

CHAPTER 2: EXPERIMENTAL PART

2.1. Chemical Reagents and Solvents.

Lauryl methacrylate (LauMA, Sigma-Aldrich, Germany, 95%), methyl methacrylate (MMA, Sigma-Aldrich, 99%), 2-(dimethylamino)ethyl methacrylate (DMAEMA, Sigma-Aldrich, Germany, 99%), glycidyl methacrylate (GMA, Sigma-Aldrich Germany, 97%) and 2-acetoacetoxy ethyl methacrylate (AcEMA over CaH_2 and DPPH, Sigma-Aldrich, Germany, 95%) were stored over CaH_2 (Sigma-Aldrich, Germany, 90-95%) and 2,2-diphenyl-1-picrylhydrazyl hydrate (DPPH, Sigma-Aldrich, Germany, 95%). Methacryloyl chloride (MaCl, Sigma-Aldrich, Germany, 97%), triethylamine (Et_3N , Merck, 99%), pyridine (Sigma-Aldrich, Germany, 99.8%), were stored over CaH_2 .

9-Anthracenemethanol (Sigma-Aldrich, Germany, 97%), HCl (1 M), NaHCO_3 (Sigma-Aldrich, Germany, 99.5%), NaCl (Himedia, >99%), anhydrous MgSO_4 (Himedia, 70%), silica gel (Merck, 60 Å, 0.04-0.063 mm), methanol (Lab-Scan, 99.9%), diethyl ether (Sigma-Aldrich, Germany, >99.8%), deuterated chloroform (CDCl_3 , Merck, 99.8%), benzene (Scharlau, >99.5%), chloroform (Sigma-Aldrich, Germany, >99%), *n*-hexane (Sigma-Aldrich, Germany, >97%), cyclohexane (Sigma-Aldrich, Germany, >97%), hydrazine monohydrate (Sigma-Aldrich, Germany, 80%), $\text{HAuCl}_4 \cdot 3\text{H}_2\text{O}$ (Sigma-Aldrich, Germany, >99.9%) and $\text{Ni}(\text{CH}_3\text{COO})_2 \cdot 4\text{H}_2\text{O}$ (Sigma-Aldrich, Germany, >99.9%), bromobenzene (Sigma-Aldrich, Germany, 98%), 1,4-diisopropenyl benzene (Sigma-Aldrich, Germany, 99%), anhydrous carbon disulfide (CS_2 , Sigma-Aldrich, Germany, >99%), NaOH (1 M), Mg (Sigma-Aldrich, Germany, 98%), dichloromethane (DCM, Sigma-Aldrich, Germany, 99%), dimethyl acetate (DMAc, Sigma-Aldrich, Germany, 99%), $\text{Pd}(\text{CH}_3\text{COO})_2$ (Sigma-Aldrich, Germany, >99.9%), 2-Cyanoprop-2-yl dithiobenzoate (2-CPDB, purity > 97%), ethylene diamine (EDA, purity \geq 99%), diethylene triamine (DETrA, purity \geq 97%), triethylene tetramine (TrETA, purity \geq 97%), tetraethylene pentamine (TEPA, purity \geq 97%) and pentaethylene hexamine (PEHA, purity \geq 97%), were used as received without further purification. 1,4-Bis[2-(thiobenzoylthiol)prop-2-yl]benzene (1,4-BTBTPB) was used as the chain transfer agent CTA for RAFT polymerization. 2,2'-azobis(isobutylnitrile) (AIBN, 95%) was recrystallized twice in ethanol (Sigma-Aldrich, Germany, 96%) and dried for 78 h under vacuum at room temperature. The cross-linker, ethylene glycol dimethacrylate (EGDMA, 98%), the initiator, 1-

methoxy-1-trimethylsiloxy-2-methyl propene (MTS, 95%), were purchased from Aldrich, Germany. The catalyst, tetrabutylammonium bibenzoate (TBABB), was synthesized in our laboratory as detailed by Dicker and coworkers¹¹⁰, and it was kept under vacuum until use. The degradable cross-linker, 2,2-dimethacryloyloxy-1-ethoxy propene (DMOEP), was synthesized in our laboratory following one of the recipes in the literature¹²¹ in dichloromethane (DCM), using 2-hydroxyethyl methacrylate (HEMA, 97%) and 2-methoxypropene (MOP), and employing *p*-toluenesulfonic acid (*p*TSA) as the catalyst of the reaction.

C₂C₁₂ cell lines were purchased from ECACC, Salisbury, Wiltshire, UK. Lipofectamine2000 was purchased from Invitrogen, UK. Dulbecco's phosphate buffered saline (D-PBS) without calcium chloride and magnesium chloride, Dulbecco's modified Eagle's medium (DMEM), OPTIMEM (reduced-serum medium (1 ×) liquid), fetal bovine serum (FBS), glutamine (glutaMAX), penicillin-streptomycin, trypsin (0.25% (1 ×) with EDTA 4Na), geneticin-selective antibiotic and trypan blue were purchased from Gibco, UK and were used for the cell culture experiments.

2.2. Purification of Monomers and Solvents for the Polymerizations.

Lauryl methacrylate (LauMA), methyl methacrylate (MMA), 2-(dimethylamino)ethyl methacrylate (DMAEMA), glycidyl methacrylate (GMA) and 2-acetoacetoxy ethyl methacrylate (AcEMA) were passed through a basic alumina column (90 Å, 0.063-0.2 mm) and distilled over DPPH. Methacryloyl chloride (MaCl), triethylamine (Et₃N) and pyridine, were distilled under reduced pressure. 9-anthrylmethyl methacrylate (AnMMA) was synthesized following a procedure reported by Demetriou et al.⁸ but with column chromatography as further purification. DMOEP was purified from the unreacted starting materials and the mono-substituted side-product, 2-[(2-methoxypropan-2-yl)oxy]ethyl methacrylate (*m*-HEMA), by column chromatography using silica gel and a solvent mixture composed of cyclohexane and diethyl ether, plus triethylamine base (1% v/v) to protect the labile DMOEP from acid hydrolysis. It is noteworthy that the acid-lability of DMOEP was so high that it would spontaneously hydrolyze in chloroform (protonated or deuterated) whose acidic impurities had not been neutralized using basic alumina. The starting composition of

the solvent mixture for chromatography was 99% v/v cyclohexane, 0% v/v diethyl ether, and 1% v/v triethylamine, which was gradually changed to a final composition of 84% v/v cyclohexane, 15% v/v diethyl ether, and 1% v/v triethylamine.

1,4-dioxane, CCl₄ and DMAc were stored in CaH₂ and distilled under reduced pressure. THF, was purchased from Fisher, UK, and was dried by being refluxed for three days over a potassium/sodium amalgam before use.

2.3. Synthesis of the AnMMA Monomer, the Chain Transfer Agent and the Degradable Cross-linker.

2.3.1. Synthesis of the AnMMA Monomer.

For the synthesis of the AnMMA monomer, 9-anthracenemethanol (6 g, 0.028 mol) was dissolved in THF (24 mL). Then, Et₃N (6 mL, 0.032 mol), pyridine (4 mL, 0.032 mol) and MaCl (4.2 mL, 0.032 mol) were added at a 20% excess, with respect to the 9-anthracenemethanol in to the reaction flask. The 4.2 mL of MaCl was added dropwise and under stirring at 0 °C, and the mixture was left to reach room temperature and it was further stirred for 1 h. Subsequently, water (20 mL) was added and the mixture was extracted with diethyl ether, followed by further extraction of the organic phase with HCl (1 M, 40 mL), then with NaHCO₃ (5% in water, 20 mL) and with NaCl (40 mL). The solvent was removed under reduced pressure and the product was purified with column chromatography (95:4:1, n-hexane: diethyl ether: Et₃N). The yield was 75%. The complete purification of the monomer and its structure are confirmed using ¹H- and ¹³C-NMR spectroscopy: ¹H NMR (500 MHz, CDCl₃) δ (ppm): 8.5 (s, s, -PhCH=Ph), 8.4-7.5 (m, -Ph), 6.3 (s, -CH₂Ph), 6.05 (s, olefinic H), 5.50 (s, olefinic H), 1.9 (s, -CH₃). ¹³C NMR (500 MHz, CDCl₃) δ (ppm): 167 (s, OCH=O), 136 (s, CH₃CH=CH₂), 131-125 (m, CHCH=CH), 124 (s, CH=CH₂), 60 (s, OCH₂CH), 19 (s, CH₃CH).

2.3.2. Synthesis of the 1,4-BTBTPB Chain Transfer Agent.

The bifunctional CTA, 1,4-bis[2-(thiobenzoylthio)prop-2-yl]benzene (1,4-BTBTPB), was prepared similarly to the synthesis of 1,3-bis-[2-(thiobenzoylthio)prop-2-yl]benzene, as described by Patton et al.¹²² In particular, 39 mmol of dithiobenzoic

acid (DTBA) was reacted with 18,6 mmol of 1,4-diisopropenyl benzene in the presence of a catalytic amount of *p*-toluenesulfonic acid. DTBA was prepared as described by Jayalakshmi et al.¹²³ The agent was purified with column chromatography (90:10, *n*-hexane: DCM) and recrystallization (2:1, *n*-hexane: diethyl ether). The yield was 47,2%.

2.3.3. Synthesis of the DMOEP Hydrolyzable Cross-linker.¹²⁴⁻¹²⁵

In a typical reaction, a DCM (200 mL) solution / dispersion of *p*TSA (28 mg, 1.56 mmol), HEMA (19 mL, 20 g, 156.55 mmol) and MOP (7.43 mL, 5.65 g, 78.33 mmol) was transferred into a 500 mL round-bottomed flask. The reaction mixture was maintained at 0 °C for 1 h in the presence of added DPPH to prevent undesirable thermal polymerization. Afterward, the mixture was filtered in order to remove the solid *p*TSA. The DCM was subsequently removed under reduced pressure using a rotary evaporator at room temperature. The resulting oily residue (yield in desired product before column chromatography = 70%) was separated from starting materials (mainly HEMA) using column chromatography (silica gel/cyclohexane : diethyl ether : triethylamine = from 99:0:1 to 84:15:1 v/v/v). A mixture of two vinylic compounds coeluted in column chromatography at the final solvent composition cyclohexane : diethyl ether : triethylamine equal to 84:15:1 v/v/v. These two compounds were the desired degradable divinyl cross-linker DMOEP (yield 15.5 g, 52%) and the monovinyl side-product m-HEMA (yeild 8.3 g, 28%) where the hydroxyl group of HEMA was protected with a methoxyketal group; to our knowledge, this is the first time that the synthesis of m-HEMA is reported and we plan to further exploit it in a future investigation. Finally, DMOEP and m-HEMA were separated from each other using vacuum distillation, in which m-HEMA distilled over at 110 °C, and DMOEP at 120 °C.

The high purity of the DMOEP cross-linker was confirmed using ¹H and ¹³C NMR spectroscopy:

¹H NMR (d₆-DMSO, δ, ppm): 1.29 [s, (CH₃)C), 6 H], 1.86 [s, (CH₃)C=CH₂), 6 H], 3.63 [t, OCOCH₂CH₂O, 4 H], 4.18 [t, OCOCH₂CH₂O, 4 H], 5.66 [s, olefinic H, trans to CO₂, 2 H], 6.01 [s, olefinic H, cis to CO₂, 2 H].

^{13}C NMR (d_6 -DMSO, δ , ppm): 18 [s, $\text{CH}_3\text{C}=\text{CH}_2$, 2 C], 24 [s, $(\text{CH}_3)_2\text{C}$, 2 C], 58 [s, $\text{OCOCH}_2\text{CH}_2\text{O}$, 2 C], 64 [s, $\text{OCOCH}_2\text{CH}_2\text{O}$, 2 C], 99 [s, $-\text{OCO}-$, 1 C], 126 [s, $\text{CH}_2=\text{C}$, 2 C], 136 [s, $\text{CH}_3\text{C}=\text{CH}_2$, 2 C], 166 [s, $\text{OC}(=\text{O})\text{C}$, 2 C].

The high purity of m-HEMA was also confirmed using ^1H and ^{13}C NMR spectroscopy:

^1H NMR (d_6 -DMSO, δ , ppm): 1.25[s, $(\text{CH}_3)_2\text{C}$, 6 H], 1.88 [s, $\text{CH}_3\text{C}=\text{CH}_2$, 3 H], 3.09 [s, CH_3O , 3 H], 3.56 [t, $\text{OCOCH}_2\text{CH}_2\text{O}$, 2 H], 4.19 [t, $\text{OCOCH}_2\text{CH}_2\text{O}$, 2 H], 5.68 [s, olefinic H, trans to CO_2 , 1 H], 6.03 [s, olefinic H, cis to CO_2 , 1 H].

^{13}C NMR (d_6 -DMSO, δ , ppm): 18 [s, $\text{CH}_3\text{C}=\text{CH}_2$, 1 C], 25 [s, $(\text{CH}_3)_2\text{C}$, 2 C], 48 [s, CH_3O , 1 C], 59 [s, $\text{OCOCH}_2\text{CH}_2\text{O}$, 1 C], 64 [s, $\text{OCOCH}_2\text{CH}_2\text{O}$, 1 C], 100 [s, $-\text{OCO}-$, 1 C], 126 [s, $\text{CH}_2=\text{C}$, 1 C], 136 [s, $\text{CH}_3\text{C}=\text{CH}_2$, 1 C], 167 [s, $\text{OC}(=\text{O})\text{C}$, 1 C].

2.4. Synthesis of Polymers and Polymer Networks.

2.4.1. GTP Synthesis of EGDMA-MMA-DMAEMA-EGDMA Amphiphilic Polymer Conetworks Based on End-linked Core-first Star Block Copolymers.

Polymer synthesis was performed using group transfer polymerization (GTP). The polymerization procedure followed for the synthesis of amphiphilic polymer conetworks (APCN) comprised four, one-pot, sequential addition steps, with the first and fourth ones involving EGDMA cross-linker polymerizations (oligomerizations), and the two intermediate ones involving polymerizations of the two comonomers, MMA and DMAEMA, in either order of addition.

The details of the polymerizations for the preparation of one of the APCNs are given below. A 100 mL round-bottomed flask, containing a magnetic stirring bar, was charged with a small amount (~10 mg) of TBABB catalyst. Subsequently, 21 mL of freshly distilled THF and 0.3 mL of MTS initiator (0.26 g, 1.48 mmol) were transferred to the flask, in this order, using dried glass syringes. This was followed by the addition of 0.28 mL of EGDMA cross-linker (0.29 g, 1.48 mmol), also using a glass syringe, under stirring (first polymerization step). The added EGDMA was immediately polymerized, resulting in a temperature increase from 29 to 31 °C. Analysis of the resulting product (oligomer mixture) using gel permeation

chromatography (GPC) indicated a number-average molecular weight, M_n , of 1400 g mol⁻¹ (M_n is the number-average molecular weight);, and a molecular weight dispersity, D (D is the molecular weight dispersity, with $D = M_w/M_n$, where M_w is the weight-average molecular weight), of 5.46, while analysis using ¹H NMR spectroscopy suggested 100% conversion of EGDMA to polymer (oligomer). The sample was also analyzed using mass spectrometry. In the second polymerization step, 4.99 mL of the DMAEMA monomer (4.65 g, 29.6 mmol) was added slowly. The polymerization of DMAEMA led to a temperature rise from 30 to 45 °C. GPC analysis of the formed “core-first” star DMAEMA homopolymer suggested that the M_n value was 12200 g mol⁻¹, while the D value was 2.52; the DMAEMA monomer conversion to polymer was quantitative, according to ¹H NMR spectroscopy. In the third polymerization step, 3.17 mL of the second monomer, MMA (2.96 g, 29.6 mmol), was slowly added, resulting in a temperature increase from 40 to 52 °C. The “core-first” star diblock copolymer product exhibited an M_n value of 21900 g mol⁻¹, and a D value of 2.60; ¹H NMR spectroscopy again showed full MMA monomer conversion to polymer. Finally, in the fourth polymerization step, 0.28 mL of EGDMA (0.29 g, 1.48 mmol) was added, which promoted gelation within seconds. The efficiency of the cross-linking reaction was high, as evidenced by attenuated total reflection Fourier-transform infrared (ATR-FTIR) spectroscopy analyses of the dried conetworks, and by measurement of the sol fraction. Regarding the former, ATR-FTIR indicated complete consumption of the EGDMA olefinic groups (absence of signal at 1637 cm⁻¹ corresponding to C=C stretching) in the conetworks. Regarding the latter, the measured sol fraction was relatively low, around 20 wt.%.

2.4.2. GTP Synthesis of Hydrolyzable MMA Networks Cross-linked with DMOEP and EGDMA

To illustrate the network synthesis procedure, we provide below as an example the preparation of the network with both hydrolyzable cores. A small amount (~10 mg, 21 μmol) of TBABB catalyst was transferred to a 100 mL round-bottomed flask. Then, 12.0 mL of freshly distilled THF and 0.3 mL MTS initiator (0.26 g, 1.48 mmol, 1 equivalent) were syringed, in this order, into the flask, followed by the addition of 1.6 mL of DMOEP cross-linker (1.78 g, 5.92 mmol, 4 equivalents) under stirring. This led to a temperature increase from 22 to 35 °C. Analysis of the resulting product

by GPC indicated an $M_n = 2920 \text{ g mol}^{-1}$ (and a $D = 4.38$), while ^1H NMR spectroscopy suggested 100% conversion of DMOEP to polymer. In the second stage, 3.2 mL of the MMA monomer (2.96 g, 29.6 mmol, 20 equivalents) was added slowly, leading to a temperature rise from 29 to 53 °C. GPC analysis of the formed “core-first” star polymer provided a M_n value of 6840 g mol^{-1} and a D value of 2.34; the MMA monomer conversion to polymer was complete, according to analysis using ^1H NMR spectroscopy. Finally, 1.6 mL of DMOEP cross-linker (1.78 g, 5.92 mmol, 4 equivalents) was added, which promoted gelation within seconds. The three other polymer networks were prepared using a similar procedure, using a THF volume for the polymerizations so that the final solids concentration in the networks was kept constant at about 35 vol%. Furthermore, the amount of EGDMA cross-linker used for the formation of one core was only 1 equivalent with respect to the MTS initiator. This was based on initial polymerization experiments which indicated that the use of 1 equivalent of EGDMA corresponded to the use of 4 equivalents of the bulkier, and, therefore, more sterically hindered and less reactive DMOEP. The four synthetic sequences employed are summarized in Figure 1.1. As already mentioned, four times more of the less efficient DMOEP cross-linker had to be used to roughly match the performance of the more reactive EGDMA cross-linker.



Figure 2.1. Synthetic sequences followed for the preparation of the end-linked MMA homopolymer networks based on interconnected “core-first” star polymers.

2.4.3. RAFT and GTP Synthesis of Linear and Star “Arm-first” GMA Homopolymers.

An “arm-first” GMA star homopolymer with a nominal arm DP of 20 ($\text{GMA}_{20}\text{-star}$) was synthesized using sequential group transfer polymerization GTP¹⁰⁸⁻¹¹² while a

similar star homopolymer of higher arm DP (nominal value of 100) (GMA₁₀₀-star) was prepared using step-wise reversible addition-fragmentation chain transfer polymerization RAFT¹¹³. The synthetic procedures followed for the preparation of each star homopolymer are described below. The synthesis of this star homopolymer was accomplished by sequential GTP with two additions.

2.4.3.1. GMA "arm-first" star homopolymer by GTP.

The synthesis of the star polymer was performed by the sequential GTP of the GMA monomer and the EGDMA cross-linker. To this end, a round-bottomed flask (100 mL), which was preloaded with a small amount (~10 mg) of TBABB, 16.3 mL of freshly distilled THF and 0.3 mL of MTS initiator (0.26 g, 1.49 mmol) were added, while the flask was kept under an inert water- and oxygen-free dry argon atmosphere for approximately 5 min. Then, 3.90 mL of GMA monomer (4.06 g, 28.6 mmol) was added dropwise (an exotherm of 20 °C was observed) and, subsequently, 1.12 mL of EGDMA cross-linker (1.18 g, 5.85 mmol) was added, which produced again an exotherm (3 °C). After each of the additions of monomer and crosslinker, small volumes (1 mL) of samples were taken out from the flask and characterized by gel permeation chromatography (GPC) and proton nuclear magnetic resonance (¹H NMR) spectroscopy. [Monomer and cross-linker conversions by ¹H NMR spectroscopy: (a) that of GMA in GMA₂₀ = 100%, theoretical MW = 2900 g mol⁻¹, *M_n* by GPC = 2000 g mol⁻¹, *D* = 1.5, (b) that of EGDMA in GMA₂₀-EGDMA₄ = 100%, *M_n* by GPC = 39500 g mol⁻¹, *D* = 1.7]. Finally, the produced polyGMA-star homopolymer was recovered by precipitation in methanol and was dried in a vacuum oven at room temperature for 48 h.

2.4.3.2. Linear and "Arm-first" Star Homopolymers of GMA by RAFT Polymerization.

The synthesis of this star homopolymer was accomplished by step-wise RAFT copolymerization of monomer and cross-linker *in bulk*. First, the synthesis and isolation of the linear GMA homopolymer precursor were performed, followed by its interconnection at one end using EGDMA cross-linker.

For the synthesis of the linear GMA precursor, AIBN (20 mg, 0.12 mmol), 2-CPDB (83 mg, 0.37 mmol) and GMA (5 mL, 36.65 mmol) were added into a small Schlenk flask. Subsequently, this mixture was degassed by three freeze-evacuate-thaw cycles, placed under an oxygen-free and dry argon atmosphere, and heated to 60 °C where it was kept for 18 h. [Monomer conversion by ^1H NMR spectroscopy: that in $\text{GMA}_{100} = 99\%$ GMA, theoretical $M_w = 14200 \text{ g mol}^{-1}$, M_n by GPC = 15300 g mol^{-1} , $D = 1.2$]. The polymerization was terminated by cooling the reaction down to room temperature, followed by its precipitation in methanol and its drying in a vacuum oven at room temperature for 48 h.

Some of this linear homopolymer was kept for further studies. For the preparation of the GMA “arm-first” star homopolymer, the polyGMA linear precursor (5.35 g, $M_n = 15300 \text{ g mol}^{-1}$, $D = 1.2$, 0.35 mmol macroCTA) and AIBN (20 mg, 0.12 mmol) were dissolved in freshly distilled DMAc (7.50 mL) and placed together with EGDMA (0.40 mL, 2.1 mmol) in a Schlenk flask. The reaction mixture was again degassed by three freeze-evacuate-thaw cycles, placed under an oxygen-free, dry argon atmosphere, and heated up to 60 °C where it was kept for 18 h. [EGDMA conversion by ^1H NMR spectroscopy = 100%, M_n by GPC-RI = $218100 \text{ g mol}^{-1}$, $D = 1.5$, M_w by GPC-SLS = $300000 \text{ g mol}^{-1}$] The polymerization flask was subsequently cooled down to room temperature, the produced polyGMA-*star* was precipitated in methanol and left to dry in a vacuum oven at room temperature for 48 h.

2.4.4. RAFT Synthesis of the AcEMA-LauMA Diblock Copolymers and the Linear AcEMA-LauMA-AnMMA Diblock Terpolymers.

2.4.4.1. Synthesis of the Diblock Copolymers.

In a round-bottomed flask, 3.5g LauMA (13.6 mmol) was transferred and dissolved in freshly distilled 1,4-dioxane (4 mL) under a dry argon atmosphere. Then, 0.06g 2-CPBD (0.27 mmol) and 0.03g AIBN (0.017 mmol) were dissolved in 1,4-dioxane and transferred into the flask. The mixture was degassed by three freeze-evacuate-thaw cycles and placed under a dry argon atmosphere at 65 °C for 18 h. The obtained LauMA₅₀ homopolymer ($M_n^{\text{GPC}} = 14900 \text{ g mol}^{-1}$, $D = 1.2$, Conversion from ^1H NMR = 98%), was added AcEMA (0.82 g, 3.4 mmol) and the reaction was continued for another 24 h under a dry argon atmosphere at 65 °C. The polymerization was

terminated by cooling the reaction down to room temperature. The polymer (4.11 g, 94% polymerization yield) was retrieved by precipitation in methanol and was left to dry under vacuum at room temperature for 48 h.

2.4.4.2. Synthesis of Diblock Terpolymers.

In a round-bottom flask, AcEMA (2.24 g, 0.0105 mol) was mixed with and dissolved in freshly distilled 1,4-dioxane (2.03 mL) under a dry argon atmosphere. 2-CPBD (0.046 g, 0.2 mmol) and AIBN (0.010 g, 0.063 mmol) were dissolved in 1,4-dioxane and transferred into the flask with the AcEMA solution in 1,4-dioxane. The mixture was degassed by three freeze-evacuate-thaw cycles and placed under a dry argon atmosphere at 65 °C for 19 h. The polymerization was stopped by cooling the reaction down to room temperature. The homopolymer (2.22 g, 99% polymerization yield) was retrieved by precipitation in methanol and was left to dry under vacuum at room temperature for 48 h. This AcEMA₅₀ homopolymer ($M_n^{\text{GPC}} = 13500 \text{ g mol}^{-1}$, $D=1.4$, 0.5 g, 0.037 mmol) in the macro-CTA for the next stage of the polymerization. For that purpose, it was transferred to round bottomed- flask and dissolved in freshly distilled 1,4-dioxane (1.95 mL) under a dry argon atmosphere AIBN (0.0036 g, 0.022 mmol) and AnMMA (0.2 g, 0.74 mmol) were dissolved in 1,4-dioxane, and together with LauMA (1.69 g, 6.7 mmol), were transferred into the flask via a syringe. The contents of the reaction flask were degassed by three freeze-evacuate-thaw cycles and maintained under a dry argon atmosphere at 65 °C for 25 h. The polymerization was terminated by cooling the reaction down to room temperature. A diblock copolymer (AcEMA_x-*b*-[LauMA_{4x}]) was also prepared using the same macro-CTA for comparison. The produced diblock terpolymer (1.7 g, 70% yield) and diblock copolymer (1.8 g, 74% yield) were retrieved by precipitation in methanol and were left to dry under vacuum at room temperature for 48 h.

2.4.5. RAFT Synthesis of AcEMA-LauMA-AcEMA Triblock Copolymers.

In a 50 mL round-bottomed flask equipped with a stirring bar, 3 mL of LauMA (2.6 g, 10 mmol) was transferred using a glass syringe. Subsequently, 47 mg of 1,4-BTBTBPB (0.1 mmol) and 10 mg of AIBN (0.0625 mmol) were dissolved in 1,4-dioxane (3 mL) and the resulting solution was transferred in to the flask. The reaction mixture was

stirred at room temperature, degassed by three freeze–evacuate–thaw cycles and heated at 65 °C for 18 h. After the passage of the 18 hours, samples were withdrawn from the polymerization flask and analyzed using GPC and ¹H NMR spectroscopy. This analysis indicated that the conversion of LauMA to polymer was 98% ($M_n^{\text{GPC}} = 22900 \text{ g mol}^{-1}$ and $D = 1.3$). Subsequently, 0.54 mL of AcEMA (0.6 g, 2.5 mmol) was added in the reaction mixture and it was allowed to polymerize at 65 °C for 19 h. The polymerization was stopped by cooling the reaction mixture down to room temperature. The produced AcEMA_{12.5}-*b*-LauMA₁₀₀-*b*-AcEMA_{12.5} was recovered by precipitation in *n*-hexane and dried at room temperature under vacuum (yield: 92%, $M_n^{\text{GPC}} = 30100 \text{ g mol}^{-1}$, $D = 1.3$).

2.4.6. RAFT Synthesis of Linear AcEMA₅₀-*b*-DMAEMA₂₀₀ Copolymer.

In a 50 mL round-bottomed flask, 1.5 mL AcEMA (1.8 g, 7.57 mmol) was transferred and dissolved in freshly distilled 1,4-dioxane (5 mL) under a dry argon atmosphere. Then, 0.033 g 2-CPBD (0.15 mmol) and 0.0156 g AIBN (0.0085 mmol) were dissolved in 1,4-dioxane and transferred into the flask. The mixture was degassed by three freeze-evacuate-thaw cycles and placed under a dry argon atmosphere at 65 °C for 18 h. The obtained AcEMA₅₀ homopolymer ($M_n^{\text{GPC}} = 9300 \text{ g mol}^{-1}$, $D = 1.2$, Conversion from ¹H NMR = 99%), was added 5.01 mL DMAEMA (4.75 g, 30.3 mmol) and the reaction was continued for another 24 h under a dry argon atmosphere at 65 °C. The polymerization was terminated by cooling the reaction down to room temperature. The 5.14 g polymer ($M_n^{\text{GPC}} = 29900 \text{ g mol}^{-1}$, $D = 1.5$, 78,5 % yield) was retrieved by precipitation in methanol and was left to dry under vacuum at room temperature for 48 h.

2.5. Characterization Methods for all the Polymers and Polymer Networks.

2.5.1. Gel Permeation Chromatography (GPC-HPLC).

The molecular weights and molecular weights distribution of different polymers were labeled with GPC using a Polymer Laboratories system equipped with a PL-Mixed "D" column. The mobile phase was tetrahydrofuran with a flow of 1 mL min⁻¹, obtained with a Waters model 515 HPLC pump. The refractive index (refractive index, RI) was measured using an ERC-7515A RI detector, which was also supplied

by Polymer Laboratories. Molecular calibration 173 weights were based on ten standard linear poly polymers (methyl methacrylate) [poly (methyl methacrylate), PMMA] (800, 2200, 6370, 12600, 23500, 41400, 89300, 201000, 392000 and 675000 g mol⁻¹), supplied by Polymer Standards Service GmbH (Mainz, Germany). The following quantities were calculated for each sample: the average number of molecular weight (M_n), the average molecular weight (M_w), the molecular weight that corresponds to the maximum of the top of the chromatogram (MW), and their polydispersity of molecular weights ($D = M_w / M_n$).

2.5.2. Nuclear Magnetic Resonance Spectroscopy (¹H and ¹³C NMR).

Confirmation of the structure of linear or star polymers, as well as of compounds of low molecular weight was achieved by ¹H NMR spectra, while in some cases and with the exception of ¹³C NMR spectra, in various secondary solvents, with the Bruker 500 MHz Avance spectrometer. In addition, from the ¹H NMR spectra the rate of conversion of terminal groups to polymers after end of each reaction.

2.5.3. Extractables of Amphiphilic Polymer Conetworks and Degradable Polymer Networks.

Extractables are defined as the mass of all reactants and polymers chains that were not incorporated into the grid during its formation. The percentage of no embedded mass of each network was calculated from the quotient of non-incorporated mass for the initial dry mass of its reactants. Not incorporated mass was analyzed by ¹H NMR spectroscopy and GPC.

2.5.4. Static Light Scattering (SLS).

The absolute weight-average molecular weight values, M_w , of the star polymer precursors to the the amphiphilic conetworks and degradable networks, and also the hydrolysis products were measured by static light scattering (SLS) in a flow configuration (GPC-SLS system) using a BI-MwA Brookhaven spectrophotometer equipped with a 30 mW red diode laser emitting at 673 nm and a multi-angle detector measuring the intensity of scattered light at seven different angles: 35, 50, 75, 90, 105,

130 and 145°. The mobile phase was THF (flow rate 1 mL min⁻¹), delivered using a Polymer Laboratories PL-LC1120 isocratic pump. Right after the pump, a single Polymer Laboratories PL-mixed “D” column was connected, followed by the BI-MwA SLS detector, which was followed by a Polymer Laboratories PL-RI 800 RI detector used to measure the RI signal. The PSS WinGPC 7 software was used for the MW calculations. The polymer samples were dissolved in HPLC-grade THF at a concentration of 2 wt%, and were filtered through 0.45 µm pore size syringe filters. The amount of dn/dC of polymeric solutions in THF was determined using an ABBE refractometer. The following Table 2.1 illustrates the values of dn/dC .

Table 2.1. Indicative values of dn/dC for each polymerization step used in SLS.

Polymerization steps	dn/dC
EGDMA ₁	0.087 ⁺
EGDMA ₁ - <i>b</i> -MMA _X X=5, 10, 15, 20, 30, 40	0.087 ⁺
EGDMA ₁ - <i>b</i> -DMAEMA _X X=5, 10, 15, 20, 30, 40	0.101525 ⁺
EGDMA ₁ - <i>b</i> -MMA _X - <i>b</i> -DMAEMA _X * X=10	0.09588
X=20	0.09593
EGDMA ₁ - <i>b</i> -MMA _X - <i>b</i> -DMAEMA _Y * X=10, Y=30	0.09566
X=15, Y=5	0.09055
EGDMA ₁ - <i>b</i> -MMA _Y - <i>b</i> -DMAEMA _X * X=10, Y=30	0.09142
X=15, Y=5	0.099
DMOEP ₄ - <i>star</i> -MMA ₂₀	0.087 ⁺

* The same dn/dC apply to grids with the same texture but different architecture. ⁺ Theoretical dn/dC

2.5.5. *Dynamic / Static Light Scattering (DLS/SLS).*

Dynamic/ Static light scattering experiments were performed to determine the nanoparticles sizes of polymers AcEMA-LauMA/ metals in organic solvents, at room temperature using an ALV/CGS-3 Compact Goniometer System equipped with 22 mW He-Ne laser operating at 632.8 nm. The scattered light was detected at 90° for DLS measurements, while for the SLS measurements the scattered light was detected at a range of 30° - 150°. All the metal-bearing solutions were used as they synthesis (0.4%). For the DLS measurement was used only one concentration of 0.4% w/w, while for the SLS measurement was used a variety of concentrations of the solutions (0.4%, 0.2% and 0.1% w/w, sometime was used 0.3% and 0.15% w/w concentration for decreased the errors). Prior to the light scattering measurements the samples were filtered using a pipette full with cotton.

2.5.6. *Mass Spectroscopy (MS) in the Core of the Star Polymer in Amphiphilic Polymer Conetworks.*

The individual molecular weights of the various oligomers in the core of the star polymer was determined using a Bruker UltraFlex III MALDI tandem time-of-flight (TOF/TOF) mass spectrometer equipped with a Nd:YAG laser emitting at 355 nm.¹²⁶ Dithranol (DIT) served as the matrix, whereas sodium trifluoroacetate (NaTFA) was employed as the cationization salt. Both DIT and NaTFA were dissolved in THF at concentrations of 20 and 10 mg mL⁻¹, respectively. The polymer (oligomer) sample was dissolved in THF at a concentration of 10 mg mL⁻¹. Solutions at matrix : sample : salt ratios equal to 10 : 2 : 1 were prepared and spotted onto the MALDI target.

2.5.7. *Degrees of Swelling (DS).*

The equilibrium degrees of swelling (DS) of the amphiphilic polymer conetworks and degradable polymer networks, in water as a function of pH, and in THF, were measured following our previously published procedures.¹¹⁹

2.5.7.1. Degrees of Swelling in Organic Solvent.

Briefly, after removing the sol fraction of the conetworks by extraction using THF for two weeks, THF-equilibrated conetwork pieces were dried in a vacuum oven at room temperature for 72 h; the DSs in THF were calculated as the ratio of the masses of the THF-swollen divided by the dried conetworks, both determined gravimetrically.

2.5.7.2. Degrees of Swelling in Water at Different pHs.

Subsequently, weighed dried conetwork pieces were transferred to vials containing water and a calculated amount of a 0.5 M HCl solution to effect the desired degree of ionization (DI) of the DMAEMA units within each conetwork piece. The samples were left to equilibrate for three weeks, and the conetwork water-swollen mass and the pH of the supernatant solution were measured; again, the DSs were calculated by dividing the water-swollen by the dried conetwork masses. The aqueous swelling results were presented by plotting the DSs and the DIs (as the left-hand-side and the right-hand-side y-axes) of each conetwork against the supernatant solution pH. Furthermore, the maximum DS (in acidic conditions, around pH 4) and the low DS (neutral conetworks, around pH 8.5) for each conetwork were plotted against conetwork structure.

2.5.8. Polarized Light Microscopy.

Dried amphiphilic polymer conetwork samples were carefully crushed to a fine powder and a small amount was examined under both parallel and crossed polarizers using a Leica DM LSP polarized light microscope, at total magnifications ranging from $50\times$ to $200\times$, and an object field of the order of 0.5 mm. A drop of water was added on top of each solid sample, leading to its complete immersion. Each sample was subsequently examined using the same magnification as for the dry sample. The examination was performed at room temperature (roughly at 20°C) without temperature control.

2.5.9. *Small-angle Neutron Scattering (SANS).*

SANS measurements on (dried) amphiphilic conetwork samples (subsequently) equilibrated in D₂O within 1 mm thickness quartz cuvettes were carried out using three different instruments: instrument D11 of the Institut Laue-Langevin (ILL) in Grenoble, France; instrument KWS-1 of the Julich Center for Neutron Science (JCNS) FRM-II, in Garching, Germany; and, the 30 m NG7 instrument at the Center for Neutron Research of the National Institute of Standards and Technology (NIST) in Gaithersburg, Maryland. The measurements on D11 were carried out with a neutron wavelength of 6 Å (FWHM 10%) for 3 sample-to-detector distances of 1.2, 8, and 34 m, using a collimation length of 8 m for the first two configurations and 34 m for the third. The efficiency of the detector was calibrated by the scattering of a 1 mm thick H₂O sample. All the data reduction was done using the program LAMP provided by ILL. The experiments on KWS-1 were performed with a neutron wavelength of 4.49 Å (FWHM 10%), for three sample-to-detector distances of 1.27, 4.97, and 19.77 m and with collimation lengths of 4, 8, and 20 m, respectively. The sample aperture was 7×7 mm², and the collimation apertures 9×9, 11×11, and 14×14 mm² for the collimation lengths of 4, 8, and 20 m, respectively. The detector calibration was done using H₂O. The data reduction was done with the program QtiKWS. The measurements at NIST involved an incident wavelength of 6 Å, and three sample-to-detector distances, 1.00, 4.00, and 13.50 m. All scattering patterns were isotropic, and therefore, the measured counts were circularly averaged, and corrected for empty cell and electronic background.

2.5.10. *High-resolution Transmission Electron Microscopy (HR-TEM).*

The HR-TEM was used for the metal-end-linked polymer conetworks. The geometrical characteristics (size and shape) and the crystalline structure adopted by the morphology of two nanocomposite conetworks were investigated by high-resolution transmission electron microscopy (HR-TEM) using a TECNAI F30 G2 S-TWIN microscope operated at 300 kV with Energy Dispersive X-ray Analysis (EDX). For the TEM investigations, a small amount of sample was placed on the holder.

2.5.11. Atomic Force Microscopy (AFM).

All the AFM images were recorded at room temperature using either a Cypher S atomic force microscope from Asylum Research / Oxford Instruments or a Dimension Icon atomic force microscope from Bruker. The latter instrument was used to collect the images in the dried state, whereas the former was employed to characterize sample immersed in water. The measurements with the Dimension Icon were performed in tapping mode using commercial Tapping Mode Etched Silicon Probes (RTESP) cantilevers of various frequencies from 300 to 400 kHz, while those with the Cypher were performed in AC mode using Arrow UHF AuD cantilevers resonating in water at 688 kHz.

2.5.11.1. AFM for Amphiphilic Polymer Conetwork.

The samples of APCNs were study after being vacuum dried (at room temperature) from THF and then all the conetworks were thermally treated by leaving them overnight in a vacuum oven at 105 °C, a temperature above the T_g of polyMMA, in order to allow the polyMMA segments to equilibrate (the T_g of the polyDMAEMA segments is much lower, 0 – 20 °C). Then were frozen in liquid nitrogen, fractured, and mounted on a special holder for irregular samples with the fresh surface facing out.

2.5.11.2. AFM for Metal-bearing Nanoparticles.

The micelles' morphology, of all polymers after the redaction of the metals (in CHCl₃, Benzene, Cyclohexane and *n*-Hexane) were recorded using the AFM. All the solutions were 0.01% w/w concentrated and added on the surface of graphite using the speed coating method. AFM, using standard silicon cantilevers with 25-75 N/m spring constant and 200-400 kHz working frequency. All images are recorded in air at room temperature, at a scan speed of 2.4 Hz.

2.5.11.3. AFM for Au-end-linked Polymer Conetworks.

The self-organization of the four of the well-defined hydrophobic polymer conetworks (with Au) in the benzene- swollen states was investigated using the AFM.

2.5.12. Powder X-ray Diffraction (*p*-XRD).

p-XRD was used to examine the crystallinity of the metal-end-linked conetworks. The measurements were carried out on a Shimadzu 6000 diffractometer using $K\alpha$ radiation ($\lambda = 0.15478$ nm). The measurements were performed in the range $10^\circ < 2\theta < 80^\circ$ with $\theta:2\theta$ scan at 2° min^{-1} (2θ). The crystallite size was calculated from the full width at half maximum (fwhm) of the diffraction peaks using Sherrer's equation.

2.5.13. Compression Tests of Amphiphilic Polymer Conetworks.

The mechanical properties of the water-swollen amphiphilic polymer conetworks were characterized in confined compression using an Instron 5944 mechanical testing system (Instron, Norwood, MA). According to the confined compression protocol, specimens with a size of 6 mm were confined within a metallic chamber. The bottom side of the chamber was in contact with a filter paper to allow fluid but not the solid material of the specimen to pass through the pores of the filter. At the top side of the chamber, a piston compressed the specimens to a specified strain (90%) with a strain rate of 0.05 mm s^{-1} . This was the slowest strain rate the used mechanical testing system could apply in order to diminish any viscoelastic effects. The specimens were compressed up to 90% strain and the developed force was recorded. From the measured force and the initial cross sectional area of the specimen, the first Piola-Kirchhoff stress was calculated. The Young's modulus was measured from the slope of the linear part of the stress-strain curve of the specimens. The stress and strain at break were taken at the point of failure of the specimen.

2.6. Hydrolysis of the Degradable Conetworks.

All DMOEP-bearing networks were hydrolyzed at room temperature and under various acidic conditions, yielding polymer solutions within 48 h. These conditions included hydrochloric acid in THF, trifluoroacetic acid in THF, or neat chloroform (not processed with basic alumina). Most of the results reported in the following are those based on hydrolysis in chloroform as this represented the mildest cleavage conditions; due to apparent star recombination, the hydrolysis of the EGDMA₁-*b*-MMA₂₀-*b*-DMOEP₄ network was repeated several times in chloroform, and was also

performed in a THF solutions of hydrochloric or trifluoroacetic acids, with essentially the same results.

As a typical example, we provide below the procedure followed for the hydrolysis of the DMOEP₄-*b*-MMA₂₀-*b*-DMOEP₄ network. A piece of 0.3 g of dried DMOEP₄-*b*-MMA₂₀-*b*-DMOEP₄ network was transferred into a glass vial to which 1 mL of chloroform was subsequently added. Complete network dissolution occurred within 48 h. The hydrolysis product was analyzed using GPC (measured $M_n = 4000 \text{ g mol}^{-1}$, $D = 1.5$; theoretically expected molecular weight = 4100 g mol^{-1}) and ¹H NMR spectroscopy (measured HEMA content in the copolymer = 46 mol%; theoretically expected HEMA content in the copolymer = 44 mol%).

2.7. Derivatization of Linear and Star GMA Homopolymers with Several Amines.

Both GMA “arm-first” *star* homopolymers were derivatized with the oligoamines EDA, DETrA, TrETA, TEPA and PEHA in DMAc. To achieve quantitative derivatizations, large excesses (30-fold molar excess) of the oligoamines were used. To illustrate the procedure, the derivatization of the higher molecular weight GMA “arm-first” *star* homopolymer using excess EDA is described in detail in the following.¹²⁷ First, 4.50 mL of EDA (4.04 g, 67.2 mmol) was dissolved in 18 mL of dry DMAc (22 % w/w) in a round-bottomed flask. In a second flask, 0.3 g of GMA₁₀₀-*star* (2.11 mmol of GMA units) was dissolved in 12 mL of dry DMAc (2.5% w/w), and was, subsequently, added dropwise into the EDA solution. The reaction mixture was left to react at 60 °C for 18 h, and it was subsequently poured into diethyl ether in order to precipitate the diamine-derivatized *star* polymer product. Extensive interconnection of this type may lead to gel formation, as was the case with our original approach using the pentafluorophenyl acrylate linear homopolymer. The product was further purified by dialysis against 2 L of distilled water, which was replaced twice a day over a course of 7 days. Finally, the purified amine-derivatized polymer product was collected by freeze-drying and was characterized using ¹H NMR spectroscopy.

2.8. DNA Transfer Using Oligoamine-grafted-GMA Polymers and AcEMA₅₀-LauMA₂₀₀-linear/Au.

All the oligoamine-grafted GMA-*star* and *linear* homopolymers and also AcEMA₅₀-LauMA₂₀₀-*linear* after complexes with Au, were evaluated for their ability to deliver to C2C12 mouse myoblast cells plasmid DNA which expressed the firefly Luciferase (Luc) gene.

2.8.1. Plasmid DNA / Polymer Transient Transfections.

C2C12 mouse myoblast cells were plated in 12-well plates at a density of 100 000 cells / well and were cultured in DMEM growth medium under standard conditions (37 °C, 5% CO₂). When the cells reached 60-70% confluence, approximately 24 h after cell plating, transient transfections were initiated.

For transfections of C2C12 myoblasts, a stock polymer solution of 3 g L⁻¹ was prepared in deionized sterile water. Various transfection solutions were then prepared using 5 to 40 µL of the polymer stock solution and gently mixing it with OPTIMEM at a final volume of 0.25 mL. The polymer / OPTIMEM solutions were incubated at room temperature for 5 min. In a separate set of 1.5 mL tubes, solutions of plasmid DNA expressing firefly luciferase (10 µL from a 0.01% w/v solution) were diluted in 0.25 mL OPTIMEM.

Furthermore, after the initial incubation, the 0.25 mL firefly luciferase plasmid DNA solutions in OPTIMEM were gently mixed with the 0.25 mL polymer solutions in OPTIMEM and were then incubated for 25 min at room temperature. During this 25 min of incubation, the luciferase plasmid-polymer complex was formed. As a control, luciferase plasmid and Lipofectamine 2000 complex at its optimum condition (based on protocol) was prepared as described above.

After the 25 min of incubation, the mixtures were incubated with the C2C12 cells for 6 h in standard cell culture conditions (37 °C, 5% CO₂). After this 6 h incubation, the cells were rinsed with PBS and supplemented with 2 mL of DMEM growth medium for an additional 24 h incubation period in standard cell culture conditions (37 °C, 5% CO₂).

2.8.2. Firefly Luciferase Assay.

Following the above-described transient transfections, the firefly luciferase activity was measured using a Dual-Luciferase® (DLRTM) Reporter Assay (Promega, USA) according to manufacturer's instructions. Briefly, the cells were harvested and lysed in 500 μL of 1X Passive Lysis Buffer (PLB) (supplied in the kit). PLB is supplied at 5X concentration and, therefore, prior to lysis it was diluted in distilled water. The lysate was vortexed and incubated for 15 min at room temperature. 100 μL of LAR II, which is the lyophilized Luciferase Assay Substrate re-suspended in Luciferase Assay Buffer II (supplied in the kit), was added in a luminometer tube. LAR II is used to initiate the firefly luciferase expression. 20 μL of the lysate was added in the luminometer tube and mixed with LAR II by pipetting. The luminometer tube was placed in the single tube luminometer (Berthold Detection Systems, Germany) and the firefly luciferase activity was measured.

2.8.3. Determination of Cell Viability.

The cytotoxicity of all polymers was also investigated. For this determination, 10 μL of the cells (~ 909 cells / μL) were mixed gently with 10 μL of Trypan Blue. Then, using 10 μL of the resulting mixture, the number of viable cells was counted using a Bio-Rad iMark™ Microplate Reader. The *toxicity* of the polymer toward the cells was calculated as one minus the ratio of the number of viable cells in the transfected well divided by the number of viable cells in the untransfected well.

2.9. Complexation of all the diblock and triblock copolymers (AcEMA-LauMA-AnMMA) with Metal Ions and Reduction in Nanoparticles.

All the diblock and triblock copolymers were complexes with three different metals ions (Au, Pd and Ni) and then reduction in nanoparticles. The way to complexes a polymer with Au is different from the way to complexes polymer with Pd or Ni.

2.9.1. Complexes with Au Metal Ions.

A polymer (diblock or triblock) (40 mg, 0.028 mmol of AcEMA units) was dissolved in chloroform (10 mL) followed by the addition of triethylamine (3.9 μL , 0.0386

μmol), after polymer dissolution completed. Then, the resulting solution was transferred in a glass vial containing $\text{HAuCl}_4 \cdot 3\text{H}_2\text{O}$ (1.1 mg, 2.79 μmol) and left to stir at room temperature until the solubilisation of the salt finished. The reduction of Au(III) ions to Au(0) was accompanied by a colour change of the solution from colorless to pink.

2.9.2. Complexes with Pd or Ni Metal Ions.

A polymer (copolymer or terpolymer) (20 mg, 0.014 mmol of AcEMA units) was dissolved in chloroform (5 mL). After the polymer dissolution finished, triethylamine (1.97 μL , 0.14 μmol) was added in the reaction and it was transferred in a glass vial containing $\text{Ni}(\text{CH}_3\text{OO})_2 \cdot 4\text{H}_2\text{O}$ (2.5 mg, 0.1 μmol). Finally, hydrazine monohydrate was added to the solution upon stirring. The solution was left to stir at 40 °C, in reflux, until the solubilisation of the salt finished. The reduction of Pd(II) ions to Pd(0) was accompanied by a colour change of the solution from orange to brown and Ni(II) ions to Ni(0) was changed from colourless to yellow.

2.10. Preparation of the Metal-end-linked Polymer Conetworks with $\text{Pd}(\text{CH}_3\text{COO})_2$ or $\text{HAuCl}_4 \cdot 3\text{H}_2\text{O}$.

A typical procedure for the preparation of a Pd-bearing copolymer nanohybrid is provided below. The particular example concerns the use of the $\text{AcEMA}_{12.5}\text{-}b\text{-LauMA}_{100}\text{-}b\text{-AcEMA}_{12.5}$ triblock copolymer together with $\text{Pd}(\text{CH}_3\text{COO})_2$. In a glass vial, 0.2 g (0.0066 mmol) of polymer was dissolved in 0.4 mL of THF and then 24 μL of Et_3N (17 mg, 0.17 mmol) was added. In another glass vial, 19 mg (0.085 mmol) of $\text{Pd}(\text{CH}_3\text{COO})_2$ was dissolved in 0.1 mL of THF. The polymer solution was added in to the solution of $\text{Pd}(\text{CH}_3\text{COO})_2$. The mixture was vigorously stirred for a few seconds, and 3 μL (0.085 mmol) of hydrazine monohydrate was subsequently added to it. The same method was also followed for the synthesis of all Au-end-linked ABA triblock copolymers but without the last step involving the addition of hydrazine monohydrate. Gel formation was observed after 1 day.

CHAPTER 3: RESULTS AND DISCUSSION

In this PhD Thesis, we worked on preparation and study of six families of polymer:

- (a) two groups of amphiphilic polymer conetworks (DMAEMA-MMA),
- (b) a family of degradable hydrophobic polymer networks,
- (c) a group of oligoamine-grafted glycidyl methacrylate linear and star homopolymers,
- (d) a family with metal-bearing nanoparticles from the chelation-driven self-assembly of diblock co- and ter-polymers,
- (e) a family with metal-end-linked polymer conetworks from the chelation-driven self-assembly of ABA triblock copolymers, and, finally
- (f) a AcEMA₅₀-*b*-DMAEMA₂₀₀ copolymer with the polyAcEMA and polyDMAEMA blocks being capable of complexing metals and genetic materials, respectively.

Figure 3.1 displays all six of these polymer and polymer network families, the type of bonding in each case and some of the results in each family.

The amphiphilic copolymer networks (EGDMA-MMA-DMAEMA-EGDMA), the MMA homopolymer networks with degradable ketal cross-linker (DMOEP) and the glycidyl methacrylate star polymer (Gly₂₀-*star*) were all synthesized using GTP. RAFT polymerization was used for the synthesis of the diblock co- (AcEMA-LauMA) and ter- (AcEMA-LauMA-AnMMA) polymers, the ABA triblock copolymers (AcEMA-LauMA-AcEMA) and the AcEMA₅₀-*b*-DMAEMA₂₀₀-*linear* diblock copolymer.

GPC and NMR spectroscopy were used to confirm successful synthesis of monomers, crosslinker (DMOEP), all soluble polymers (star and linear), as such, were used for the calculation of molecular weight and monomer's conversions. Furthermore, the degrees of swelling of the networks at different total solids concentrations, different pH, different solvents or different temperatures were determined. MALDI-TOF was employed to identify the various species constituting the oligomeric EGDMA cores of the star polymers. The compressive stress and strain at break of the amphiphilic polymer conetworks was also determined. Nanophase separation within the amphiphilic polymer conetworks was investigated using SANS, AFM and polarized microscopy, whereas lamellar mesophase with long-range order was observed for the

EGDMA₁-*b*-MMA₃₀-*b*-DMAEMA₁₀-*b*-EGDMA₁ conetwork. All networks bearing the degradable ketal crosslinker were hydrolyzed under mildly acidic conditions and the products were characterized in terms of their size and composition using GPC and NMR spectroscopy. Characterization of the network hydrolysis products indicated that their size was not always the expected.

All three GMA homopolymers, GMA₂₀-*star*, GMA₁₀₀-*star* and GMA₁₀₀-*linear*, were derivatized with the five oligoamines, EDA, DETrA, TrETA, TEPA and PEHA and the AcEMA₅₀-*b*-DMAEMA₂₀₀-*linear* was complexed with Au. Then, all the oligoamine-grafted glycidyl methacrylate homopolymers and AcEMA₅₀-*b*-DMAEMA₂₀₀-Au star copolymer were evaluated for their ability to deliver to C2C12 mouse myoblast cells *plasmid*-DNA which expressed the Luc gene and for cytotoxicity. We have shown that the odd-even effect is also in action in totally abiotic systems. With the exception of the PEHA-grafted polymers, all oligoamine-grafted star homopolymers presented higher, albeit moderate, transfection efficiencies when the oligoamine-grafts possessed an even number of nitrogen atoms than an odd number. The odd-even effect was also observed for the cytotoxicity of the oligoamine-grafted GMA₁₀₀-*linear* and oligoamine-grafted GMA₁₀₀-*star* homopolymers, while the cytotoxicity for the oligoamine-grafted GMA₂₀-*stars* slightly increased with the number of ethylene imine repeating units. Also, recording AcEMA₅₀-*b*-DMAEMA₂₀₀-*linear*, we observed that Luc expression was high (1.35×10^6) using only the linear copolymer, without Au, but it tripled (4.0×10^6 at 15 μ L) when the copolymer was previously complexed with Au, without an increase in cytotoxicity.

The stabilization of nanoparticles was studied in different organic solvents (*n*-hexane, cyclohexane, benzene, CHCl₃), after the combination of all the AcEMA-LauMA and AcEMA-LauMA-AnMMA polymers with three different metal ions (Au, Pd, Ni). The size of the Au and Pd crystallites in the Au- and Pd-end-linked polymer conetworks were determined using *p*-XRD and the diameter of the nanoparticles using TEM.

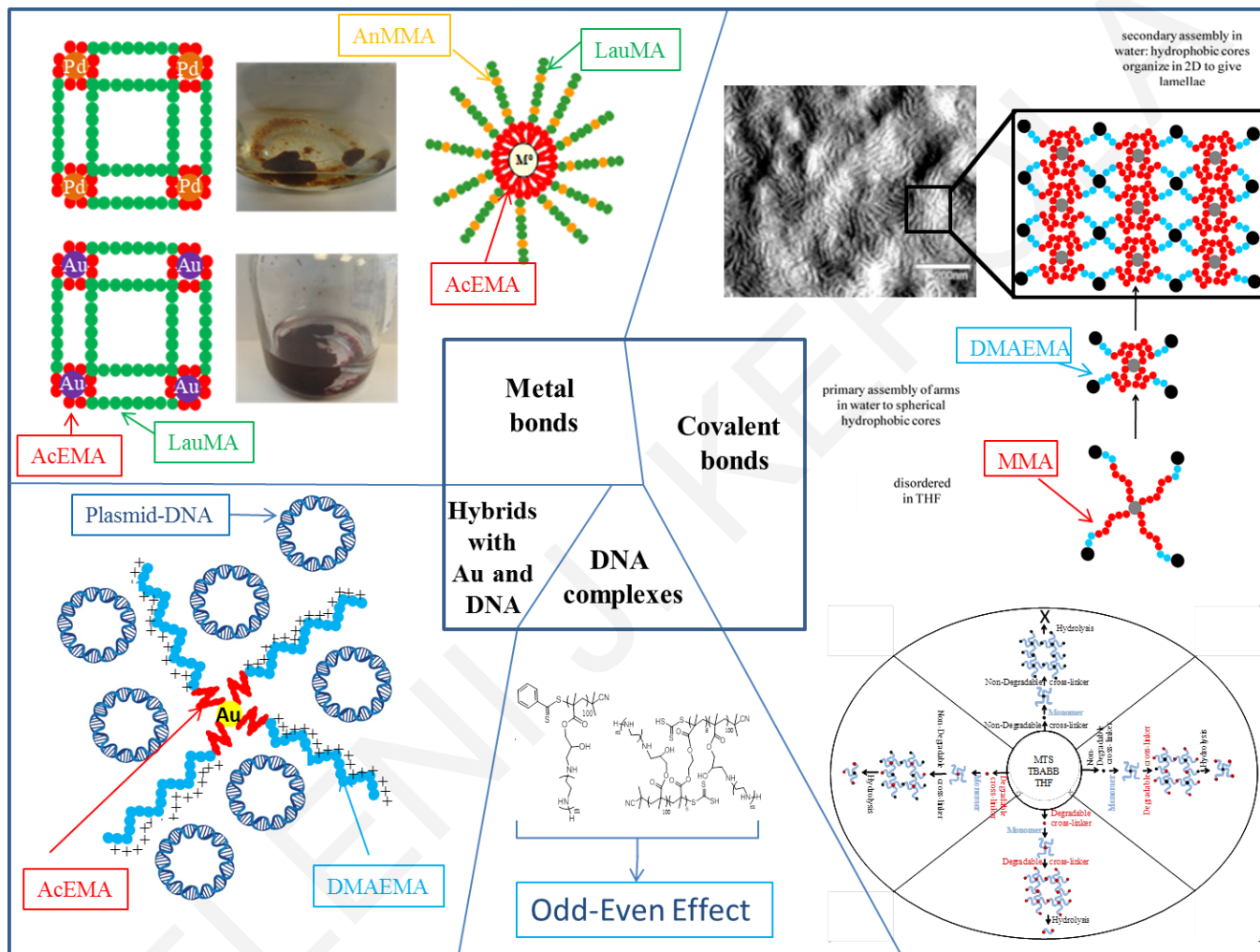


Figure 3.1. Graphical representation of the various projects under taken in this PhD Thesis.

3.1. Amphiphilic Polymer Conetworks Based on End-Linked “Core-First” Star Block Copolymers: Structure Formation with Long-Range Order.^a

In this first section, we present, the one-pot preparation of APCNs comprising end-linked amphiphilic “core-first” star block copolymers that self-organize, some forming lamellae with long-range order, as evidenced by microscopy and scattering. To the best of our knowledge, this is the first crosslinked polymer system that internally assembles with such high regularity. The APCNs were prepared in the disordered state in tetrahydrofuran (THF), by the one-pot sequential group transfer polymerization (GTP, a type of oxyanionic polymerization) of crosslinker (EGDMA), hydrophobic monomer (MMA), hydrophilic comonomer (DMAEMA), and again crosslinker, as illustrated in Figure 3.2. The chemical structures of the monomers and crosslinker are also shown in the figure. A “core-first” amphiphilic star block copolymer was produced after the third step of the synthetic procedure, which was end-linked at the final addition step, yielding the APCN.

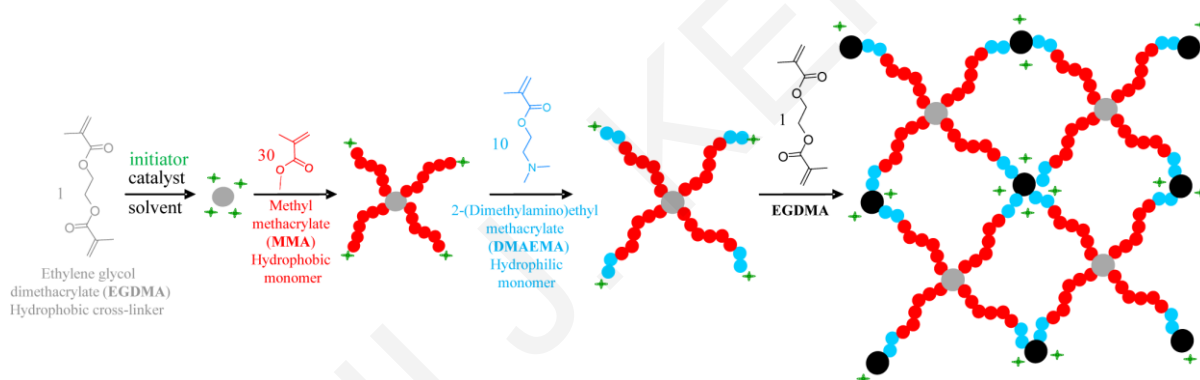


Figure 3.2. Schematic representation of the procedure followed for APCN preparation *via* sequential GTP.

This work concerns eight (co)networks based on end-linked “core-first” star (co)polymers, six of which were amphiphilic star block copolymers of DMAEMA (ionizable hydrophilic component) and MMA (nonionic hydrophobic component), and the remaining two were the star homopolymers of DMAEMA and MMA. The overall (nominal) degree of polymerization of the arms of all the star (co)polymers was fixed to 40.

^a Reprinted with permission from *ACS Macro Letters* **2015**, *4*, 1163–1168. Copyright 2015, American Chemical Society.

The six amphiphilic star block copolymers differed in terms of their composition, with nominal MMA contents of 25, 50 and 75 mol%, and their arm architecture, covering both the MMA-DMAEMA and the DMAEMA-MMA block sequences. Simplified schematic representations of the building blocks of all (co)networks synthesized, *i.e.*, the “core-first” star (co)polymers, are illustrated in Figure 3.3 below.

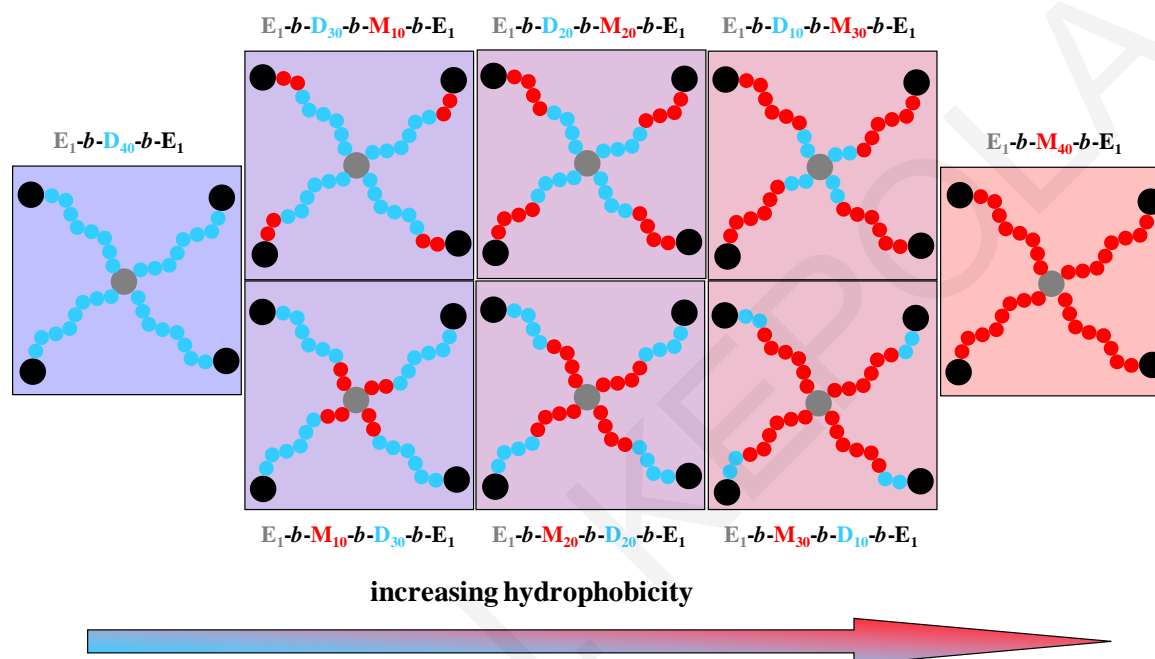


Figure 3.3. Schematic representations of the “core-first” star (co)polymer building blocks, precursors to the eight (co)networks. E, M and D are further abbreviations for EGDMA, MMA and DMAEMA, respectively. The hydrophobic MMA units are shown in red, the hydrophilic DMAEMA units are presented in light blue, the first EGDMA cores are displayed in grey, and the second EGDMA cores are painted black.

3.1.1. GPC Traces of the Star (Co)polymers.

GPC was employed to analyze the molecular weight distributions of all the soluble precursors to the (co)networks, *i.e.*, the EGDMA core oligomers, the “core-first” star homopolymers, and the “core-first” star block copolymers. The GPC traces of all these precursors are displayed in Figure 3.4. The molecular weight distributions were very heterogeneous, as the GPC traces of all precursors were bimodal or even trimodal, manifesting the presence of populations with two or three different sizes. This heterogeneity arose from the bifunctionality of the EGDMA cross-linker (two vinyl groups available for addition

reactions), which, at the employed 1 : 1 molar ratio of EGDMA to the MTS initiator, allowed the generation of a multitude of species to constitute the core of the star polymer (see results on core oligomer analysis using MALDI-TOF in Figure 3.5). Despite the heterogeneities, after each subsequent monomer addition, the distributions were shifted to earlier elution times, corresponding to higher molecular weights, as expected.

ELENI J. KEPOLA

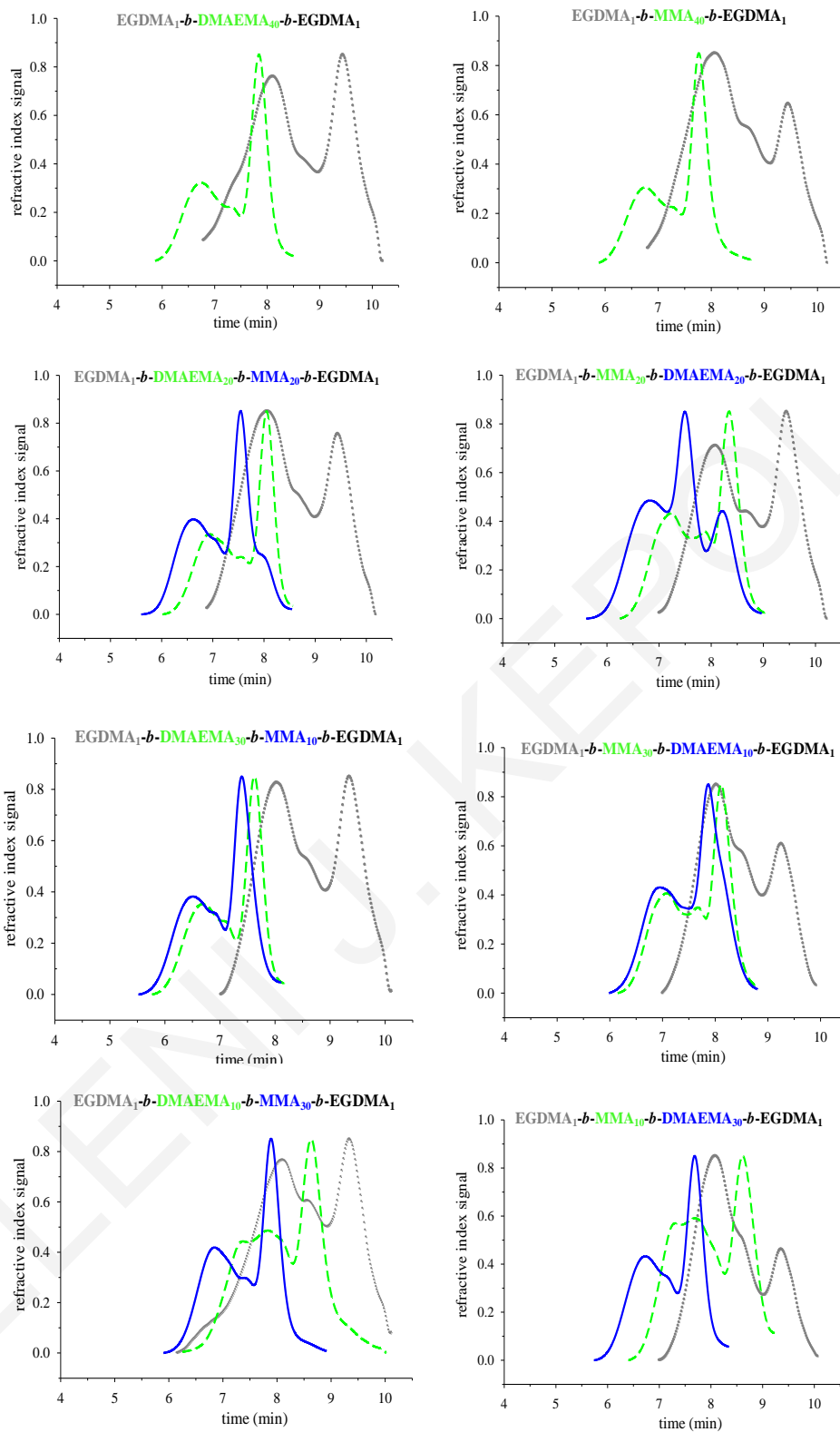


Figure 3.4. GPC traces of all the soluble precursors to the (co)networks based on the end-linked “core-first” star (co)polymers. The traces for the EGDMA core oligomers, the “core-first” star homopolymers, and the “core-first” star block copolymers are shown in grey dotted lines, in light green dashed lines, and in blue continuous lines, respectively.

3.1.2. Molecular Weights and Compositions of the Star (Co)polymers.

From these GPC traces, the molecular weights (the number-average molecular weights, M_n , and the peak molecular weights, M_p) and the molecular weight dispersities, relative to linear PMMA standards, were calculated and are listed in Table 3.1 together with the star block copolymer compositions (in terms of the mol% content in DMAEMA units) calculated using ^1H NMR spectroscopy. The first column under the GPC results lists the M_p values. As mentioned above, each sample had two or three peaks, corresponding to two or three M_p values. Regarding the cores, the M_p values for the two main peaks were typically 800 and 8000 g mol^{-1} , with the third peak presenting an M_p value intermediate between those of the two main peaks, around 2000 g mol^{-1} , and this peak not being very intense, resembling almost a shoulder rather than a clear peak. The overall molecular weight distributions of the core exhibited M_n and D values of typically around 1400 g mol^{-1} and 5.0, respectively. Regarding the final star (co)polymers, the M_p values for the two main peaks were typically 10000 and 80000 g mol^{-1} , with the third peak being again subtle, and presenting an M_p value of around 25000 g mol^{-1} . The overall molecular weight distributions of the final star (co)polymers exhibited M_n and D values of around 20000 g mol^{-1} and 2.5, respectively. The much lower molecular weight dispersities of the final star (co)polymers as compared to those of the initial EGDMA oligomer cores might be attributed to the increased steric hindrance in the former structure, conferred by the newly-formed arms which rendered star-star coupling more difficult. Finally, the table shows that the experimentally (by ^1H NMR spectroscopy) determined DMAEMA content in the star copolymers was very close to the one expected on the basis of the comonomer feed ratio.

Table 3.1. Molecular weight (relative) and composition characteristics of the soluble precursors to the (co)networks based on end-linked “core-first” star (co)polymers.

Network Number	Polymer Structure	GPC Results			DMAEMA (mol%)	
		M_p (g mol ⁻¹)	M_n (g mol ⁻¹)	\bar{D}	Theory	¹ H NMR
1	EGDMA ₁	700 6800	1300	5.99	-	-
	EGDMA ₁ - <i>b</i> -DMAEMA ₄₀	10900 26100 76800	16800	2.63	100	100
2	EGDMA ₁	600 1500 7400	1400	5.96	-	-
	EGDMA ₁ - <i>b</i> -MMA ₄₀	12600 28500 74600	15700	2.72	0	0
3	EGDMA ₁	600 2300 8600	1200	5.03	-	-
	EGDMA ₁ - <i>b</i> -MMA ₂₀	4500 10600 32000	7400	2.85	0	0
	EGDMA ₁ - <i>b</i> -MMA ₂₀ - <i>b</i> -DMAEMA ₂₀	5700 20100 66400	13800	3.23	50	46
4	EGDMA ₁	600 1700 7400	1400	5.46	-	-
	EGDMA ₁ - <i>b</i> -DMAEMA ₂₀	7700 17800 59100	12200	2.52	100	100
	EGDMA ₁ - <i>b</i> -DMAEMA ₂₀ - <i>b</i> -MMA ₂₀	18400 42800 94300	21900	2.60	50	47
5	EGDMA ₁	800 1900 7900	1400	4.40	-	-
	EGDMA ₁ - <i>b</i> -DMAEMA ₃₀	15900 38100	24500	2.21	100	100

		83900				
	EGDMA ₁ - <i>b</i> -DMAEMA ₃₀ - <i>b</i> -MMA ₁₀	23900 54100 112000	33000	2.26	75	74
6	EGDMA ₁	800 1800 8400	1600	4.11	-	-
	EGDMA ₁ - <i>b</i> -DMAEMA ₁₀	1100 10200 30200	4300	3.09	100	100
	EGDMA ₁ - <i>b</i> -DMAEMA ₁₀ - <i>b</i> -MMA ₃₀	10000 21900 62600	15000	2.61	25	24
7	EGDMA ₁	900 2100 8100	2000	3.47	-	-
	EGDMA ₁ - <i>b</i> -MMA ₃₀	6800 15000 41600	10000	2.62	0	0
	EGDMA ₁ - <i>b</i> -MMA ₃₀ - <i>b</i> -DMAEMA ₁₀	10500 53000	11900	2.76	25	24
8	EGDMA ₁	800 7200	1600	4.40	-	-
	EGDMA ₁ - <i>b</i> -MMA ₁₀	2800 11900 32900	5400	2.88	0	0
	EGDMA ₁ - <i>b</i> -MMA ₁₀ - <i>b</i> -DMAEMA ₃₀	27600 76800	20400	2.74	75	75

3.1.3. Average Number of Arms in Star Polymers.

To determine the absolute weight-average molecular weight, M_w , of the star polymers, static light scattering (SLS) was performed on a particular star sample. To secure sufficient sample quantity, the synthesis of star homopolymer number 2 (“core-first” star MMA homopolymer, EGDMA₁-*b*-MMA₄₀) was repeated, but without performing the final EGDMA addition (which would have led to gel formation). The thus-produced star polymer was characterized using SLS in THF. From the constructed Zimm plot, an M_w value of 885 000 g mol⁻¹ was determined, which corresponded to 206 (= 885 000 g mol⁻¹ / 4 299 g mol⁻¹) arms; 4 299 g

mol^{-1} is the nominal molecular weight of a linear arm comprising 40 MMA monomer repeating units ($40 \times 100 \text{ g mol}^{-1} = 4\,000 \text{ g mol}^{-1}$), one EGDMA unit (198 g mol^{-1}), and one MTS initiator unit after removal of the trimethylsilyl group (101 g mol^{-1}). It is pointed out that this is the average number of arms in the multimodal distribution. The number of arms in the higher-molecular weight peak may reach even higher values.¹²⁸

3.1.4. Extractables from the (Co)networks.

Table 3.2. summarizes the percentage, composition and molecular weight characteristics of the extractables from the (co)networks. The percentage of the extractables (sol fraction) ranged between 15 and 30 wt.%. The relatively low percentage of extractables (<50%) demonstrated the rather successful incorporation of the star building block into the networks. The M_n values of the extractables, shown in Table 3.2, in all cases, except for the homopolymer ($E_1-b-D_{40}-b-E_1$) network and $E_1-b-M_{20}-b-D_{20}-b-E_1$, were lower than their star polymers (Table 3.2) which can be attributed to the early deactivation of the stars which subsequently could not be integrated into the networks.

Table 3.2. Characteristics of the extractables from the amphiphilic polymer conetworks of this study, including their sol fraction, composition and molecular weight.

Chemical Structure of APCN ¹	Percentage (wt.%)	¹ H NMR Spectroscopy Results (MMA, mol%)	GPC Results	
			M_n (g mol^{-1})	\bar{D}
$E_1-b-M_{40}-b-E_1$	24.4	23.7	11400	1.87
$E_1-b-D_{40}-b-E_1$	19.4	-	10200	2.55
$E_1-b-M_{20}-b-D_{20}-b-E_1$	22	11.7	5190	1.82
$E_1-b-D_{20}-b-M_{20}-b-E_1$	21	6.6	9910	2.86
$E_1-b-D_{30}-b-M_{10}-b-E_1$	15.4	1.4	7650	3.59
$E_1-b-D_{10}-b-M_{30}-b-E_1$	29.5	19	9680	3.96
$E_1-b-M_{10}-b-D_{30}-b-E_1$	16.6	4.6	6930	3.14
$E_1-b-M_{30}-b-D_{10}-b-E_1$	26	19.2	5310	1.67

¹ E: EGDMA, M: MMA, D: DMAEMA

3.1.5. Species Identification in the EGDMA Core.

MALDI-TOF was utilized to identify the various species constituting the oligomeric EGDMA core of the star polymers. Figure 3.5 displays the recorded mass spectrum for such a core, which indicates, in different colors, the various families of conjugates formed between the EGDMA cross-linker and the MTS initiator (indicated as “I” in the figure). The prevalent families of conjugates, in decreasing abundance, are: I_2 -EGDMA_x ($x = 2 - 5$), I_3 -EGDMA_x ($x = 2 - 8$), I_4 -EGDMA_x ($x = 5 - 8$), I_5 -EGDMA_x ($x = 8 - 13$), and I_6 -EGDMA_x ($x = 12 - 13$). This plethora of species is due to the low molar ratio of EGDMA to MTS (= 1 : 1) on the one hand, and on the other hand due to the existence of two olefinic groups in EGDMA. It will be shown later that this size heterogeneity in the core, which is passed on to the star polymers in the form of a multimodal distribution in the numbers of arms, does not interfere with microphase separation within the conetworks in water. Microphase separation is apparently more influenced by the arm length and composition, both of which are highly homogeneous.

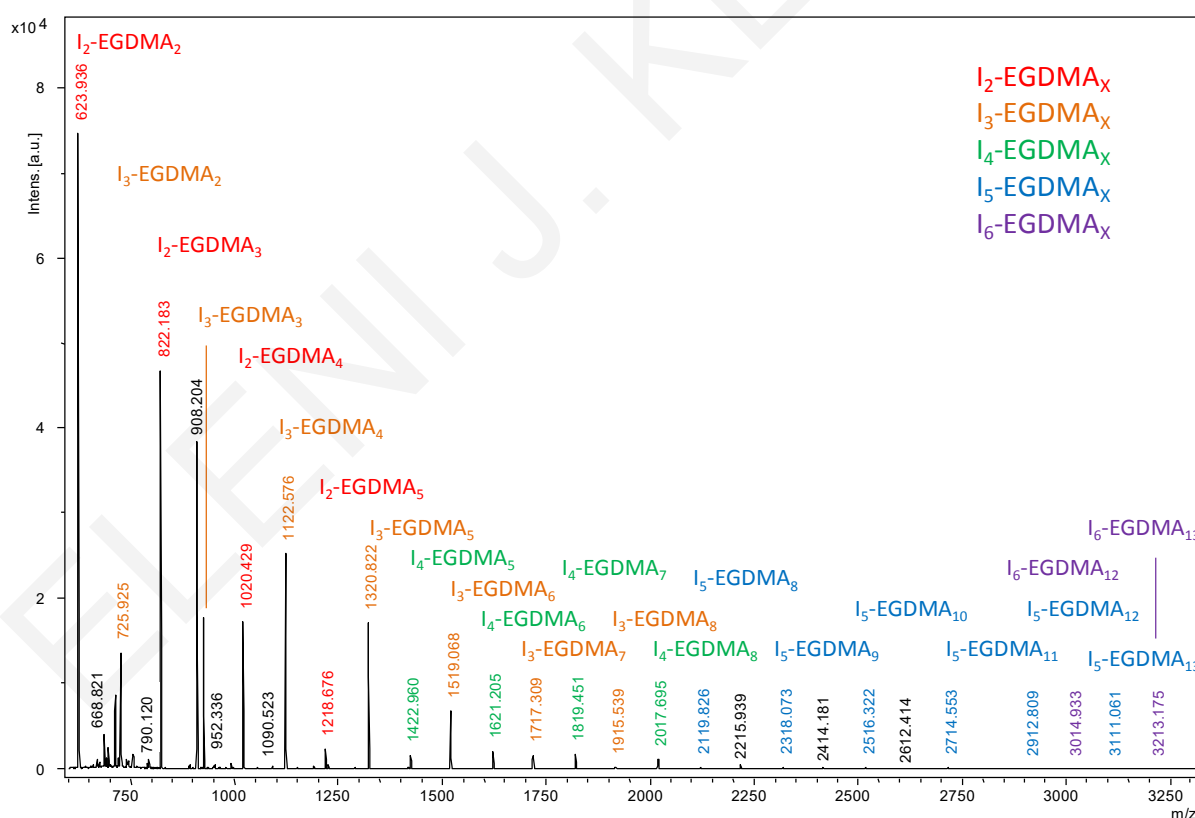


Figure 3.5. MALDI-TOF spectrum of the EGDMA oligomeric core of a star polymer, involving various conjugates of EGDMA with the MTS initiator (I).

3.1.6. Effect of pH on the Aqueous Degrees of Swelling.

The degrees of swelling (DS) of all the (co)networks were measured in water within a supernatant solution pH range between 2 and 12. At each pH, the degree of ionization (DI) of the DMAEMA units was calculated from the amount of HCl added relative to the number of DMAEMA units present in each sample. The results are presented in Figure 3.6 for all (co)networks, in which DS (left-hand-side y-axis) and DI (right-hand-side y-axis) are plotted against the supernatant solution pH. As swelling was driven by the ionization of the DMAEMA units, the swelling curves followed the ionization curves, consistent with previous studies of others^{39,129} and our own¹¹⁹. Thus, the DSs were low at pH values above 7 where the DMAEMA units were not ionized; whereas they increased rather abruptly at pH values below 7 where the DMAEMA units started to get ionized (the effective p*K* value of the DMAEMA units within the networks is about 7).

Ionization of the DMAEMA units favors network swelling via two mechanisms: (a) the increase in the osmotic pressure established by the chloride counteranions accumulated to balance the positive charge of the DMAEMA units, and (b) the electrostatic repulsions between the positively charged polymer chains. The decrease in the DSs of the (co)networks at pH values below 2 probably arose from charge screening in the conetworks, due to the high ionic strength of the solution imparted by the relatively high concentration of HCl present in this very acidic environment.

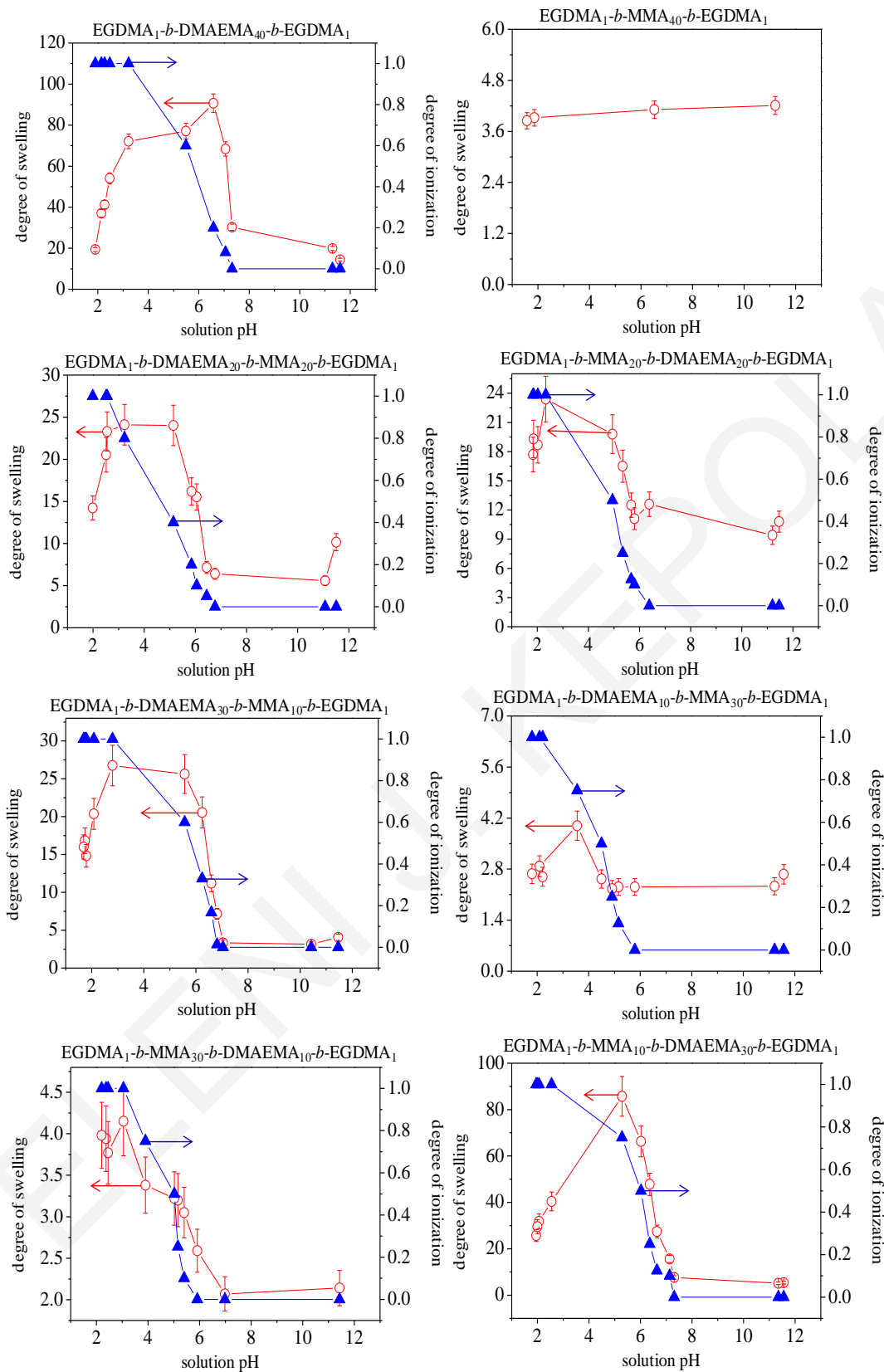


Figure 3.6. pH-Dependence of the swelling and ionization degrees of all the (co)polymer (co)networks.

3.1.7. Effect of (Co)polymer Composition and Architecture on the Degrees of Swelling.

To examine the effect of conetwork composition and architecture on the DSs, the DSs of all (co)networks at some characteristic conditions are plotted in Figure 3.7. These characteristic conditions were swelling maximum of the charged gel in low pH water (between pH 2.5 and 5.5, taken from Figure 3.6), low DS of the uncharged gel in pure water (pH between 6 and 7, again extracted from Figure 3.6), and in THF (uncharged gels). In Figure 3.7, the DSs are plotted against conetwork composition (DMAEMA mol%), with conetwork architecture indicated through the use of open (MMA-*b*-DMAEMA) or closed (DMAEMA-*b*-MMA) symbols. The DSs in pure and in acidified water increased as the DMAEMA content increased. In particular, the DSs in low pH water increased from about 4 up to 90 as the DMAEMA content increased from 0 to 100 mol%. These DSs were higher compared to those in pure water and in THF because of the full ionization of the DMAEMA units at acidic pH. Comparing the effect of polymer architecture on the DSs in water, both pure and acidic water, all conetworks with MMA-*b*-DMAEMA (M-D) architecture swelled more than those with DMAEMA-*b*-MMA (D-M) architecture, indicating better hydration in the former case.

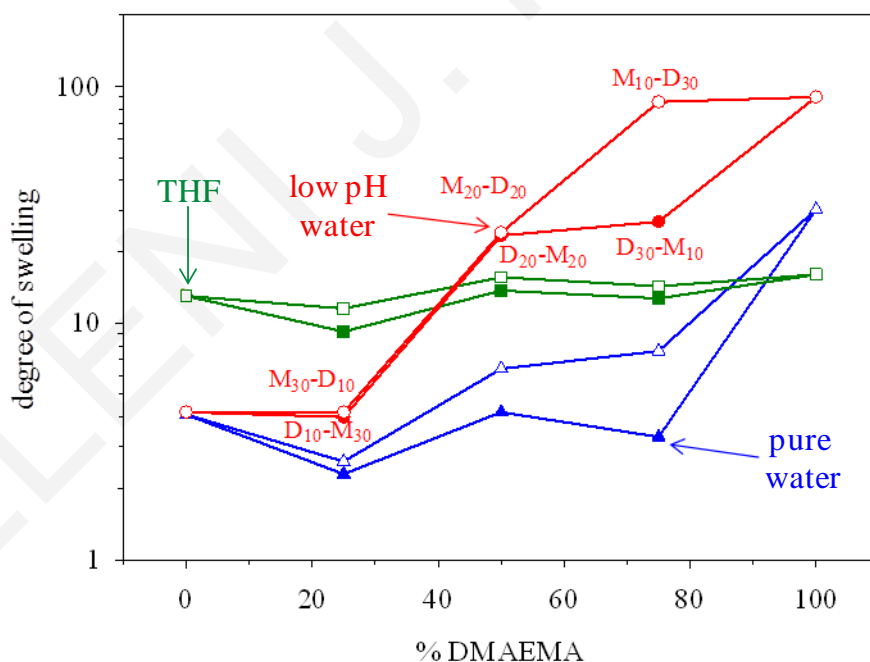


Figure 3.7. Degrees of swelling of all the (co)polymer (co)networks in pure (blue) and in acidic (red) water, and in THF (green), plotted against (co)network composition for the two (co)network architectures: MMA-*b*-DMAEMA (open symbols) and DMAEMA-*b*-MMA (closed symbols). M is MMA and D is DMAEMA.

3.1.8. Structure of the Conetworks in the Bulk and in Water.

The self-organization of the APCNs in the dry and the D₂O-swollen states was investigated using AFM and SANS, respectively, whereas the presence of anisotropic phases in the water-swollen conetworks was examined *via* polarized light microscopy.

3.1.8.1. Structure in the Bulk.

AFM images before thermal annealing. Figure 3.8 shows the AFM phase images of all the (co)networks of this study after being vacuum dried (at room temperature) from THF. All images displayed a grainy structure, with the grain size increasing with the polyMMA content, from *ca.* 15 to 70 nm. The DMAEMA homopolymer network (Sample 1) presented almost no grain features, the DMAEMA-rich APCNs, Samples 5 and 8, exhibited some more grainy structure, and the equimolar and MMA-rich conetworks displayed more grainy features. The MMA homopolymer network, Sample 2, showed the most intense grainy structure, with the largest spheroidal grains having a size of about 70 nm, much larger than the contour length of the arms of the stars of 10 nm (40 units \times 0.252 nm per monomer repeating unit¹³²).

Furthermore, since this network was not expected to form any thermodynamically stable structure, it was concluded that the structure obtained was due to the glassy nature of polyMMA (glass transition temperature, T_g , of about 100 °C). This may also imply that the grainy structure in the images of the other samples was due to the frozen polyMMA segments as well.

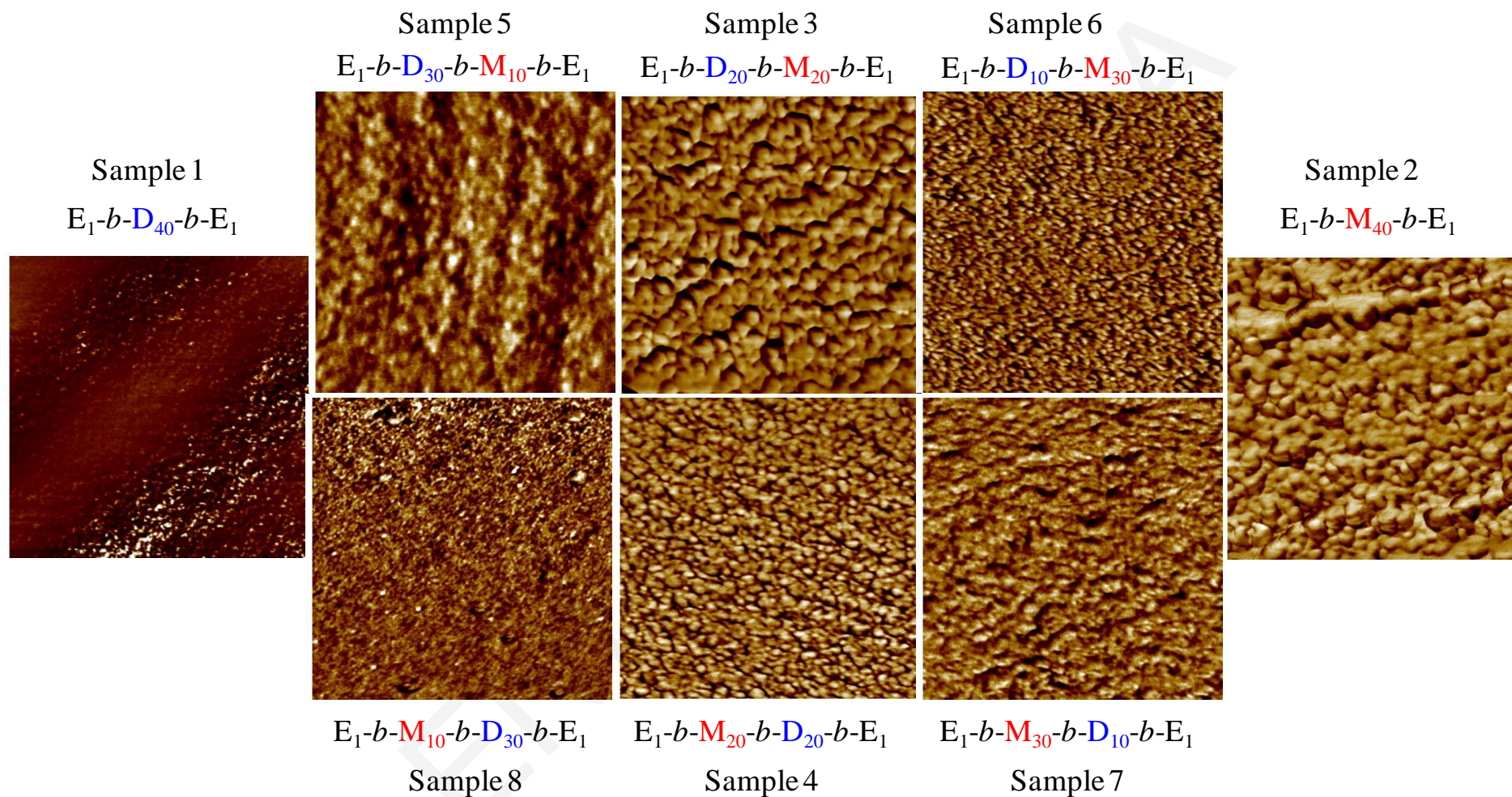


Figure 3.8. Atomic force microscopy phase images of all the (co)networks of this study in the bulk before thermal annealing. Image dimensions are 1000 nm × 1000 nm. E is EGDMA, D is DMAEMA and M is MMA.

AFM images after thermal annealing. To investigate this hypothesis, we thermally treated all (co)network samples by leaving them overnight in a vacuum oven at 105 °C, a temperature above the T_g of polyMMA, in order to allow the polyMMA segments to equilibrate (the T_g of the polyDMAEMA segments is much lower, 0 – 20 °C), and then letting them to slowly cool down to attain their lowest energy configuration. The AFM phase images of the thus-thermally annealed (co)networks are presented in Figure 3.9. These images largely differ from those of the untreated samples, as most of them lost their grainy structure; exceptions were the DMAEMA-rich ones (Samples 5 and 8) which exhibited a less grainy initial (before annealing) structure due to their low MMA content. The most striking change concerned the MMA homopolymer network which, after thermal annealing, became essentially featureless, confirming the hypothesis that the grainy structure was due to the glassy polyMMA segments. An equally important change occurred in Sample 7, whose grainy structure was transformed to lamellae with long-range order and a spacing of 15 nm. To our knowledge, this is the first well-defined morphology observed with APCNs synthesized and cross-linked in the disordered state. Sample 6 which is the architectural isomer of Sample 7 (also MMA-rich but with the reverse star block architecture) also underwent a dramatic morphological transformation upon thermal annealing but did not give lamellae; instead, it gave a structure with a rather short range order, with features intermediate between spheres and cylinders. The difference in the morphologies exhibited by annealed Samples 6 and 7 highlights the importance of molecular architecture on the phase behavior of APCNs. Equimolar Sample 3 displayed a similar morphology to Sample 6 but with less order. Samples 4, 5 and 8 presented smaller structural features and even shorter-range order.

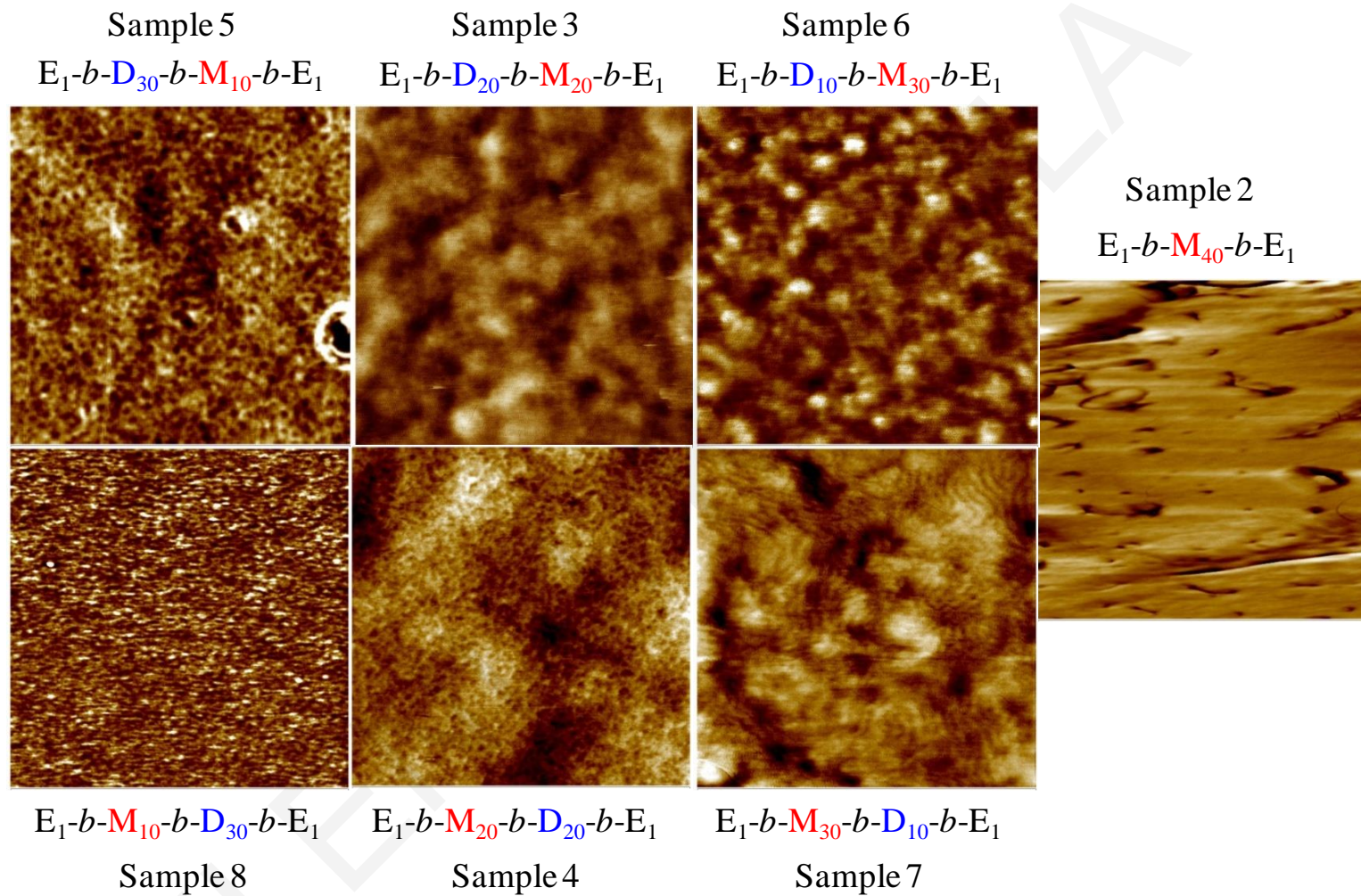


Figure 3.9. Atomic force microscopy phase images of all the (co)networks of this study in the bulk, after thermal annealing at 105 °C. Image dimensions are 500 nm × 500 nm. E is EGDMA, D is DMAEMA and M is MMA.

An even clearer, highly-ordered lamellar structure was obtained by imaging Sample 7 under water, as shown in Figure 3.10. The lamellar morphology with long-range order exhibited by Sample 7 is in agreement with theory and experiments on linear diblock copolymers with components of mild mutual incompatibility such as the two methacrylates involved here, DMAEMA and MMA. In particular, the composition of the present system is 24 mol% in DMAEMA, which corresponds to 33 wt.%, which is just above the cylinder-to-lamella transition boundary of 32 wt.% in the morphology phase diagram for linear diblock copolymers.¹³⁰

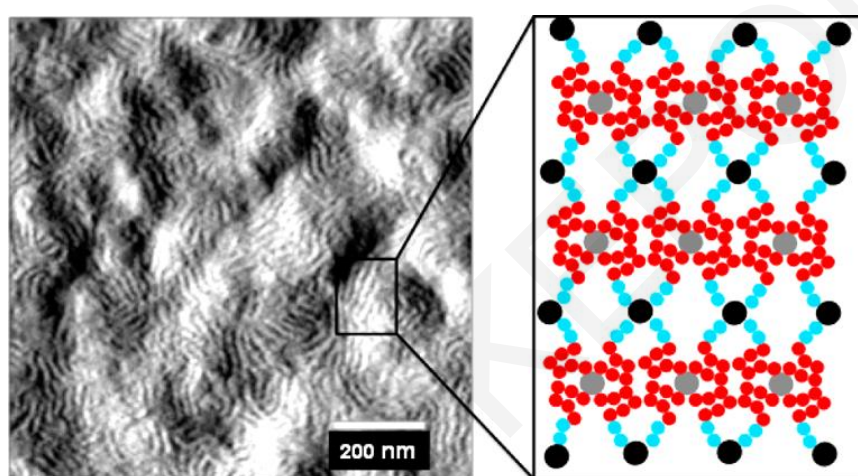


Figure 3.10. Structure formation with long-range order exhibited by Sample EGDMA₁-*b*-MMA₃₀-*b*-DMAEMA₁₀-*b*-EGDMA₁ in water, as observed using AFM (phase mode). Secondary assembly in water: hydrophilic cores organized in 2D to give lamellae.

However, this comparison is made with the reservation that the morphology of a linear block copolymer system may not be the same as that exhibited by the corresponding interlinked star block copolymer system, because polymer architecture also has an important effect on copolymer morphology. For instance, end-linked conetworks based on ABA triblock copolymers¹³¹⁻¹³² and melts of (non-interlinked) star block copolymers¹³³ have phase diagrams different from that of the corresponding linear diblock copolymer, as a result of the restriction of the configurational space accessible by the chains, imposed by the presence of crosslinks. Nonetheless, the morphology observed here for conetwork Sample 7 coincides with that for the corresponding linear diblock copolymer. Furthermore, it is also important to stress that this morphology is only obtained after thermal processing. Thus, conetworks

formed by the crosslinking of block copolymer systems appear to be able to access the classical diblock copolymer morphologies, provided appropriate annealing is performed.

3.1.8.2. Structure in Solution.

Following the characterization of the structure of the APCNs in the solid state, we proceeded to the characterization of their structure in equilibrium swelling in D₂O using SANS. In all of these experiments, the DMAEMA units in the (co)networks were practically uncharged as no acid was added (aqueous pH between 5.5 and 7.5, depending on conetwork composition, with the more hydrophobic conetworks presenting the lower pH values and the more hydrophilic the higher). The first experiments were performed without thermal annealing and the obtained SANS profiles of all (co)networks are plotted in Figure 3.11, whereas the SANS profiles of the thermally treated (at 105 °C in a vacuum oven overnight) samples are displayed in Figure 3.12.

Figure 3.11 shows that the six non-annealed APCNs exhibited a correlation peak at intermediate q -values, indicating microphase separation, a result of the presence of long enough polyMMA hydrophobic segments within the amphiphilic material. These q -values at the intensity maxima, q_{max} , ranged between 0.022 and 0.043 Å⁻¹, corresponding to spacings between the scattering centers ($= 2\pi/q_{max}$) in the range between 29 and 15 nm, and increasing (in most cases) with the content in hydrophilic polyDMAEMA (Table 3.3), as expected. Furthermore, the MMA-rich APCN with M-D architecture (Sample 7) most interestingly exhibited a double peak, with the minor peak located at a q -value exactly twice that of the major peak, indicative of a lamellar morphology and in agreement with the AFM image of annealed Sample 7 (Figures 3.8 and 3.9). Careful inspection of all the SANS profiles would reveal that Samples 3, 4 and 5 exhibited a secondary shoulder (rather than a peak), also suggesting some longer-range order. In previous investigations of the APCN structure, SANS and SAXS sometimes revealed profiles bearing a correlation peak plus a secondary shoulder, but never a clear secondary peak, as was the case with Sample 7 in the present study.

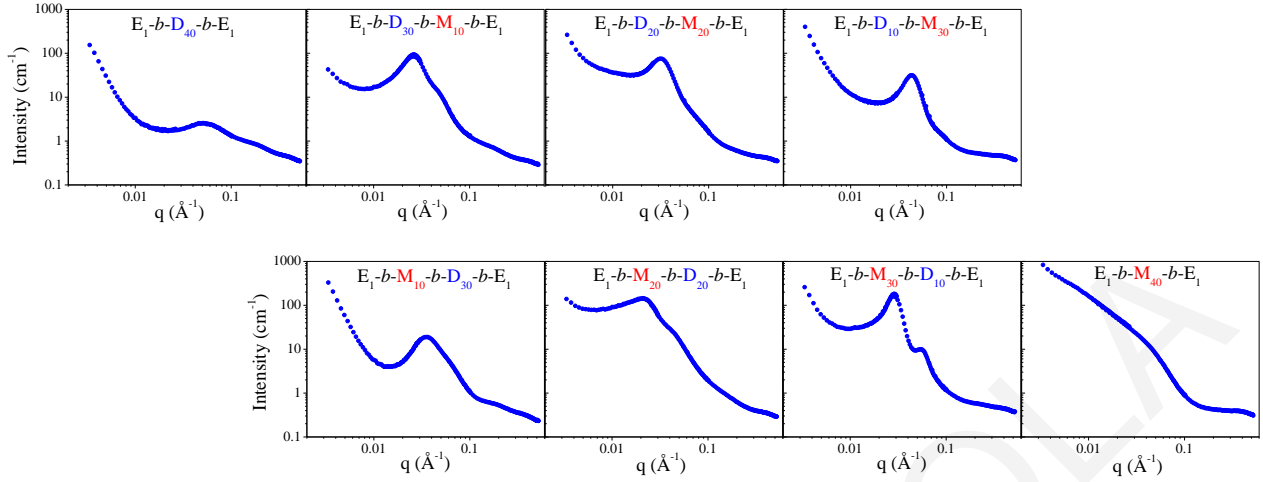


Figure 3.11. Small-angle neutron scattering profiles of the unprocessed (not thermally-annealed) (co)networks in D_2O . These data were collected at the National Institute of Standards and Technology (NIST), in Gaithersburg, Maryland in the USA. E is EGDMA, D is DMAEMA and M is MMA.

Table 3.3. Locations of peak maxima in the SANS profiles of all the (co)networks in D_2O , both before and after thermal annealing, and corresponding correlation distances.

Network number	Network structure	Not annealed samples		Annealed samples	
		q_{max} (\AA^{-1})	$2\pi/q_{max}$ (nm)	q_{max} (\AA^{-1})	$2\pi/q_{max}$ (nm)
1	EGDMA ₁ -b-DMAEMA ₄₀ -b-EGDMA ₁	0.05138	12	0.02657	24
5	EGDMA ₁ -b-DMAEMA ₃₀ -b-MMA ₁₀ -b-EGDMA ₁	0.02616	24	0.02808	22
4	EGDMA ₁ -b-DMAEMA ₂₀ -b-MMA ₂₀ -b-EGDMA ₁	0.03199	20	0.03511	18
6	EGDMA ₁ -b-DMAEMA ₁₀ -b-MMA ₃₀ -b-EGDMA ₁	0.04296	15	0.04506	14
8	EGDMA ₁ -b-MMA ₁₀ -b-DMAEMA ₃₀ -b-EGDMA ₁	0.03554	18	0.03678	17
3	EGDMA ₁ -b-MMA ₂₀ -b-DMAEMA ₂₀ -b-EGDMA ₁	0.02170	29	0.02585	24
7	EGDMA ₁ -b-MMA ₃₀ -b-DMAEMA ₁₀ -b-EGDMA ₁	0.02852	22	0.03183	20
2	EGDMA ₁ -b-MMA ₄₀ -b-EGDMA ₁	0.05438	12	0.06206	10

The DMAEMA and MMA homopolymer networks displayed only a shallow SANS peak and a long tail, respectively, a result of the lack of hydrophobic scattering centers or a consequence of inability to swell in D₂O resulting in weak scattering contrast.

Knowing from the AFM experiments that thermal treatment of the APCN samples in the bulk helped induce structure formation through equilibration, we decided to thermally anneal the (co)networks and re-run them in D₂O using SANS. The thus-acquired SANS profiles are plotted in Figure 3.12 and did not present any significant changes as compared to the profiles of untreated samples in Figure 3.11. The shapes of most SANS profiles in Figure 3.12 are identical to those in Figure 3.11; an exception to this observation was the MMA homopolymer network, whose tailing SANS profile was transformed to one with a shallow shoulder, possibly a result of the elimination of the pores in this network arising from its thermal collapse, also manifested as the disappearance of the grainy structure in the AFM images. Furthermore, the positions of q_{max} remained largely unchanged upon annealing (Table 3.3), with the observed small increase in q_{max} (corresponding to a reduction in the spacing between the scattering centers) possibly being again due to pore elimination in the polyMMA microphase. It may be noteworthy, however, that the second order peak in Sample 7 became more pronounced after thermal treatment. Thus, we may conclude that the self-assembly of APCNs in a selective solvent such as water readily attains equilibrium without the aid of thermal annealing, because the solvent facilitates equilibration.

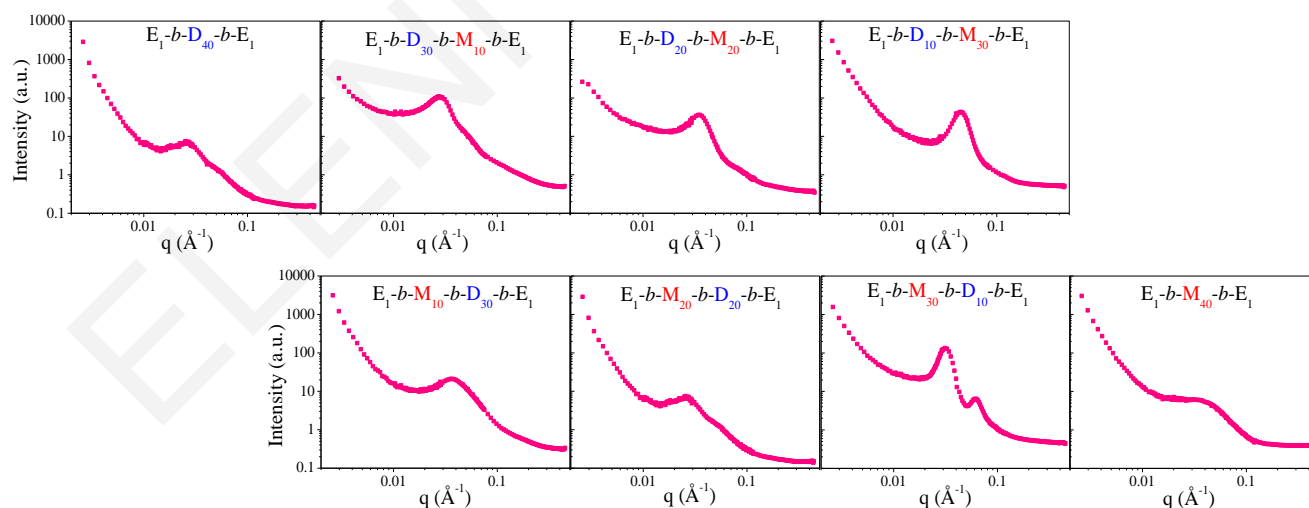


Figure 3.12. Small-angle neutron scattering profiles of the thermally-annealed (at 105 °C) (co)networks in D₂O. These data were collected at the Jülich Center for Neutron Scattering (JCNS) in Garching, Germany. E is EGDMA, D is DMAEMA and M is MMA.

3.1.9. Anisotropic Nanophases.

Self-assembly into anisotropic nanophases, such as lamellae or cylinders, leads to birefringence, a property resulting from at least one of the two nanophases exhibiting refractive indices which are different in different directions. Birefringence can be readily observed under a polarized light microscope. Because one of our samples, Sample 7, clearly exhibited a lamellar morphology (both from AFM in water and in the bulk, and from SANS in D₂O), and most of the remaining samples displayed shoulders and tails in their SANS profiles in addition to the main correlation peak, we examined all APCNs in H₂O using polarized light microscopy. Figure 3.13 shows the images from polarized light microscopy for all APCNs plus the two homopolymer networks; for these experiments, dried samples of the (co)networks were finely ground, placed on the microscope glass slide, to which one drop of deionized water was added. Four of the samples presented birefringence, as manifested by the multiple colors in the images. These were Samples 3, 5, 6 and 7, from which Sample 7 exhibited the most intense color variation, in agreement with the SANS results. It is noteworthy that the three other samples that displayed birefringence, Samples 3, 5 and 6, are the APCNs with D-M star architecture, suggesting that this architecture may favor the formation of anisotropic morphologies. The coloration in the samples clearly comes from the bulk of the ground particles and not from reflections from surface planes cut in irregular ways. Some particles exhibit clear birefringence and some other not, but this cannot be an artifact of the way the samples are ground and measured because the thickness of these samples is much larger than the lamellar order parameter. Note that the two homopolymer networks did not show any birefringence, consistent with our expectation.

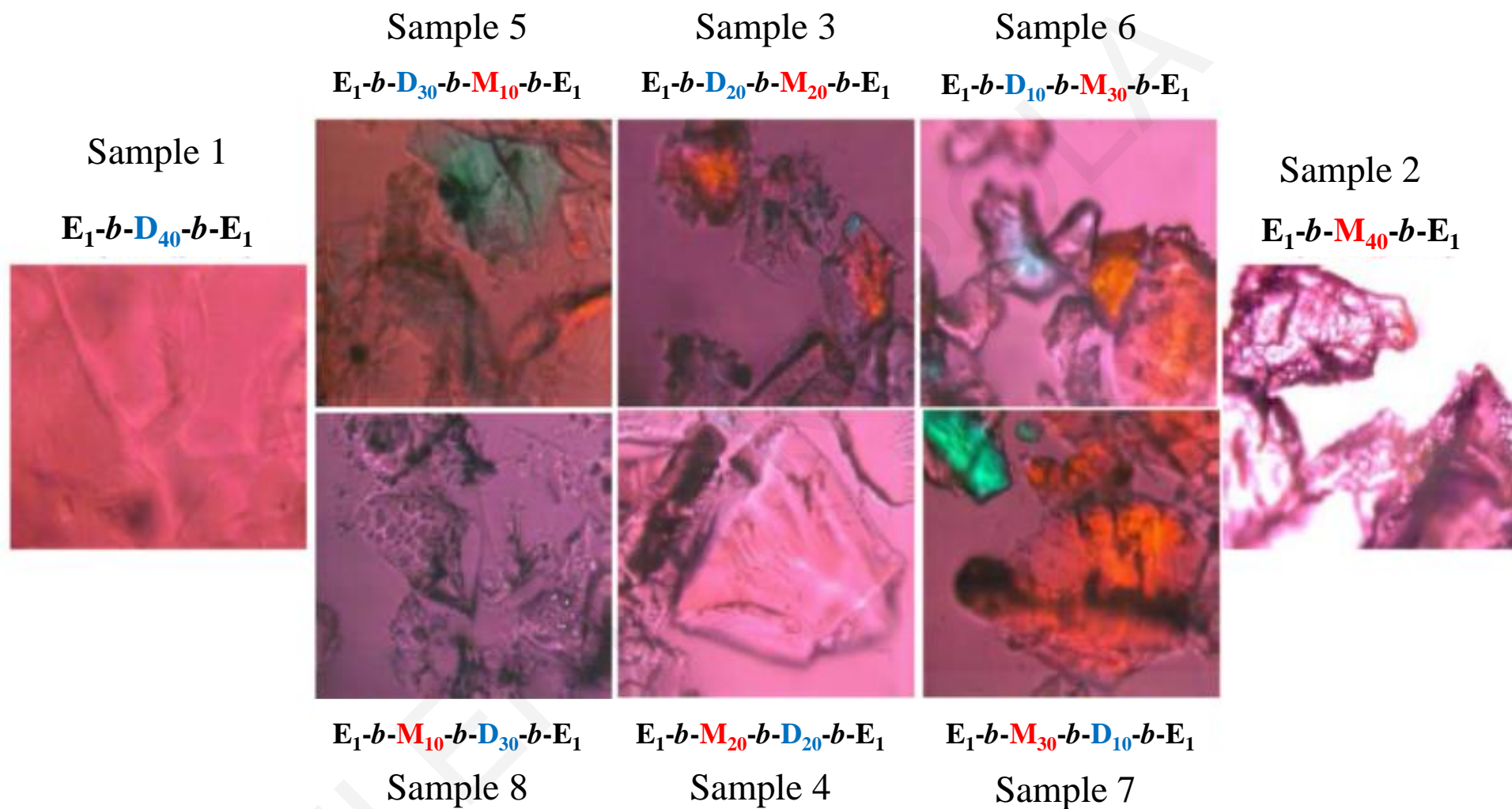


Figure 3.13. Polarized light microscopy images of all the (co)networks swollen in water. E is EGDMA, D is DMAEMA and M is MMA.

3.1.10. Mechanical Properties.

The mechanical properties of all (co)networks swollen in water were characterized in uniaxial compression, and the stress and strain at break, and the Young's modulus were determined. The values of these three determined parameters are displayed in the three parts of Figure 3.14, with the dashed green straight line in the bottom of the plot in Figure 3.14(a) interconnecting the points corresponding to the two homopolymer networks and represents the expected stress at break values of the APCNs, if a simple proportionality law applied. The measured stress at break values for most APCNs lies above the dashed line, indicating a synergistic behavior. This synergy has also been observed for the tensile strength of linear block copolymers in the bulk, but its extent was much smaller.¹³⁴⁻¹³⁵ The stress at break for the best-ordered APCN, EGDMA₁-*b*-MMA₃₀-*b*-DMAEMA₁₀-*b*-EGDMA₁, is much higher than the proportionality law dictates, suggesting a very strong synergy, and indicating that the high structural regularity in this sample may provide a most efficient energy dissipation mechanism, possibly via thin-layer or “fibril” yielding.¹³⁶⁻¹³⁷ The particular value of the compressive strength in this sample (~14 MPa) is very close to that of double-network hydrogels (~17 MPa)¹³⁸⁻¹³⁹ which represent one of the most mechanically robust hydrogel systems developed to date.

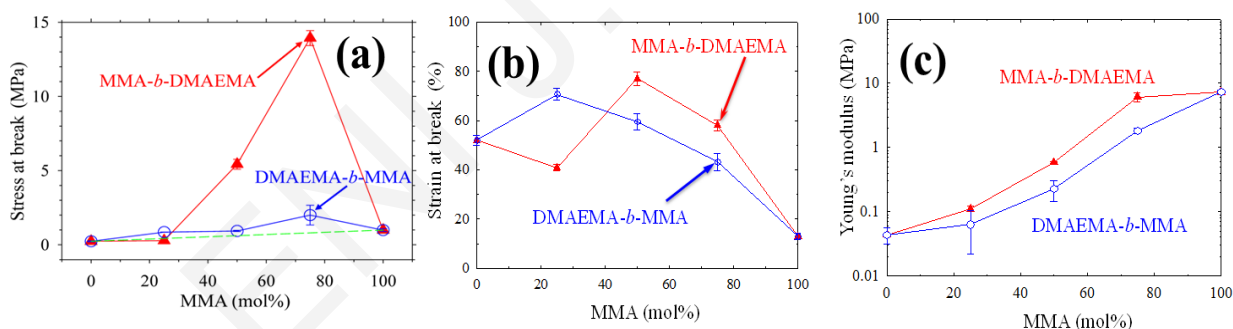


Figure 3.14. Compressive (a) stress and (b) strain at break, and (c) Young's modulus of all (co)networks equilibrium-swollen in water.

Figure 3.14(c) shows that the Young's modulus in compression of the (co)networks increases with their content in the glassy component, polyMMA, as expected, with the conetworks with M-D architecture presenting higher values than their D-M counterparts. In contrast, the compressive strain at break (Figure 3.14(b)) increases (in most cases) with the conetwork content in the more ductile component, polyDMAEMA, again as expected, and, once again, with the M-D conetworks displaying superiority when compared to the D-M conetworks.

However, the highest strain at break was exhibited by the EGDMA₁-*b*-MMA₂₀-*b*-DMAEMA₂₀-*b*-EGDMA₁ conetwork rather than by EGDMA₁-*b*-MMA₃₀-*b*-DMAEMA₁₀-*b*-EGDMA₁ which exhibited the highest stress at break.

3.1.11. Confirmation of the APCN Long-range Structure.

To confirm the correctness of our results regarding the phase separation with long-range order within the particular APCN sample, the SANS characterization of the EGDMA₁-*b*-MMA₃₀-*b*-DMAEMA₁₀-*b*-EGDMA₁ APCN sample in D₂O was repeated, and the collected SANS profile is illustrated in Figure 3.15(a) below. The profile is very similar to those for the same sample displayed in Figures 3.11 and 3.12, again presenting the second-order peak, and confirming long-range order in the self-assembled structure. We even went one step further, and repeated the synthesis of the above-mentioned sample, and characterized it using SANS in D₂O. The relevant SANS profile is depicted in Figure 3.15(b), and this is very similar to the previous ones.

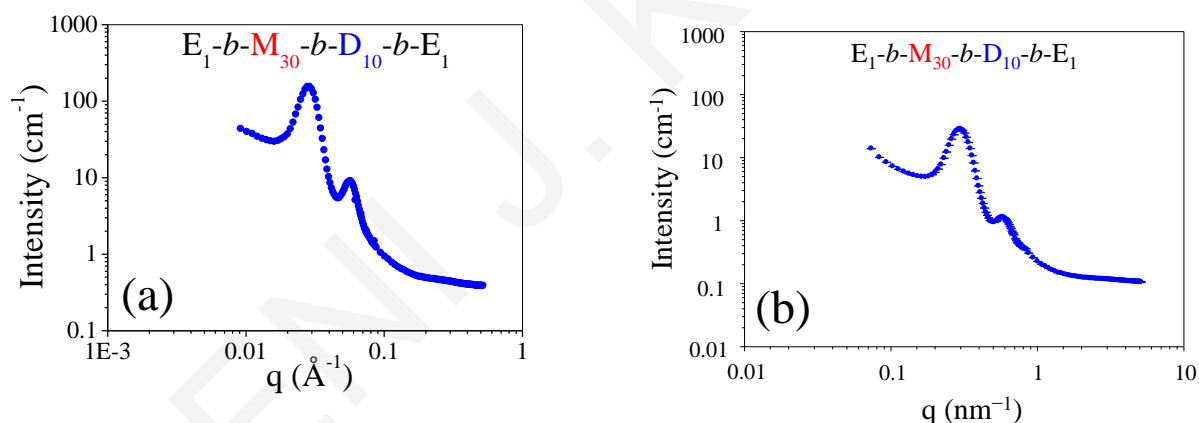


Figure 3.15. Small-angle neutron scattering profiles of EGDMA₁-*b*-MMA₃₀-*b*-DMAEMA₁₀-*b*-EGDMA₁ in D₂O. (a) Originally-synthesized sample, and, (b) repeated synthesis. These SANS data were collected at the Institut Laue-Langevin (ILL) in Grenoble, France.

3.1.12. Conclusions.

In summary, the results from this section of this Thesis offer the first APCN hydrogel, based on cross-linked star block copolymers, self-organizing in water into a lamellar mesophase with long-range order, a behavior previously known only for non-cross-linked block copolymer systems. The mechanical properties of the well-ordered system are clearly superior to those of its homologues, which, together with the facile, one-pot preparation using

readily available components, are expected to render the present system popular for applications in medicine and biotechnology.

For convenience, Figure 3.16 summarizes the structural characterization results only for sample EGDMA₁-*b*-MMA₃₀-*b*-DMAEMA₁₀-*b*-EGDMA₁. The figure displays the AFM image of the water-equilibrated sample, (part (a)), the SANS profile of the thermally-annealed sample equilibrated in D₂O (part (b)), and the optical image of the water-equilibrated sample as observed under a polarized light microscope (part (c)).

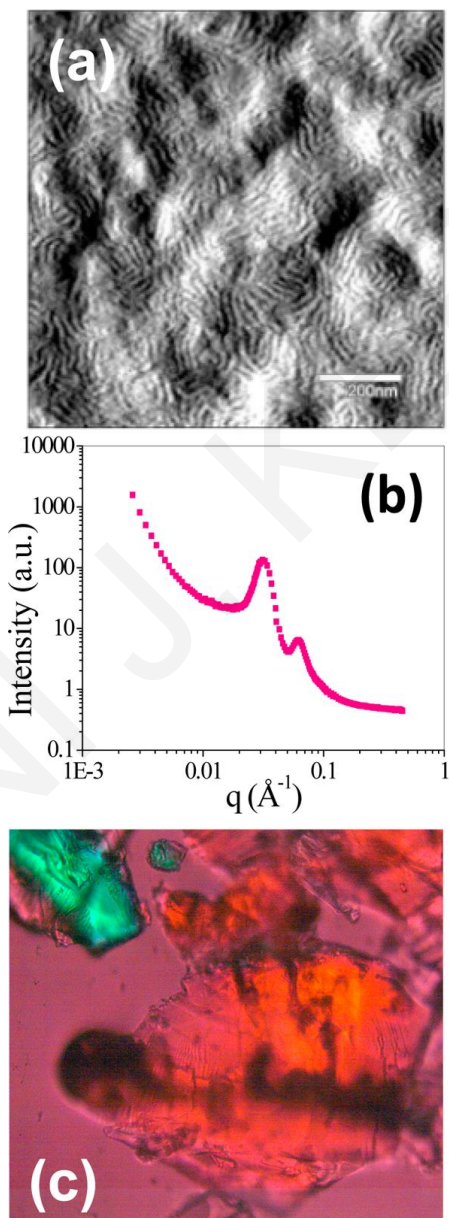


Figure 3.16. Structure formation with long-range order exhibited by sample EGDMA₁-*b*-MMA₃₀-*b*-DMAEMA₁₀-*b*-EGDMA₁ in water, as observed using (a) AFM (phase mode), (b) SANS (in D₂O), and (c) polarized light microscopy with image dimensions 625 μm × 625 μm.

3.2. Amphiphilic Polymer Conetworks Based on End-Linked “Core-First” Hydrophobic Star Block Copolymers: Synthesis and Characterization.^b

Until now, phase separation on the nanoscale and the resulting morphologies appear to be key APCN properties, crucial for their applications. However, the obtained morphologies are most often rather distorted and less regular¹⁴¹ compared to those formed by linear block copolymers in the bulk. This is due to the presence of the crosslinks in APCNs which hinder chain relaxation to lowest energy conformations. The presence of the crosslinks is even more important when chain entanglements or other network defects occur. In these cases, the covalent interconnections imposed by the crosslinks make these imperfections impossible to eliminate, and prevent the system from equilibrating to highly regular morphologies.

Thus, a major aim in this Thesis is to design, prepare and characterize APCNs with better-organized nanophase separated structures. The design relies on APCN fabrication using amphiphilic star block copolymers¹⁴² as building blocks. The more compact nature and the usually large molecular weight of star polymers are expected to introduce fewer network defects related to chain entanglements, and, therefore, allow for more regular organization of the nanophases in the phase separated state. Although most of APCNs already prepared from amphiphilic star block copolymers presented nanophase separation with only short-range order,¹⁴³⁻¹⁴⁹ some recent reports, including the results in the previous section in this Thesis, revealed morphologies with longer-range order.^{31,150-151} In these latter reports, a rather low amount of crosslinker was used, so as to allow more freedom to the polymer segments to reach a lowest-energy configuration, resulting in the formation of better-ordered morphologies within the APCNs. Thus, in the study in this section, a lower-than-usual crosslinker loading was employed too, together with a higher hydrophobic content in most samples. More hydrophobic APCN samples would swell less in water, thereby exposing any defects to only a smaller extent, favoring morphologies with longer-range order.

^b Reprinted with permission from *Macromolecular Symposia* **2017**, 372, 69 – 86. Copyright 2017, Wiley-VCH.

Herein, we report on the preparation and structural characterization of six APCN based on end-linked amphiphilic “core-first” star block copolymers, comprising MMA and DMAEMA as the monomer repeating units in the hydrophobic and hydrophilic blocks, respectively, and exclusively based on the MMA-DMAEMA block sequence. The structures of the six star block copolymer building block are schematically illustrated in Figure 3.17. The various star building blocks differed either in the arm composition or in the arm molecular weight, with four out of the six block copolymers being rich in the hydrophobic MMA component. APCN synthesis was again accomplished *via* the one-pot, sequential GTP of crosslinker, hydrophobic monomer, hydrophilic monomer, and cross-linker again.

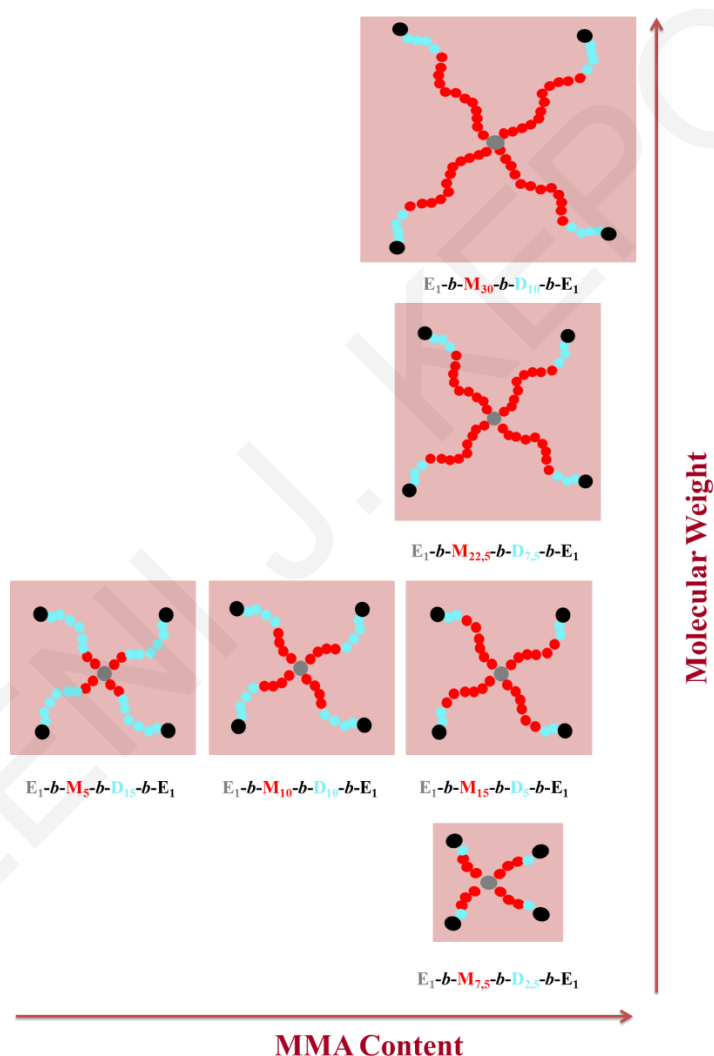


Figure 3.17. Schematic representations of the “core-first” star block copolymer building blocks, precursors to the six conetworks. E, M and D are further abbreviations for EGDMA, MMA and DMAEMA, respectively. The hydrophobic MMA units are shown in red, the hydrophilic DMAEMA units are presented in light blue, the first EGDMA cores are displayed in grey, and the second EGDMA cores are painted black.

The soluble precursors to the APCNs, *i.e.*, the star homopolymers, the star block copolymers and the initial cross-linker cores, were characterized in terms of their composition, size and size dispersity. The degrees of swelling in THF were found to increase with the molecular weight of the arms of the stars of the APCNs, whereas the degrees of swelling in water increased with the content in hydrophilic units in the arms of the constituting stars. Small-angle neutron scattering indicated that most APCNs nanophase separated in D₂O, whereas polarized light microscopy showed that all APCNs were birefringent both in water and in the dried state.

3.2.1. Species Identification in the EGDMA Core.

Figure 3.18 displays the MALDI-TOF mass spectra for the cores of the star block copolymers constituting the six APCNs. The spectra cover the molecular weight range from about 1000 to 3700 g mol⁻¹, but the signal intensity is only significant upto molecular weights of approximately 1800 g mol⁻¹, with species with molecular weights above 2500 g mol⁻¹ exhibiting extremely low intensities. The spectra for the six cores should be the same, as they all concern species resulting from the reaction between one molecule of EGDMA cross-linker and one molecule of MTS initiator.

Indeed, they are all similar, with differences among them arising from differences in detection sensitivity above 2500 g mol⁻¹. Below, we focus on the analysis of the MALDI-TOF mass spectrum of core 2 (precursor to APCN with chemical structure EGDMA₁-*b*-MMA_{22.5}-*b*-DMAEMA_{7.5}-*b*-EGDMA₁), exhibiting the greatest number of peaks; the MALDI-TOF mass spectra of the other cores display peaks also present in the spectrum of core 2.

Table 3.4 below identifies the peaks exhibited by the MALDI-TOF mass spectrum of core 2. In this analysis, it was taken into account that the molecular weight of one EGDMA unit is 198.22 g mol⁻¹, while that of one MTS residue, after loss of its trimethylsiloxy group, is 101.1 g mol⁻¹. The species identified comprise from 2 to 7 MTS initiator residues, and from 4 to 15 EGDMA crosslinker units, with the number of EGDMA units being equal to or greater than the number of MTS residues for all species identified. The most abundant peaks in the spectra are indicated in boldface in the table; these are the species bearing three initiator residues and 4 or 5 EGDMA units; this implies that the majority of the star polymers would bear around three arms.

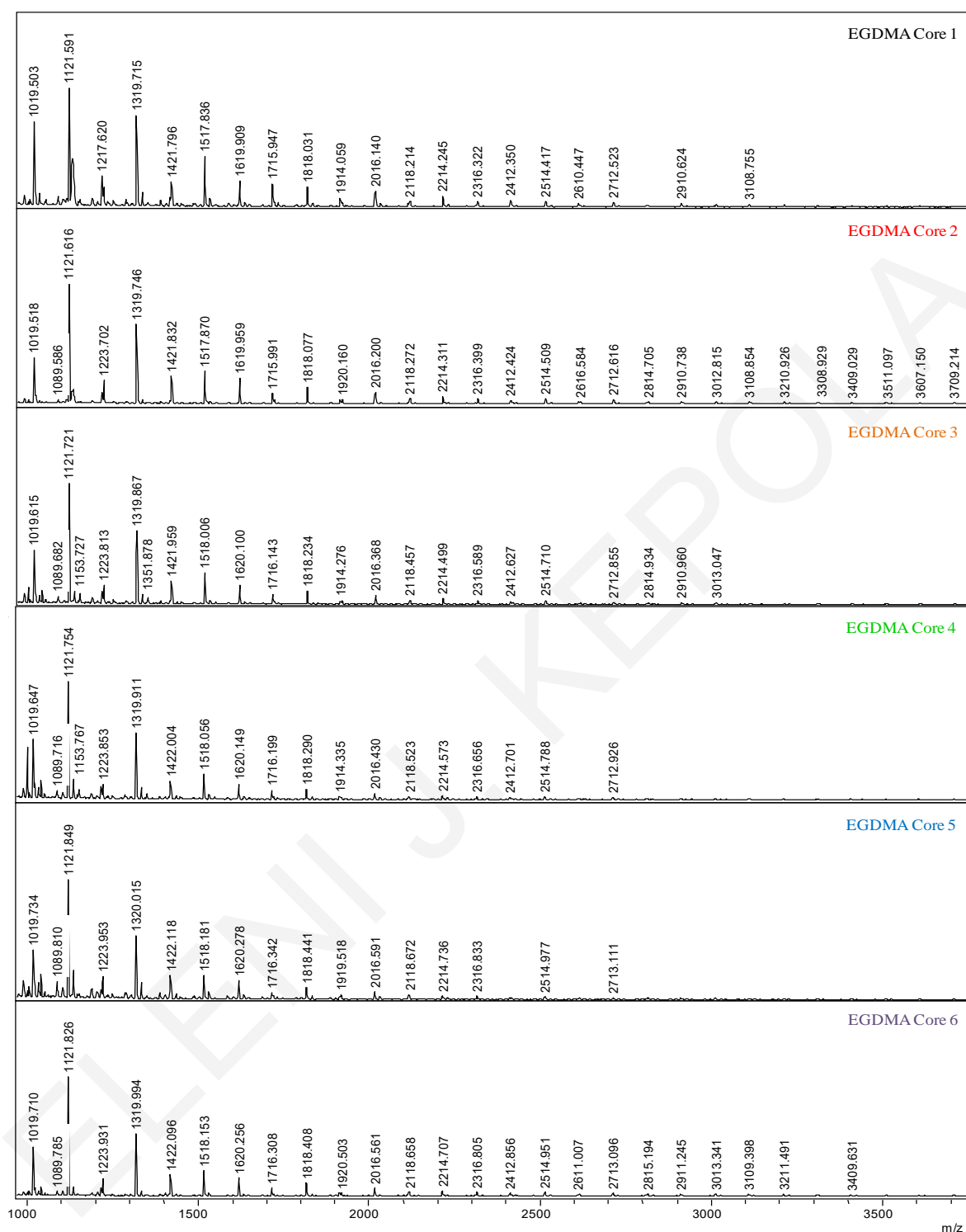


Figure 3.18. MALDI-TOF spectra of the EGDMA oligomeric cores of the star block copolymer precursors to the six amphiphilic polymer conetworks, each exhibiting various peaks corresponding to conjugates between the EGDMA crosslinker and the MTS initiator.

Table 3.4. Molecular weights and identification of the species with general formula MTS_x - $EGDMA_y$, present in the MALDI-TOF mass spectrum of core 2 (Figure 3.18), corresponding to the star block copolymer precursor to the amphiphilic polymer conetwork with chemical structure $EGDMA_1$ - b - $MMA_{22.5}$ - b - $DMAEMA_{7.5}$ - b - $EGDMA_1$.

x	2	3	4	5	6	7
y						
4	1019.520	1121.616	1223.702			
5		1319.746	1421.832			
6		1517.870	1619.959			
7		1715.991	1818.077	1920.160		
8			2016.200	2118.272		
9			2214.311	2316.399		
10			2412.424	2514.509	2616.580	
11				2712.616	2814.710	
12				2910.738	3012.820	
13				3108.854	3210.930	
14				3308.929	3409.030	3511.097
15					3607.150	3709.214

3.2.2. GPC Traces of the Star Copolymers.

Figure 3.19 plots the GPC traces (RI signal) for all the soluble precursors to the APCNs synthesized in this study, *i.e.*, the star polymers and their core, and also those of the sol fraction extracted from the conetworks. The core of the star polymers and the star polymers themselves present GPC traces which correspond to very broad molecular weight distributions, covering the whole range of elution volumes from the column, from 4 to 10 mL. These GPC traces display both a low-molecular-weight portion, with a peak in the range from 8.25 to 9.25 mL, and a high-molecular-weight portion, with a peak in the range from 6.5 to 7.5 mL. For the cores, the area under the high-molecular-weight peaks is larger than that under the low-molecular-weight peaks, suggesting a greater abundance (by weight) of cores with a higher initiator functionality. However, for the star homopolymers, the area under the high-molecular-weight peaks is equal to or smaller than that under the low-molecular-weight peaks, indicating that most of the polymerized MMA monomer was assimilated in core species possessing a smaller number of initiator residues, possibly favored by a weaker steric hindrance. This trend is also preserved for the amphiphilic star block copolymers, in which

the area under the lower-molecular-weight peak further grows relative to that under the higher-molecular-weight peak.

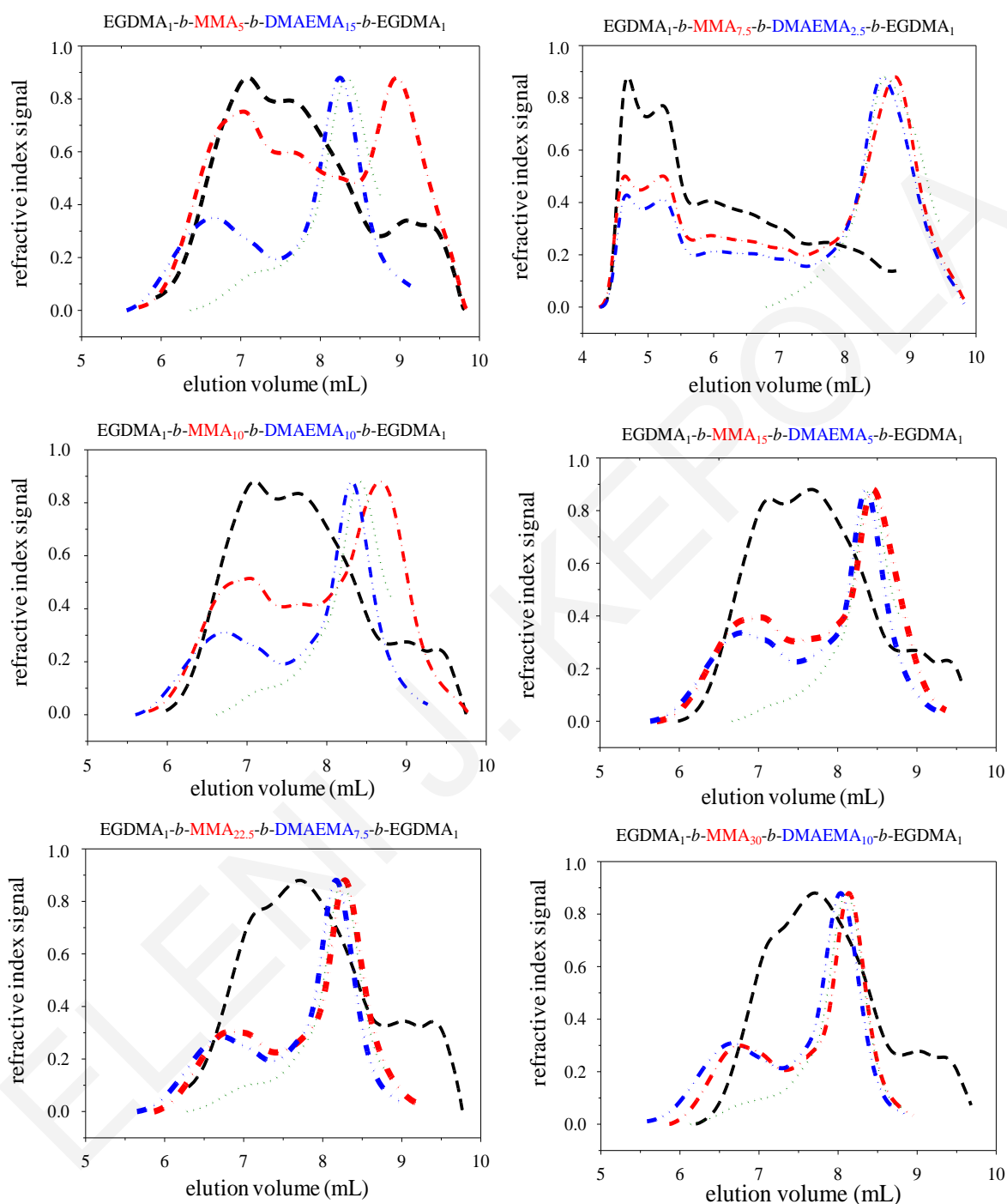


Figure 3.19 GPC traces for all soluble precursors to the six amphiphilic polymer conetworks, and the extractables from the conetworks. The traces of the EGDMA core oligomers are shown in black dashed lines, those of the MMA star homopolymers are presented in red dashed-dotted lines, those of the MMA-DMAEMA star block copolymers are displayed in blue dashed-double dotted lines, and those of the extractables are exhibited in green dotted lines.

However, for all polymers, both the lower- and the higher-molecular-weight peaks shifted to lower elution volumes upon each polymerization step, from the initial EGDMA polymerization, followed by the MMA polymerization and the DMAEMA polymerization, suggesting that all species further grew as more monomer repeating units were introduced into the system. Finally, the GPC traces of the extractables almost coincided with the lower-molecular-weight portion of the GPC trace of the corresponding amphiphilic star block copolymers, suggesting that the sol fraction mainly consisted of star block copolymers with a relatively small numbers of arms.

3.2.3. Molecular Weights and Compositions

Table 3.5 summarizes the molecular weight characteristics for all soluble precursors to the APCNs calculated from the GPC traces using the RI signal for the cores, together with the compositions of the star polymers determined using ^1H NMR spectroscopy. ^1H NMR spectroscopy was also used to determine monomer-to-polymer conversion which was found to be quantitative in all cases. The compositions of the star block copolymers from ^1H NMR spectroscopy were very close to the theoretical values calculated from the comonomer feed ratios, also consistent with the complete monomer polymerization mentioned above.

With one exception, the (number-average) molecular weights of the cores determined using GPC ranged from 2 850 to 4 130 g mol^{-1} , in fair agreement with the molecular weights determined using MALDI-TOF mass spectrometry. Their molecular weight dispersities were very high, ranging from 5.55 and 8.86, due to the very broad GPC traces in Figure 3.18, arising from the multiple conjugations between EGDMA units and MTS residues. The exception mentioned above concerned core 5, the precursor to the star polymers constituting APCN with the final polymer chemical structure $\text{EGDMA}_1\text{-}b\text{-MMA}_{7.5}\text{-}b\text{-DMAEMA}_{2.5}\text{-}b\text{-EGDMA}_1$. As all polymerizations were designed to yield APCNs at a final polymer concentration of 30 wt.%, the core of the above-mentioned APCN was prepared at the highest EGDMA concentration in the first step (due to the lowest arm DP), resulting in a core with an extremely high molecular weight (see that the relevant GPC trace in Figure 3.18 approaches the high-molecular-weight resolution limit of the GPC column), 25 500 g mol^{-1} , and a similarly extremely high molecular weight dispersity of 33.1.

Table 3.5. Compositions, molecular weights, and molecular weight dispersities of the soluble precursors to the amphiphilic polymer conetworks. The calculated number of arms of the star polymers is also listed.

Sample Number	Polymer Chemical Structure	MMA Content (mol%)		GPC Results		
		¹ H NMR	Theory	M_n (g mol ⁻¹)	\mathcal{D}	No. of Arms ¹
1	EGDMA ₁ (core 1)	0	0	3 180	5.55	-
	EGDMA ₁ - <i>b</i> -MMA ₃₀	100	100	69 300	4.49	21
	EGDMA ₁ - <i>b</i> -MMA ₃₀ - <i>b</i> -DMAEMA ₁₀	73	75	33 200	3.14	7
2	EGDMA ₁ (core 2)	0	0	2 850	6.36	-
	EGDMA ₁ - <i>b</i> -MMA _{22.5}	100	100	44 900	4.21	18
	EGDMA ₁ - <i>b</i> -MMA _{22.5} - <i>b</i> -DMAEMA _{7.5}	73	75	18 100	1.70	5
3	EGDMA ₁ (core 3)	0	0	4 130	5.56	-
	EGDMA ₁ - <i>b</i> -MMA ₁₅	100	100	41 000	3.35	23
	EGDMA ₁ - <i>b</i> -MMA ₁₅ - <i>b</i> -DMAEMA ₅	76	75	12 000	1.05	5
4	EGDMA ₁ (core 4)	0	0	3 440	7.85	-
	EGDMA ₁ - <i>b</i> -MMA ₁₀	100	100	39 900	1.84	31
	EGDMA ₁ - <i>b</i> -MMA ₁₀ - <i>b</i> -DMAEMA ₁₀	51	50	14 800	1.01	5
5	EGDMA ₁ (core 5)	0	0	25 500	33.1	-
	EGDMA ₁ - <i>b</i> -MMA _{7.5}	100	100	12 500	2.30	41
	EGDMA ₁ - <i>b</i> -MMA _{7.5} - <i>b</i> -DMAEMA _{2.5}	73	75	11 500 000	1.04	8000
6	EGDMA ₁ (core 6)	0	0	3 160	8.86	-
	EGDMA ₁ - <i>b</i> -MMA ₅	100	100	141 000	1.73	180
	EGDMA ₁ - <i>b</i> -MMA ₅ - <i>b</i> -DMAEMA ₁₅	27	25	9 460	1.03	3

¹ Calculated as the ratio of the molecular weight of the star polymer divided by the theoretical molecular weight of one arm, with the latter molecular weight also including the contribution from the EGDMA cross-linker unit of 198.22 g mol⁻¹, and the MTS initiator residue, after loss of its trimethylsilyl group, of 101.10 g mol⁻¹.

Again with the exception of APCN 5, the M_n of the MMA star homopolymers determined using GPC ranged from 39 900 to 141 000 g mol⁻¹, whereas those of the MMA-DMAEMA star block copolymers ranged from 9 460 to 33 200 g mol⁻¹. In all cases, the average molecular weights of the star block copolymers were lower than those of their parent star homopolymers due to the incorporation of the incoming DMAEMA monomer repeating units in the lower-molecular-weight portion of the GPC trace of the star homopolymer, also manifested by a large drop in the molecular weight dispersity of the star block copolymers (ranging from 1.01 to 3.14) as compared to the star homopolymers (ranging from 1.73 to 4.49). The numbers of arms in the star polymers were calculated by dividing the star polymer

M_n , from GPC, by the theoretical arm molecular weight, and are also listed in Table 3.5. The numbers of arms of the star homopolymers (except for that corresponding to APCN 5) ranged from 18 to 180, whereas those of the star block copolymers (again with the exception of that of APCN 5) were expectedly lower, ranging from 3 to 7. This latter range of numbers of arms is in fair agreement with the findings of mass spectrometry (Table 3.4) which indicated that the dominating species in the cores of the star polymers bore three initiator residues. The molecular weight of the star block copolymer corresponding to APCN 5, based on an extremely polydisperse core, was extremely high, $11\,500\,000\text{ g mol}^{-1}$, possessing an extremely high number of arms, 8 000.

3.2.4. Extractables.

Table 3.6 summarizes the characteristics of the extractables from the APCNs, as these were characterized using gravimetry, ^1H NMR spectroscopy and GPC. The table lists the mass of the extractables as a percentage relative to the total mass of polymerized monomers and crosslinker (sol fraction), the composition, the number-average molecular weight, and molecular weight dispersity of the extractables, together with the theoretical composition and theoretical molecular weight of the arms of the corresponding star block copolymers constituting the APCNs. The sol fraction was relatively high, ranging from 25 to 35% w/w, arising from the rather low loading of crosslinker, especially at the fourth polymerization step, in order to facilitate phase separation on the nanoscale with longer-range order. Examining the first three samples in the table, it appears that the sol fraction increases with the overall arm DP of the stars, from 20 to 40.

This trend can be attributed to a decrease in crosslinking within the APCNs as the arm DP increases. A lower cross-linking density is more likely to allow defects related to missing interconnections, leading to a higher sol fraction.

The composition (molar percentage of MMA in the polymer) of the extractables in Table 3.6 is very close to the composition of the star block copolymers (Table 3.5) and also close to the theoretical composition of the arms of the stars (Table 3.6), indicating that the extractables are composed of copolymers having the targeted composition for the particular APCN. This also implies that, upon the removal of the sol fraction, the remaining gel fraction of the APCN continues to have the initially targeted composition.

Table 3.6. Characteristics of the extractables from the amphiphilic polymer conetworks of this study, including their sol fraction, composition and molecular weights.

Chemical Structure of Amphiphilic Polymer Conetwork	Extractables (% w/w)	MMA Content (mol%)		Theoretical Molecular Weight of Arm	GPC Results	
		¹ H NMR	Theory		M_n (g mol ⁻¹)	\bar{D}
		EGDMA ₁ - <i>b</i> -MMA ₃₀ - <i>b</i> -DMAEMA ₁₀ - <i>b</i> -EGDMA ₁	35.3	81		
EGDMA ₁ - <i>b</i> -MMA _{22.5} - <i>b</i> -DMAEMA _{7.5} - <i>b</i> -EGDMA ₁	32.2	82	75	3731	4900	2.42
EGDMA ₁ - <i>b</i> -MMA ₁₅ - <i>b</i> -DMAEMA ₅ - <i>b</i> -EGDMA ₁	24.9	80	75	2587	3980	2.17
EGDMA ₁ - <i>b</i> -MMA ₁₀ - <i>b</i> -DMAEMA ₁₀ - <i>b</i> -EGDMA ₁	26.0	53	50	2873	4120	2.59
EGDMA ₁ - <i>b</i> -MMA _{7.5} - <i>b</i> -DMAEMA _{2.5} - <i>b</i> -EGDMA ₁	31.7	72	75	1443	1690	2.85
EGDMA ₁ - <i>b</i> -MMA ₅ - <i>b</i> -DMAEMA ₁₅ - <i>b</i> -EGDMA ₁	28.9	30	25	3158	4470	2.57

The (number-average) molecular weight of the extractables is higher (almost twice as high) than the theoretical molecular weight of the arm of the star, exhibiting relatively high molecular weight dispersities, between 2.2 and 2.9, indicating that the extractables comprise star and hyperbranched copolymers of rather small molecular weight, in agreement with the coincidence of the GPC traces of the extractables with the lower-molecular-weight portion of the GPC trace of the corresponding star block copolymer in Figure 3.19.

3.2.5. Effect of pH on the Aqueous Degrees of Swelling.

Figure 3.20 presents plots, one for each of the six APCNs prepared in this study, with their degrees of swelling in water as a function of the pH of the supernatant solution. Each plot also shows the degree of ionization of the APCN, and its variation with the supernatant solution pH. The aqueous degrees of swelling start to increase as the pH is lowered. This critical pH below which the swelling degrees start to increase highly depends on the composition of the APCNs; the more hydrophobic the APCN, the lower the critical pH. In particular, the critical swelling pH for the four hydrophobic APCNs is 4.5 – 5.0, whereas for the two more hydrophilic APCNs this critical pH is higher, 6.5 for sample EGDMA₁-*b*-MMA₁₀-*b*-DMAEMA₁₀-*b*-EGDMA₁, and 8.5 for sample EGDMA₁-*b*-MMA₅-*b*-DMAEMA₁₅-*b*-EGDMA₁. At very low pH, 2.5 – 3.0, the degrees of swelling start to decrease again.

The above observations can be explained as follows (see also discussion of results in Figure 3.6). The increase in the aqueous degrees of swelling as the supernatant solution pH is initially lowered (pH below 4.5 – 8.5, depending on APCN composition) is due to the

ionization of the DMAEMA weakly basic monomer repeating units in the APCNs, which start to become ionized below pH 8.5.

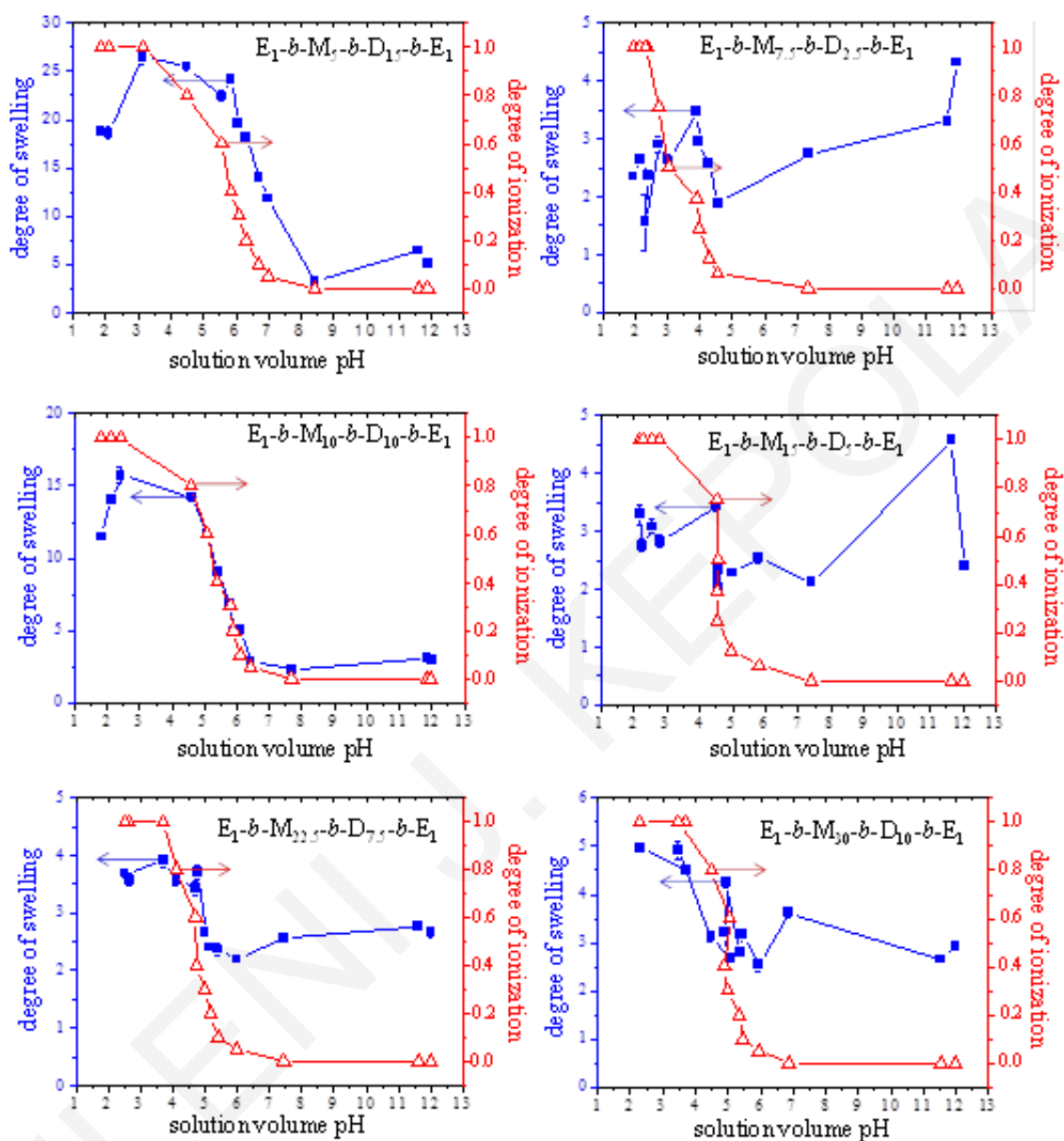


Figure 3.20. pH-Dependence of the swelling and ionization degrees for all amphiphilic polymer conetworks equilibrated in aqueous media. In the figure labels, E, M and D are further abbreviations for EGDMA, MMA and DMAEMA, respectively.

Ionization of these units establishes Coulombic repulsive forces among the polymer chains and creates an osmotic pressure within the system due to the accumulated chloride counteranions to the protonated tertiary amine groups in the DMAEMA units, both of which

lead to APCN swelling. Thus, this part of the swelling behavior is driven by electrostatics, as can also be confirmed by the observation that the degree of swelling curve follows the degree of ionization curve in this portion of the plots.

The fact that the critical swelling pH is lower for the more hydrophobic APCNs can be attributed to the greater repulsive and osmotic forces necessary to overcome the attractive forces generated by the stronger hydrophobic association dominating within these APCNs, before substantial aqueous swelling can occur. Finally, the reduced aqueous swelling measured in the very low pH region can be attributed to the high ionic strength created by the relatively high concentration of HCl required to establish these acidic pH values.

From each of the plots in Figure 3.20, two characteristic aqueous degrees of swelling are taken: first, the maximum swelling degree in the acidic pH range, and, second, the degree of swelling in water near neutral pH conditions, just before swelling starts to increase. These two characteristic swelling degrees are plotted in Figure 3.21, together with the degrees of swelling in THF. Figure 3.21 (a) displays the degrees of swelling for the three APCNs of different MMA-DMAEMA arm compositions but constant overall arm DP of 20, while Figure 3.21 (b) presents the swelling degrees of the four APCNs possessing varying overall arm DPs but constant MMA-to-DMAEMA molar ratio (= 3:1) in the arm.

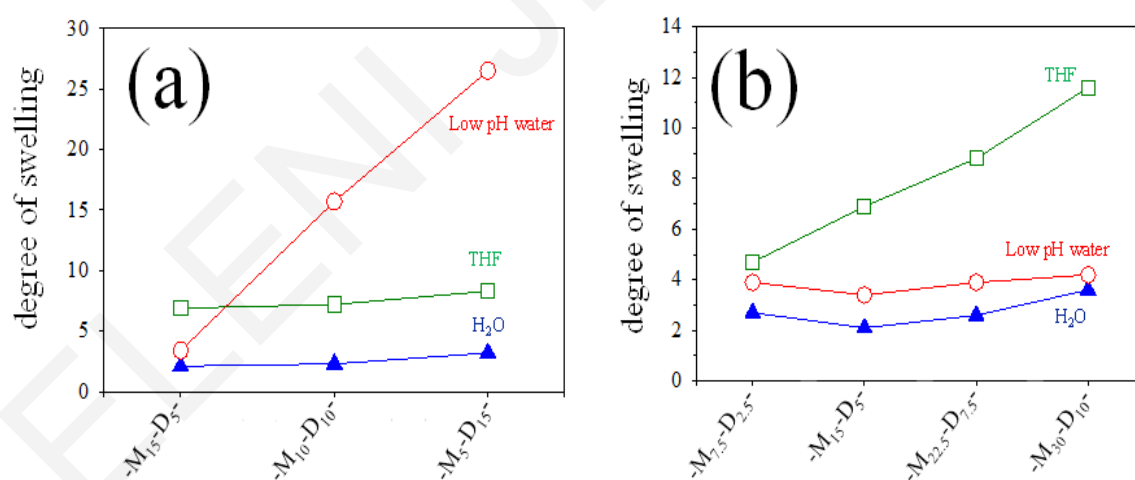


Figure 3.21. Degrees of swelling of all the amphiphilic polymer conetworks in pure water, in acidic water, and in tetrahydrofuran (THF). (a) Effect of the composition of the arm of the star block copolymer. (b) Effect of the degree of polymerization of the arm of the star block copolymer. In the *x*-axis labels, M and D represent further abbreviations for MMA and DMAEMA, respectively.

Figure 3.21 (a) shows that the degrees of swelling in THF for APCNs made up of star block copolymers comprising arms of different MMA-DMAEMA composition but the same overall DP are nearly independent of the APCN structure, spanning a range of values only between 7 and 8. This can be explained by considering that THF is a non-selective solvent, *i.e.*, THF dissolves equally well the MMA and DMAEMA monomer repeating units, and that the arms have the same length as they have the same DP. Figure 3.21 (a) also indicates that the swelling degrees in pure water are very low, and slightly increase with the arm content in the hydrophilic DMAEMA monomer repeating units, from a lower value of about 2 to a highest value of approximately 3. In pure water, the relatively high MMA content, 25 – 75 mol%, drives the APCNs into a rather collapsed state, in which the DMAEMA content has only a slight effect on swelling as it is in its uncharged state. In contrast, when the DMAEMA units are fully charged under acidic conditions, the degrees of swelling in low pH water, also plotted in Figure 3.21 (a), greatly increase with the DMAEMA content, rising from a value of about 3 for a DMAEMA content of 25 mol% up to a value of 27 for a DMAEMA content of 75 mol%.

The trends in the degrees of swelling are rather different in Figure 3.21 (b), focusing on the effect of arm length at constant arm composition. For this group of APCNs, the swelling degrees in the non-selective THF increase with arm DP, as expected, from about 4.5 to 11.5 for arm DPs from 10 to 40, respectively. In contrast, the degrees of swelling in water, either pure or acidic, are almost arm DP-independent, as all four APCNs are based on star block copolymers whose arms have the same composition, namely, 25 mol% of hydrophilic DMAEMA monomer repeating units. This rather low DMAEMA content is the reason why the aqueous degrees of swelling are so low, with values of about 2.5 in pure water and 3.5 in acidic water. The higher swelling degrees in acidic water as compared to the corresponding values in pure water are justified by the ionization of the DMAEMA units under the former conditions and their neutrality in the latter conditions.

3.2.6. Structure of the Conetworks in Water.

Figure 3.22 illustrates the SANS profiles for all APCNs prepared in this study. Part (a) of the figure presents the SANS profiles for the three APCNs of different MMA-DMAEMA arm compositions but constant overall arm DP of 20, whereas part (b) displays the SANS profiles for the four APCNs possessing varying overall arm DPs but having constant MMA-to-

DMAEMA molar ratio in the arm. With one exception, the APCNs possessed SANS profiles exhibiting a clear correlation peak. The APCN whose SANS profile did not display a clear correlation peak was EGDMA₁-*b*-MMA_{7.5}-*b*-DMAEMA_{2.5}-*b*-EGDMA₁ (sample #4), comprising stars with the shortest arms, which apparently are too short to allow for formation of organized and correlated hydrophobic domains. The formation of a correlation peak in the SANS profile is consistent with the internal organization within the APCNs, with the hydrophobic polyMMA segments clustering together to avoid contact with D₂O. Apparently, the stiffness of the very short polymer segments in sample #4 prevented the hydrophobic segments from segregating and forming separate hydrophobic domains. In addition, we observe for all the samples an increase in intensity at low q that scales roughly with $q^{-3} - q^{-4}$, a scaling that is typically observed for polymer networks.¹¹⁸

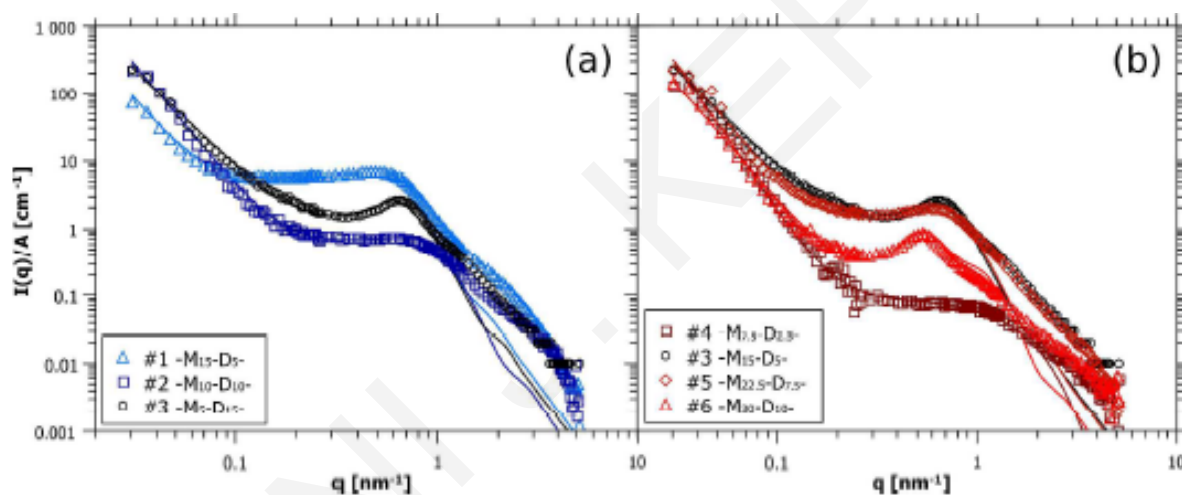


Figure 3.22. Small-angle neutron scattering (SANS) profiles for all the amphiphilic polymer conetworks in D₂O in the pure state (obtained by dividing by the factor A that takes into account incomplete filling of the cells). The curves fitted with eqs. 1 and 2 are given as solid lines. (a) Effect of the composition of the arm of the star block copolymer. (b) Effect of the degree of polymerization of the arm of the star block copolymer.

From the q -value of the correlation peak, q_{max} , one can estimate the average distance between the hydrophobic polyMMA cores, d , as $d = 2 \pi / q_{max}$. The q_{max} and d values extracted from the SANS profiles are listed in Table 3.7. Examining first the effect of arm composition, at constant arm DP, on d , it seems that APCNs based on star block copolymers with more hydrophilic arms have their hydrophobic cores spaced further apart, at 9.8 nm for samples #2 and #3, and at 12.9 nm for sample #1. This can be attributed to the greater aqueous swelling

of the more hydrophilic APCN sample (see also Figure 3.21) and, in general, the experimentally observed spacings nicely reflect the molecular architecture of the samples and their extent of swelling (DS). For instance, examining the effect of arm DP, at constant arm composition, on d , it appears that longer arms lead to hydrophobic cores which are spaced further apart, at 9.8 nm for sample #3, 10.9 nm for sample #5, and 11.8 nm for sample #6. This is in agreement with our expectation that APCNs based on star block copolymers with longer arms would have their building blocks located further away from each other, and it is also consistent with the aqueous DSs of the APCNs presented in Figure 3.21.

Table 3.7. Position of the intensity maximum, q_{max} , distance between the scattering centers, d , hydrophobic volume fraction, Φ , radius of hydrophobic core, R , and star aggregation number (both obtained from the peak position q_{max}) within the unit cell for the amphiphilic polymer conetworks of this study in D₂O, as obtained using small-angle neutron scattering.

Sample Number	Chemical Structure of Amphiphilic Polymer Conetwork	q_{max} (nm ⁻¹)	d^1 (nm)	DS^2	Φ^3	R^4 (nm)	N_{agg}^5
1	EGDMA ₁ - <i>b</i> -MMA ₅ - <i>b</i> -DMAEMA ₁₅ - <i>b</i> -EGDMA ₁	0.49	12.9	3.15	0.0757	3.4	41
2	EGDMA ₁ - <i>b</i> -MMA ₁₀ - <i>b</i> -DMAEMA ₁₀ - <i>b</i> -EGDMA ₁	0.64	9.8	2.1	0.202	3.6	18
3	EGDMA ₁ - <i>b</i> -MMA ₁₅ - <i>b</i> -DMAEMA ₅ - <i>b</i> -EGDMA ₁	0.64	9.8	2.0	0.323	4.2	20
4	EGDMA ₁ - <i>b</i> -MMA _{7.5} - <i>b</i> -DMAEMA _{2.5} - <i>b</i> -EGDMA ₁	----	----	2.8	0.229	----	----
3	EGDMA ₁ - <i>b</i> -MMA ₁₅ - <i>b</i> -DMAEMA ₅ - <i>b</i> -EGDMA ₁	0.64	9.8	2.0	0.323	4.2	20
5	EGDMA ₁ - <i>b</i> -MMA _{22.5} - <i>b</i> -DMAEMA _{7.5} - <i>b</i> -EGDMA ₁	0.57	10.9	2.3	0.282	4.4	17
6	EGDMA ₁ - <i>b</i> -MMA ₃₀ - <i>b</i> -DMAEMA ₁₀ - <i>b</i> -EGDMA ₁	0.53	11.8	3.2	0.204	4.3	8.7

¹ Calculated as: $d = 2\pi/q_{max}$.

² Equilibrium degree of swelling in water.

³ Calculated from the conetwork theoretical chemical structure and the aqueous degree of swelling as: $\Phi = [(\text{molecular weight of the hydrophobic block for one arm, including, in addition to the polyMMA block, the initiator residue and one cross-linker unit}) / (\text{overall molecular weight of one arm, including both blocks, the initiator residue and two cross-linker units})] / (\text{degree of swelling in water})$.

⁴ Estimated as: $R = d \times (3\Phi/4\pi)^{1/3}$, based on the assumption of a simple cubic lattice.

⁵ Number of star block copolymers aggregated within one unit cell which possesses one scattering center.

Subsequently, we combined the determined spacing between the scattering centers with the APCN composition, together with the experimentally measured aqueous DSs of the APCNs to estimate the volume fraction of hydrophobic segments in the system, Φ , and from that the radius, R , of the equivalent spherical hydrophobic core (completely compacted) under the assumption of a simple cubic lattice geometry, as well as the number of star block copolymers aggregating within a unit cell. The results from these calculations are listed in Table 3.7. As expected, the Φ - and R -values both increase with the APCN content in

hydrophobic MMA monomer repeating units (samples #1, #2 and #3) and constant overall arm DP, from 7.6 to 32% and 3.4 to 4.2 nm, respectively. Also expectedly, the Φ - and R -values both remain approximately constant at a constant APCN molar content in hydrophobic MMA monomer repeating units (samples #3, #5 and #6) and varying overall arm DP, ranging between only 20 to 32% and 4.2 to 4.4 nm, respectively. In contrast, the aggregation numbers of the stars within the unit cells, N_{agg} , were approximately equal to 20 in most cases, as it was to be expected due to having the same preparation process. Exceptions were exhibited by the most hydrophilic APCN system displaying a larger aggregation number of 41, reflecting its greater ability toward rearrangement facilitated by its lower hydrophobicity / lower glass transition temperature, and by the hydrophobic APCN system with the greatest arm DP presenting a lower aggregation number of 9, indicating its difficulty for rearrangement effected by its higher hydrophobicity / higher glass transition temperature.

The scattering curves in Figure 3.22 were also analyzed somewhat more quantitatively with respect to intensity and shape of the SANS curves. For this purpose, we describe the scattering intensity by:

$$I(q) / A = {}^1N \cdot P(q) \cdot S(q) + D \cdot q^{-n} \quad (1)$$

$$P(q) = (SLD_{agg} - SLD_{solv})^2 \cdot (4\pi \cdot R_{sph})^3 \cdot \left(\frac{\sin(q \cdot R_{sph}) - q \cdot R_{sph} \cdot \cos(q \cdot R_{sph})}{(q \cdot R_{sph})^3} \right)^2 \quad (2)$$

where $P(q)$ is the form factor given in eq. 2, and $S(q)$ is the structure factor of the system, 1N the number density of scattering domains, and A a factor that takes into account that the networks had to be filled as granular material into the cuvettes and partly there was also not sufficient material to completely fill the cuvettes (A was determined from the incoherent background that arises largely from the H atoms of the polymer). It might be noted that this type of modeling was also successful for describing similar systems, as, for instance, amphiphilic polydimethylsiloxane – poly(ethylene glycol) (PDMS-PEG) conetworks,¹⁴¹ cross-linked star polymers¹⁴² or Tetronic-based amphiphilic star-block copolymers.¹⁴³ SLD_{agg} and SLD_{solv} are the scattering lengths of domain and solvent, respectively, and R_{sph} the sphere radius. For SLD_{agg} we just assumed polyMMA with a density of 1.18 g/mL and for SLD_{solv} the presence of D₂O and the hydrophilic chains of the polymer (as well as the

hydrophobic chains not contained in the aggregates). For our modelling, we smeared the form factor $P(q)$ by assuming a log-normal distribution of the radii with a polydispersity index of 0.20. Finally the term $D \cdot q^{-n}$ takes care of the experimentally observed upturn of intensity at low q , which is due to the overall network structure described by a fractal exponent n (which in our case was mostly in the range of 3.4 – 3.6).

As the structural details of the present APCNs are certainly rather complicated, we approached the modelling of the SANS data with a rather simple model in which the scattering domains are described by homogeneous spheres and a hard sphere structure factor,¹⁴⁴ which is needed to reproduce the correlation peaks. In our model we assumed now a certain fraction B of the polyMMA to be contained in the hydrophobic domains, while the remaining part was counted into the solvent. The shape of the scattering curve at higher q ($q > 0.7 - 1 \text{ nm}^{-1}$) is determined by the form factor $P(q)$ and it, therefore, allows to determine the domain radius R_{sph} . The position of the scattering peak determines the number density 1N of the scattering domains and the hard sphere radius R_{HS} then allows to adjust the effective hard sphere repulsion, which is modulated by the polymer blocks that connect the different hydrophobic domains. Knowing 1N and using the degrees of swelling given in Figures 3.20 and 3.21, one can calculate with the domain radius R_{sph} the theoretical scattering curves. However, they would be substantially higher in intensity than the experimental data, which can be taken into account by the factor B of the contained fraction of polyMMA in the hydrophobic domains. This is a realistic assumption, as these are highly constrained polymer conetworks, where not all chains can easily become incorporated into the hydrophobic domains. From this analysis, we could then determine the mass fraction B of MMA/EGDMA that is included in these domains. The determined R_{sph} , R_{HS} , Φ_{HS} , B , and n are summarized in Table 3.8.

Table 3.8. Parameters obtained from fitting the SANS data with eqs. 1-2: hard sphere volume fraction Φ_{HS} , radius R_{sph} , hard sphere radius R_{HS} , fraction of the MMA contained in the hydrophobic domains, B , and fractal exponent n .

Sample Number	Chemical Structure of Amphiphilic Polymer Conetwork	Φ_{HS}	R_{sph} (nm)	R_{HS} (nm)	B	n
1	EGDMA ₁ - <i>b</i> -MMA ₅ - <i>b</i> -DMAEMA ₁₅ - <i>b</i> -EGDMA ₁	0.16	3.0	4.3	1.25	3.6
2	EGDMA ₁ - <i>b</i> -MMA ₁₀ - <i>b</i> -DMAEMA ₁₀ - <i>b</i> -EGDMA ₁	0.13	2.0	3.1	0.29	3.6
3	EGDMA ₁ - <i>b</i> -MMA ₁₅ - <i>b</i> -DMAEMA ₅ - <i>b</i> -EGDMA ₁	0.25	2.6	4.2	0.30	2.9
4	EGDMA ₁ - <i>b</i> -MMA _{7.5} - <i>b</i> -DMAEMA _{2.5} - <i>b</i> -EGDMA ₁	----	1.2	----	0.06	4.3
3	EGDMA ₁ - <i>b</i> -MMA ₁₅ - <i>b</i> -DMAEMA ₅ - <i>b</i> -EGDMA ₁	0.25	2.6	4.2	0.30	2.9
5	EGDMA ₁ - <i>b</i> -MMA _{22.5} - <i>b</i> -DMAEMA _{7.5} - <i>b</i> -EGDMA ₁	0.18	2.4	3.9	0.23	3.5
6	EGDMA ₁ - <i>b</i> -MMA ₃₀ - <i>b</i> -DMAEMA ₁₀ - <i>b</i> -EGDMA ₁	0.25	2.0	5.5	0.13	3.4

For the first series (samples #1-3), it is interesting to note that the hydrophobic domain is expectedly substantially larger for the case of having a MMA₁₅ block instead of a MMA₁₀ block, but it is then largest for the shortest MMA₅ block. This apparent discrepancy may be explained by the fact that the small size of the MMA 5 block together with its connection to the relatively long DMAEMA 15 hydrophilic block convey to the former block a large flexibility, which, in turn, allows to a large number of MMA 5 blocks to assemble into relatively large domains. Here the fraction B is even 1.25, while for samples #2 and #3 it is ~ 0.3, and this value larger than 1 may indicate some incorporation of EGDMA into the hydrophobic domain. Looking at series 2 (samples #3-6) interestingly one finds the largest hydrophobic domains for the samples with intermediate length (#3 and #5). Obviously a very short MMA block does not allow for formation of larger domains, but the network with the longest intermediate block then seems to have too pronounced constraints for forming large hydrophobic domains, as further confirmed by the low value of B . Here simply the distance to neighboring network points might become too large to have polyMMA blocks from different network points to be able to join into one hydrophobic domain.

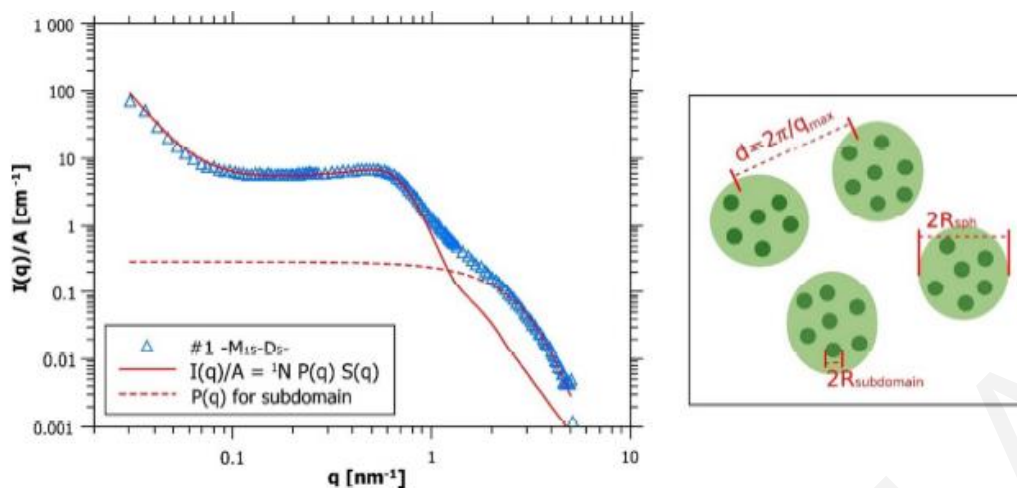


Figure 3.23. Small-angle neutron scattering (SANS) profile for sample #1 (EGDMA₁-*b*-MMA₅-*b*-DMAEMA₁₅-*b*-EGDMA₁ in D₂O) showing the scattering of subdomains with a size of ~ 0.8 nm at high q and a schematic representation of the corresponding structures (right).

However, it should be noted that this is not an exclusive interpretation of the data, as this fraction B of polyMMA contained in the domains is basically arising from the lower-than-expected intensity. However, this effect could also be achieved by having a higher fraction of aggregated polyMMA but in domains that are not homogeneous in MMA but also contain some of the other polymer and D₂O, for instance as connecting material between subdomains. Such a scenario would lead to a corresponding reduction of scattering intensity that is directly proportional to the amount of contained material other than MMA. Actually for some samples there is good evidence for such a scenario as shown in Figure 3.23, where one can see at higher q the typical scattering pattern of globular objects of a size of ~0.8 nm. In general, it can be seen in Figure 3.22 that the fitted curves at higher q underestimate the intensity, which could be attributed partly to chain scattering but also strongly hint to internal inhomogeneities of the hydrophobic domains. Accordingly one may assume here a structure of larger hydrophobic spherical domains which are substructured into smaller hydrophobic domains and then contain in addition some of the remaining polymer and D₂O, as depicted in Figure 3.23. However, it has to be said that a more detailed description in terms of contained material in the hydrophobic domains (given by B) and a swelling of these domains by other polymer and water is hampered by the fact that these parameters, as well as the domain radius R_{sph} , all have a similar effect on the scattering intensity and, therefore, are strongly interrelated.

Further examination of the SANS profiles in Figure 3.22 leads to the identification of a shoulder in the SANS profile of sample #6, on the right-hand-side of the correlation peak,

appearing at about twice the value of q_{max} . Similar shoulders, but of lower intensity, can also be observed in the SANS profiles of samples #3 and #5. These shoulders are attributed to smeared second-order peaks, thereby indicating a trend within these samples to a more pronounced long-range ordering, and, correspondingly, more regular morphologies, similar to those formed by linear block copolymers in the bulk. To qualitatively test this hypothesis, we imaged all APCN samples under a polarized light microscope to examine them for birefringence. Birefringence is exhibited by materials possessing refractive indices which are different in two different directions within the material, such as those organized into anisotropic morphologies, *e.g.*, lamellae and cylinders. Thus, a slight multiple coloration within the samples might be an indication for organization into an anisotropic morphology, even just locally.

3.2.7. Anisotropic Nanophases.

Figure 3.24 displays the polarized light microscopy images for all APCN samples prepared in this study. The samples were imaged both in the dried state and also after equilibration in water. All images present multiple coloration and are, therefore, birefringent, indicating the possible formation of anisotropic nanophases, even to a limited length-scale. Birefringence is more intense for the samples in water than in the dried state, consistent with our expectation that the introduction of a selective solvent, such as water, would more strongly drive nanophase separation.

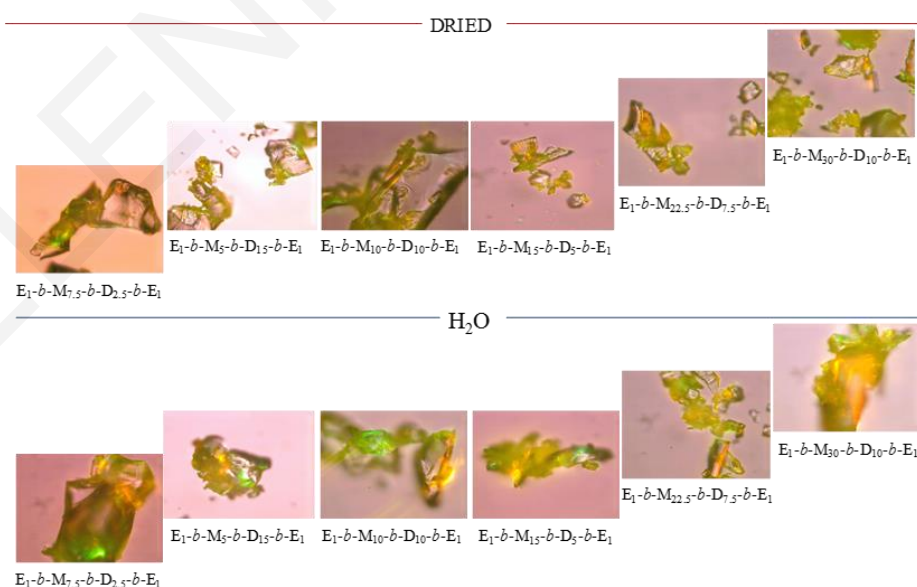


Figure 3.24. Polarized light microscopy images for all the amphiphilic polymer conetworks, in the dried state and in water-swollen states.

3.2.8. Conclusions.

This study presented the preparation and characterization of six novel amphiphilic polymer conetworks, where we varied systematically the arm architecture, *i.e.*, the lengths of the hydrophilic and hydrophobic blocks. All, except the one with the shortest arms, exhibited a correlation peak when equilibrated in D₂O, as deduced from small-angle neutron scattering (SANS), consistent with internal self-assembly and nanophase separation. In addition to the correlation peak, some of the samples also presented a shoulder in their scattering profile, at twice the q -value of the correlation peak, indicating a trend for internal organization with a longer range ordering. From a simple SANS model, the size of the hydrophobic domains can be deduced and become correlated with the molecular architecture of the polymer conetworks. Furthermore, there is good indication that actually the 4-6 nm sized hydrophobic domains are not homogeneous in structure, but they actually are themselves built up from smaller (1.2-1.6 nm sized) subdomains. Our results demonstrate that the molecular architecture of the amphiphilic polymer conetworks is successfully translated into their mesoscopic structure and thereby this approach allows for a rational design of such systems. Future studies will aim at developing amphiphilic polymer conetworks yielding morphologies with longer-range order, by better controlling the distribution of the arm numbers at the crosslinking junctions.

3.3. Networks Based on “Core-first” Star Hydrophobic Homopolymers End-linked Using a Degradable Ketal Cross-Linker: Synthesis, Characterization and Cleavage.^c

To better characterize the molecular structure of the networks in the two previous sections, in this section we designed a study to give us the number of arms at the (secondary) cores where the star building blocks are interconnected. This involved the design, preparation and use of a degradable dimethacrylate crosslinker, together with the non-degradable EGDMA, to prepare cleavable networks based on end-linked MMA “core-first” star homopolymers. In particular, sequential group transfer polymerization of crosslinker, MMA monomer, and crosslinker again was used to prepare cleavable polymer networks based on interconnected “core-first” star polymers. By employing a degradable and a non-degradable crosslinker, four networks were prepared. While cleavage of the degradable crosslinker residues led to complete polymer network dissolution, the degradation products did not always display the expected molecular weight features. These products were the expected in the case of the network prepared using only the degradable crosslinker (monomodal size distribution with the expected low molecular weight) and also in the case of the network prepared using first the degradable and then the non-degradable crosslinker (bimodal size distribution including high molecular weight star polymers), but not so in the case of the network prepared using first the non-degradable and then the degradable crosslinker, where the expected high molecular weight star polymer component was missing due to star recombination after hydrolysis.

^c Reprinted with permission from *Macromolecular Chemistry and Physics* **2018**, 219, 1700404. Copyright 2018, Wiley-VCH

3.3.1. Synthesis and Characterization of the DMOEP Crosslinker.

The acid-labile DMOEP crosslinker was prepared by the reaction between HEMA and MOP in the presence of *p*TSA catalyst in DCM¹⁴⁵ as shown in Figure 3.25.

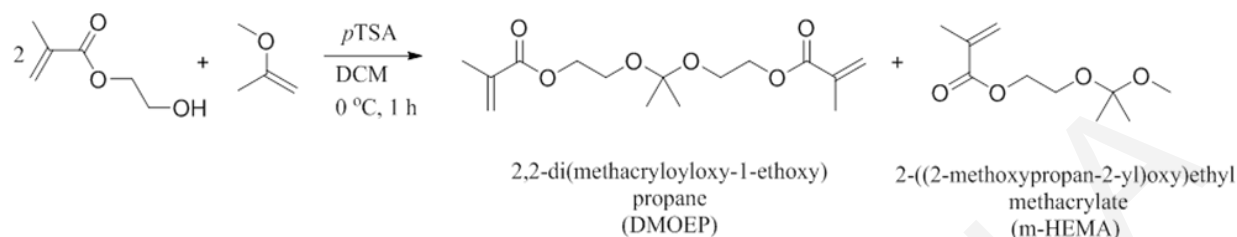


Figure 3.25. Chemical reaction leading to the formation of the 2,2-di(methacryloyloxy-1-ethoxy)propane (DMOEP) crosslinker accompanied by the formation of the mono-substituted side-product 2-[(2-methoxypropan-2-yl)oxy]ethyl methacrylate (m-HEMA).

The HEMA to MOP molar ratio was fixed at the 2:1 stoichiometric molar ratio in order to maximize the yield in DMOEP production. Typical yields of the reaction for the preparation of DMOEP (from the crude) were 70%, whereas the yield of the purified product after column chromatography and distillation was 50%. The ¹H and ¹³C NMR spectra of purified DMOEP are displayed in Figure 3.26, whereas those of purified m-HEMA are given in Figure 3.27.

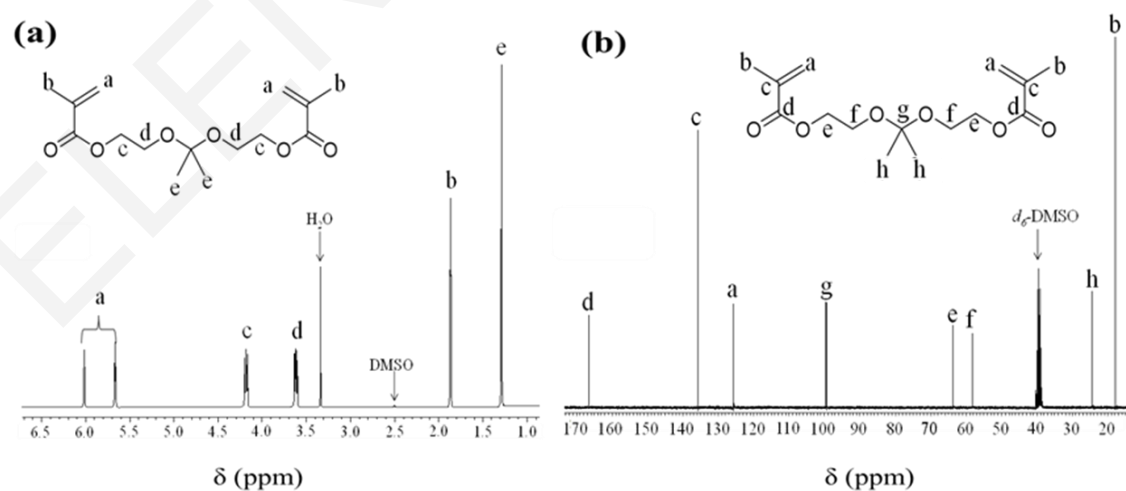


Figure 3.26. (a) ¹H and (b) ¹³C NMR spectra of the 2,2-di(methacryloyloxy-1-ethoxy)propane (DMOEP) crosslinker in *d*₆-DMSO.

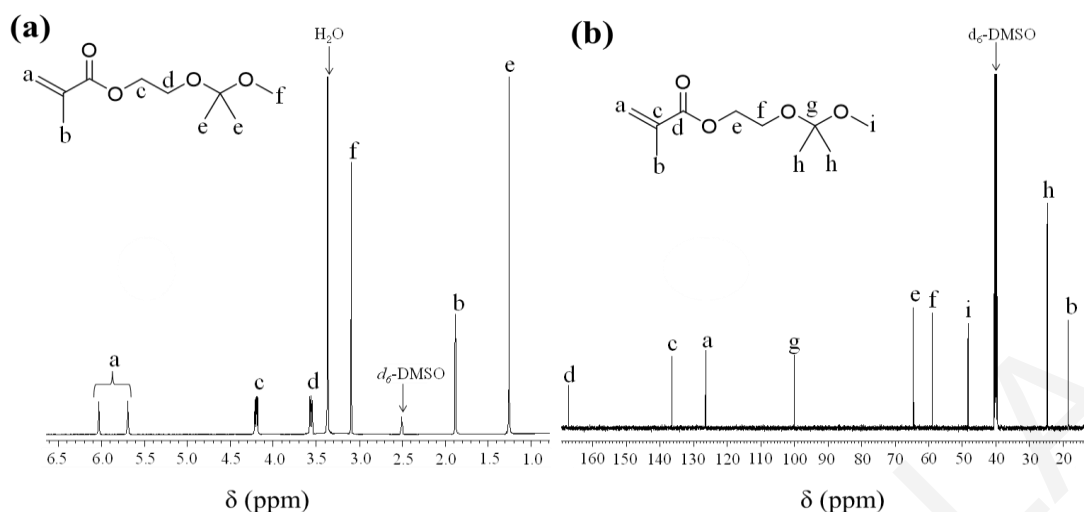


Figure 3.27. (a) ^1H and (b) ^{13}C NMR spectra of 2-[(2-methoxypropan-2-yl)oxy]ethyl methacrylate (m-HEMA) in d_6 -DMSO.

3.3.2. Synthesis of Hydrolyzable End-Linked Networks of MMA Based on EGDMA and DMOEP Crosslinkers.

Figure 3.28 shows the synthetic routes leading to the preparation of all four networks of this section. These networks included one network with both hydrolyzable cores (DMOEP₄-*b*-MMA₂₀-*b*-DMOEP₄), one network with both non-hydrolyzable cores (EGDMA₁-*b*-MMA₂₀-*b*-EGDMA₁), and two other polymer networks with both hydrolyzable and not hydrolyzable cores, and differing from each other as to which core is hydrolyzable, the first (DMOEP₄-*b*-MMA₂₀-*b*-EGDMA₁) or the second (EGDMA₁-*b*-MMA₂₀-*b*-DMOEP₄). Note that, while the non-hydrolyzable cores comprised one EGDMA unit, the hydrozable ones consisted of four DMOEP units because preliminary experiments experiment on the synthesis of “core-first” star polymers indicated that a DMOEP₄ core could yield “core-first” star homopolymers with MMA₂₀ arms of roughly the same size as those obtained using an EGDMA₁ core.

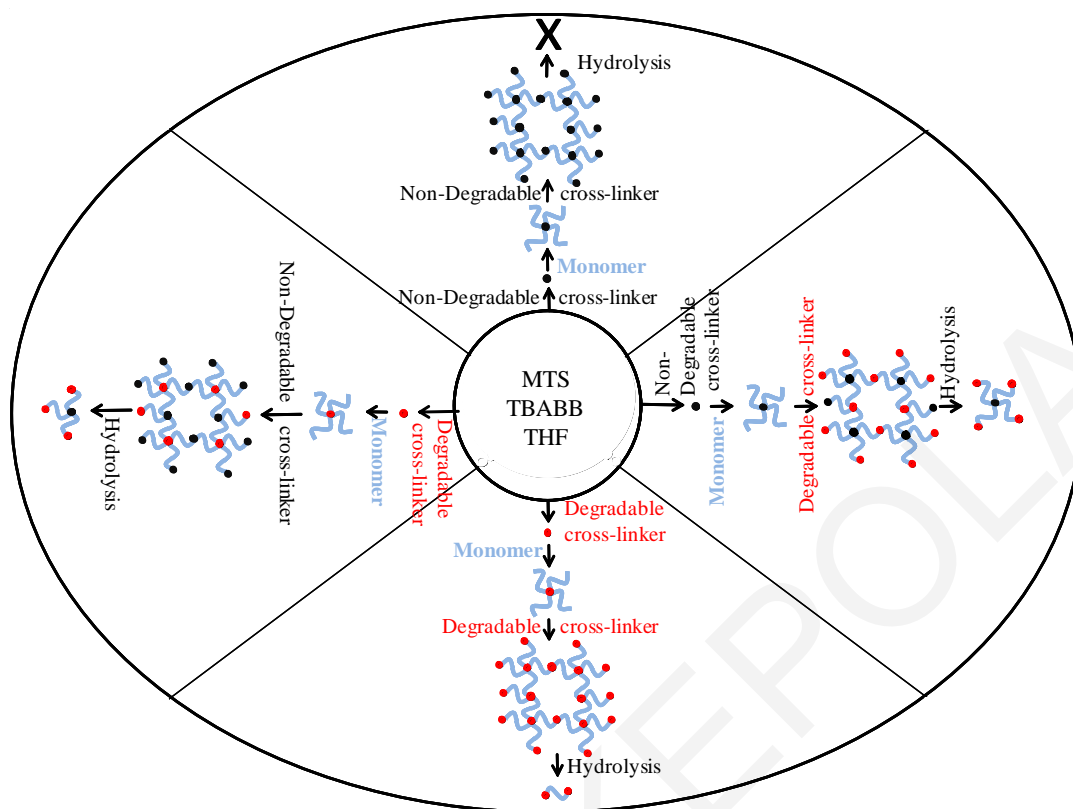


Figure 3.28 Synthesis and hydrolysis of networks based on end-linked “core-first” star MMA homopolymers using the four possible combinations of degradable and non-degradable crosslinkers.

3.3.3. GPC Traces of the Star Homopolymers.

Figure 3.29 presents the GPC traces of all the precursors to all the polymer networks (cores and “core-first” star homopolymers), the extractables from the networks, and the network hydrolysis products. The GPC traces of all cores (shown in red dotted lines) were broad, and displayed, in most cases, two main peaks (in the case of the EGDMA_{1-b}-MMA_{20-b}-DMOEP₄ network, the higher molecular weight peak degenerated to a shoulder), plus a third, lower molecular weight population in the form of a shoulder. The two main peaks in the GPC traces of the DMOEP-based cores were closer to each other, compared to those in the EGDMA-based cores which were more clearly separated from each other. This difference may be attributed to the greater polymerization reactivity of the less sterically hindered EGDMA crosslinker whose faster polymerization kinetics may lead to more heterogeneous polymeric products.

The GPC traces of all “core-first” star homopolymers (shown in blue dashed lines) were also broad, reflecting the shape of the GPC traces of their parent cores, and were expectedly shifted to shorter elution times, indicating polymer growth arising from the incorporation of MMA in the polymer structure. These GPC traces were also, in most cases, bimodal (in the case of the DMOEP₄-*b*-MMA₂₀-*b*-EGDMA₁ network, the higher molecular weight peak degenerated to a shoulder), with a much wider separation of the two peaks in the GPC traces in the case of the two EGDMA-based “core-first” star polymers compared to the DMOEP-based ones. In general, the GPC traces of the EGDMA-based cores and “core-first” star homopolymers in the present investigation were similar to those in our previous work on (non-degradable) amphiphilic polymer conetworks based on interconnected “core-first” star block copolymers, described in Sections 3.1 and 3.2 of this Thesis.³¹⁻³²

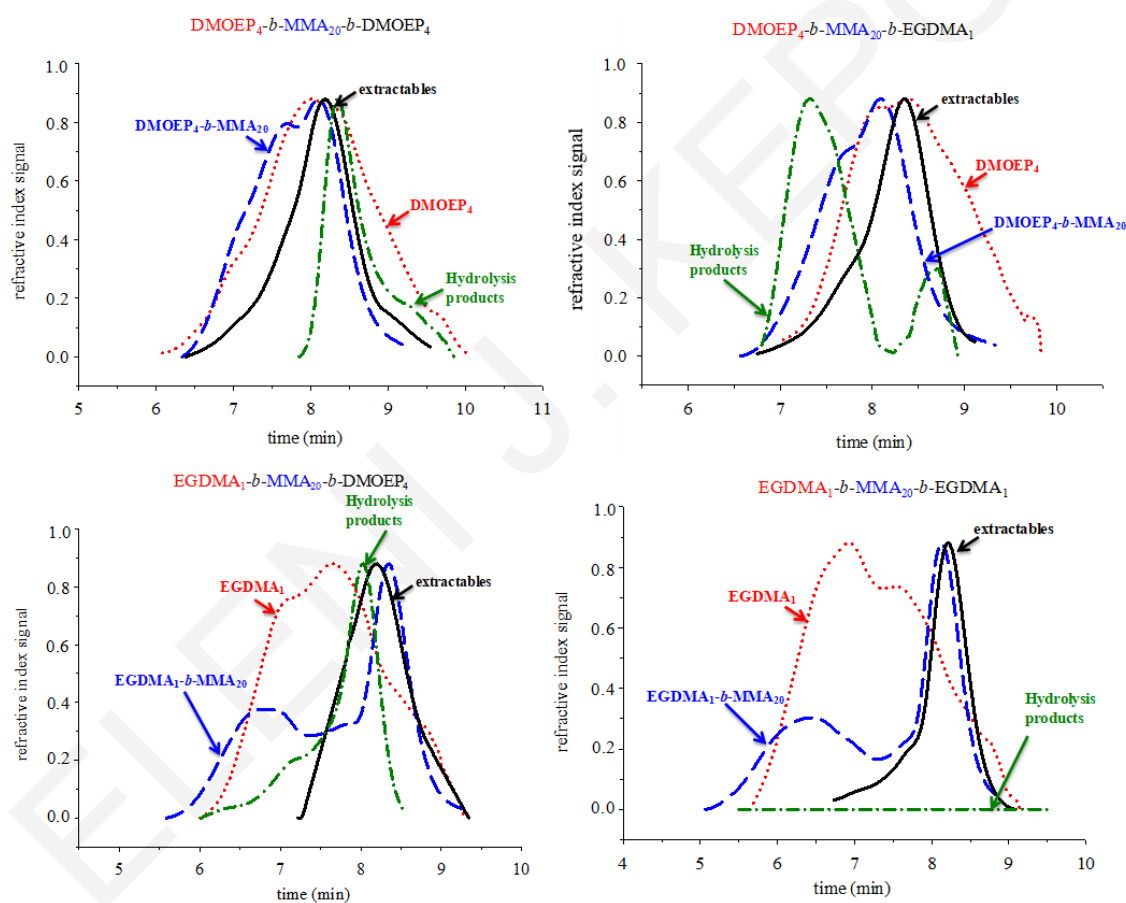


Figure 3.29. GPC traces of all the precursors to all MMA homopolymer networks synthesized, the extractables from the networks, and the hydrolysis products of the networks. The traces of the cores appear in red dotted curves, those of the star homopolymers in blue dashed lines, those of the hydrolysis products in green dashed-dotted lines, and those of the extractables in black continuous lines.

The GPC traces of all the extractables (shown in black continuous lines) from the networks were monomodal and much narrower than those corresponding to the network precursors, but displayed a long tailing toward shorter elution times, particularly the ones corresponding to networks with a DMOEP-based (primary) core. The GPC traces of the extractables from all polymer networks, but particularly those from networks with EGDMA-based (primary) cores, largely overlapped with the lower molecular weight peak of the “core-first” star polymer precursor.

Finally, the GPC traces of the network hydrolysis products (shown in green dashed-dotted lines) presented the following features. First, the GPC trace of the sample obtained after the hydrolysis processing of the polymer network with both EGDMA cores, EGDMA₁-*b*-MMA₂₀-*b*-EGDMA₁, displayed no polymer peaks, because this network cannot be hydrolyzed. Then, the GPC trace of the hydrolysis products of the polymer network with both DMOEP cores, DMOEP₄-*b*-MMA₂₀-*b*-DMOEP₄, was essentially monomodal, corresponding to a rather low molecular weight (longer elution time), lower than that of the corresponding extractables. Next, the GPC trace of the hydrolysis products of the polymer network containing both cross-linkers, and with the structure DMOEP₄-*b*-MMA₂₀-*b*-EGDMA₁, was bimodal, with the higher molecular weight peak (shorter elution time) exhibiting a higher molecular weight than the corresponding “core-first” star polymer (blue dashed line). Note, however, that the above-mentioned “core-first” star polymer has a primary core based on DMOEP (star polymer structure: DMOEP₄-*b*-MMA₂₀), whereas the network hydrolysis product, which is also a star polymer, has a secondary core based on EGDMA (star polymer structure: HEMA₈-*b*-MMA₂₀-*b*-EGDMA₁, where HEMA₈ represents the hydrolysis product of the DMOEP₄ core). The facts that the latter star polymer bears the more efficient EGDMA as its core component plus the inclusion of eight HEMA units per arm explain its shorter elution time (higher molecular weight) compared to its “core-first” star polymer precursor with a DMOEP core.

Lastly, the GPC trace of the hydrolysis products of the polymer network containing both cross-linkers, but with the structure EGDMA₁-*b*-MMA₂₀-*b*-DMOEP₄, was unexpectedly almost monomodal, with a peak at longer elution times (lower molecular weights), plus a shoulder at shorter elution times. The GPC trace for these hydrolysis products (expected star polymer structure: EGDMA₁-*b*-MMA₂₀-*b*-HEMA₈) was expected to be shifted to shorter elution times compared to its “core-first” star precursor polymer (structure: EGDMA₁-*b*-MMA₂₀) due to the extra 8 HEMA units added to the former structure. This appears to be

true for the lower molecular weight peaks (compare blue and green GPC traces at longer elution times), but not so at shorter elution times. Instead, a clear high molecular weight peak is totally missing from these hydrolysis products, and only a shoulder is present in this molecular weight range. This can be attributed to coupling among the network hydrolysis products, leading to formation of microgels / aggregates comprising (irreversibly) reconnected star polymers. This explanation is supported by the following observations. First, the solution of the hydrolysis products of this network was rather cloudy, but became clear after filtration through a syringe microfilter for sample preparation for GPC, apparently due to retention of the microgels onto the microfilter. Second, GPC experiments where both the amounts of network sample and solvent were carefully controlled indicated incomplete (by ~70%) area peak recovery in the case of the hydrolysis product of the particular polymer network; complete area peak recovery was recorded for the hydrolysis products of the two other hydrolyzable polymer networks.

The hydrolysis of samples from this polymer network using chloroform was repeated several times, but the same results were obtained. Network hydrolysis was also performed using stronger acids, and, in particular, THF solutions of hydrochloric acid or trifluoroacetic acid, but the star recombination was again observed and the results were again the same.

One may ask the question why the hydrolysis products (at least their higher molecular weight fraction) of the polymer network with the structure EGDMA₁-*b*-MMA₂₀-*b*-DMOEP₄ would recombine, but not so those of the DMOEP₄-*b*-MMA₂₀-*b*-EGDMA₁ network. This may be due to the fact that the hydrolysis products of the former network are of higher molecular weight than those of the latter, and, consequently, have many more reactive arm tips through which they can be covalently connected.

It would be useful to compare the results of the present study with those of a previous study of ours¹⁷⁻²⁴ on degradable polymer networks also prepared by GTP, but based on interconnected “arm-first” and “in-out” rather than “core-first” polyMMA stars. The hydrolysis products of the networks of the previous study, possessing a primary degradable core and a secondary non-degradable core, also exhibited a molecular weight greater than those of the network precursors. The hydrolysis products of the networks of the previous investigation, but possessing a primary non-degradable core and a secondary degradable core, were completely soluble (clear polymer solution) but of very high molecular weight, just above 5.000.000 g mol⁻¹. This extreme molecular weight indicated the strong tendency of those hydrolysis products to also reconnect into large aggregates. The fact that those

hydrolysis products maintained their solubility might be due to the fact those previous networks were based on “arm-first”, and, subsequently, “in-out”, star polymers, in which the extra star arms offered greater steric hindrance as compared to the present “core-first” star polymers, thus more efficiently disfavoring star-star coupling.

3.3.4. Molecular Weights, Absolute Molecular Weights and Compositions.

The number-average molecular weights, M_n , and the molecular weight dispersities, D , corresponding to the GPC traces displayed in Figure 3.29 were calculated relative to linear polyMMA standards (GPC-RI), and are listed in Table 3.9, together with the absolute weight-average molecular weights, M_w , (GPC-SLS) and calculated star numbers of arms. The calculated relative M_n and D values for the cores of the four star polymers ranged between 2200 and 12700 g mol⁻¹, and 2.5 and 5.7, respectively, with the values of both quantities for the EGDMA-based cores being higher than those of the DMOEP-based ones due to the higher reactivity of EGDMA. The M_n values for the “core-first” star homopolymers were higher than those of their parent cores, an exception being the “core-first” star polymer of the network with the structure EGDMA₁-*b*-MMA₂₀-*b*-EGDMA₁, where the discrepancy may be attributed to effects of high molecular weight dispersity. The table also lists the relative peak molecular weights, M_p , from which one can see that all “core-first” star polymers were bimodal, with the higher molecular weight peak of the EGDMA-based stars possessing a higher molecular weight than the corresponding peak of the DMOEP-based star polymers. The D values for the “core-first” star polymers with DMOEP cores were lower than those of the parent cores. This was also the case for one of the “core-first” star polymers with EGDMA core, for which its D value was slightly lower than that of its parent core. However, the reverse was true for the other “core-first” star polymer with EGDMA core, for which its D value was higher than that of the precursor core.

Table 3.9. Relative number-average molecular weights, M_n , and absolute weight-average molecular weights, M_w , and DMOEP content in the precursors to the polymer networks. The calculated numbers of arms of the star polymers are also listed.

Polymer Structure	GPC-RI			GPC-SLS		DMOEP Content (mol%)	
	M_p ($g\ mol^{-1}$)	M_n ($g\ mol^{-1}$)	D	M_w ($g\ mol^{-1}$)	no. of arms ^a	¹ H NMR	theory
DMOEP ₄ - <i>b</i> -MMA ₂₀ - <i>b</i> -DMOEP ₄							
DMOEP ₄	7410	2920	4.38	-	-	100.0	100.0
DMOEP ₄ - <i>star</i> -MMA ₂₀	12600 ^b	21100 ^b	1.25 ^b	15300	4.6	13.5	16.7
	6270 ^b	4310 ^b	1.20 ^b				
	6270 ^c	6840 ^c	2.34 ^c				
DMOEP ₄ - <i>b</i> -MMA ₂₀ - <i>b</i> -EGDMA ₁							
DMOEP ₄	3790	2220	2.53	-	-	100.0	100.0
DMOEP ₄ - <i>star</i> -MMA ₂₀	15100 ^b	15400 ^b	1.05 ^b	26900	8.1	11.8	16.7
	6670 ^b	4680 ^b	1.19 ^b				
	6670 ^c	5880 ^c	1.92 ^c				
EGDMA ₁ - <i>b</i> -MMA ₂₀ - <i>b</i> -EGDMA ₁							
EGDMA ₁	45500	12700	4.22	-	-	0.0	0.0
EGDMA ₁ - <i>star</i> -MMA ₂₀	102000 ^b	84000 ^b	1.84 ^b	18100	7.9	0.0	0.0
	5930 ^b	5740 ^b	1.29 ^b				
	5930 ^c	9430 ^c	7.53 ^c				
EGDMA ₁ - <i>b</i> -MMA ₂₀ - <i>b</i> -DMOEP ₄							
EGDMA ₁	13300	3950	5.66	-	-	0.0	0.0
EGDMA ₁ - <i>star</i> -MMA ₂₀	58400 ^b	53500 ^b	1.42 ^b	19500	8.5	0.0	0.0
	8520 ^b	15400 ^b	1.05 ^b				
	4120 ^b	3650 ^b	1.09 ^b				
	4120 ^c	6330 ^c	5.14 ^c				

^a Number of arms = (absolute M_w of star polymer) / (molecular weight of MTS-EGDMA₁-*b*-MMA₂₀ or MTS-DMOEP₄-*b*-MMA₂₀).

^b Calculation on individual peaks.

^c Calculation on whole GPC trace (overall molecular weight distribution).

Despite the differences in the molecular weights of the individual peaks, the overall absolute weight-average molecular weights, M_w , for the four star polymers were similar, around 20 000 $g\ mol^{-1}$, corresponding to about 5 to 8 arms per star polymer. This similarity in the values of the numbers of arms of all MMA star homopolymers confirms the equivalence of four DMOEP units to one EGDMA unit mentioned before.

The DMOEP content in the two “core-first” star polymers bearing it was determined using ¹H NMR spectroscopy by ratioing the areas of the characteristic peaks of the cross-linker and the

monomer. The signals from the six ketal protons at 3.7 ppm were used as the characteristic peaks for the DMOEP residues, whereas the signals from the three methoxy protons at 3.6 ppm were the most characteristic peaks for the MMA units. This calculation provided a DMOEP experimental content of 12-13 mol%, slightly lower than the value of 17 mol% expected from the polymerization feed ratio. The lower experimental value compared to the theoretical might be due to an underestimation in the DMOEP peak area in the ^1H NMR spectra, arising from peak broadening because of the reduced mobility of the DMOEP residues in the cores of the star polymers.

3.3.5. Extractables.

Table 3.10 lists the results from the characterization of the extractables from the polymer networks, and also the degrees of swelling in THF of the networks themselves. The percentage of the extractables (sol fraction) was rather high for all polymer networks, ranging between 29 and 46%. The lowest values of the extractables were displayed by the two networks cross-linked (in the final polymerization step) using the DMOEP cross-linker (29 and 31%), whereas the highest by those crosslinked using EGDMA (39 and 46%). The faster network formation accomplished using EGDMA may be the reason why a larger amount of polymer was not incorporated in the network, compared to the case when the more sterically-hindered DMOEP was used.

The M_n values of the extractables (GPC traces shown in Figure 3.29) were rather low, ranging from 4700 - 7200 g mol^{-1} , corresponding to the molecular weights of the lower molecular weight peak of the “core-first” star polymers. The D values of the extractables were between 2.0 and 2.9, corresponding to the monomodal GPC traces shown in Figure 3.29, which, however, presented tailing toward shorter elution times.

Table 3.10. Percentage, and molecular weight and composition characteristics of the extractables from the networks.

Polymer Network Structure	Characteristics of Extractables from Polymer Networks					
	Percentage (%)	GPC Results			DMOEP Content (mol%)	
		M_p ($g\ mol^{-1}$)	M_n ($g\ mol^{-1}$)	\bar{D}	1H NMR	Theory
DMOEP ₄ - <i>b</i> -MMA ₂₀ - <i>b</i> -DMOEP ₄	29	5700	5800	2.6	0.0	28.6
DMOEP ₄ - <i>b</i> -MMA ₂₀ - <i>b</i> -EGDMA ₁	46	5600	7200	2.9	0.0	16.7
EGDMA ₁ - <i>b</i> -MMA ₂₀ - <i>b</i> -EGDMA ₁	39	5400	5400	2.0	0.0	0.0
EGDMA ₁ - <i>b</i> -MMA ₂₀ - <i>b</i> -DMOEP ₄	31	4300	4700	2.3	0.0	16.7

These values were slightly higher than those of the “core-first” star polymers with DMOEP cores, but much lower than those of the “core-first” star polymers with EGDMA cores. No DMOEP was detected by 1H NMR spectroscopy in the extractables of the polymer networks. This may imply that either the extractables were linear polymers or only small, not detectable, amounts of DMOEP were incorporated in the extractables. Because the \bar{D} values determined for the extractables from the DMOEP-containing polymer networks (2.3 – 2.9) were much higher than those expected for linear homopolymers prepared using GTP (1.2 – 1.5), the latter scenario seems more likely.

3.3.6. Degrees of Swelling in THF.

Table 3.11 shows the DSs in THF for all polymers networks. The DSs possessed values which ranged between 5 and 9, which are rather low. Three out of four networks displayed DS values of around 5.

Table 3.11. Degrees of swelling of the networks in THF.

Polymer Network Structure	Degree of Swelling in THF
DMOEP ₄ - <i>b</i> -MMA ₂₀ - <i>b</i> -DMOEP ₄	5.0 ± 0.5
DMOEP ₄ - <i>b</i> -MMA ₂₀ - <i>b</i> -EGDMA ₁	8.6 ± 0.5
EGDMA ₁ - <i>b</i> -MMA ₂₀ - <i>b</i> -EGDMA ₁	5.5 ± 0.7
EGDMA ₁ - <i>b</i> -MMA ₂₀ - <i>b</i> -DMOEP ₄	5.3 ± 2.0

3.3.7. Size and Composition of the Polymer Network Hydrolysis Products.

The products of network hydrolysis under mildly acidic conditions (“acidic” chloroform) were characterized in terms of their size and composition, and the results are summarized in Table 3.12. For the polymer network with both hydrolyzable crosslinker cores, the hydrolysis products exhibited molecular weights with values very close to the theoretically calculated value of 4180 g mol^{-1} , and a D value of 1.5, typical for linear polymers prepared using GTP. Furthermore, the HEMA content in these hydrolysis products was 46 mol%, close to the value of 44 mol% expected on the basis of the feed ratio during the polymerizations in network preparation.

Table 3.12. Size and composition characteristics of the polymer network hydrolysis products.

Polymer Structure	Theoretical Molecular Weight (g mol^{-1})	Absolute M_w (g mol^{-1})	Results from GPC			HEMA content (mol%)	
			M_p (g mol^{-1})	M_n (g mol^{-1})	D	$^1\text{H NMR}$	theory
HEMA ₈ - <i>b</i> -MMA ₂₀ - <i>b</i> -HEMA ₈	4180	6420	4800	4000	1.5	46	44.4
HEMA ₈ - <i>b</i> -MMA ₂₀ - <i>b</i> -EGDMA ₁	-	72500	12200	12200	1.1	24	28.6
			4500	4200	1.1		
EGDMA ₁ - <i>b</i> -MMA ₂₀ - <i>b</i> -EGDMA ₁	No hydrolysis						
EGDMA ₁ - <i>b</i> -MMA ₂₀ - <i>b</i> -HEMA ₈	-	24800	22300	20500	1.1	23	28.6
			5100	4400	1.1		
			5100	7700	1.7		

The absolute M_w value for the hydrolysis product of the DMOEP₄-*b*-MMA₂₀-*b*-EGDMA₁ polymer network, HEMA₈-*b*-MMA₂₀-*b*-EGDMA₁, was higher than that for EGDMA₁-*b*-MMA₂₀-*b*-HEMA₈, the hydrolysis product of its isomeric network with the structure EGDMA₁-*b*-MMA₂₀-*b*-DMOEP₄. This can be attributed to the prevalence of the higher molecular weight peak in the former hydrolysis product (see Figure 3.29) and the prevalence of the lower molecular weight peak in the latter product due to the formation of large aggregates, as explained before. The corresponding average numbers of arms for the two hydrolysis products are 22 and 7.4. The HEMA content in these two hydrolysis products was 23 and 24 mol%, in good agreement with the theoretically expected value of 29 mol%.

3.3.8. Conclusions.

A degradable, ketal-based, dimethacrylate crosslinker was synthesized and used to prepare cleavable polymer networks of MMA using sequential GTP in three steps. These three steps involved crosslinker addition in the first step, followed by MMA addition in the second step, and completed by addition of crosslinker again in the third and final step. In each of the two crosslinker additions, either the degradable ketal cross-linker or a non-degradable crosslinker was used. These sums up to four possibilities, corresponding to four polymer networks, all of which were prepared in this investigation, characterized, and subjected to hydrolysis. Regarding the polymerization part, it is noteworthy that the three GTP steps required for the preparation of one polymer network took in total about 30 min, a particularly short time, especially when compared to alternate preparation methods, *e.g.*, controlled radical polymerization, which may take almost 1 day per polymerization step.

The products after the second polymerization step were “core-first” star polymers of MMA, which presented a bimodal size distribution. The lower molecular weight population of these stars possessed about the same molecular weight in all four preparations. However, the higher molecular weight population had higher molecular weight in the two cases when the non-degradable crosslinker had been used, as compared to the two cases when the degradable, ketal crosslinker had been used. This is thought to arise from the smaller size of the non-degradable crosslinker, presenting a smaller steric hindrance, and, therefore, being more reactive toward its polymerization.

Exposing the polymer networks containing the degradable ketal crosslinker to mildly acidic hydrolysis conditions led to complete network dissolution. Characterization of the network hydrolysis products indicated that their size was not always the expected. In particular, in two cases, the network hydrolysis products had the expected molecular weights and molecular weight distributions. However, in the third case, the larger hydrolysis products irreversibly recombined to form even larger covalent aggregates which escaped size and composition characterization, despite repeating the hydrolysis experiment several times, and using even stronger hydrolysis reagents.

3.4. Oligoamine-grafted Glycidyl Methacrylate Linear and Star Homopolymers: Odd-Even Correlated Transfection Efficiency.

Unlike the previous three sections that explored star polymers as building blocks for the preparation of crosslinked polymer networks, this section employs free (non-crosslinked) star polymers for a biomedical application, namely transfer to biological cells (transfection) of genetic material. Past research in our group,¹⁴⁷⁻¹⁵² has indicated that star polymers are better transfectants than linear polymers.

The specific aim in this study is to investigate whether the odd-even effect on DNA transfection efficiency, presented by oligoamine-substituted poly(amino acid)s, is more general, also holding for totally abiotic synthetic polymers (two “arm-first” star polymers and one linear polymer, all based on glycidyl methacrylate, GMA) non-viral gene vehicles. To this end, three series of oligoamine-grafted polyGMAs, bearing oligoamine side-groups with one to five ethylene imine repeating units, were synthesized and evaluated for their ability to deliver the firefly luciferase plasmid DNA *in vitro*. The oligoamines employed were EDA, DETrA, TrETA, TEPA and PEHA, comprising one, two, three, four and five ethylene imine repeating units, respectively, the same as those employed by Kataoka and coworkers.⁵³ These oligoamines were grafted onto methacrylate (the two star polymers and the linear polymer) backbones *via* the nucleophilic attack of the primary amine groups onto the glycidyl ring of the GMA monomer repeating units. One linear GMA homopolymer with a DP of 100, as well as two “arm-first” star GMA homopolymers with arm DPs of 20 and 100 were employed for the preparation of the oligoamine-grafted polymers. Before resorting to the ring-opening reaction, the grafting was attempted *via* a pentafluorophenyl¹⁴⁶ substitution reaction using a pentafluorophenyl acrylate homopolymer. However, this attempt was unsuccessful as undesired gelation was observed even when a large excess of the oligoamine (50 ×) relative to the reactive pentafluorophenyl acrylate repeating units was used during this polymer modification reaction. In order to avoid gel formation, we subsequently tried to protect the one end of the oligoamines using phthalic anhydride. However, both the synthesis and purification of the mono-phthalimide-protected oligoamines proved more difficult than originally anticipated. Thus, we next elected to use a readily available methacrylate backbone, polyGMA, which has a reactive epoxide ring side-group onto which the oligomeric amines could be readily grafted, without any undesired gel formation.⁵⁷

3.4.1. Synthesis Oligoamine-grafted Glycidyl Methacrylate Linear and Star Homopolymers.

Two “arm-first” star homopolymers of GMA with EGDMA crosslinker cores, and one linear homopolymer of GMA, were prepared, and subsequently functionalized with each of the five oligoamines. One of the star polymers had shorter arms, each of which with a DP of 20, and it was prepared by sequential GTP using MTS as initiator, TBABB as catalyst, and THF as solvent. The second star polymer had longer arms, each with a DP of 100, and it was synthesized by step-wise RAFT polymerization in the presence of linear polyGMA macroRAFT CTA, AIBN as radical source, and DMAc as solvent. For both star homopolymers, EGDMA served as the cross-linking agent, at a crosslinker to initiator (EGDMA : MTS) molar ratio of 4 : 1 for GMA₂₀-star, and a crosslinker to linear macroCTA (EGDMA : macroCTA) molar ratio of 6 : 1 for GMA₁₀₀-star. RAFT polymerization was chosen instead of GTP for the synthesis of GMA₁₀₀-star in order to readily reach the higher arm DP at sufficiently high monomer conversion, and high crosslinking efficiency.

3.4.2. Molecular Weights and Compositions.

The successful formation of the GMA star homopolymers was confirmed using GPC and ¹H NMR spectroscopy. The ¹H NMR spectra indicated that the GMA monomer conversion to polymer was 100 and 80% for the GTP and RAFT polymerizations, respectively, while EGDMA was fully polymerized in both polymerizations. In addition, the star homopolymers (before precipitation) and their linear precursors were characterized using GPC, and the obtained GPC traces are plotted in Figure 3.30.

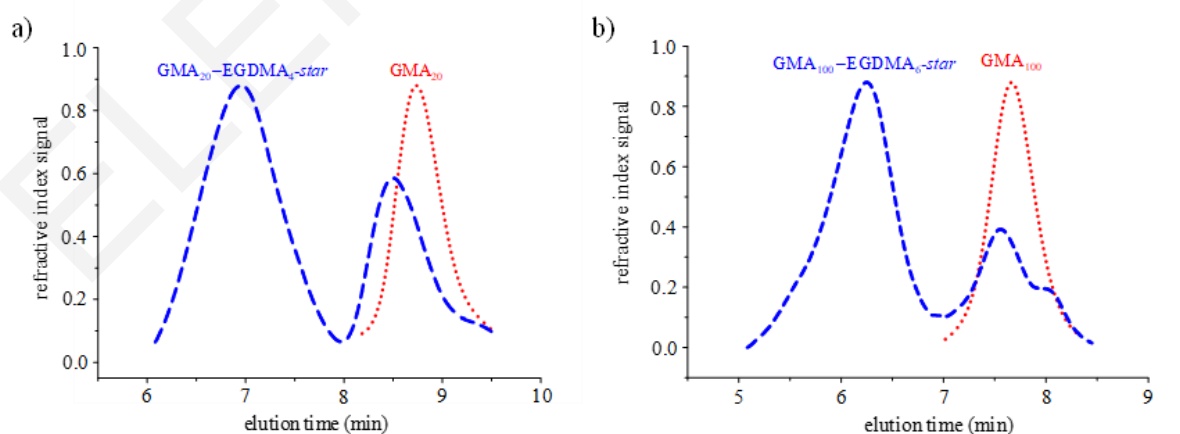


Figure 3.30. GPC traces of the GMA₂₀-star and GMA₁₀₀-star homopolymers together with those of their linear precursors.

The molecular weights calculated from these traces are listed in Table 3.13. The table also shows the theoretical molecular weights of the arms. GPC indicates that the M_n values of the linear polymer arms were reasonably close to the theoretically calculated molecular weight values. The molecular weight dispersities (\mathcal{D}) of the two linear polymers, GMA₂₀ and GMA₁₀₀, were 1.5 and 1.2, respectively. The GPC traces of the two star polymers were bimodal with one peak due to the star homopolymer and the other due to a small fraction of unattached arm. Their \mathcal{D} values were 1.5 and 1.7 for the GMA₂₀-star and GMA₁₀₀-star, respectively.

Table 3.13 Theoretical structures, monomer and crosslinker conversions, molecular weights, molecular weight dispersities, arm DPs and number of arms of the GMA star homopolymers.

Theoretical Polymer Structure ¹	Theoretical MW ² (g mol ⁻¹)	¹ H NMR monomer conversion (mol %)	GPC	
			M_n (g mol ⁻¹)	\mathcal{D}
GMA ₂₀	2940	GMA: 100	2000	1.5
GMA ₂₀ -star by GTP	-----	EGDMA: 100	39500	1.7
			2600	1.2
GMA ₁₀₀	14400	GMA: 80	15300	1.2
GMA ₁₀₀ -star ³ by RAFT	-----	GMA: 100 EGDMA:100	218100	1.5
			15100	1.3

¹ GMA: glycidyl methacrylate, EGDMA: ethylene glycol dimethacrylate.

² (Monomer MW) × (Targeted degree of polymerization) × (Monomer conversion from ¹H NMR) + MW_{initiator}.

³ Absolute M_w could not be determined due to the formation of unreasonably large aggregates.

3.4.3. Derivatization of GMA the Linear and Star Homopolymers with the Oligoamines.

Subsequently, all three GMA homopolymers, GMA₂₀-star, GMA₁₀₀-star and GMA₁₀₀, were derivatized with the five oligoamines, EDA, DETrA, TrETA, TEPA and PEHA, through the nucleophilic attack of the terminal primary amine group onto the epoxy group of GMA, in DMAc at 60 °C during the course of an 18 h reaction.¹²⁷ Figure 3.31 illustrates the synthetic procedure followed for the introduction of the oligoamine pendant groups to the GMA₁₀₀-star and the GMA₁₀₀-linear homopolymers. Note that a large (30 ×) excess of oligoamine relative to each GMA monomer repeating unit was employed to minimize the possibility for

interconnection between different polymer chains *via* the termini of the oligoamine molecules. Extensive interconnection of this type may lead to gel formation, as was the case with our original approach using the pentafluorophenyl acrylate linear homopolymer.

The introduction of the pendant oligoamine side-groups to polyGMAs was quantified using ^1H NMR spectroscopy on the products purified by dialysis. Figure 3.32 shows the ^1H NMR spectrum of the original GMA_{100} -*star* polymer along with those resulting from its grafting with the five oligoamines, (GMA_{100} -EDA)-*star*, (GMA_{100} -DETrA)-*star*, (GMA_{100} -TrETA)-*star*, (GMA_{100} -TEPA)-*star*, and (GMA_{100} -PEHA)-*star*. The reaction was driven to near-completion as can be seen from the almost complete disappearance of ring proton “d” at 3.2 ppm from the parent polymer, and the replacement of ring protons “e” at 2.7 and 2.9 ppm also from the original polymer by protons “e” and “f” in the daughter polymers.

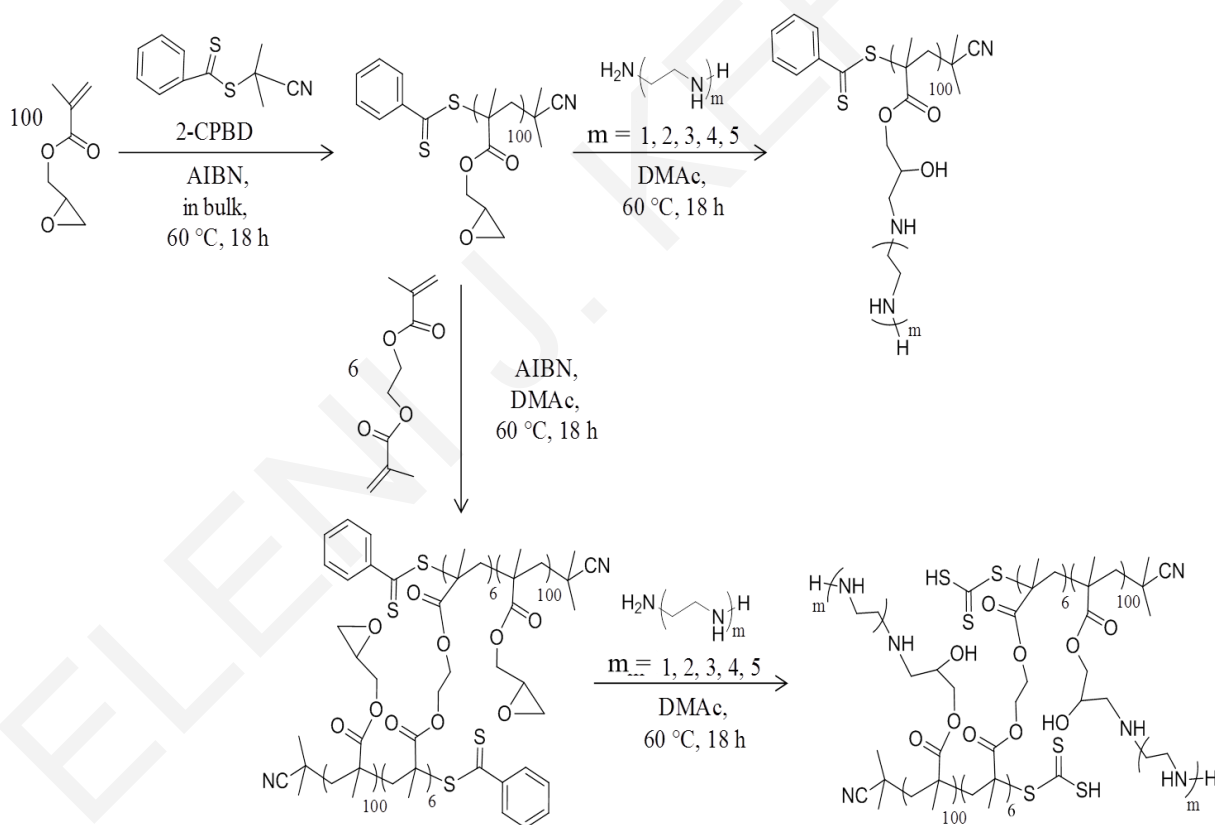


Figure 3.31. Synthetic routes followed for the preparation of the oligoamine-grafted GMA_{100} -*star* and GMA_{100} -*linear* homopolymers through RAFT polymerization and subsequent oligoamine grafting onto the ethylene oxide ring.

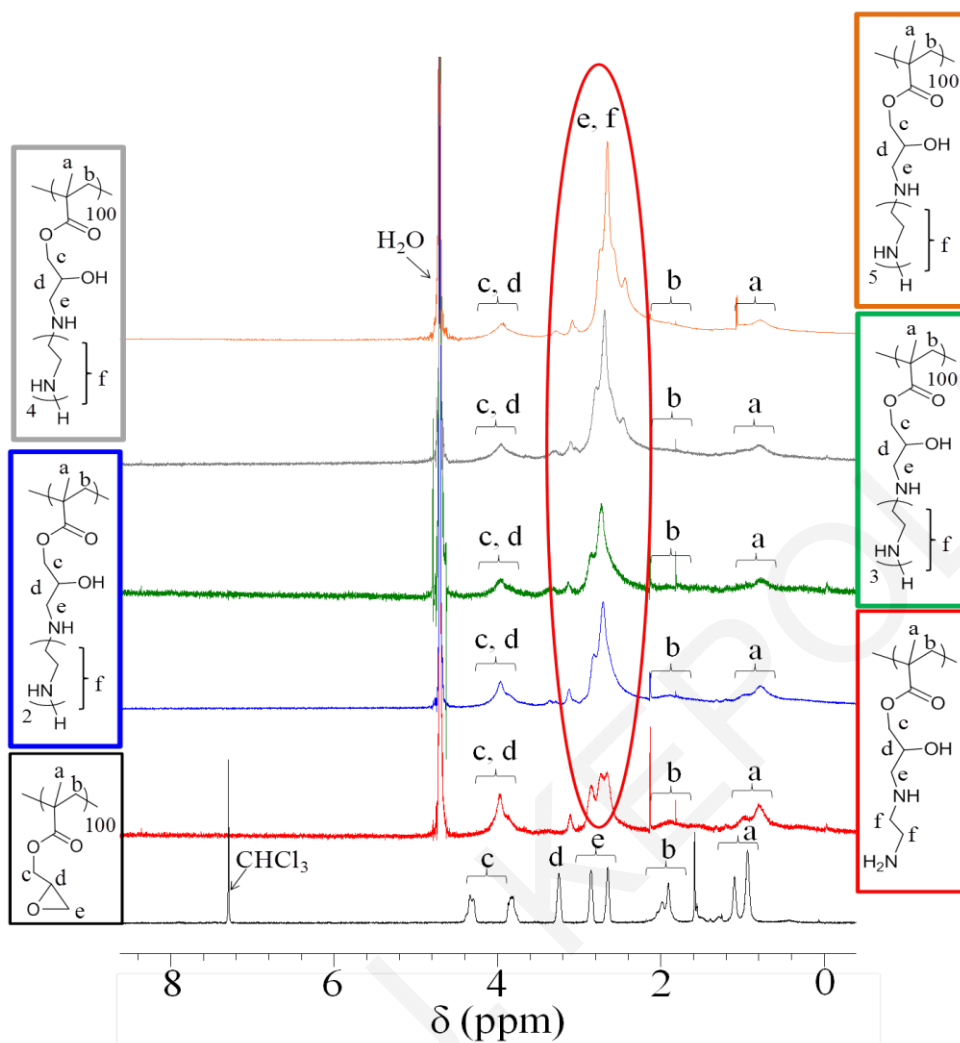


Figure 3.32. ^1H NMR spectrum of the GMA_{100} -*star* homopolymer in CDCl_3 , overlaid with those of the oligoamine-grafted GMAs: $(\text{GMA}_{100}\text{-EDA})\text{-star}$, $(\text{GMA}_{100}\text{-DETrA})\text{-star}$, $(\text{GMA}_{100}\text{-TrETA})\text{-star}$, $(\text{GMA}_{100}\text{-TEPA})\text{-star}$ and $(\text{GMA}_{100}\text{-PEHA})\text{-star}$ in D_2O .

3.4.4. Evaluation of the Oligoamine-grafted PolyGMAs as Plasmid DNA Transfectants.

All $(\text{GMA}_{20}\text{-amine})\text{-star}$ and $(\text{GMA}_{100}\text{-amine})\text{-star}$ as well as all $(\text{GMA}_{100}\text{-amine})\text{-linear}$ polymers were evaluated for their ability to deliver to mouse myoblast cells plasmid DNA which expressed the Luc gene. Figures 3.33-3.35 show the dependence of Luc expression and cell viability on the polymer (concentration of all polymer solutions was 3 g L^{-1}) loading used for all $(\text{GMA}_{20}\text{-amine})\text{-star}$, $(\text{GMA}_{100}\text{-amine})\text{-star}$ and $(\text{GMA}_{100}\text{-amine})\text{-linear}$ polymers. In these figures, the amount of polymer used was varied from 5 to 30 μL (15 to 90 μg) for the $(\text{GMA}_{20}\text{-amine})\text{-stars}$, 5 to 18 μL (15 to 54 μg) for the $(\text{GMA}_{100}\text{-amine})\text{-stars}$, and 5 to 40 μL (15 to 120 μg) for the $(\text{GMA}_{20}\text{-amine})\text{-linear}$ polymers, while the amount of

plasmid DNA was kept constant at 1000 ng. At this point, it should be mentioned that, for all polymers grafted with PEHA, the polymer amount used was kept between 5 and 15 μL (15 to 45 μg). This loading was found to be the least toxic.

Figure 3.33 shows that Luciferase expression by C2C12 mouse myoblast cells transfected using polyplexes of *plasmid* DNA with (GMA₂₀-amine)-*stars* grafted with EDA or TrETA was higher than that by cells transfected using polyplexes of *plasmid* DNA with (GMA₂₀-amine)-*stars* grafted with DETrA, TEPA or PEHA. The same trend, but in a more pronounced way, was also presented by (GMA₁₀₀-amine)-*stars* (Figure 3.34) where luciferase expression for DETrA, TEPA and PEHA was negligible. The above trend was very much weakened in the case of (GMA₁₀₀-amines)-*linear* polymers, presented in Figure 3.35, where the odd-even effect was only observed for the lowest polymer loading (10 μL), while for the other amounts, an increase in the number of the ethylene imine repeating units gave a lower transfection efficiency.

In these experiments, the cytotoxicity of the polyplexes was also determined. The polyplexes based on (GMA₂₀-amine)-*stars* presented a slight decrease in cell viability as the number of ethylene imine units in the pendant increased, for all polymer loadings. For the other two polymers, (GMA₁₀₀-amine)-*stars* and (GMA₁₀₀-amine)-*linears*, the cytotoxicity was higher for the polyplexes involving DETrA and TEPA compared to those involving EDA and TrETA. From this study, it was also observed that with the exception of (GMA₁₀₀-DETrA)-*star* and (GMA₁₀₀-TEPA)-*star*, the cytotoxicity of all oligoamine-grafted GMA polymers increased (within experimental error) with polymer loading, in agreement with our previous work.¹⁴⁷⁻¹⁵² The cytotoxicities of (GMA₁₀₀-DETrA)-*star* and (GMA₁₀₀-TEPA)-*star* remained constant. For all series, the Luc expression of polyplexes involving PEHA was lower than or equal to these of the other oligoamines due to the lower polymer loading used during transfection with the PEHA-bearing polymers. At the same polymer loadings, the cytotoxicity of PEHA-grafted polymers was very high.

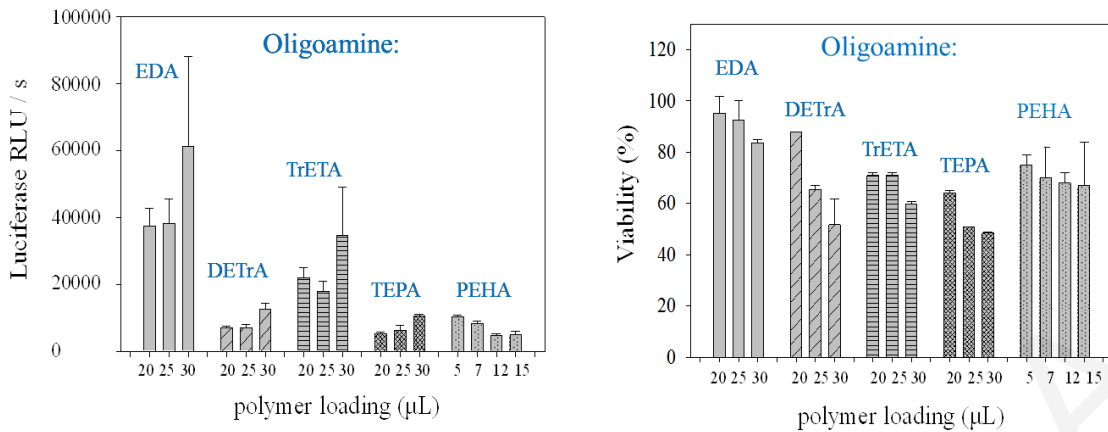


Figure 3.33. Dependence of Luc expression and cell viability on the amount of polymer at a constant amount of plasmid DNA for the (GMA₂₀-amine)-*star* homopolymers.

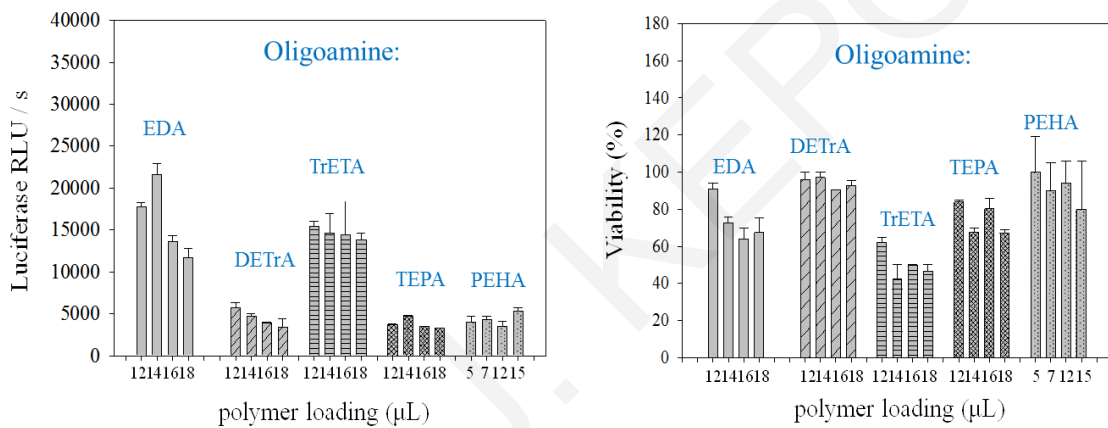


Figure 3.34. Dependence of Luc expression and cell viability on the amount of polymer at a constant amount of plasmid DNA for the (GMA₁₀₀-amine)-*star* homopolymers.

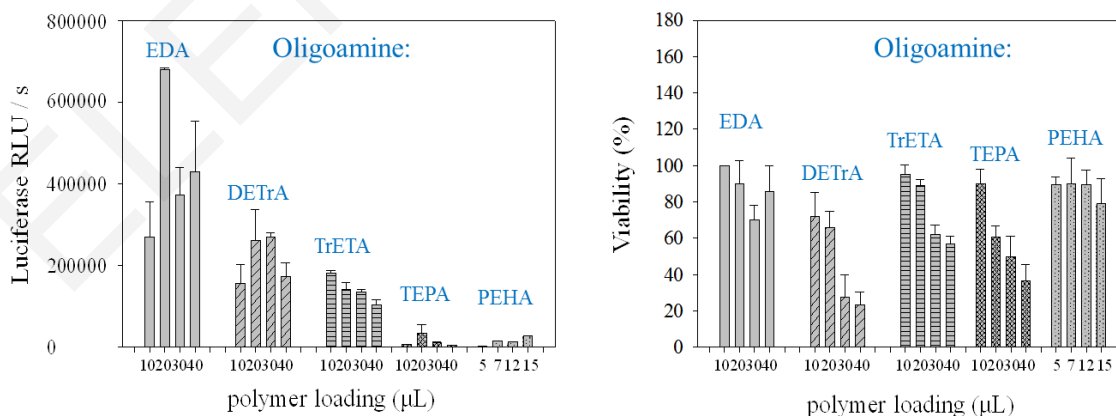


Figure 3.35. Dependence of Luc expression and cell viability on the amount of polymer at a constant amount of plasmid DNA for the (GMA₁₀₀-amine)-*linear* homopolymers.

It is clear that transfection efficiencies presented by oligoamine-grafted polymers with an even number of nitrogens were higher than those with an odd number of nitrogens. Comparing our results with Kataoka's findings,⁵³ where *N*-substituted polyaspartamides possessing an odd number of nitrogens units presented higher efficiencies. They ascribed this effect to the higher buffering capacity of the polymer with an even number of nitrogen units, as well as to their capability to disrupt membrane integrity selectively at endosomal pH, leading to highly effective endosomal escape of the polyplexes.

Comparing the structural characteristics of our polymers, the different effect can be attributed to the small difference in the structure of the two types of polymers. In Kataoka's polymers, the oligoamines are attached to the main chain through a terminal nitrogen atom which becomes part of an amide group; this amide nitrogen is incapable of accepting a proton and, therefore, it does not participate in the complexation with DNA. In contrast, in our polymers, all nitrogens in the oligoamine remain aminic and chargeable, even after their attachment to the main chain, and thus participate in polyplex formation.

In the case of PEHA, the transfection efficiency for both linear and star homopolymers was negligible and did not follow the odd-even trend. Similar transfection efficiencies for GMA-TEPA and GMA-PEHA have been reported in the literature.¹²⁷

Despite the similarities of our results with those in previous studies (odd-even effect), the transfection efficiencies in these studies were different. This may be attributed to the different cell types in the various studies. Pun's¹²⁷ and Kataoka's groups⁵³⁻⁵⁴ used cancer cell lines, HeLa and Huh-7 cells, respectively, compared with mouse myoblast cells used in this work. It is well-known that malignant cancer cells express different molecules or receptors on their cell surface compared to normal cells, and this may lead to special binding interactions of oligoamine-based polymers with cancer cells, facilitating the penetration of these complexes through the cell membranes and leading to higher transfection efficiencies.

To conclude, we have shown that the odd-even effect is also in action in the present study, implying that this effect is more general, and also applicable to totally abiotic transfection systems, in addition to the substituted poly(amino acid)s. Despite the generality of this effect, the difference in transfection efficiencies should be studied and elucidated. Thus, a lot of unanswered questions remain and should be resolved in order to elucidate the precise structure-function relationship between complexes and transfection efficiencies, including

specific interactions between amine-based polycations and malignant or normal cell surface receptors and molecules.

3.4.5. Conclusions.

In the present study we have shown that the odd-even effect is also in action in totally abiotic systems, in addition to the poly(amino acid)-based ones already reported in the literature. In particular, two series of GMA-based star homopolymers with arm DP of 20 and 100, as well as a series of linear GMA-based homopolymers with DP of 100 were successfully synthesized using GTP and RAFT polymerizations, and were grafted with the oligoamines EDA, DETrA, TrETA, TEPA and PEHA, possessing one to five ethylene imine repeating units. With the exception of the PEHA-grafted polymers, all oligoamine-grafted star homopolymers presented higher, albeit moderate, transfection efficiencies when the oligoamine-grafts possessed an even number of nitrogen atoms than an odd number. This trend was also followed by oligoamine-grafted linear homopolymers at low polymer loadings. The odd-even effect was also observed for the cytotoxicity of oligoamine-grafted GMA_{100} -linear and oligoamine-grafted GMA_{100} -star homopolymers, while the cytotoxicity for oligoamine-grafted GMA_{20} -stars slightly increased with the number of ethylene imine repeating units.

3.5. Metal-bearing Nanoparticles From the Chelation-driven Self-assembly of Diblock Co- and Ter-polymers: Preparation and Characterization with Atomic Force Microscopy and Dynamic Light Scattering.

Building on the previous section of this Doctoral Thesis on “arm-first” star homopolymers, in this section we present the preparation and characterization of hybrid metal-organic nanoparticles comprising diblock copolymer arms interconnected using metals *via* one of the blocks. To this end, a series of diblock copolymers composed of a metal-chelating short block and a longer relatively non-polar block were synthesized using reversible addition-fragmentation chain-transfer (RAFT) polymerization, along with cyano-2-propyl dithiobenzoate as chain transfer agent. 2-(Acetoacetoxy)ethyl methacrylate (AcEMA) served as the metal-chelating monomer, whereas lauryl methacrylate (LauMA) were employed as the non-polar one. Also, two AcEMA-LauMA diblock terpolymers were synthesized with the LauMA block doped with a fluorescent monomer, 9-anthrylmethyl methacrylate (AnMMA). All the polymers were characterized in terms of their molecular weights and compositions using gel permeation chromatography and ^1H NMR spectroscopy, respectively. Subsequently, the diblock co- and ter-polymers were dissolved in non-polar organic solvents to solubilize various metal salts, resulting in the formation of polymeric micelles loaded with metal in their core. The size and the morphology of these micelles were characterized using light scattering and atomic force microscopy, respectively.

In this study, we used the ability of amphiphilic block copolymers to create various organized nanomorphologies in solution due to microphase separation (as we presented in previous sections) and makes them ideal templates for the localization of metals on the nanoscale.

3.5.1. Synthesis and Characterization of the AnMMA Monomer.

The fluorescent AnMMA monomer was synthesized and purified in our laboratory. Its synthesis involves esterification of the corresponding alcohol with methacryloyl chloride in the presence of a mixture of triethylamine and pyridine bases, as shown in Figure 3.36.

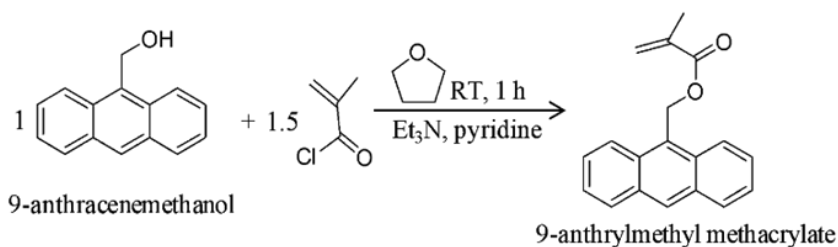


Figure 3.36. Chemical reaction leading to the formation of the monomer 9-anthrylmethyl methacrylate (AnMMA) via the esterification of 9-anthracenemethanol with methacryloyl chloride.

As expected, a rise in temperature was observed during the esterification reaction. The AnMMA was purified by column chromatography, to obtain the pure monomer in 75% yield.

The complete purification of the monomer and its structure were confirmed using ^1H - and ^{13}C -NMR spectroscopy. Figure 3.37 presents the ^1H - and ^{13}C -NMR spectra of AnMMA.

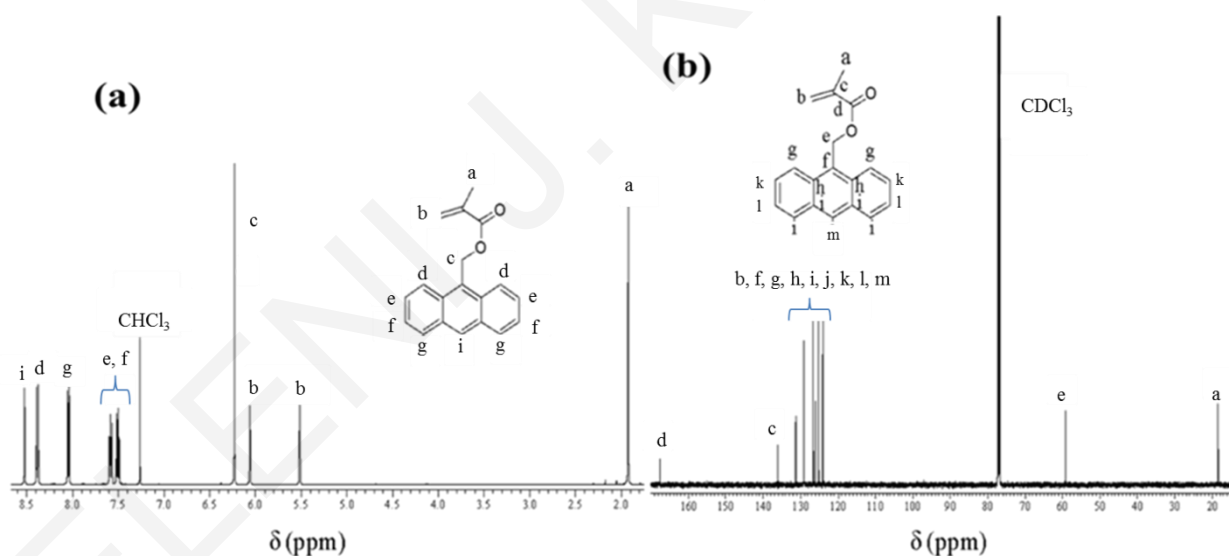


Figure 3.37. (a) ^1H and (b) ^{13}C NMR spectra of the purified AnMMA monomer in CDCl_3 .

3.5.2. Synthesis of Linear Diblock AcEMA-*b*-LauMA Copolymers AcEMA-*b*-(LauMA-co-AnMMA) Terpolymers.

All the polymers were synthesized using reversible addition-fragmentation chain transfer (RAFT) polymerization. Sequential monomer addition was used for the copolymer synthesis, whereas step-wise monomer addition was employed for the preparation of the terpolymers,

because of the high degree of polymerization in the second addition for the preparation of the LauMA plus AnMMA block, as presented in Figure 3.38.

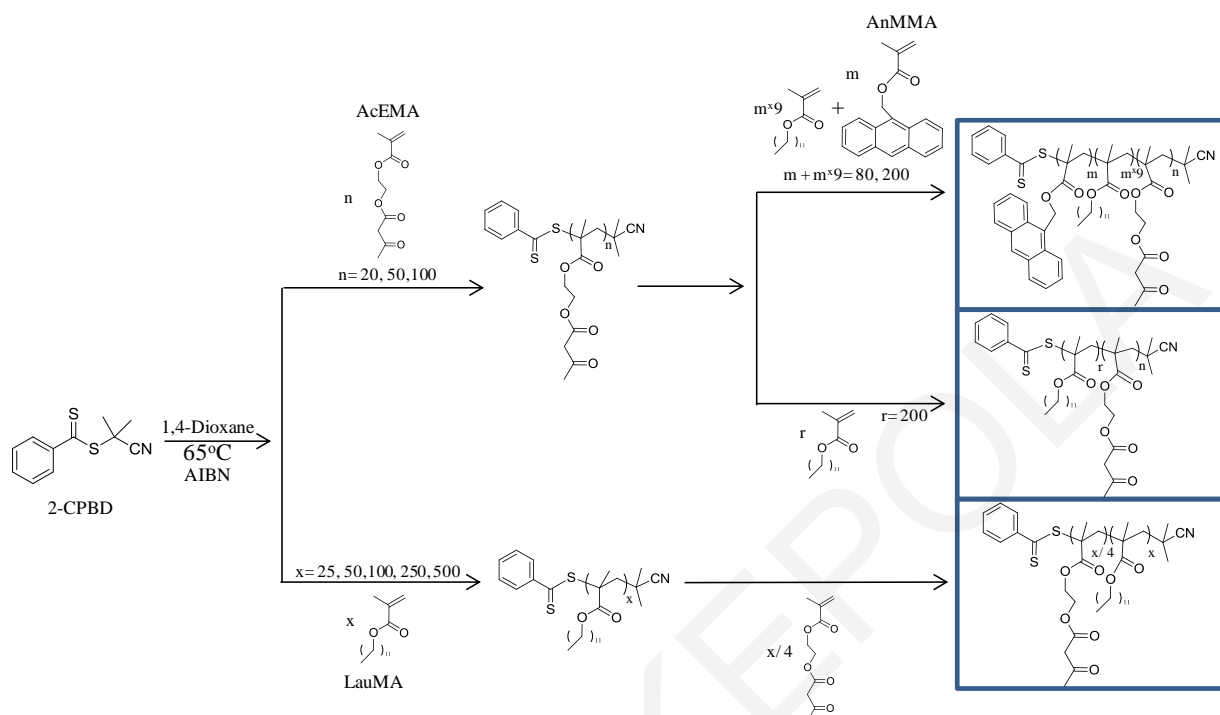


Figure 3.38. Synthesis of the diblock copolymers and terpolymers by RAFT polymerization.

3.5.3. Molecular Weights and Compositions.

Table 3.14 presents the molecular weights and compositions of the nine synthesized diblock polymers, as well as their precursor homopolymers. The number-average molecular weights, M_n , determined by GPC were close to the theoretical molecular weights expected on the base of the monomer: CTA ratio in the synthesis and taking into account the conversion of the monomers to polymer, with the latter having values above 85%.

The molecular weight, dispersity, D , of the polymers were in most cases low, 1.2-1.3. The compositions of the polymers as determined using ^1H NMR spectroscopy were in most cases very close to the theoretically expected.

Table 3.14. Molecular weights and compositions of the linear diblock copolymers and terpolymers determined using GPC and ¹H NMR, respectively.

Polymers	MW _{theor.} ^a (g mol ⁻¹)	GPC		AcEMA / AnMMA (mol%)		Monomer Conversion (%)	Gravimetric yield ^b (%)
		M _n (g mol ⁻¹)	Đ	¹ H NMR	Theory		
Step-wise Method							
AcEMA ₁₀₀	21200	20000	1.3	100	100	99	88
AcEMA _{100-b} -(LauMA _{180-co} - AnMMA ₂₀)	65300	87900	2.4	47 / 8	33 / 7	86 / 87	
AcEMA ₅₀	10700	13500	1.4	100	100	100	73
AcEMA _{50-b} -(LauMA _{180-co} - AnMMA ₂₀)	60000	70800	1.9	19 / 6	20 / 8	96 / 98	
AcEMA ₅₀	10700	13500	1.4	100	100	100	75
AcEMA _{50-b} -LauMA ₂₀₀	61000	71400	1.8	19	20	99	
AcEMA ₂₀	4300	5600	1.2	100	100	100	98
AcEMA _{20-b} -(LauMA _{72-co} - AnMMA ₈)	24600	30800	1.9	26 / 5	20 / 8	99 / 100	
Sequential Method							
LauMA ₂₅	6300	6600	1.2	0	0	99	96
LauMA _{25-grad} -AcEMA _{6.25}	7600	8700	1.2	22	20	100 / 95	
LauMA ₅₀	12500	14900	1.2	0	0	98	96
LauMA _{50-grad} -AcEMA _{12.5}	15100	16700	1.3	22	20	99 / 97	
LauMA ₁₀₀	25200	20000	1.2	0	0	99	99
LauMA _{100-grad} -AcEMA ₂₅	30300	23900	1.3	22	20	99 / 96	
LauMA ₂₅₀	61000	36300	1.2	0	0	96	99
LauMA _{250-grad} -AcEMA _{62.5}	74300	59800	1.2	21	20	96 / 100	
LauMA ₅₀₀	124500	92100	1.2	0	0	98	95
LauMA _{500-grad} -AcEMA ₁₂₅	150000	106400	1.5	21	20	98 / 94	

^a (Molecular weight of monomer) × (Degree of polymerization) × (monomer conversion of ¹H NMR). ^b (mass of polymer) / (total mass of monomers).

3.5.4. Polymer Complexation with Three Different Metals (Au, Pd, Ni) in Selective and Non-selective Organic Solvents.

The linear diblock copolymers and terpolymers were complexed with three different metal salts of Au, Pd and Ni, in four different organic solvents, non-selective (the solvent can dissolve all monomer repeating units) and selective (the solvent cannot dissolve the AcEMA monomer repeating units) as to the solubility of the AcEMA units. Figure 3.39 shows the two different methods where using the selective solvent (for AcEMA) the linear copolymer makes micelles, but when using non selective solvent, the linear copolymers stayed as linear structure, which is more difficult for nanoparticles synthesis.

All the metal-bearing nanoparticle solutions, with different metals and different solvents, were characterized using atomic force microscopy (AFM) for their morphologies and sizes, and also for their sizes using dynamic light scattering.

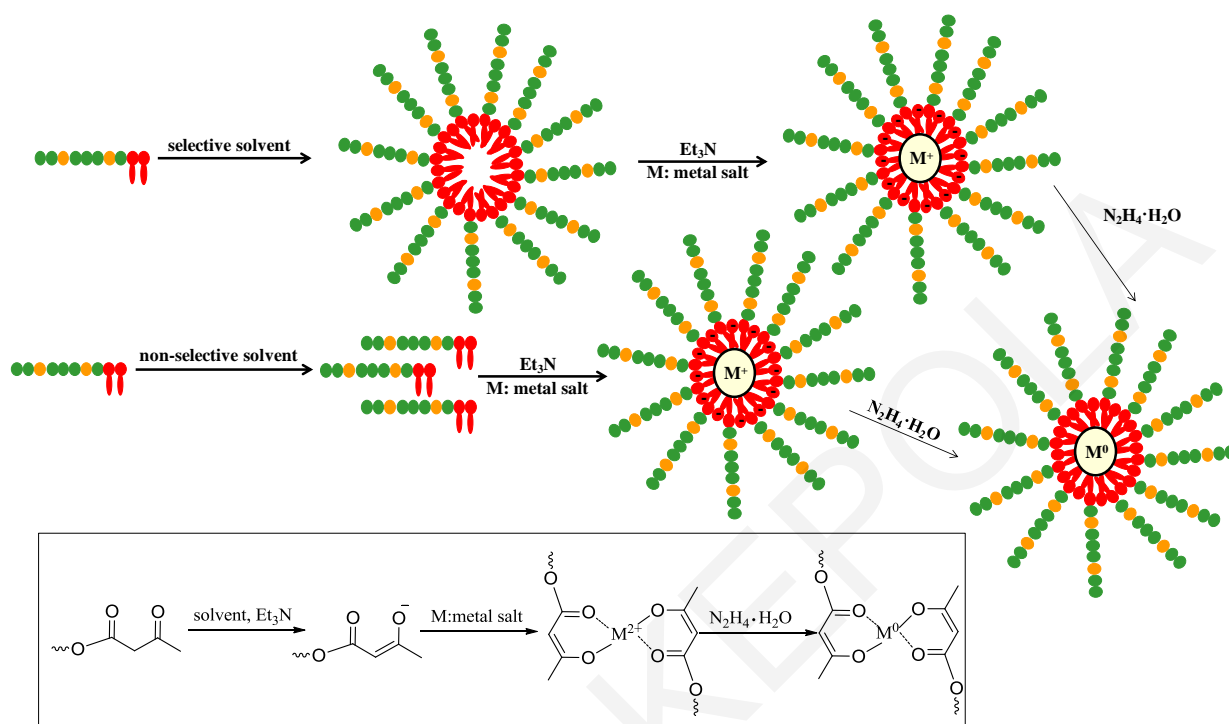


Figure 3.39. Fabrication of metal-bearing nanoparticles in selective and non-selective organic solvents.

3.5.5. Characterization of Nanoparticles Stability in Organic Solvents.

After characterizing all the co-and ter-polymers in terms of their molecular weights, their composition and their ability to make complexes with three different metals (Au, Pd, Ni), they were characterized in terms of their stability in organic solvents (chloroform, *n*-hexane, benzene and cyclohexane).

The most stable solutions were those in chloroform (B) and benzene (A) because the polyLauMA stabilizing portion is better soluble in these than in the other two solvents, *n*-hexane (D) and cyclohexane (C). Benzene was a better solvent for LauMA and AcEMA, so the micelles of the AnMMA-containing diblock were more stable in solution. In *n*-hexane and cyclohexane the micelles settle down after 48-72 hours. This was confirmed by observing the samples for more than 72 hours and the related photographs are shown in Figure 3.40.

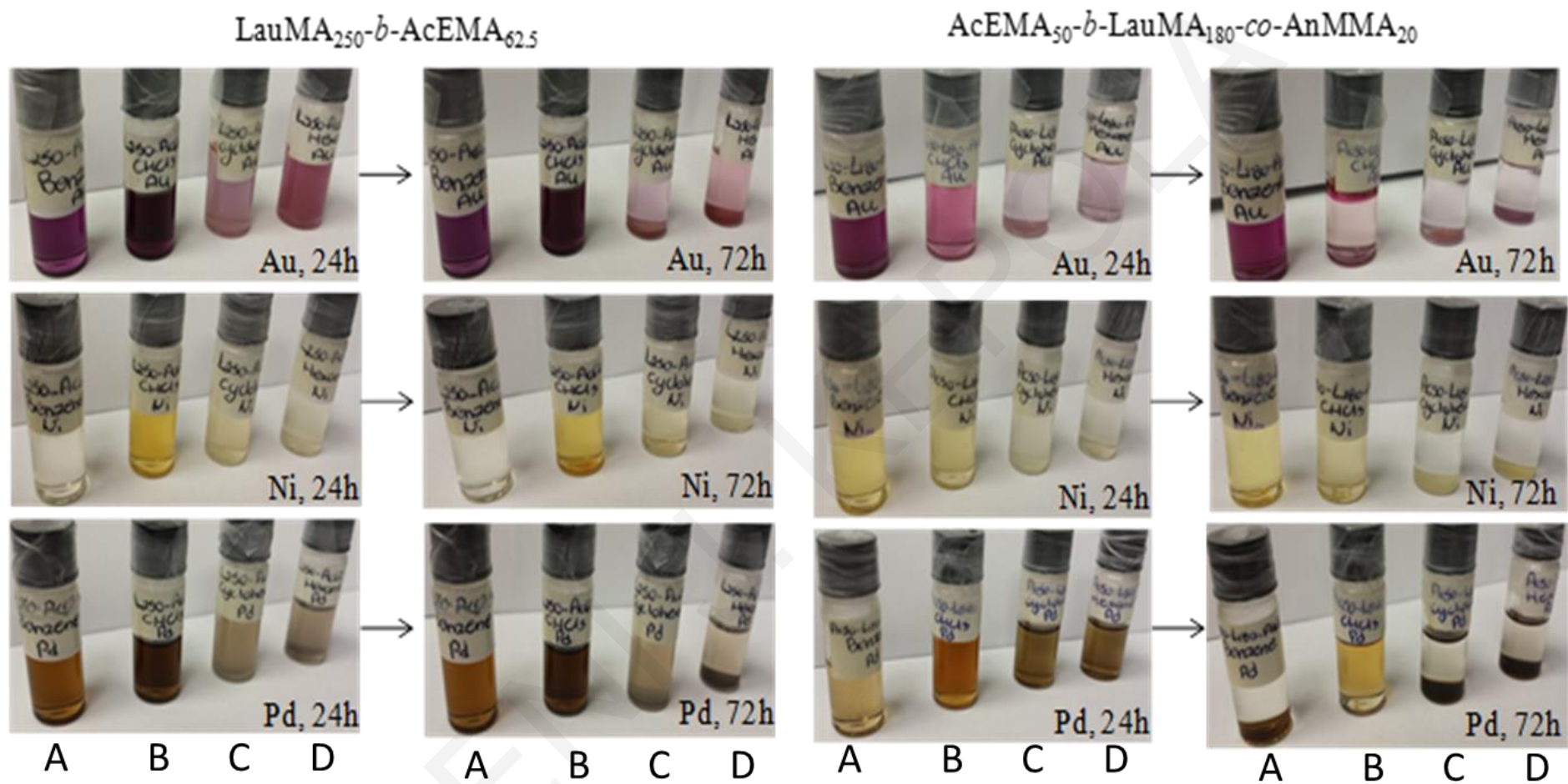


Figure 3.40. Photographs of one linear diblock copolymer and one linear diblock terpolymer complexed with three different metals (Au, Ni, Pd) in four different solvents. The photographs were taken after 24 h and 72 h from the complexations. A: Benzene, B: CHCl_3 , C: Cyclohexane, D: *n*-Hexane

3.5.6. Surface Morphology.

Several polymer-metal complexes were characterized using AFM. The complexes resulted from the combination of the four different copolymers, with and without AnMMA, in four different organic solvents, and with three different metals. The images obtained are shown in Figure 3.41. Table 3.15 summarizes the mean values of the radii of the particles from the images in Figure 3.41.

Figure 3.41 shows that the complexes were predominantly spherical in shape, as for example in the case of AcEMA₅₀-*b*-LauMA₂₀₀ with Pd in chloroform. However, in some cases, a cylindrical shape was observed, such as, for example, the complex of LauMA₂₅₀-*b*-AcEMA_{62.5} with Pd in cyclohexane. In the absence of metal, the copolymers in chloroform did not give large particles because chloroform is a non-selective solvent for the two segments, polyAcEMA and polyLauMA. When the solvents were selective, aggregates were observed, particularly when the samples were not filtered at all. Images with red frames correspond to samples that were not filtered, and clearly showed large aggregates.

Table 3.15 shows that polymers with higher molecular weights gave larger particles in less polar solvents such as *n*-hexane or cyclohexane, with the exception of the complexes with Pd where larger sizes were observed in chloroform. In most samples, there was a large polydispersity in particle size.

Finally, the Ni complexes exhibited many aggregates, even after cotton filtration. Complexes with Pd showed almost no aggregates but were ellipsoidal in shape. Au complexes exhibited aggregates but exhibited a more uniform spherical shape mainly in benzene and chloroform.

The non-metallic AcEMA₂₀-*b*-(LauMA₇₂-*c**o*-AnMMA₈) samples formed vesicles. However, after complexing with the metals, the vesicles were transformed into spherical micelles.

Solvents	AcEMA ₅₀ - <i>block</i> -LauMA ₂₀₀ $M_n = 71400 \text{ g mol}^{-1}$				AcEMA ₅₀ - <i>block</i> -(LauMA ₁₈₀ - <i>co</i> -AnMMA ₂₀) $M_n = 70800 \text{ g mol}^{-1}$			
	No metal	Metal in Nanoparticle			No metal	Metal in Nanoparticle		
		Ni	Pd	Au		Ni	Pd	Au
<i>n</i> -Hexane								
Cyclohexane								
Benzene								
CHCl ₃								

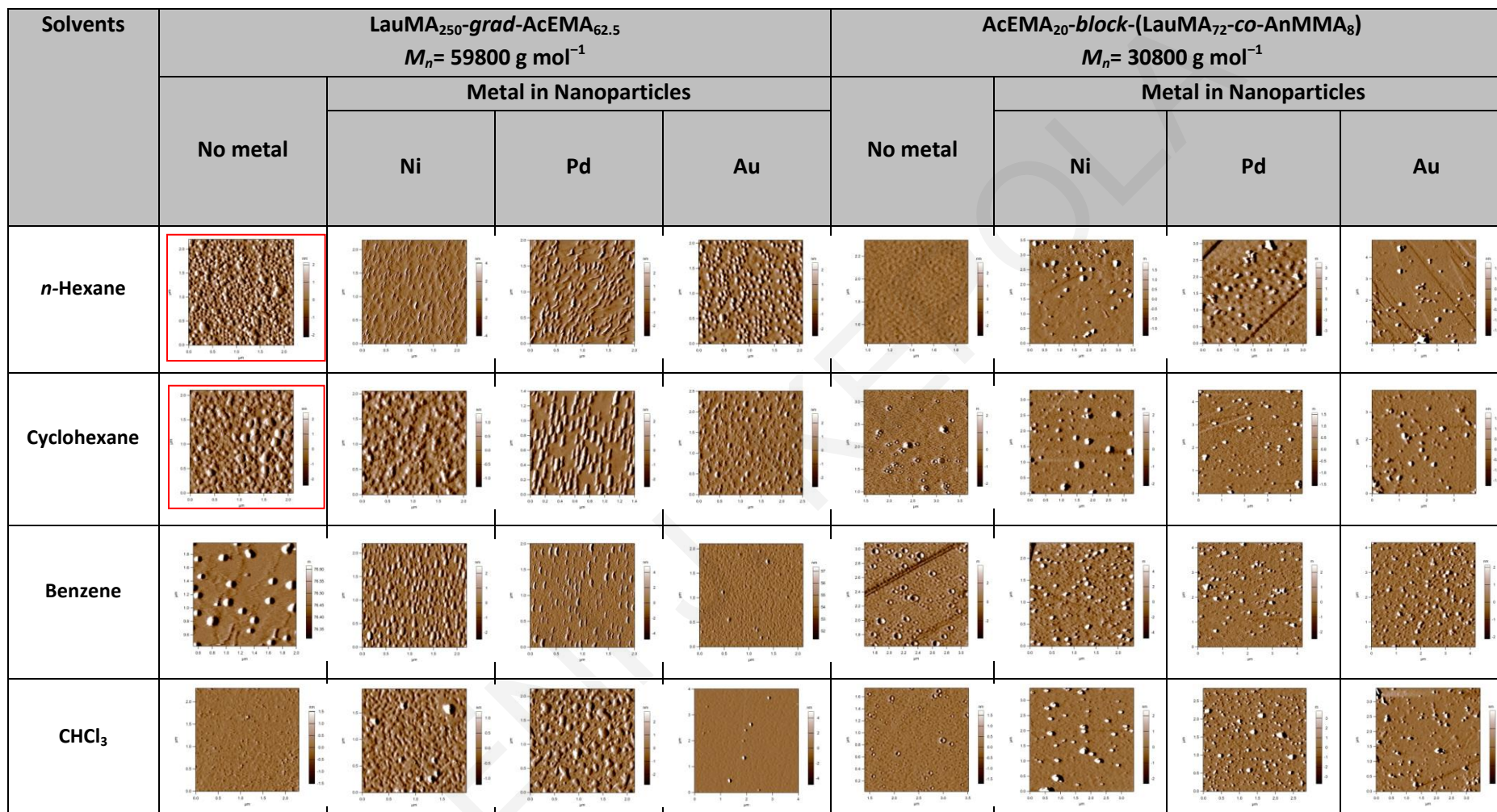


Figure 3.41. AFM images (4 μm x 4 μm) of the hybrid metal-organic nanoparticles cast from solutions in four different organic solvents.

Table 3.15. Radii of the major micelle populations and their mean values obtained from the AFM images in Figure 3.41.

AcEMA₅₀-block-LauMA₂₀₀, Theoretical R= 63.5 nm								
Solvents	No metals		Ni		Pd		Au	
	Radius of Major Populations R (nm)	Average R (nm)	Radii of Major Populations R (nm)	Average R (nm)	Radii of Major Populations R (nm)	Average R (nm)	Radii of Major Populations R (nm)	Average R (nm)
<i>n</i>-Hexane	Very large aggregate	Very large aggregate	125 90 60 45	80 Very large aggregate	50 40	45	50 35	43
Cyclohexane	Very large aggregate	Very large aggregate	90 70 50	70 Very large aggregate	72 45 23	47	57 45 35	46
Benzene	11 6	9	65 58 46	56	58 42 15	38	20 14	17
CHCl₃	No micelles	No micelles	No micelles	62	48 42	45	29 14	22
AcEMA₅₀-block-(LauMA₁₈₀-co-AnMMA₂₀), Theoretical R = 63.5 nm								
<i>n</i>-Hexane	42 22	32	150 90 Very large aggregate	120	95 68 54	72	150 80 55	95
Cyclohexane	55 35 15	35	190 140 55	142	125 65 31 21	61	100 95 54	83
Benzene	55	55	66 25	46	No micelles	19	54 24 17	32
CHCl₃	No micelles	No micelles	No micelles	46	Very large aggregate 44 27	36	No micelles	18

LauMA₂₅₀-<i>block</i>-AcEMA_{62.5}, Theoretical <i>R</i> = 79 nm								
<i>n</i>-Hexane	160 110 40	103	Length: Width: 76 20 50 18	Length Width: 64 18	Length: Width: 152 66 86 40	Length Width: 120 52	No micelles	45
Cyclohexane	75 55 35	55	50 40	45	Length: Width: 164 20 140 44 112 32	Length: Width: 138 42	95 67 50	71
Benzene	68 45 35	74	Length: Width: 150 84 110 60 80 36	Length: Width: 114 60	Length: Width: 154 76 132 52 106 22	Length: Width: 130 50	49 38 19	35
CHCl₃	No micelles	No micelles	97 45	71	Very large aggregate 89 44	67	No micelles	40
AcEMA₂₀-<i>block</i>-(LauMA₇₂-<i>co</i>-AnMMA₈), Theoretical <i>R</i> = 25 nm								
<i>n</i>-Hexane	26 9	18	150 100 70	100	50 22	36	50 31 10	30
Cyclohexane	27 12 6	15	150 50 10	70	51 20	35	50 31	41
Benzene	30 14 10	18	175 50 15 10	62	No micelles	24	32 16	24
CHCl₃	No micelles	No micelles	75 50	62	45 15 10 5	18	38 22 10	23

3.5.7. Absolute Molecular Weights and Radii of the Nanoparticles.

After the samples were characterized by AFM without being further filtered using syringe microfilters due to the difficulty in doing so, the same samples were characterized by static and dynamic light scattering to confirm the sizes of the complexes determined above using AFM, as well as to calculate the absolute molecular weights using a Zimm plot. Samples of DLS was used 0.4 % of sample concentration in 90°, while in SLS were used three different concentrations (0.4, 0.2, and 0.1 %) in a range of angles from 30-150°. Table 3.16 shows the results obtained for one of the polymers, the AcEMA₂₀-*b*-(LauMA₇₂-*co*-AnMMA₈) terpolymer, in four different solvents with three different metals.

Table 3.16. Absolute molecular weights and size characteristics of the nanoparticles formed by the AcEMA₂₀-*b*-(LauMA₇₂-*co*-AnMMA₈) terpolymer and its complexes with three metals in four solvents.

Polymer with	GPC	SLS			DLS	AFM	$N=M_w/M_n$	$N_{metal}/N_{no\ metal}$
	M_n (g/mol) GPC	M_w (g/mol)	R_g (nm)	A_2 (mol dm ³ /g ²)	R_h (nm)	Average R (nm)		
No metal/ CHCl ₃	30800	3.3×10 ⁴	42	6.7×10 ⁻¹⁰	8	-	1	1
Au/CHCl ₃	30800	9.0×10 ⁷	21	-7.7×10 ⁻¹⁰	52	23	2922	2922
Pd/CHCl ₃	30800	4.3×10 ⁸	120	-9.0×10 ⁻⁹	86 11 Average: 49	18	13961	13961
Ni/CHCl ₃	30800	1.7×10 ⁷	74	1.2×10 ⁻⁸	81 11 Average: 46	62	552	552
No metal/ <i>n</i> -Hexane	30800	8.8×10 ⁸	232	2.3×10 ⁻¹⁰	123 25 Average: 74	24	28571	1
Au/ <i>n</i> -Hexane	30800	5.1×10 ⁹	200	5.8×10 ⁻¹¹	484	30	165584	6
Pd/ <i>n</i> -Hexane	30800	3.1×10 ⁹	251	1.9×10 ⁻¹⁰	115 29 Average: 72	36	100649	4

Ni/ <i>n</i> -Hexane	30800	3.2×10^9	233	4.0×10^{-11}	798	100	103896	22
No metal/ Benzene	30800	6.9×10^5	70	8.6×10^{-6}	23	18	22	1
Au/ Benzene	30800	9.6×10^7	32	3.0×10^{-9}	68 16 Average: 42	24	3117	142
Pd/ Benzene	30800	7.3×10^7	90	1.8×10^{-8}	272 28 Average: 150	24	2370	108
Ni/ Benzene	30800	2.2×10^8	177	8.7×10^{-11}	455	62	7143	325
No metal/ Cyclohexane	30800	4.2×10^8	616	7.3×10^{-10}	152 77 Average: 115	15	13636	1
Au/ Cyclohexane	30800	1.3×10^9	160	6.5×10^{-11}	641	41	42208	3
Pd/ Cyclohexane	30800	3.1×10^9	202	8.1×10^{-10}	90 10 Average: 50	35	100649	7
Ni/ Cyclohexane	30800	2.9×10^9	276	2.3×10^{-10}	737	70	94156	7

The nanoparticle sizes determined using DLS / SLS (R_h and R_g , but also M_w and N) were large, much larger than those determined using AFM, again confirming the sensitivity of DLS/ SLS to larger particles. It is concluded that the best polymer - metal complexes, either by the less of aggregates in the samples of them or due to their stability in solution were the gold complexes in benzene and chloroform.

3.5.8. Conclusions.

Polymer-metal micellar nanohybrids consisting of well-defined methacrylate block copolymers comprising an organic-solvent soluble block and a metal-binding block, and metal nanoparticles (MNPs) of one of the metals Ni, Pd or Au, were fabricated. The complexes resulted from the combination of four different copolymers, with and without AnMMA, in four different organic solvents, and with three different metals. The complexes

with Ni exhibited the greatest number of aggregates in solution, even after filtering with cotton. The complexes with Pd contained virtually no aggregates, but, when observed, they were oval in some solutions. Complexes with Au showed a few samples of aggregates but had more uniformly spherical shape mainly in benzene and chloroform. It is concluded that the best polymer-metal complexes, judging both from the small concentration of aggregates and their high stability in solution were the complexes with gold in benzene and chloroform.

ELENI J. KEPOLA

3.6. Metal-end-linked Polymer Conetworks from the Chelation-driven Self-assembly of ABA Triblock Copolymers: Preparation and Characterization.

The previous section in this Doctoral Thesis presented hybrid nanoparticles held together by metal coordination bonds, whereas the first three sections dealt with covalently crosslinked polymer networks. This section intends to combine these two above-mentioned concepts by showing the preparation of polymer networks interconnected *via* metal coordination bonds. The organic parts of the networks were AcEMA-LauMA-AcEMA triblock copolymers, while the linking metal was either gold or palladium. The ABA triblock copolymers were synthesized using RAFT polymerization and employing the in-house-prepared bifunctional chain transfer agent, 1,4-BTBTPB. Five different AcEMA-LauMA-AcEMA copolymers of different molecular weights but the same AcEMA mol fraction were prepared.

3.6.1. RAFT Synthesis of the AcEMA-LauMA-AcEMA Triblock Copolymers.

The ABA triblock copolymers were synthesized using sequential RAFT polymerization, employing the in-house-prepared bifunctional CTA 1,4-BTBTPB and AIBN initiator in 1,4-dioxane as solvent. Figure 3.42 below illustrates the two-step synthetic route followed for the preparation of these ABA triblock copolymers.

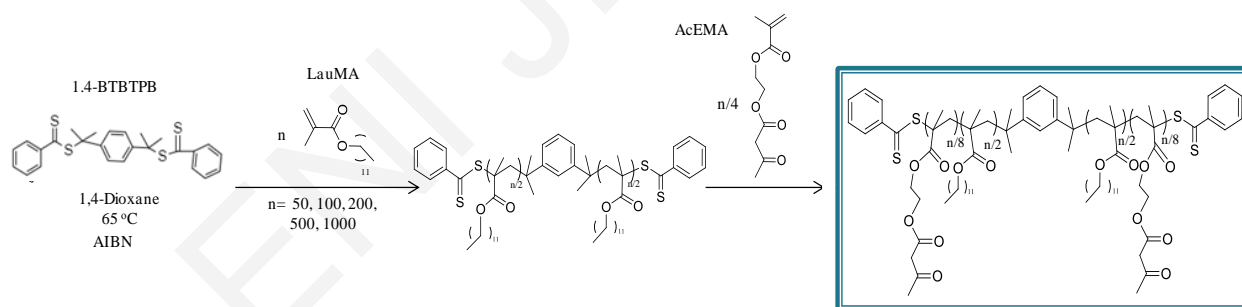


Figure 3.42. Synthetic route followed for the preparation of the AcEMA-LauMA-AcEMA triblock copolymers by the two-step sequential RAFT polymerization using a bifunctional CTA in 1,4-dioxane at 65 °C.

3.6.2. Molecular Weights and Compositions.

The synthesized ABA triblock copolymers covered a broad range of molecular weights, from 16800 to 186900 g mol⁻¹, but had a constant AcEMA content of 20 mol%. The molecular weight and composition characteristics of these copolymers, determined using GPC and ¹H NMR spectroscopy, respectively, are presented in Table 3.17.

Table 3.17. Chemical structures, molecular weights and compositions of the prepared metal-chelating AcEMA-LauMA-AcEMA triblock copolymers.

(Co)polymer Structure	Theor. MW ¹ (g mol ⁻¹)	GPC		AcEMA (mol %)		Monomer conversion (mol%) LauMA / AcEMA	Mass Recovery ² (%)
		M _n (g mol ⁻¹)	Đ	¹ H NMR	Theory		
LauMA ₅₀	12600	15400	1.3	0	0	99	88
AcEMA _{6.25} - <i>b</i> -LauMA ₅₀ - <i>b</i> -AcEMA _{6.25}	14900	16800	1.3	22	20	99 / 87	
LauMA ₁₀₀	24900	22900	1.3	0	0	98	92
AcEMA _{12.5} - <i>b</i> -LauMA ₁₀₀ - <i>b</i> -AcEMA _{12.5}	28400	30100	1.3	20	20	98 / 90	
LauMA ₂₀₀	48300	45300	1.2	0	0	95	90
AcEMA ₂₅ - <i>b</i> -LauMA ₂₀₀ - <i>b</i> -AcEMA ₂₅	56200	46700	1.3	23	20	97 / 92	
LauMA ₅₀₀	114300	99200	1.3	0	0	90	91
AcEMA _{62.5} - <i>b</i> -LauMA ₅₀₀ - <i>b</i> -AcEMA _{62.5}	122200	107300	1.4	22	20	96 / 92	
LauMA ₁₀₀₀	231100	136500	1.8	0	0	91	86
AcEMA ₁₂₅ - <i>b</i> -LauMA ₁₀₀₀ - <i>b</i> -AcEMA ₁₂₅	272300	186900	1.8	17	20	91 / 73	

¹ Homopolymer: (Molecular weight of LauMA monomer) × (Targeted degree of polymerization) × (LauMA homopolymer to polymer conversion by ¹H NMR spectroscopy) and (Co)Polymer: (Theoretical MW for Homopolymer) + [(Molecular weight of AcEMA) × (Targeted degree of polymerization) × (AcEMA monomer to polymer conversion by ¹H NMR spectroscopy)] ² (Mass of polymer recovered) / (Mass of monomers loaded).

3.6.3. Complexation with Metals Leading to the Formation of Hybrid Networks.

The AcEMA-LauMA-AcEMA triblock copolymers were used for complexation (through the AcEMA units in the terminal blocks) with gold or palladium metal ions in tetrahydrofuran. In the case of the palladium-containing networks, gelation took place upon reduction *via* the addition of N₂H₄·H₂O, after 30 – 60 min. In the case of the gold-containing networks, gelation was observed after 2 – 3 hours after the addition of Et₃N. These processes are schematically illustrated in Figure 3.43, where the photographs of the hybrid networks obtained after crosslinking with palladium (dark orange) and gold (dark purple) are also given.

For all the networks, after dissolving the copolymer in the non-selective tetrahydrofuran, triethylamine was added to enolize the AcEMA units in the copolymers, followed by the introduction of the metal salts.

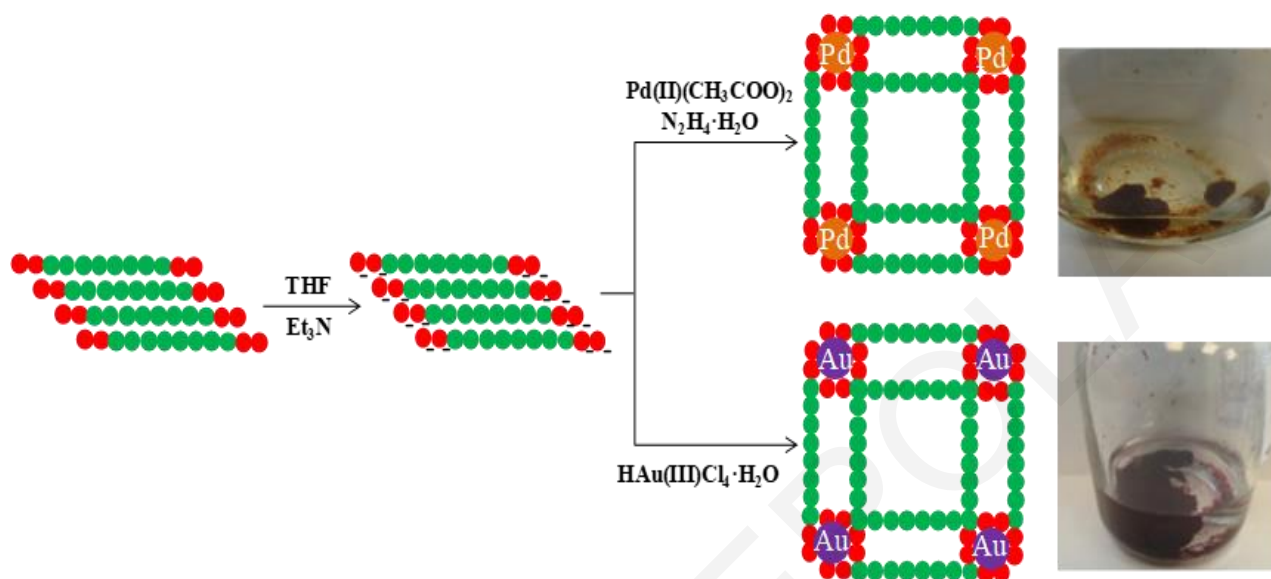


Figure 3.43. Schematic representation of the procedure followed for the formation of the metal-end-linked ABA triblock copolymer conetworks, and photographs of the final products.

3.6.4. Degrees of Swelling in *n*-Hexane.

The metal-end-linked ABA triblock copolymer conetworks were transferred to *n*-hexane for better stabilization (compared to THF), where they were equilibrated. Their equilibrium degrees of swelling in *n*-hexane were measured and are given in Table 3.18. All degrees of swelling were relatively low (< 14), manifesting the compact nature of the conetworks. The degrees of swelling did not depend on the molecular weight of the copolymers but on the length of the LauMa block vs. the length of the AcEMA block.

Table 3.18. Degrees of swelling in *n*-hexane of the gold- and palladium-end-linked AcEMA-LauMA-AcEMA triblock copolymer conetworks.

Metal-end-linked Polymer Conetworks	Degrees of Swelling	
	in <i>n</i> -Hexane	
	Au	Pd
AcEMA _{6.25} - <i>b</i> -LauMA ₅₀ - <i>b</i> -AcEMA _{6.25}	11.5 ± 0.1	8.8 ± 0.6
AcEMA _{12.5} - <i>b</i> -LauMA ₁₀₀ - <i>b</i> -AcEMA _{12.5}	2.7 ± 0.2	4.8 ± 0.1
AcEMA ₂₅ - <i>b</i> -LauMA ₂₀₀ - <i>b</i> -AcEMA ₂₅	6.8 ± 0.1	7.0 ± 0.2
AcEMA _{62.5} - <i>b</i> -LauMA ₅₀₀ - <i>b</i> -AcEMA _{62.5}	7.4 ± 0.2	9.7 ± 0.6
AcEMA ₁₂₅ - <i>b</i> -LauMA ₁₀₀₀ - <i>b</i> -AcEMA ₁₂₅	13.5 ± 0.4	12.1 ± 0.1

Figure 3.44 shows the dependence of the DSs in *n*-hexane on the LauMA DPs for the Au-end-linked and Pd-end-linked-conetworks. With the exception of [LauMA₅₀-BT]-AcEMA_{12.5}, we observed that as the LauMA DP increases, the DS in *n*-hexane increases too, in both cases.

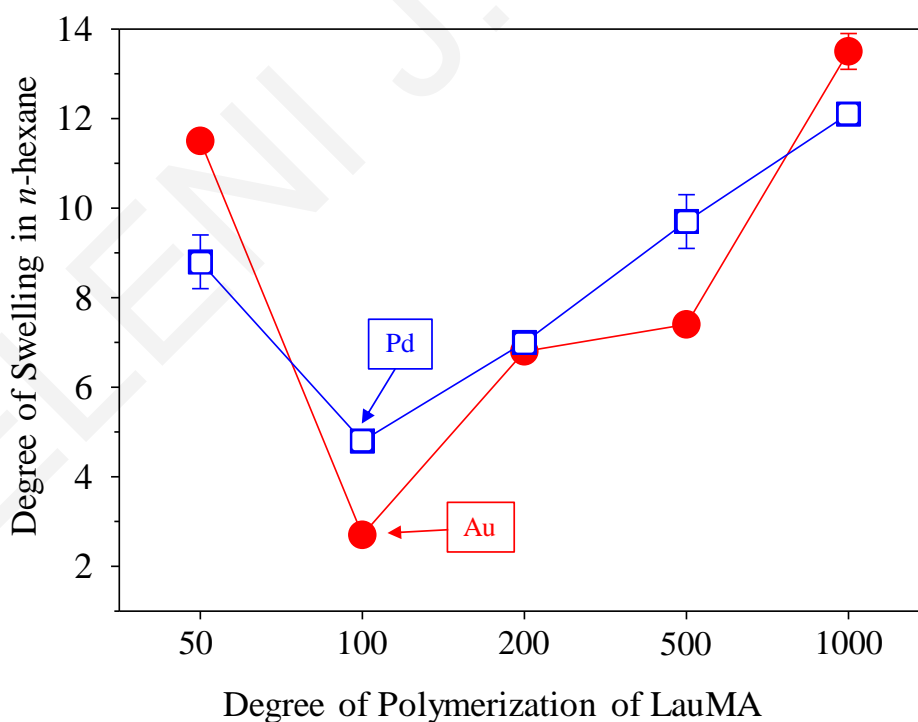


Figure 3.44. Dependence of the degrees of swelling in *n*-hexane on the degree of polymerization of the LauMA mid-block of the Au- and Pd-end-linked-conetworks.

3.6.5. Size of the Au and Pd Crystallites in the Au- and Pd-end-linked Polymer Conetworks.

Samples from all metal-end-linked ABA triblock copolymer conetworks in *n*-hexane were vacuum-dried, and the morphology was characterized using powder X-ray diffraction (*p*-XRD).¹⁵³ The *p*-XRD profiles of the Pd- or Au-end-linked conetworks are shown in Figure 3.45. The three vertical lines on the *x*-axis are drawn at the positions (angles) of the known (from literature)¹⁵³ characteristic peaks of the crystalline form of Pd or Au.

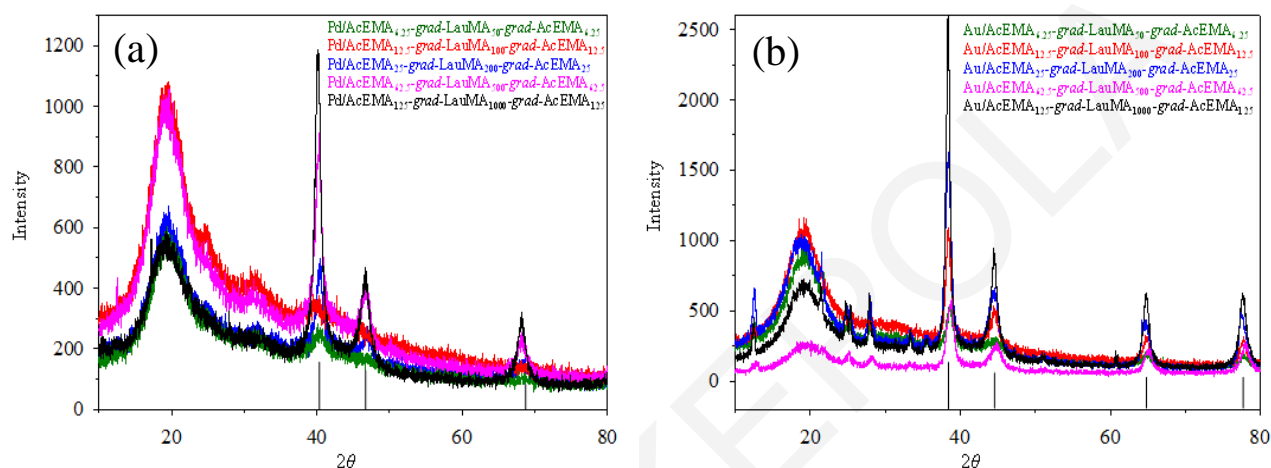


Figure 3.45. *p*-XRD profiles of the (a) Pd- and (b) Au-end-linked AcEMA-LauMA-AcEMA copolymer conetworks.

The *p*-XRD profiles of all five Pd-end-linked conetworks displayed peaks at the positions of the three vertical lines, confirming the presence of reduced (crystalline-metallic) Pd or Au. The average sizes of the crystallites, *L*, were calculated using Scherrer's equation and are displayed in Table 3.19. The crystallites in the Au-end-linked conetworks were 4.6-5.6 nm, whereas those in the Pd-end-linked conetworks were 4.5-4.8 nm, slightly smaller than those in the Au-end-linked conetworks. In both cases, the crystallite size was independent of the copolymer molecular weight.

Table 3.19. Sizes of the Au and Pd metal crystallites in the dried Au- and Pd-end-linked AcEMA-LauMA-AcEMA triblock copolymer conetworks.

ABA Triblock Copolymers	L^a (nm)	
	Au	Pd
AcEMA _{6.25} - <i>b</i> -LauMA ₅₀ - <i>b</i> -AcEMA _{6.25}	4.6 ± 0.1	4.5 ± 0.1
AcEMA _{12.5} - <i>b</i> -LauMA ₁₀₀ - <i>b</i> -AcEMA _{12.5}	5.4 ± 0.1	4.7 ± 0.3
AcEMA ₂₅ - <i>b</i> -LauMA ₂₀₀ - <i>b</i> -AcEMA ₂₅	5.6 ± 0.3	4.6 ± 0.1
AcEMA _{62.5} - <i>b</i> -LauMA ₅₀₀ - <i>b</i> -AcEMA _{62.5}	5.4 ± 0.1	4.7 ± 0.1
AcEMA ₁₂₅ - <i>b</i> -LauMA ₁₀₀₀ - <i>b</i> -AcEMA ₁₂₅	5.6 ± 0.2	4.8 ± 0.2

^aCalculated using Scherrer's equation: $L = (K \times \lambda) / (B \times \cos\theta)$, θ position (angle) of the peak, $K=0.99$, λ radiation wavelength with $\lambda = 1.54184 \text{ \AA}$, and B peak width at half height of $2\theta = 40^\circ$

3.6.6. Diameters of the Nanoparticles within the Au- and Pd-end-linked Polymer Conetworks.

Then, characterization of four out of the ten metal-end-linked polymer conetworks was performed using high-resolution transmission electron microscopy (TEM), and the obtained images are displayed in Figure 3.46. The crosslinker cores, comprising the metal nanoparticles, appear dark in the TEM images.

In both Au-end-linked polymer conetworks, the average diameter of the crosslinker cores was about 50 nm. For the Pd-end-linked polymer conetworks, the average diameter of the the nanoparticles (crosslinker) cores was about 13 nm. The average diameters of crosslinker cores were larger than the average metal crystallite sizes determined using *p*-XRD, indicating that each cross-linker core consisted of many crystallites.

The average diameters of the crosslinker cores comprising either metal was greater when the conetwork was based on the lower molecular weight copolymer, possibly due to the weaker steric hindrance arising from the shorter polyLauMA chains. Also, the diameters of the crosslinker cores, comprising Au were greater than those comprising Pd because of the use of hydrazine in the case of Pd, affects the formation of nanoparticles. The average diameter of nanoparticles was independent of the reducing agent concentration.¹⁵⁴

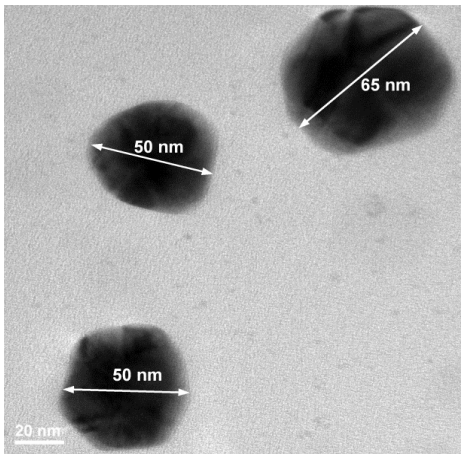
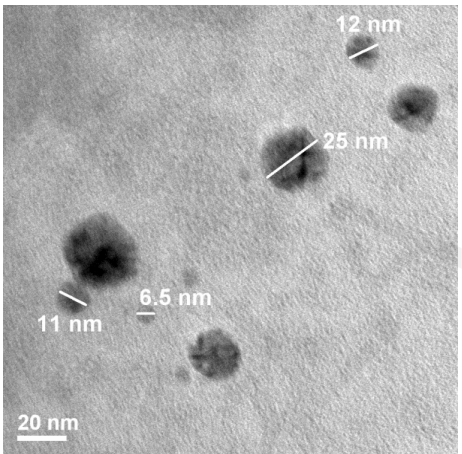
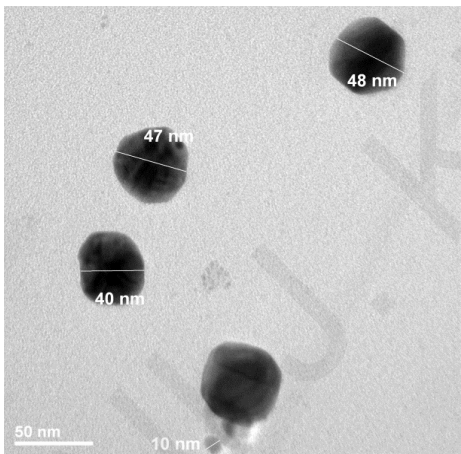
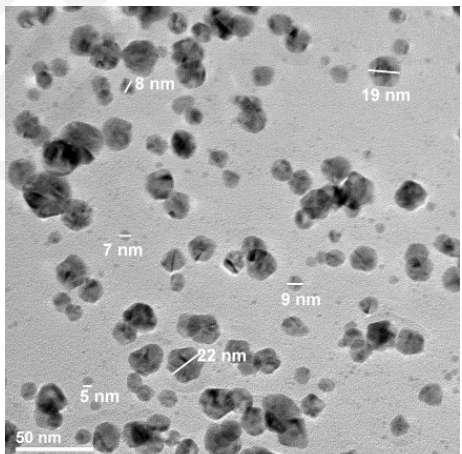
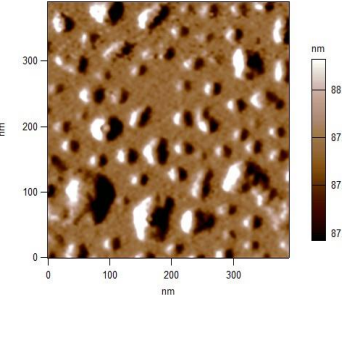
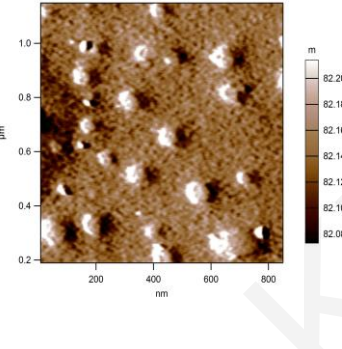
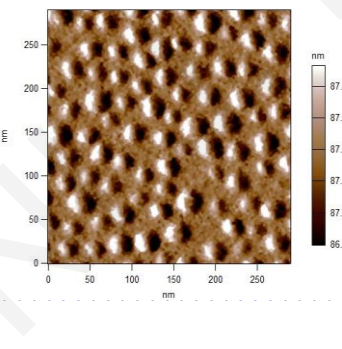
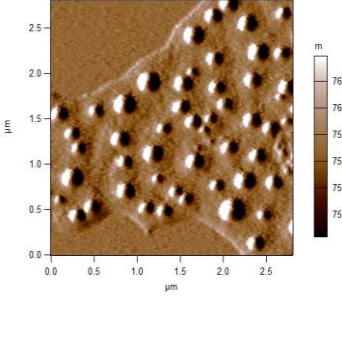
ABA polymer conetworks	Au	Pd
AcEMA ₂₅ - <i>b</i> -LauMA ₂₀₀ - <i>b</i> -AcEMA ₂₅		
AcEMA _{62.5} - <i>b</i> -LauMA ₅₀₀ - <i>b</i> -AcEMA _{62.5}		

Figure 3.46. TEM images of four polymer conetworks, two based on Au- and two based Pd-end-linked ABA triblock copolymers.

3.6.7. Surface Morphology of the Au-end-linked Polymer Conetworks.

Finally, the self-organization of four Au-end-linked polymer conetworks in the benzene-swollen states was investigated using AFM. Figure 3.47 shows the AFM phase images of four of the polymers of this study after being swollen in benzene and being vacuum dried (at room temperature). All images displayed a spherical structure, with the network size increasing with the polyLauMA content. As the DPs of the polyLauMA block increased, the spherical structures increased and therefore the size of nanoparticles. The AcEMA_{62.5}-*b*-

LauMA₅₀₀-*b*-AcEMA_{62.5} conetwork showed the most intense spherical structure, as expected, with the largest nanoparticles having an average size from 90 to 160 nm (contour length of the arms of the star equal to 126 nm (500 units × 0.252 nm per monomer repeating unit)). The sizes of the remaining conetworks are listed in Figure 3.47. The AcEMA₁₂₅-*b*-LauMA₁₀₀₀-*b*-AcEMA₁₂₅ was not investigated because it was not dissolving in benzene and in any other non-polar and polar solvents.

ABA Copolymer in Benzene	AFM Images of Conetworks with Au	Theoretical Size of Spherical Nanopart. ¹ (nm)	Average Size of Nanopart. (nm)
$A_{12.5}\text{-}b\text{-}LauMA_{50}\text{-}b\text{-}A_{12.5}$		13	4 - 16
$A_{25}\text{-}b\text{-}LauMA_{100}\text{-}b\text{-}A_{25}$		25	4 - 25
$A_{50}\text{-}b\text{-}LauMA_{200}\text{-}b\text{-}A_{50}$		50	13 - 60
$A_{62.5}\text{-}b\text{-}LauMA_{500}\text{-}b\text{-}A_{62.5}$		126	90 - 160

¹DP_{LauMA} × 0.252

Figure 3.47. Atomic force microscopy phase images of the four conetworks with Au in benzene with the theoretical size of their nanoparticles and the average sized calculated from the AFM images.

3.6.8. Conclusions.

In this section supramolecular polymer conetworks were prepared *via* metal–ligand coordination. This was achieved by mixing AcEMA-LauMA-AcEMA triblock copolymers and one of the metal salts, Pd(CH₃COO)₂ or HAuCl₄·3H₂O in THF. All degrees of swelling were relatively low (< 14), independent of triblock copolymer molecular weight, manifesting the compact nature of the networks. TEM indicated that networks with gold and palladium, possessed crosslinker cores with diameters which were larger when the ligating polymer was smaller as that causes a smaller steric hindrance. The average diameters of the crosslinker cores were larger than the average *L* values of the metal crystallites within them, as determined by *p*-XRD, indicating that each crosslinker core consists of many crystallites. Finally, the average size of nanoparticles and the self-organization was determined using AFM and as the DPs of the polyLauMA increased the average size of the nanoparticles increased and that because of the larger crosslinker cores.

3.7. Synthesis of a linear AcEMA₅₀-*b*-DMAEMA₂₀₀ Copolymer Complexed with Au for use in Gene Delivery.

Finally, in this section, a dual complexation (both with a metal and DNA) was performed, with the preparation of an AcEMA₅₀-*b*-DMAEMA₂₀₀ copolymer with one part being able to complex with genetic material (DMAEMA) and the other with gold (AcEMA). The AcEMA₅₀-*b*-DMAEMA₂₀₀-linear copolymer was synthesized also using RAFT polymerization, and the obtained copolymer was complexed *in situ* by Au cations (metal-linked copolymer) followed by reduction of the Au. The reason that Au was chosen is because it is biocompatible, so the metal-linked copolymer was used in complexation with DNA and transferred in to C2C12 mouse myoblast cells.

3.7.1. Molecular Weights and Compositions.

The Table 3.20 shows the molecular weight and monomer conversion, for the linear homopolymer (AcEMA₅₀) and the linear diblock copolymer (AcEMA₅₀-*b*-DMAEMA₂₀₀).

Table 3.20. Chemical structures, molecular weights, monomer conversion and composition of the prepared AcEMA₅₀-*b*-DMAEMA₂₀₀-linear copolymer.

Polymer	MW _{theory} (g mol ⁻¹)	GPC		Monomer Conversion (%)	Polymer Composition (mol%)	
		<i>M_n</i>	<i>Đ</i>	¹ H NMR	Theory	¹ H NMR
AcEMA ₅₀ -linear	7600	9300	1.2	99	100	99
AcEMA ₅₀ - <i>b</i> -DMAEMA ₂₀₀ -linear	39000	29900	1.5	100 / 90	25 / 75	25 / 68

The molecular weights of the linear polymers were reasonably close to the theoretical expectations. The molecular weight dispersity of the homopolymer was low, at 1.2, whereas that of the copolymer was somewhat higher, at 1.5, indicating an increase in size heterogeneity upon the growth of the homopolymer to its daughter diblock copolymer.

3.7.2. Luciferase Expression and Cytotoxicity.

The cationic linear AcEMA₅₀-*b*-DMAEMA₂₀₀ copolymer was used to transfer genetic material, first without complexing it with Au and then by complexing it with Au, in C2C12 mouse myoblast cells. In the latter case, several linear copolymer chains assembled together around an Au core, giving a larger binding surface for the DNA chains. Subsequently, the polymer - DNA complexes were transferred to C2C12 mouse myoblast cells in order to express the firefly luciferase gene (luciferase, Luc). Transfection experiments were performed with respect to the amount of polymer in the polymer - DNA complex, while the amount of DNA was kept constant at 1000 µg.

Luc expression was found to be quite high (1.35×10^6) with the linear diblock copolymer in the absence of Au and with low cytotoxicity. The largest expression of Luc was presented in 20 µL of polymer. However, when the copolymer was first complexed with Au and then used for transfection, it was observed that Luc expression tripled (4.0×10^6 at 15 µL) and the cytotoxicity remained low. This comparison is shown in Figure 3.47. It is good to note that Lipofectamine (a commercially available lipid-loved molecule suitable for transfection of nucleic acids into eukaryotic cells) showed Luc expression of the same order of magnitude as AcEMA₅₀-*b*-DMAEMA₂₀₀ / Au (9.0×10^6).

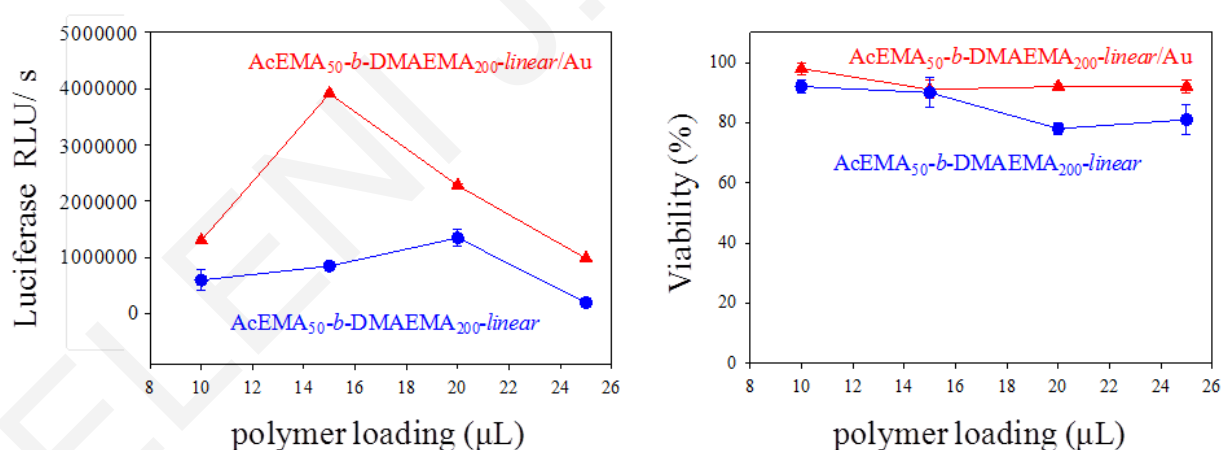


Figure 3.48. Comparison of the results of Luc expression (left) for the two transfections (red results after Au complexation and blue before complexation) and cytotoxicity (right).

3.7.3. Conclusions.

Luc expression was high (1.35×10^6) using the linear diblock copolymer (AcEMA₅₀-*b*-DMAEMA₂₀₀) without Au, but tripled (4.0×10^6 at 15 μ L) when the copolymer was previously complexed with Au, without an increasing cytotoxicity.

ELENI J. KEPOLA

CHAPTER 4: CONCLUSIONS AND FUTURE WORK

4.1. Conclusions

In this PhD Thesis, the successful formation and characterization of six families of polymers and polymer networks is reported. One of our most important results is the self-organizing in water of the amphiphilic polymer conetwork with the structure EGDMA₁-*b*-MMA₃₀-*b*-DMAEMA₁₀-*b*-EGDMA₁ into a lamellar mesophase with long-range order, a behavior previously known only for non-cross-linked block copolymer systems. The mechanical properties of this well-ordered system were clearly superior to those of its homologues, which, together with its facile, one-pot preparation using readily available components, are expected to render the present system popular for applications in medicine and biotechnology. Then, another amphiphilic polymer network family was synthesized where we varied systematically the arm architecture, *i.e.*, the lengths of the hydrophilic and hydrophobic blocks. All, except the one with the shortest arms, exhibited a correlation peak when equilibrated in D₂O, as deduced from SANS, consistent with internal self-assembly and nanophase separation. In addition to the correlation peak, some of the samples also presented a shoulder in their scattering profile, at twice the *q*-value of the correlation peak, indicating a trend for internal organization with a longer-range ordering. Our results demonstrate that the molecular architecture of the amphiphilic polymer conetworks is successfully translated into their mesoscopic structure and thereby this approach allows for a rational design of such systems.

Next part not only intends to describe the synthesis of a complex polymer network architecture, readily convertible to solution, but also to showcase its facile preparation. A degradable, ketal-based, dimethacrylate cross-linker was synthesized and used to prepare cleavable polymer networks of MMA using sequential GTP in three steps. These three steps involved crosslinker addition in the first step, next followed by MMA addition in the second step, and completed by the addition of crosslinker again in the third and final step. In each of the two crosslinker additions, either the degradable ketal crosslinker or a non-degradable crosslinker was used. These sums up to four possibilities, corresponding to four polymer networks, all of which were prepared in this investigation, characterized, and subjected to hydrolysis. The lower molecular weight population of these stars possessed about the same molecular weight in all four preparations. However, the higher molecular weight population had higher molecular weight in the two cases when the non-degradable crosslinker had been used, as compared to the two cases when the degradable, ketal crosslinker had been used.

This is thought to arise from the smaller size of the non-degradable cross-linker, presenting a lower steric hindrance, and, therefore, being more reactive toward its polymerization. Exposing the polymer networks containing the degradable ketal crosslinker to mildly acidic hydrolysis conditions led to complete network dissolution. Characterization of the network hydrolysis products indicated that their size was not always the expected. In particular, in two cases, the network hydrolysis products had the expected molecular weights and molecular weight distributions. However, in the third case, the larger hydrolysis products irreversibly recombined to form even larger covalent aggregates which escaped size and composition characterization, despite repeating the hydrolysis experiment several times, and using even stronger hydrolysis reagents.

Regarding the family with the oligoamine-grafted polymers (oligoamine-grafted GMA₁₀₀-*linear*, oligoamine-grafted GMA₂₀-*star* and oligoamine-grafted GMA₁₀₀-*star* homopolymers), we showed that the odd-even effect is also in action in totally abiotic systems, in addition to the poly(amino acid)-based ones already reported in the literature by Kataoka and co-workers. With the exception of the PEHA-grafted polymers, all oligoamine-grafted star homopolymers presented higher, albeit moderate, transfection efficiencies when the oligoamine-grafts possessed an even number of nitrogen atoms rather than an odd number. This trend was also followed by oligoamine-grafted linear homopolymers at low polymer loadings. The odd-even effect was also observed for the cytotoxicity of the oligoamine-grafted GMA₁₀₀-*linear* and oligoamine-grafted GMA₁₀₀-*star* homopolymers, while the cytotoxicity for oligoamine-grafted GMA₂₀-*stars* slightly increased with the number of ethylene imine repeating units.

In the next two families, we used metal ions as a crosslinker. At first, polymer-metal micellar nanohybrids were synthesized, consisting of well-defined methacrylate-based block copolymers comprising an organic-solvent soluble block, a metal-binding block, and metal nanoparticles of Ni, Pd or Au. The complexes resulted from the combination of four different copolymers, with and without AnMMA in four different organic solvents, and three different metals. The complexes with Ni exhibited most aggregates in solution, even after filtering with cotton. The complexes with the Pd showed virtually no aggregates, but when observed, they were ellipsoid in some solutions and the complexes with Au showed a few samples of aggregates but had more uniformly spherical shape mainly in benzene and chloroform. It was concluded that the best polymer-metal complexes, either based on a small number of the very low aggregates in the samples or based on the complex stability in solution were the Au

complexes in benzene and chloroform. So, we focused first on the Au complexes and then on those of Pb, to prepare supramolecular polymer conetworks via metal–ligand coordination by mixing AcEMA-LauMA-AcEMA triblock copolymers and metal salts in THF, without forming aggregates or precipitates. The bonding between the polymer and the metal was nearly independent of the degree of polymerization of the AcEMA ligating blocks. All degrees of swelling were relatively low (< 14), manifesting the compact nature of the networks. TEM indicated larger nanoparticles (with both Au and Pd) when the networks were based on block copolymers of lower molecular weights due to the weaker steric hindrances arising from the shorter polyLauMA chains. The average diameters of crosslinker cores were larger than the average sizes of the metal crystallites determined by *p*-XRD, indicating that each crosslinking core consisted of many crystallites. Finally, the average size of the nanoparticles was determined using AFM, and that this size increased as the DPs of the polyLauMA blocks increased.

Finally, we synthesized an AcEMA₅₀-*b*-DMAEMA₂₀₀-*linear* copolymer which is a combination of a polyAcEMA block which can bind to metals, leading to star formation, and a polyDMAEMA block which can complex with DNA. The AcEMA₅₀-*b*-DMAEMA₂₀₀-*linear* copolymer was synthesized using RAFT polymerization and then, the copolymer was complexed in situ by the reduction of the Au cations ligated onto a metal-linked copolymer. The reason that Au was chosen is because it is biocompatible, so the metal-linked copolymer was used in complexation with DNA and transferred in C2C12 cells. Luc expression was high (1.35×10^6) using only the linear copolymer, without Au, but it tripled (4.0×10^6 at 15 μ L) when the copolymer was previously complexed with Au, without increased in the cytotoxicity.

4.2. Future Work

Future work should aim at expanding and deepening the present research projects. Perhaps the main direction that could be followed is the formation of amphiphilic polymer conetworks yielding morphologies with longer-range order, by better controlling the distribution of the arm numbers at the cross-linking junctions. This, longer-range order would in turn, lead to an enhancement in the mechanical properties of the conetworks, and, in particular, their stress and strain of break.

Another possibility for future work may involve the preparation and study of degradable amphiphilic polymer conetworks, using the same “core-first” star polymer preparation route by GTP, together with the same, ketal-containing dimethacrylate cross-linker, but employing two monomer additions, one hydrophilic and one hydrophobic. The hydrolysis might even be possible to perform in water. As self-assembly phenomena are expected to take place in water, it would be interesting to explore aqueous hydrolyzability as a function of the composition and the molecular weights of the constituting, linear amphiphilic block copolymer segments.

The part of the oligoamine-grafted polymers may also be extended in the future by using new oligoamines, either of biological or synthetic origin. This should be followed by study of the cytotoxicity and transfection efficiency of the complexes, and observation whether the odd-even effect.

Moreover, new experiments may be performed using polymers that bind with metals ions. This may involve use of new polymers, new metal ions, new solvents, or a combination of the above.

Finally, we may study the effect of the DP in the $\text{AcEMA}_n\text{-}b\text{-DMAEMA}_m\text{-linear}$ copolymer on the gene delivery efficiency in order to optimize the expression of Luc.

CHAPTER 5: BIBLIOGRAPHY

1. R. J. Hunter, *Foundations of Colloid Science*, Vol. II, Clarendon Press, New York, 1989, Chapter. 12.
2. P. Atkins, J. dePaula, *Physical Chemistry*, 7th έκδ, Oxford University Press, New York, 2002, Page 700.
3. I. Manners, *Synthetic Metal-Containing Polymers*, WILEY-VCH Verlag GmbH & Co. KGaA, Weinheim, Germany, 2004.
4. D. W. Pack, A. S. Hoffman, S. Pun, P. S. Stayton, “Design and development of polymers for gene delivery”, *Nat. Rev.* **2005**, *4*, 581 – 593.
5. C. Burda, X. B. Chen, R. Narayanan, M. A. El-Sayed, “Chemistry and Properties of Nanocrystals of Different Shapes”, *Chem. Rev.* **2005**, *105*, 1025 – 1102.
6. D. V. Talapin, J. S. Lee, M. V. Kovalenko, E. V. Shevchenko, “Prospects of Colloidal Nanocrystals for Electronic and Optoelectronic Applications”, *Chem. Rev.* **2010**, *110*, 389 – 458.
7. C. J. Murphy, T. K. Sau, A. M. Gole, C. J. Orendorff, J. Gao, L. Gou, S. E. Hunyadi, T. Li, “Anisotropic Metal Nanoparticles: Synthesis, Assembly, and Optical Applications”, *J. Phys. Chem. B* **2005**, *109*, 13857 – 13870.
8. M. Demetriou, T. Krasia-Christoforou, “Well-defined diblock copolymers possessing fluorescent and metal chelating functionalities as novel macromolecular sensors for amines and metal ions”, *J. Polym. Sci., Part A: Polym. Chem.* **2012**, *50*, 52 – 60.
9. K. Iliopoulos, G. Chatzikyriakos, M. Demetriou, T. Krasia-Christoforou, S. Couris, “Preparation and nonlinear optical response of novel palladium-containing micellar nanohybrids”, *Opt. Material* **2011**, *33*, 1342 – 1349.
10. M. Demetriou, T. Krasia-Christoforou, “Synthesis and characterization of well-defined block and statistical copolymers based on lauryl methacrylate and 2-(acetoacetoxy)ethyl methacrylate using RAFT-controlled radical polymerization”, *J. Polym. Sci., Part A: Polym. Chem.* **2008**, *46*, 5442 – 5451.
11. R. Freitag, *Synthetic Polymers for Biotechnology and Medicine*, Landes Bioscience: Georgetown, Texas, 2003, Chapter 2, 19 – 37.
12. T. Merdan, J. Kopeček, T. Kissel, “Prospects for cationic polymers in gene and oligonucleotide therapy against cancer”, *Adv. Drug Deliv. Rev.* **2002**, *54*, 715 – 758.

13. M. E. Seitz, M. E. Wiseman, I. Hilker, J. Loos, M. Tian, J. Li, M. Goswami, V. M. Litvinov, S. Curtin, M. Bulters, "Influence of silicone distribution and mobility on the oxygen permeability of model silicone hydrogels", *Polymer* **2017**, *118*, 150 – 162.
14. G. Guzman, S. S. Es-haghi, T. Nugay, M. Cakmak, "Drug Delivery: Zero-Order Antibiotic Release from Multilayer Contact Lenses: Nonuniform Drug and Diffusivity Distributions Produce Constant-Rate Drug Delivery", *Adv. Healthcare Mater.* **2017**, *6*, 1600775.
15. B. Ozcelik, K. D. Brown, A. Blencowe, K. Ladewig, G. W. Stevens, J.-P. Y. Scheerlinck, K. Abberton, M. Daniell, G. G. Qiao, "Biodegradable and Biocompatible Poly(Ethylene Glycol)-based Hydrogel Films for the Regeneration of Corneal Endothelium" *Adv. Healthcare Mater.* **2014**, *3*, 1496 – 1507.
16. I. Schoenfeld, S. Dech, B. Ryabenky, B. Daniel, B. Glowacki, R. Ladisch, J. C. Tiller, "Investigations on diffusion limitations of biocatalyzed reactions in amphiphilic polymer conetworks in organic solvents", *Biotechnol. Bioeng.* **2013**, *110*, 2333 – 2342.
17. E. Themistou, C. S. Patrickios, "Synthesis and characterization of star polymers and cross-linked star polymer model networks containing a novel, silicon-based, hydrolyzable cross-linker", *Macromolecules* **2004**, *37*, 6734 – 6742.
18. E. Themistou, C. S. Patrickios, "Synthesis and Characterization of Polymer Networks and Star Polymers Containing a Novel, Hydrolyzable Acetal-Based Dimethacrylate Cross-Linker", *Macromolecules* **2006**, *39*, 73 – 80.
19. D. Kafouris, E. Themistou, C. S. Patrickios, "Synthesis and Characterization of Star Polymers and Cross-Linked Star Polymer Model Networks with Cores Based on an Asymmetric, Hydrolyzable Dimethacrylate Cross-Linker", *Chem. Mater.* **2006**, *18*, 85 – 93.
20. E. Themistou, C. S. Patrickios, "Star polymers and polymer networks containing a novel, hydrolyzable diacetal-based dimethacrylate cross-linker: Synthesis, characterization, and hydrolysis kinetics", *Macromolecules* **2007**, *40*, 5231–5234.
21. E. Themistou, A. Kanari, C. S. Patrickios, "Thermolyzable polymer networks and star polymers containing a novel, compact, degradable acylal-based dimethacrylate cross-linker: Synthesis, characterization, and thermolysis" *J. Polym. Sci., Part A: Polym. Chem.* **2007**, *45*, 5811 – 5823.

22. E. Themistou, C. S. Patrickios, "A Cleavable Network Based on Crosslinked Star Polymers Containing Acid-Labile Diacetal Crosslinks: Synthesis, Characterization and Hydrolysis", *Macromol. Chem. Phys.* **2008**, *209*, 1021 – 1028.
23. E. Themistou, C. S. Patrickios, "Degradable polymer networks and star polymers based on mixtures of two cleavable dimethacrylate crosslinkers: Synthesis, characterization, and degradation", *J. Polym. Sci., Part A: Polym. Chem.* **2009**, *47*, 5853 – 5870.
24. M. Elladiou, C. S. Patrickios, "A dimethacrylate cross-linker cleavable under thermolysis or alkaline hydrolysis conditions: synthesis, polymerization, and degradation", *Chem. Commun.* **2016**, *52*, 3135 – 3138.
25. M. D. Rikkou, C. S. Patrickios, "Polymers prepared using cleavable initiators: Synthesis, characterization and degradation", *Prog. Polym. Sci.* **2011**, *36*, 1079 – 1097.
26. M. D. Rikkou, C. S. Patrickios, "Well-Defined Networks with Precisely Located Cleavable Sites: Structure Optimization and Core Functionality Determination", *Macromolecules* **2008**, *41*, 5957 – 5959.
27. M. D. Rikkou, E. Loizou, L. Porcar, P. Butler, C. S. Patrickios, "Degradable Amphiphilic End-Linked Conetworks with Aqueous Degradation Rates Determined by Polymer Topology", *Macromolecules* **2009**, *42*, 9412 – 9421.
28. M. Rikkou-Kalourkoti, E. Loizou, L. Porcar, K. Matyjaszewski, C. S. Patrickios, "End-linked, amphiphilic, degradable polymer conetworks: synthesis by sequential atom transfer radical polymerization using a bifunctional, cleavable initiator", *Polym. Chem.* **2012**, *3*, 105 – 116.
29. M. Rikkou-Kalourkoti, C. S. Patrickios, "Synthesis and Characterization of End-Linked Amphiphilic Copolymer Conetworks Based on a Novel Bifunctional Cleavable Chain Transfer Agent", *Macromolecules* **2012**, *45*, 7890 – 7899.
30. M. Elladiou, A. S. Kalogirou, C. S. Patrickios, "Symmetrical polymer systems prepared using a degradable bifunctional atom transfer radical polymerization initiator: Synthesis, characterization, and cleavage", *J. Polym. Sci., Part A: Polym. Chem.* **2017**, *55*, 2342 – 2355.
31. E. J. Kepola, E. Loizou, C. S. Patrickios, E. Leontidis, C. Voutouri, T. Stylianopoulos, R. Schweins, M. Gradzielski, C. Krumm, J. C. Tiller, M. Kushnir, C. Wesdemiotis, "Amphiphilic Polymer Conetworks Based on End-Linked "core-First" Star Block Copolymers: Structure Formation with Long-Range Order", *ACS Macro Letters* **2015**, *4*, 1163 – 1168.

32. E. J. Kepola, K. Kyriacou, C. S. Patrickios, M. Simon, M. Gradzielski, M. Kushnir and C. Wesdemiotis, “Amphiphilic Polymer Conetworks Based on Interconnected Hydrophobic Star Block Copolymers: Synthesis and Characterization”, *Macromolecular Symposia* **2017**, 372, 69 – 86.
33. E.J. Kepola, C. S. Patrickios, “Networks Based on “Core-First” Star Polymers End-Linked Using a Degradable Ketal Cross-Linker: Synthesis, Characterization, and Cleavage”, *Macromolecular Chemistry and Physics* **2018**, 219, 1700404.
34. K. Matyjaszewski, A. H. E. Müller, *Controlled and Living Polymerizations: From Mechanisms to Applications*: WILEY-VCH Verlag GmbH & Co. KGaA, 2009.
35. O. W. Webster, “Living Polymerization Methods”, *Science* **1991**, 251, 887 – 893.
36. K. Matyjaszewski, Y. Gnanou, L. Leibler, “Macromolecular engineering: precise synthesis, materials properties, applications,” 1η Έκδοση 2011, Εκδόσεις Wiley, Νέα Υόρκη, Ηνωμένες Πολιτείες Αμερικής.
37. W. Li, T. Tanaka, “Phase transitions of gels,” *Annu. Rev. Mater. Sci.* **1992**, 22, 243 – 277.
38. S. Hirotsu, “Phase transition of a polymer gel in pure and mixed solvent media,” *J. Phys. Soc. Jpn.* **1987**, 56, 233 – 242.
39. R. A Siegel, B. A. Firestone, “pH-dependent equilibrium swelling properties of hydrophobic polyelectrolyte copolymer gels,” *Macromolecules* **1988**, 21, 3254 – 3259.
40. T. Tanaka, I. Nishio, S. –T. Sun, S. U. Nishio, “Collapse of gels in an electric field,” *Science* **1982**, 218, 467 – 469.
41. M. Irie, D. Kungwachakun, “Photoresponsive polymers. Mechanochemistry of polyacrylamide gels having triphenylmethane leuco derivatives,” *Makromol. Chem. Rapid Commun.* **1985**, 5, 829 – 832.
42. C. S. Patrickios, T. K. Georgiou, “Covalent amphiphilic polymer networks,” *Curr. Opin. Colloid Interface Sci.* **2003**, 8, 2223 – 2232.
43. G. Erdodi, J. P. Kennedy, “Amphiphilic conetworks: definition, synthesis, applications,” *Prog. Poly. Sci.* **2006**, 31, 1 – 18.
44. H. Kamata, Y. Akagi, Y. –K. Kariya, U. Chang, T. Sakai, “Nonswellable hydrogel without mechanical hysteresis”, *Science* **2015**, 343, 873 – 875.
45. E. Demosthenous, S. C. Hadjiyannakou, M. Vamvakaki, C. S. Patrickios, “Synthesis and Characterization of Polyampholytic Model Networks: Effects of Polymer Composition and Architecture,” *Macromolecules* **2002**, 35, 2252 –2260.

46. K. S. Pafiti, Z. Philippou, E. Loizou, L. Porcar, C. S. Patrickios, “End-Linked Poly[2-(dimethylamino)ethyl Methacrylate]–Poly(methacrylic acid) Polyampholyte Conetworks: Synthesis by Sequential RAFT Polymerization and Swelling and SANS Characterization,” *Macromolecules* **2011**, *44*, 5352 – 5362.
47. K. S. Pafiti, M. Elladiou, C. S. Patrickios, ““Inverse Polyampholyte” Hydrogels from Double-Cationic Hydrogels: Synthesis by RAFT Polymerization and Characterization”, *Macromolecules* **2014**, *47*, 1819 – 1827.
48. A. P. Constantinou, M. Elladiou, C. S. Patrickios, “Regular and Inverse Polyampholyte Hydrogels: A Detailed Comparison” , *Macromolecules* **2016**, *49*, 3869 – 3880.
49. S. N. Georgiades, M. Vamvakaki, C. S. Patrickios, “Synthesis and characterization of double-hydrophilic model networks based on cross-linked star polymers of poly (ethylene glycol) methacrylate and methacrylic acid”, *Macromolecules* **2002**, *35*, 4903 – 4911.
50. E. Loizou, A. I. Triftaridou, T. K. Georgiou, M. Vamvakaki, C. S. Patrickios, “Cationic Double-Hydrophilic Model Networks: Synthesis, Characterization, Modeling and Protein Adsorption Studies”, *Biomacromolecules* **2003**, *4*, 1150 – 1160.
51. X. B. Dou, Y. Hu, N. N. Zhao, F. J. Xu, “Different types of degradable vectors from low-molecular-weight polycation-functionalized poly(aspartic acid) for efficient gene delivery.” *Biomaterials* **2014**, *35*, 3015 – 3026.
52. K. Itaka, T. Ishii, Y. Hasegawa, K. Kataoka, “Biodegradable polyamino acid-based polycations as safe and effective gene carrier minimizing cumulative toxicity.” *Biomaterials* **2010**, *31*, 3707 – 3714.
53. H. Uchida, K. Miyata, M. Oba, T. Ishii, T. Suma, K. Itaka, N. Nishiyama, K. Kataoka, “Odd–even effect of repeating aminoethylene units in the side chain of N-substituted polyaspartamides on gene transfection profiles”. *J. Am. Chem. Soc.* **2011**, *133*, 15524 – 15532.
54. H. Uchida, K. Itaka, T. Nomoto, T. Ishii, T. Suma, M. Ikegami, K. Miyata, M. Oba, N. Nishiyama, K. Kataoka, “Modulated protonation of side chain aminoethylene repeats in N-substituted polyaspartamides promotes mRNA transfection.” *J. Am. Chem. Soc.* **2014**, *136*, 12396 – 12405.
55. X. Dong, L. Lina, J. Chen, H. Tian, C. Xiao, Z. Guo, Y. Li, Y. Wei, X. Chen, “Multi-armed poly (aspartate-g-OEI) copolymers as versatile carriers of pDNA/siRNA,” *Acta Biomaterialia* **2013**, *9*, 6943 – 6952.

56. C. Scholz, P. Kos, E. Wagner, “Comb-like oligoaminoethane carriers: change in topology improves pDNA delivery,” *Bioconjugate Chem.* **2014**, *25*, 251 – 261.
57. D. Salakhieva, V. Shevchenko, C. Nemeth, B. Gyarmati, “Structure–biocompatibility and transfection activity relationships of cationic polyaspartamides with (dialkylamino) alkyl and alkyl or hydroxyalkyl side groups.” *Int. J. Pharm.* **2017**, *517*, 234 – 246.
58. P. Alexandridis, M. Tsianou, “Block copolymer-directed metal nanoparticle morphogenesis and organization”, *Eur. Polym. J* **2011**, *47*, 569 – 583.
59. P. Alexandridis, “Gold nanoparticle synthesis, morphology control, and stabilization facilitated by functional polymers”, *Chem. Eng. Technol.* **2011**, *34*, 15 – 28.
60. R. Shenhar, T. B. Norsten, V. M. Rotello, “Polymer-mediated nanoparticle assembly: structural control and applications”, *Adv. Mater.* **2005**, *17*, 657-669.
61. B. C. Sih, M. O. Wolf, “Metal nanoparticle-conjugated polymer nanocomposites”, *Chem. Commun.* **2005**, 3375 – 3384.
62. A. U. Czaja, N. Trukhan, U. Mueller, “Industrial applications of metal–organic frameworks”, *Chem. Soc. Rev.*, **2009**, *38*, 1284 – 1293.
63. L. J. Murray, M. Dinca, J. R. Long, “Hydrogen storage in metal–organic frameworks”, *Chem. Soc. Rev.*, **2009**, *38*, 1294 – 1314.
64. N. Yanai, K. Kitayama, Y. Hijikata, H. Sato, R. Matsuda, Y. Kubota, M. Takata, M. Mizuno, T. Uemura, S. Kitagawa, “Gas detection by structural variations of fluorescent guest molecules in a flexible porous coordination polymer”, *Nat. Mater.*, **2011**, *10*, 787 – 793.
65. S. Kitagawa, R. Kitaura and S. Noro, “Functional Porous Coordination Polymers”, *Angew. Chem., Int. Ed.*, **2004**, *43*, 2334 – 2375.
66. T. Rossow, S. Hackelbusch, P. van Assenbergh, S. Seiffert, “A modular construction kit for supramolecular polymer gels”, *Polym. Chem.* **2013**, *4*, 2515 – 2527.
67. J. B. Beck, S. J. Rowan, “Multistimuli, Multiresponsive Metallo-Supramolecular Polymers”, *J. Am. Chem. Soc.* **2003**, *125*, 13922 – 13923.
68. W. Weng, J. B. Beck, A. M. Jamieson, S. J. Rowan, “Understanding the Mechanism of Gelation and Stimuli-Responsive Nature of a Class of Metallo-Supramolecular Gels”, *J. Am. Chem. Soc.* **2006**, *128*, 11663–11672.
69. M. Burnworth, L. Tang, J. R. Kumpfer, A. J. Duncan, F. L. Beyer, G. L. Fiore, S. J. Rowan, C. Weder, “Optically healable supramolecular polymers”, *Nature* **2011**, *472*, 334 – 337.

70. F. Mpekris, M. Achilleos, E. Vasile, T. Krasia-Christoforou and T. Stylianopoulos, “Mechanical properties of structurally-defined magnetoactive polymer (co)networks”, *RSC Advances* **2015**, *5*, 20011 – 20019.
71. P. Papaphilippou, M. Christodoulou, O.-M. Marinica, A. Taculescu, L. Vekas, K. Chrissafis, and T. Krasia-Christoforou, “Multiresponsive Polymer Conetworks Capable of Responding to Changes in pH, Temperature, and Magnetic Field: Synthesis, Characterization, and Evaluation of Their Ability for Controlled Uptake and Release of Solutes”, *ACS Applied Materials & Interfaces* **2012**, *4*, 2139 – 2147.
72. M. Achilleos, T. Krasia-Christoforou, C. S. Patrickios, “Amphiphilic Model Conetworks Based on Combinations of Methacrylate, Acrylate, and Styrenic Units: Synthesis by RAFT Radical Polymerization and Characterization of the Swelling Behavior”, *Macromolecules*, **2007**, *40*, 5575 – 5581.
73. U. S. Schubert, C. Eschbaumer, “Macromolecules Containing Bipyridine and Terpyridine Metal Complexes: Towards Metallosupramolecular Polymers”, *Angew. Chem., Int. Ed.* **2002**, *41*, 2892 – 2926.
74. B. G. G. Lohmeijer, U. S. Schubert, “Playing LEGO with macromolecules: Design, synthesis, and self-organization with metal complexes”, *J. Polym. Sci. Polym. Chem.* **2003**, *41*, 1413 – 1427.
75. H. Hofmeier, U. S. Schubert, “Recent developments in the supramolecular chemistry of terpyridine–metal complexes”, *Chem. Soc. Rev.* **2004**, *33*, 373 – 399.
76. J. D. Fox, S. J. Rowan, “Supramolecular Polymerizations and Main-Chain Supramolecular Polymers”, *Macromolecules* **2009**, *42*, 6823 – 6835.
77. D. H. Lee, S. H. Han, W. Joo, J. K. Kim, J. Huh, “Phase Behavior of Polystyrene-block-poly(4-vinylpyridine) Copolymers Coordinated by Metal Chloride”, *Macromolecules* **2008**, *41*, 2577 – 2583.
78. A. Noro, Y. Sageshima, S. Arai, Y. Matsushita, “Preparation and Morphology Control of Block Copolymer/Metal Salt Hybrids via Solvent-Casting by Using a Solvent with Coordination Ability”, *Macromolecules* **2010**, *43*, 5358 – 5364.
79. A. Noro, S. Matsushita, H. Xudong, M. Hayashi, Y. Matsushita, “Thermoreversible Supramolecular Polymer Gels via Metal–Ligand Coordination in an Ionic Liquid”, *Macromolecules* **2013**, *46*, 8304 – 8310.
80. S. Yang, J. S. Chen, H. Korner, T. Breiner, C. K. Ober, M. D. Poliks, “Reworkable Epoxies: Thermosets with Thermally Cleavable Groups for Controlled Network Breakdown”, *Chem. Mater.* **1998**, *10*, 1475 – 1481.

81. X. Chen, F. Wudl, A. K. Mal, H. Shen, S. R. Nutt, "New Thermally Remendable Highly Cross-Linked Polymeric Materials", *Macromolecules* **2003**, *36*, 1802 – 1807.
82. H. Okamura, T. Terakawa, M. Shirai, " Photo- and thermal curing of tri-functional methacrylate with degradable property", *Res. Chem. Intermed* **2009**, *35*, 865 – 878.
83. D. S. Muggli, A. K. Burkoth, S. A. Keyser, H. R. Lee, K. S. Anseth, " Reaction Behavior of Biodegradable, Photo-Cross-Linkable Polyanhydrides", *Macromolecules* **1998**, *31*, 4120 – 4125.
84. E. Ruckenstein, H. Zhang, " A Novel Breakable Cross-Linker and pH-Responsive Star-Shaped and Gel Polymers", *Macromolecules* **1999**, *32*, 3979 – 3983.
85. J. B. Lee, K. W. Chun, J. J. Yoon, G. Park, " Controlling Degradation of Acid-Hydrolyzable Pluronic Hydrogels by Physical Entrapment of Poly(lactic acid-co-glycolic acid) Microspheres", *Macromol. Biosci* **2004**, *4*, 957 – 962.
86. J. K. Oh, C. Tang, H. Gao, N. V. Tsarevsky, K. Matyjaszewski, " Inverse Miniemulsion ATRP: A New Method for Synthesis and Functionalization of Well-Defined Water-Soluble/Cross-Linked Polymeric Particles", *J. Am. Chem. Soc.* **2006**, *128*, 5578 – 5584.
87. H. Brondsted, J. Kopeček, " Hydrogels for site-specific oral drug delivery: synthesis and characterization", *Biomaterials* **1991**, *12*, 584 – 592.
88. S. Kim, K. E. Healy, " Synthesis and Characterization of Injectable Poly(N-isopropylacrylamide-co-acrylic acid) Hydrogels with Proteolytically Degradable Cross-Links", *Biomacromolecules* **2003**, *4*, 1214 – 1223.
89. J. A. Moss, S. Stokols, M. S. Hixon, F. T. Ashley, J. Y. Chang, K. D. Janda, " Solid-Phase Synthesis and Kinetic Characterization of Fluorogenic Enzyme-Degradable Hydrogel Cross-linkers", *Biomacromolecules* **2006**, *7*, 1011 – 1016.
90. C. M. Henry, " Special delivery: alternative methods for delivering drugs improve performance, convenience and patient compliance", *Chem. & Eng. News* **2002**, *80*, 39 – 47.
91. L. G. Griffith, "Polymeric Biomaterials", *Acta Mater.* **2000**, *48*, 263 – 277.
92. Y. Lu, C. A. Aguilar, S. Chen, "Shaping Biodegradable Polymers as Nanostructures: Fabrication and Application", *Drug Discov Today Technol.* **2005**, *2(1)*, 97 – 102.
93. Y. J. Kwon, S. M. Standley, A. P. Goodwin, E. R. Gillies, J. M. J. Fréchet, " Directed Antigen Presentation Using Polymeric Microparticulate Carriers Degradable at Lysosomal pH for Controlled Immune Responses", *Molecular Pharmaceutics* **2004**, *1*, 83 – 91.

94. L. Shi, C. Berkland, “ pH-Triggered Dispersion of Nanoparticle Clusters“, *Adv. Mater.* **2006**, *18*, 2315 – 2319.
95. N. Bhuchar, R. Sunasee, K. Ishihara, T. Thundat, R. Narain, “ Degradable thermoresponsive nanogels for protein encapsulation and controlled release“, *Bioconjugate Chem.* **2012**, *23*, 75 – 83.
96. X. Hu, T. Yang, R. Gu, Y. Cui, C. Yuan, H. Ge, W. Wu, W. Li, Y. Chen, “ A degradable polycyclic cross-linker for UV-curing nanoimprint lithography“, *J. Mater. Chem. C* **2014**, *2*, 1836 – 1843.
97. J. Lederberg, “Cell genetics and hereditary symbiosis“, *Physiological Reviews* **1952**, *32*, 403 – 430.
98. H. Finbarr, “Chapter 1 – The Function and Organization of Plasmids“. In Nicola Casali, Andrew Presto (eds.). “*E. Coli Plasmid Vectors: Methods and Applications. Methods in Molecular Biology.*“ **2003**, *235*, 1– 5.
99. F. Stanley “Microbial Genomics: Standing on the Shoulders of Giants“. Microbiology Society.
100. J. Sinkovics, J. Horvath, A. Horak, “The origin and evolution of viruses (a review)“. *Acta Microbiologica et Immunologica Hungarica* **2003**, *45*, 349 – 390.
101. C. Smillie, M. P. Garcillán-Barcia, M. V. Francia, E. P. Rocha, F. de la Cruz, “Mobility of plasmids.“ *Microbiology and Molecular Biology Reviews* **2010**, *74*, 434 – 452.
102. C. M. Thomas, D. Summers, Bacterial Plasmids. Encyclopedia of Life Sciences, 2008.
103. T. J. Gibson, P. Smyth, M. Semsarilar, A. P. McCann, W. J. McDaid, M. C. Johnston, C. J. Scott, E. Themistou, “ Star polymers with acid-labile diacetal-based cores synthesized by aqueous RAFT polymerization for intracellular DNA delivery.“ *Polym. Chem.* **2020**, *11*, 344 – 357.
104. B. Erman, M. M. Demir, M. A. Gulgun, Y. Z. Menciloglu, S. S. Abramchuk, E. E. Makheva, A. R. Khokhov, V. G. Matveeva, M. G. Sulman, “ Palladium Nanoparticles by Electrospinning from Poly(acrylonitrile-co-acrylic acid)–PdCl₂ Solutions. Relations between Preparation Conditions, Particle Size, and Catalytic Activity“, *Macromolecules* **2004**, *37*, 1787 – 1792.
105. R. B. Grubbs, “Hybrid metal–polymer composites from functional block copolymers“, *J. Polym. Sci., Part A: Polym. Chem.* **2005**, *43*, 4323 – 4336.

106. D. Astruc, "Palladium Nanoparticles as Efficient Green Homogeneous and Heterogeneous Carbon–Carbon Coupling Precatalysts: A Unifying View", *Inorg. Chem.* **2007**, *46*, 1884 – 1894.
107. K. Iliopoulos, G. Chatzikyriakos, M. Demetriou, T. Krasia-Christoforou, S. Couris, "Preparation and nonlinear optical response of novel palladium-containing micellar nanohybrids", *Optical Materials* **2011**, *33*, 1342 – 1349.
108. O. W. Webster, W. R. Hertler, D. Y. Sogah, W.B. Farnham, T.V. RajanBabu, "Group-transfer polymerization. 1. A new concept for addition polymerization with organosilicon initiators," *J. Am. Chem. Soc.* **1983**, *105*, 5706 – 5708.
109. D. Y. Sogah, W. R. Hertler, O. W. Webster, G. M. Cohen, "Group transfer polymerization. Polymerization of acrylic monomers," *Macromolecules* **1987**, *20*, 1473 – 1488.
110. I. B. Dicker, G. M. Cohen, W. B. Farnham, W. R. Hertler, E. D. Laganis, D. Y. Sogah, "Oxyanions catalyze group-transfer polymerization to give living polymers," *Macromolecules* **1990**, *23*, 4034 – 4041.
111. O. W. Webster, "Group transfer polymerization: A critical review of its mechanism and comparison with other methods for controlled polymerization of acrylic monomers," *Adv. Polym. Sci.* **2004**, *167*, 1 – 34.
112. A. B. Lowe, N. C. Billingham, S. P. Armes, "Synthesis and characterization of zwitterionic block copolymers," *Macromolecules* **1998**, *31*, 5991 – 5998.
113. Moad, G.; Rizzardo, E. and Thang S. H. "Living Radical Polymerization by the RAFT Process – A Second Update," *Aust. J. Chem.* **2009**, *62*, 1402 – 1472.
114. D. A. Skoog, F. J. Holler, T. A. Nieman, Principles of Instrumental Analysis: 5th Edition, Kostaraki Athens Publications, 2007, Chapt. 28, 844 – 891.
115. J. McMurry, Organic Chemistry: 1st Edition, University Editions of Crete: Heraklion, 1998, Chapt. 13, 559 – 569.
116. D. Kiserow, K. Prochazka, C. Ramireddy, Z. Tuzar, P. Munk, S. E. Webber, "Fluorimetric and quasi-elastic light scattering study of the solubilization of nonpolar low-molar-mass compounds into water-soluble block-copolymer micelles", *Macromolecules* **1992**, *25*, 461 – 469.
117. J.-J. Yu, S. N. Magonov, "Application of Atomic Force Microscopy (AFM) in Polymer Materials." *Agilent Technologies, Inc.* **2007**, *25*, 5989 – 6926.

118. F. Horkay, P. J. Basser, A.-M. Hecht, E. Geissler, "Osmotic and SANS Observations on Sodium Polyacrylate Hydrogels in Physiological Salt Solutions." *Macromolecules* **2000**, *22*, 8329 – 8333.
119. K. S. Pafiti, E. Loizou, C. S. Patrickios, L. Porcar, "End-linked semifluorinated amphiphilic polymer conetworks: synthesis by sequential reversible addition–fragmentation chain transfer polymerization and characterization", *Macromolecules* **2010**, *43*, 5195 – 5204.
120. D. Suckau, A. Resema, M. Schuerenberg, P. Hufnagel, J. Franzen, A. Holle, "A novel MALDI LIFT-TOF/TOF mass spectrometer for proteomics", *A. Anal. Bioanal. Chem.* **2003**, *376*, 952 – 965.
121. W. Li, J. A. Yoon, K. Matyjaszewski, "Dual-Reactive Surfactant Used for Synthesis of Functional Nanocapsules in Miniemulsion", *J. Am. Chem. Soc.* **2010**, *132*, 7823 – 7825.
122. D. L. Patton, M. Mullings, T. Fulghum and R. C. Advincula, "A Facile Synthesis Route to Thiol-Functionalized α,ω -Telechelic Polymers via Reversible Addition Fragmentation Chain Transfer Polymerization", *Macromolecules* **2005**, *38*, 8597 – 8602.
123. R. Jayalakshmi, S. R. Ramadas and C. N. Pillai, "Michael Addition of Dithiobenzoic Acid to α,β -Unsaturated Ketones. A New Series of Dithioesters", *Org. Prep. Proc. Int.* **1981**, *13*, 71 – 79.
124. W. H. Heath, F. Palmieri, J. R. Adams, B. K. Long, J. Chute, T. W. Holcombe, S. Zieren, M. J. Truitt, J. L. White, C. G. Willson, "Degradable Cross-Linkers and Strippable Imaging Materials for Step-and-Flash Imprint Lithography", *Macromolecules* **2008**, *41*, 719 – 726.
125. D. L. Roberts, Y. Ma, S. E. Bowles, C. M. Janczak, J. Pyun, S. S. Saavedra, C. A. Aspinwall, "Polymer-Stabilized Phospholipid Vesicles with a Controllable, pH-Dependent Disassembly Mechanism", *Langmuir* **2009**, *25*, 1908 – 1910.
126. D. Suckau, A. Resema, M. Schuerenberg, P. Hufnagel, J. Franzen, A. Holle, "A novel MALDI LIFT-TOF/TOF mass spectrometer for proteomics", *Anal. Bioanal. Chem.* **2003**, *376*, 952–965.
127. H. Wei, J. A. Pahang, S. H. Pun, "Optimization of brush-like cationic copolymers for nonviral gene delivery", *Biomacromolecules* **2013**, *14*, 275 – 284.

128. H. Eschwey, M. L. Hallensleben, W. Burchard, 'Preparation and some properties of star-shaped polymers with more than hundred side chains', *Makromol. Chem.* **1973**, *173*, 235 – 239.
129. O. E. Philippova, D. Hourdet, R. Audebert, A. R. Khokhlov, "pH-responsive gels of hydrophobically modified poly (acrylic acid)", *Macromolecules* **1997**, *30*, 8278 – 8285.
130. M. W. Matsen, F. S. Bates, "Block copolymer microstructures in the intermediate-segregation regime", *J. Chem. Phys.* **1996**, *106*, 2436 – 2448.
131. M. Karbarz, Z. Stojek, C. S. Patrickios, "ABA triblock copolymer-based model networks in the bulk: Effect of the number of arms on microphase behaviour", *Polymer* **2005**, *46*, 7456 – 7462.
132. M. Karbarz, Z. Stojek, T. K. Georgiou, C. S. Patrickios, "Microphase separation in ABA triblock copolymer-based model conetworks in the bulk: Effect of loop formation", *Polymer* **2006**, *47*, 5182 – 5186.
133. M. W. Matsen, M. Schick, "Microphase separation in starblock copolymer melts", *Macromolecules* **1994**, *27*, 6761 – 6767.
134. R. Weidisch, M. Stamm, D. W. Schubert, M. Arnold, H. Budde, S. Höring, "Correlation between Phase Behavior and Tensile Properties of Diblock Copolymers", *Macromolecules* **1999**, *32*, 3405 – 3411.
135. R. Weidisch, G. H. Michler, M. Arnold, S. Hofmann, M. Stamm, R. Jérôme, "Synergism for the Improvement of Tensile Strength in Block Copolymers of Polystyrene and Poly(n-butyl methacrylate)", *Macromolecules* **1997**, *30*, 8078 – 8080.
136. G. H. Michler, H. H. Kausch, R. Adhikari, "Modeling of Thin Layer Yielding in Polymers", *J. Macromol. Sci., Part B: Phys.* **2006**, *45*, 727 – 739.
137. G. H. Michler, R. Adhikari, W. Lebek, S. Goerlitz, R. Weidisch, K. Knoll, "Morphology and Micromechanical Deformation Behavior of Styrene/Butadiene-Block Copolymers. I. Toughening Mechanisms in Assymmetric Star Block Copolymers", *J. Appl. Polym. Sci.* **2002**, *85*, 683 – 700.
138. J. P. Gong, Y. Katsuyama, T. Kurokawa, Y. Osada, "Double Network Hydrogels with Extremely High Mechanical Stenght", *Adv. Mater.* **2003**, *15*, 1155 – 1158.
139. V. X. Truong, M. P. Ablett, S. M. Richardson, J. A. Hoyland, A. P. Dove, "Simultaneous Orthogonal Dual-Click Approach to Tough, in-Situ-Forming Hydrogels for Cell Encapsulation", *J. Am. Chem. Soc.* **2015**, *137*, 1618 – 1622.

140. T. K. Georgiou, M. Vamvakaki, C. S. Patrickios, "Microphase separation under constraints: A molecular thermodynamic theory for polyelectrolytic amphiphilic model networks in water", *Polymer* **2004**, *45*, 7341 – 7355.
141. T. Hiroi, S. Kondo, T. Sakai, E. P. Gilbert, Y.-S. Han, T.-H. Kim, M. Shibayama, "Fabrication and Structural Characterization of Module-Assembled Amphiphilic Conetwork Gels", *Macromolecules* **2016**, *49*, 4940 – 4947.
142. M. Vamvakaki, C. S. Patrickios, P. Lindner, M. Gradzielski, "Amphiphilic Networks Based on Cross-Linked Star Polymers: A Small-Angle Neutron Scattering Study", *Langmuir* **2007**, *23*, 10433 – 10437.
143. K. Mortensen, M. Annaka, "Structural Study of Four-Armed Amphiphilic Star-Block Copolymers: Pristine and End-Linked Tetronic T1307", *ACS Macro Lett.* **2016**, *5*, 224 – 228.
144. N. W. Ashcroft, J. Lekner, "Structure and Resistivity of Liquid Metals", *Phys. Rev.* **1966**, *145*, 83 – 90.
145. G. Hild, "Model Networks Based on 'Endlinking' Processes: Synthesis, Structures and Properties", *Prog. Polym. Sci.* **1998**, *23*, 1019 – 1149.
146. M. Eberhardt, R. Mruk, R. Zentel, P. Théato, "Synthesis of pentafluorophenyl (meth)acrylate polymers: New precursor polymers for the synthesis of multifunctional materials", *Eur. Polym. J.* **2005**, *41* (7), 1569 – 1575.
147. K. S. Pafiti, N. P. Mastroiannopoulos, L. A. Phylactou, C. S. Patrickios, "Hydrophilic Cationic Star Homopolymers Based on a Novel Diethanol-*N*-Methylamine Dimethacrylate Cross-Linker for siRNA Transfection: Synthesis, Characterization, and Evaluation", *Biomacromolecules* **2011**, *12*, 1468 – 1479.
148. K. S. Pafiti, N. P. Mastroiannopoulos, L. A. Phylactou, C. S. Patrickios, "Cationic star polymer siRNA transfectants interconnected with a piperazine-based cationic cross-linker", *Biomed. Eng. Res.* **2011**, *1*, 29 – 38.
149. K. S. Pafiti, C. S. Patrickios, E. N. Yamasaki, T. K. Georgiou, N. P. Mastroiannopoulos, L. A. Phylactou, "Cationic star polymer siRNA transfectants interconnected with a piperazine-based cationic cross-linker", *Eur. Polym. J.* **2012**, *48*, 1422 – 1430.
150. T. K. Georgiou, M. Vamvakaki, C. S. Patrickios, E. N. Yamasaki, L. A. Phylactou, "Nanosopic cationic methacrylate star homopolymers: synthesis by group transfer polymerization, characterization and evaluation as transfection reagents", *Biomacromolecules* **2004**, *5*, 2221 – 2229.

151. T. K. Georgiou, M. Vamvakaki, L. A. Phylactou, C. S. Patrickios, "Synthesis, characterization, and evaluation as transfection reagents of double-hydrophilic star copolymers: effect of star architecture", *Biomacromolecules* **2005**, *6*, 2990 – 2997.
152. T. K. Georgiou, L. A. Phylactou, C. S. Patrickios, "Synthesis, characterization, and evaluation as transfection reagents of ampholytic star copolymers: effect of star architecture", *Biomacromolecules* **2006**, *7*, 3505 – 3512.
153. S. Harish, J. Mathiyarasu, K. L. N. Phani, V. Yegnaraman, "Synthesis of conducting polymer supported Pd nanoparticles in aqueous medium and catalytic activity towards 4-nitrophenol reduction", *Catalysis Letters*, **2009**, 128 – 197.
154. C.- C. Wang, D. – H. Chen and T. – C. Huang, "Synthesis of palladium nanoparticles in water-in-oil microemulsions", *Colloids and Surfaces A: Physicochem. Eng. Aspects* **2001**, *189*, 145 – 154.
155. G. H. Lathe, C. R. J. Ruthven, "The Separation of Substances on the Basis of Their Molecular Weights, Using Columns of Starch and Water," *Biochem J.* **1956**, *62*, 665 – 674.
156. J. C. Moore, "Gel permeation chromatography. I. A new method for molecular weight distribution of high polymers." *J. Polym. Sci.*, **1964**, *2*, 835 – 843.
157. B.H. Zimm, "Molecular Theory of the Scattering of Light in Fluids," *J. Chem. Phys.* **1945**, *13*, 141 – 145.
158. B.H. Zimm, "The Scattering of Light and the Radial Distribution Function of High Polymer Solutions," *J. Chem. Phys.* **1948**, *16*, 1093 – 1099.
159. R. G. Kirste, W. A. Kruse, J. Schelten, "Die bestimmung des tragheitsradius von polymethylmethacrylat im glaszustand durch neutronenbeugung." *Makromol. Chem.* **1973**, *162*, 299 – 303.
160. J. Schelten, G. D. Wignall, D. G. H. Ballard, "Chain conformation in molten polyethylene by low angle neutron scattering." *Polymer* **1974**, *15*, 682 – 685.
161. J. C. H. Spence, H. R. Kolars, G. Hembree, C. J. Humphreys, J. Barnard, R. Datta, C. Kock, F. M. Ross, J. F. Justo, "Imaging dislocation cores - the way forward". *Phil. Mag.* **2006**, *86*, 4781 – 4796.
162. C. Kisielowski, B. Freitag, M. Bischoff, H. van Lin, S. Lazar, G. Knippels, P. Tiemeijer, M. van der Stam, S. von Harrach, M. Stekelenburg, M. Haider, H. Muller, P. Hartel, B. Kabius, D. Miller, I. Petrov, E. Olson, T. Donchev, E. A. Kenik, A. Lupini, J. Bentley, S. Pennycook, A. M. Minor, A. K. Schmid, T. Duden, V. Radmilovic, Q. Ramasse, R. Erni, M. Watanabe, E. Stach, P. Denes, U. Dahmen, "Detection of single

atoms and buried defects in three dimensions by aberration-corrected electron microscopy with 0.5 Å information limit.” *Microscopy and Microanalysis* **2008**, *14*, 469 – 477.

163. “Basics of Polarizing Microscopy”, OLYMPUS, https://web.archive.org/web/20161215160659/http://research.physics.berkeley.edu/yildiz/Teaching/PHYS250/Lecture_PDFs/polarization%20microscopy.pdf

164. B.D. Cullity, Elements of X-ray Diffraction Addison Wesley Mass, **1978**, Chapter 14.

165. D. O. Sparkman, “Mass spectrometry desk reference. Pittsburgh: Global View Pub”, **2000**.

ANNEX I



Amphiphilic Polymer Conetworks Based on End-Linked "Core-First" Star Block Copolymers: Structure Formation with Long-Range Order

Author: Eleni J. Kepola, Elena Loizou, Costas S. Patrickios, et al

Publication: ACS Macro Letters

Publisher: American Chemical Society

Date: Oct 1, 2015

Copyright © 2015, American Chemical Society

PERMISSION/LICENSE IS GRANTED FOR YOUR ORDER AT NO CHARGE

This type of permission/license, instead of the standard Terms & Conditions, is sent to you because no fee is being charged for your order. Please note the following:

- Permission is granted for your request in both print and electronic formats, and translations.
- If figures and/or tables were requested, they may be adapted or used in part.
- Please print this page for your records and send a copy of it to your publisher/graduate school.
- Appropriate credit for the requested material should be given as follows: "Reprinted (adapted) with permission from (COMPLETE REFERENCE CITATION). Copyright (YEAR) American Chemical Society." Insert appropriate information in place of the capitalized words.
- One-time permission is granted only for the use specified in your request. No additional uses are granted (such as derivative works or other editions). For any other uses, please submit a new request.



Networks Based on "Core-First" Star Polymers End-Linked Using a Degradable Ketal Cross-Linker: Synthesis, Characterization, and Cleavage

Author: Costas S. Patrickios, Eleni J. Kepola

Publication: Macromolecular Chemistry and Physics

Publisher: John Wiley and Sons

Date: Dec 11, 2017

© 2017 WILEY-VCH Verlag GmbH & Co. KGaA, Weinheim

Order Completed

Thank you for your order.

This Agreement between 20, ΑΡΤΕΜΟΥ ΦΡΑΝΤΖΕΣΚΟΥ ("You") and John Wiley and Sons ("John Wiley and Sons") consists of your license details and the terms and conditions provided by John Wiley and Sons and Copyright Clearance Center.

Your confirmation email will contain your order number for future reference.

License Number 4800990080474

License date Apr 02, 2020

[Printable Details](#)

Licensed Content

Licensed Content Publisher	John Wiley and Sons
Licensed Content Publication	Macromolecular Chemistry and Physics
Licensed Content Title	Networks Based on "Core-First" Star Polymers End-Linked Using a Degradable Ketal Cross-Linker: Synthesis, Characterization, and Cleavage
Licensed Content Author	Costas S. Patrickios, Eleni J. Kepola
Licensed Content Date	Dec 11, 2017
Licensed Content Volume	219
Licensed Content Issue	1
Licensed Content Pages	11

Order Details

Type of use	Dissertation/Thesis
Requestor type	Author of this Wiley article
Format	Print and electronic
Portion	Full article
Will you be translating?	No



Amphiphilic Polymer Conetworks Based on Interconnected Hydrophobic Star Block Copolymers: Synthesis and Characterization

Author: Eleni J. Kepola, Kyriacos Kyriacou, Costas S. Patrickios, et al

Publication: Macromolecular Symposia

Publisher: John Wiley and Sons

Date: Apr 19, 2017

© 2017 WILEY-VCH Verlag GmbH & Co. KGaA, Weinheim

Order Completed

Thank you for your order.

This Agreement between 20, ΑΡΤΕΜΟΥ ΦΡΑΝΤΖΕΣΚΟΥ ("You") and John Wiley and Sons ("John Wiley and Sons") consists of your license details and the terms and conditions provided by John Wiley and Sons and Copyright Clearance Center.

Your confirmation email will contain your order number for future reference.

License Number 4800990476069

License date Apr 02, 2020

Licensed Content

Licensed Content Publisher John Wiley and Sons
Licensed Content Publication Macromolecular Symposia
Licensed Content Title Amphiphilic Polymer Conetworks Based on Interconnected Hydrophobic Star Block Copolymers: Synthesis and Characterization
Licensed Content Author Eleni J. Kepola, Kyriacos Kyriacou, Costas S. Patrickios, et al
Licensed Content Date Apr 19, 2017
Licensed Content Volume 372
Licensed Content Issue 1
Licensed Content Pages 18

Order Details

Type of use Dissertation/Thesis
Requestor type Author of this Wiley article
Format Print and electronic
Portion Full article
Will you be translating? No

[Printable Details](#)

ELENI J. KEPOLA